

# Final Report

## Group 18 - Sustainable Air Taxi

### Authors

Martijn Hoogeslag	5027772	Maarten Krikke	5102111
Baturay Kumbaroğlu	5050480	Sergiu Priboi	5000327
Theodor Falat	5053617	Vlad Buzetelu	5040604
Tarek Abdelrazek	4993004	Bas van Leeuwen	4834925
Julien Svensson	5006651	Jared Vermeulen	4809467



This page is intentionally left blank.

# Contents

Preface	vii	6.2 Fuel Tank Geometry . . . . .	38
1 Executive Overview	1	6.2.1 Geometry Support Blocks . . . . .	39
2 Introduction	10	6.3 Fuel Tank Operations . . . . .	41
3 Sustainable Development Strategy	11	6.3.1 Boil-off Process . . . . .	41
3.1 Life Cycle Assessment . . . . .	11	6.3.2 Loads Fuel Tank. . . . .	44
3.2 Design Philosophy . . . . .	11	6.3.3 Miscellaneous Concepts of the Fuel System . . . . .	45
4 Design Tools	13	7 Propulsion System	47
4.1 Initial parameters . . . . .	13	7.1 Engine. . . . .	47
4.2 Class I Weight Estimation . . . . .	14	7.1.1 Electric Motor Considerations. . .	47
4.3 Preliminary Sizing . . . . .	14	7.1.2 Propeller Considerations. . . . .	49
4.3.1 Wing & Power Loading . . . . .	15	7.1.3 Matching the Propeller with the Motor . . . . .	53
4.3.2 Wing Sizing . . . . .	16	7.2 Fuel Cells . . . . .	57
4.4 Class II Weight Estimation. . . . .	16	7.2.1 Fuel cell operation . . . . .	57
4.4.1 Powertrain Mass Estimation. . . .	16	7.3 Air compressor . . . . .	60
4.4.2 Tank Mass Estimation . . . . .	18	7.3.1 Air supply system. . . . .	60
4.5 Aircraft Sizings . . . . .	18	7.3.2 Compressor power requirement. .	62
4.6 Wing and Empennage Sizings. . . . .	18	7.3.3 Expander system . . . . .	62
4.6.1 Center of Gravity Extrusion . . . .	18	7.4 Operational Pressure of Fuel Cells . . . .	62
4.7 Stability and Control . . . . .	20	7.5 Humidifier . . . . .	63
4.7.1 Methodology . . . . .	20	7.6 Hydrogen re-usage . . . . .	64
4.8 Landing Gear Positioning . . . . .	22	7.7 Temperature Control. . . . .	64
4.9 Iteration Technique . . . . .	22	7.8 Numerical values. . . . .	65
4.10 Flight Envelope. . . . .	23	7.8.1 General subsystem values . . . . .	65
4.10.1 Maneuver Diagram. . . . .	24	7.8.2 Fuel cell sizing . . . . .	65
4.10.2 Gust Loading Diagram . . . . .	24	7.9 Materials . . . . .	66
4.10.3 Diagram and Conclusions . . . . .	25	7.9.1 Electrolyte Materials . . . . .	66
4.11 Results. . . . .	26	7.9.2 Electrode/Catalyst Materials. . . .	67
5 Fuselage and Landing Gear Design	27	7.9.3 Anode/Cathode Catalyst . . . . .	67
5.1 Cabin Cross-section and Layout . . . . .	27	7.10 Hydrogen Environmental Impact . . . . .	67
5.2 Fuselage, Fuel Tank Placement and Cargo Compartment . . . . .	28	7.11 Battery . . . . .	69
5.2.1 Fuselage Layout and Dimensions .	29	7.12 Propulsion System Integration . . . . .	70
5.2.2 Cargo Compartment . . . . .	30	8 Wing Design	73
5.2.3 Structural Considerations . . . . .	30	8.1 Airfoil Selection and Planform Design . .	73
5.3 Landing Gear Design and Storage. . . . .	31	8.2 Wing Box Design . . . . .	76
5.3.1 Tyre Sizing. . . . .	31	8.2.1 Sustainable Design Philosophy . .	76
5.3.2 Landing Gear Positioning . . . . .	32	8.2.2 Structural Design . . . . .	77
5.3.3 Landing Gear Retraction and Storage . . . . .	34	8.3 Aileron Design . . . . .	80
5.3.4 Load Transfer and Impact Safety .	35	8.4 High Lift Devices . . . . .	82
6 Fuel Tank Design	36	8.5 Wing Box Layout . . . . .	82
6.1 Fuel Tank Material . . . . .	36	8.6 Drag Calculations . . . . .	84
6.1.1 Shell Material . . . . .	36	9 Empennage Design and Final Aircraft Lay- out	86
6.1.2 Insulation Material . . . . .	36	9.1 Tail Sizing and Positioning. . . . .	86
6.1.3 Supporting Material . . . . .	37	9.2 Final Layout of Aircraft. . . . .	89

10	Verification and Validation	92	13.3	Operational profit	112
10.1	Sizing Tools Verification	92	13.3.1	Operation Profit Manufacturer	112
10.1.1	Unit Tests	92	13.3.2	Operation Profit Operator	112
10.1.2	Convergence Test	93	13.4	Return on Investment	113
10.1.3	Extreme Value Test	93	13.4.1	Return on Investment manufac-	114
10.1.4	Sensitivity Test	93	turer		
10.2	Aero-tools verification	95	13.4.2	Return on Investment operator	114
10.3	Python Tools Validation	95	13.5	Future Prospects	114
11	Production plan	97	14	Operations and Logistics	115
11.1	General Production Plan	97	14.1	Operations	115
11.2	System specific production plan	97	14.2	RAMS	116
11.2.1	Aerodynamic Surfaces	98	14.2.1	Reliability	116
11.2.2	Fuselage	99	14.2.2	Availability	117
11.2.3	Fuel Tank	99	14.2.3	Maintainability	117
11.2.4	Power System	100	14.2.4	Safety	118
11.2.5	Total Assembly	101	15	Technical risk assessment	119
11.3	Sustainable Production	101	15.1	Assessment of Previously Identified	
12	Impact Analysis	102	Technical Risks		119
12.1	Operational Impact	102	15.2	Identification and Mitigation of New	
12.1.1	Foreground Emissions	102	Technical Risks		122
12.1.2	Background Emissions	102	15.3	Updated Risk Matrices	123
12.2	Manufacturing	104	16	Compliance matrix	125
12.3	End of life	106	17	Conclusions and Recommendations	130
13	Market Analysis	108	17.1	Conclusions	130
13.1	Market Situation Air Taxi	108	17.2	Recommendations for the Future	132
13.1.1	Unit Price Air Taxi	108	References		136
13.1.2	Market Space for the Air Taxi	109	A	DSE project logic diagrams	139
13.2	Cost break-down Structure	109	A.1	DSE diagrams	139
13.2.1	Cost break-down Manufacturer	109	A.2	Post DSE diagrams	139
13.2.2	Cost Break-down Operator	111			



# Nomenclature

<b>Abbreviations</b>			$\eta_{FC}$	Real efficiency of PEMFC	-
			$\eta_{ohmic}$	Ohmic losses	-
AR	Aspect Ratio	-	$\gamma$	Ratio of specific heats	-
BP	Bipolar plates	-	$\lambda$	Stoichiometric ratio	-
CG	Centre of Gravity	-	$\lambda$	taper ratio	-
CL	Catalyst layer	-	$\nu$	Poisson's ratio	-
EOL	End of Life	-	$\rho$	density	$kg/m^3$
EPS	Expanded polystyrene	-	$\sigma_y$	Yield Strength	MPa
FCAS	Fuel cell air supply	-	$\sigma_{cc}$	Crippling stress	MPa
GDL	Gas diffusion layer	-	$\sigma_{cr}$	Critical buckling stress	MPa
GFC	Gas flow channels	-	$\tau$	Shear Strength	MPa
GWP	Global Warming Potential	$kgCO_2 - eq$	$\tau_a$	Aileron effectiveness	-
MAC	Mean Aerodynamic Chord	m	$A$	Cross sectional area	$m$
MEA	Membrane electrode assembly	-	$B$	Area of a stringer	$m^2$
MLG	Main Landing Gear	-	$b$	Wing span	m
MPL	Micro-porous layer	-	$c$	Chord	m
MTOM	Max take-off mass	kg	$C_D$	Drag coefficient	-
MTOW	Max take-off weight	N	$C_L$	Lift coefficient of the 3D wing	-
NLG	Nose Landing Gear	-	$C_l$	Lift coefficient of the 2D wing	-
OEM	Operational empty mass	kg	$C_M$	Moment coefficient of the 3D wing	-
OEW	Operational empty weight	N	$C_m$	Moment coefficient of the 2D wing	-
PEMFC	Polymer electrolyte fuel cell	-	$C_P$	Propeller power coefficient	-
PFSA	Perfluorosulfonic acid polymer	-	$c_p$	Isobaric specific heat	$J \cdot kg^{-1} \cdot K^{-1}$
<b>Symbols</b>			$C_T$	Propeller thrust coefficient	-
			$C_{D_0}$	zero lift drag coefficient	-
$\alpha$	Angle of attack	°	$C_{d_{min}}$	minimum drag coefficient of 2D wing	-
$\eta_c$	Efficiency of compressor	-	$C_{l_\alpha}$	Slope of the 2D lift curve	-
$\eta_{act}$	Activation losses	-	$C_{l_{\delta\alpha}}$	aileron control derivative	-
$\eta_{conc}$	Concentration losses	-	$C_{l_{des}}$	Design lift coefficient of the airfoil	-
$\eta_{FC,max}$	Theoretical maximum efficiency of PEMFC	-	$C_{l_{max}}$	maximum lift coefficient of 2D wing	-
			$C_{l_p}$	roll damping coefficient	-

$E$	Young's Modulus	GPA	$P_e$	Power generated by fuel cell	W
$e$	Oswald efficiency factor	-	$q$	Shear flow	N/m
$E_{thermo}$	Thermodynamically predicted fuel cell voltage output	V	$r$	Radius	m
$F$	Applied force	N	$S_{ref}$	Surface area of the wing	$m^2$
$G$	Shear Modulus	MPA	$S_{wf}$	Area of the high lift devices projected on the wing	$m^2$
$I_{xx}$	Moment of inertia around x-axis	$m^4$	$sf$	safety factor	-
$J$	Propeller advance ratio	-	$T$	Torsion	$Nm$
$L$	Lift	N	$T_1$	Atmospheric temperature	K
$M_x$	Moment around x-axis	Nm	$V_c$	Voltage that each cell in a fuel stack produce	V
$n_{ult}$	Ultimate load factor	-	$V_{rot}$	Rotational speed	RPM or RPS
$P$	Roll Rate	rad/s	$V_{tip}$	Propeller tip speed	m/s
$P_1$	Atmospheric pressure	bar	$W$	Weight	N
$P_2$	Compressor outlet pressure	bar	$W_{PL}$	Payload weight of the aircraft	N
$P_c$	Power generated by fuel cell	W	$z_{max}$	distance to x-axis	m

# Preface

To finish the bachelor degree Aerospace Engineering at the TU Delft a challenging project needs to be completed by a group of 10 students. After 10 weeks of hard working, a lot of coding and many design options we are proud to present the final results within this report. As a team we had the 'honour' to investigate the future of sustainable aviation. We, as group 18, enjoyed the entire duration of this project and gained new insights on the opportunities of flying with a small environmental impact.

After the project we want to thank our principal tutor Jos Sinke and our coaches Sven Westerbeek and Boris Kruljevic, for their great support, guidance and constructive feedback. Furthermore, special thanks to Derk-Jan van Heerden, CEO of AELS, who provided us with a lot of information regarding modern recycling of aircraft. We want to express our gratitude towards all other staff members, friends and family who supported us during the past weeks.

*Group 18 Delft, June 21, 2022*

# Executive Overview

This report acts as a follow-up to the midterm report containing the final trade-off winning design, which is further analysed in this final report. As a short summary to what has been decided after the midterm, the trade-off winner contains a propulsion system based on liquid hydrogen with a battery attached to it, making up a hybrid design. It uses fuel cells in combination with an electric motor as energy conversion mechanism and is powered by two wing mounted propeller engines, and features a high wing configuration with a T-tail. All of these choices are reflected upon in the final report.

The process of deciding the winning design choice consisted of applying the previously mentioned trade-off process on 6 different design options. The trade-off was conducted by choosing criteria, which are sustainability, performance, aircraft and airport operations and cost. Each of these received sub-criteria scored with individual grades on a scale from 1 to 7. Each criteria also has a weight, with sustainability being the most important. In the end it was found that design 5 scores highest, mostly thanks to its high scoring in terms of sustainability and performance.

In terms of performance, design 5 scores relatively high due to its low estimated operational empty weight of 4494 kg and for its relatively low drag profile. In terms of velocity it loses to its jet propelled counterparts but scores quite well for the payload-range analysis. Thanks to liquid hydrogen being its propellant, the design has to store less fuel for a trip of the same length, enabling it to carry more weight. In terms of sustainability, the design scores top points winning that trade-off criteria. Thanks to its liquid hydrogen propulsion system, the aircraft emits very little greenhouse gases into the environment and the potential of green liquid hydrogen production further increases its prospects regarding sustainability. After a calculation, it was found that using an energy density of 77,900 kWh per million standard cubic feet of hydrogen, the amount of CO<sub>2</sub> emitted is only 0.28 kg per kilowatt hour. Thanks to the use of fuel cells, hydrogen is not processed at a large enough temperature to form NO<sub>x</sub> emissions. The fuel cell powertrain also is low in noise production compared to a combustion engine. In the end, design 5 is the most sustainable option.

In terms of cost, the winning design does not score as high as other designs. This is due to the complexity of the fuel cell in combination with liquid hydrogen as propellant and a battery. The technology involved in the propulsion system is rather new and creating it implies both additional manufacturing and research costs. Regarding maintenance, fuel cells are difficult to maintain and, of course, the cryogenic tank that would store the liquid hydrogen is also expensive. Furthermore, since storing and refueling liquid hydrogen is rather difficult, the design scores low in the operations criteria. Irrespective, operations has a small weight assigned to it, making it possible for the final design to win. The final trade-off table with all the scores is in Table 1.1.

**Table 1.1:** General trade-off table

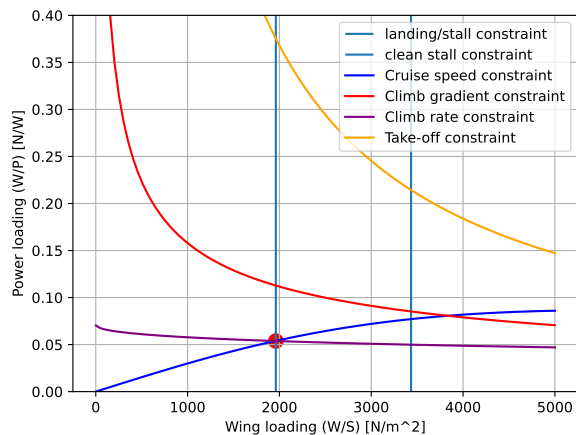
	Overall	Cost (15%)	Sustainability (35%)	Operations (20%)	Performance (30%)	Total
1	<b>H<sub>2</sub> liquid combustion</b>	3.8	4.1	3.05	7	4.72
2	<b>Electric (batteries)</b>	2.15	5.3	3.8	1	3.24
3	<b>Ammonia liquid</b>	5.05	2.5	4.95	5.5	4.27
4	<b>Methane liquid</b>	2.7	2.15	4.35	6	3.83
5	<b>H<sub>2</sub> liquid fuel cell + batteries</b>	3.85	6.8	2.65	4.75	4.91
6	<b>H<sub>2</sub> gas fuel cells</b>	3.9	6.5	2.3	1	3.62

In this fourth and final report, which concludes the series of reports documenting the Sustainable Air Taxi design process, a detailed design of the aircraft is conducted. The report begins with describing the software tools

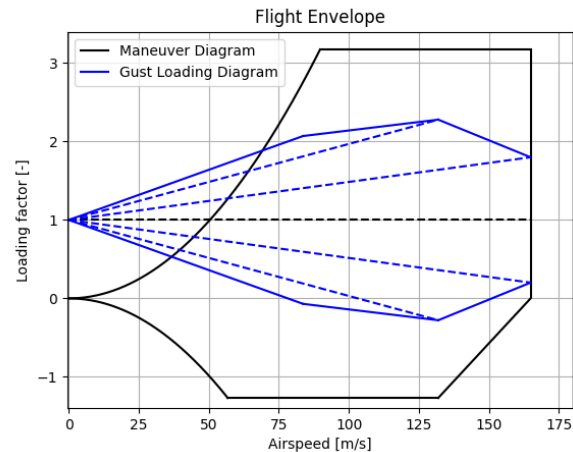
that are used in this design process. The tools are created using Python and they are used to come up with the aircraft's most important parameters which are then used in further calculations. With more than 4800 lines of code, the tools also require Verification & Validation. The V&V process is also described in this report. Afterwards, the inside of the aircraft is analysed and the fuselage is sized. This is important because the Sustainable Air Taxi promises a comfortable experience for its passengers. Next to that, detailed CAD images of the aircraft's model are presented along with the landing gear developed in the same section. Because of the difficulty to store liquid hydrogen onboard the aircraft, the fuel tank design has a chapter of its own as well. After the fuel tank's geometry is established, a very thorough explanation of the propulsion system choice is given. This includes the choice of the engine, the energy conversion system, which are fuel cells, and the architecture of said fuel cells. The next subsystem to be designed is the wing for which an aerodynamic analysis is performed using XFLR5 aerodynamic software. With the important loads acting on the wing during flight found, the structure of the wing is engineered. High lift devices, flaps, and other control surfaces such as the ailerons are designed in this section and preliminarily integrated. A sensitivity analysis is done for the tools that are used to find the most critical parameters. A more detailed production plan than the one in the midterm report is shown next. After all the analyses are completed, the empennage is placed on the aircraft and a final aircraft layout is visualised using CATIA renders. Being an important aspect of the Sustainable Air Taxi, the market analysis is expanded upon based on the previous reports to show the economic competitiveness of the Air Taxi. Operations and logistics are explored afterwards to show how the Sustainable Air Taxi should be handled. Finally, some updates from the previous reports such as a technical risk assessment, a work flow diagram and a work breakdown structure are presented. A compliance matrix is also created in order to keep track of all the set requirements and whether the design complies with them or not. In the end, a conclusions and recommendations presented to give an outlook into the future of the Sustainable Air Taxi.

The first step in the design process of the Sustainable Air Taxi is finding initial parameters that can be used to create further iterations of the design, until an operational empty weight of the aircraft can be found. These parameters are either estimated using similar aircraft of the same size and mission, assumed, or chosen based on literature. These parameters are then used as input for the Python tools that create the aircraft design itself.

The primary tool in the set creates the design point of the aircraft which helps find the necessary wing loading  $\frac{W}{S}$  for the mission at hand. For a range of 1500 km and 475  $\frac{km}{h}$  velocity, it is found that an exact value of the wing loading of 1961  $\frac{N}{m^2}$  is required, as is shown in Figure 1.1. This plot shows all the constraints that are set for the mission and that together make up the design space. The power loading, also present in this plot, is an important aspect of propeller aircraft in general and is used in the propeller design later on.



**Figure 1.1:** Power loading versus wing loading diagram including the design point (red dot)



**Figure 1.2:** CS-23 regulated flight envelope of the design

Class I and Class II estimations are the subsequent tools. They use the provided wing loading from the previous file, and begin making estimations on the aircraft's weight. Class I finds an initial maximum take-off and operational empty weight, and then Class II creates subsystem weights based on the geometry of each component. They are all added up in the end to create an iteration. This is reiterated multiple times until the solution for the weight converges.

With this operational empty weight a center of gravity range can be found which is a necessary input for stability and controllability analysis, as well as for positioning components of the aircraft. Next, the stability of the aircraft is analysed in another file, and a scissor plot is created, and then the empennage and landing gear sizing are done, here the code reiterates until a solution converges once again. Finally, in order to check that the aircraft complies with CS-23 regulations, a flight envelope is conceived in Figure 1.2. This flight envelope gives the loading factors that the aircraft may reach under extreme conditions.

As it is already mentioned, the code reiterates until it converges to a final solution. The code is explained more thoroughly in this report. However, a simplified version of how the program actually behaves is shown in the N2 chart in Figure 1.3. The elements in the main diagonal represent a file that exists within the tools, the cells in the vertical direction represent the outputs of said files, and the elements in the horizontal direction are the required inputs. The iteration process is shown in Figure 1.4.

<b>Class I</b>	OEW	OEW	Fuel Weight	Fuel Weight		
	<b>Preliminary Sizing</b>	Aircraft Dimensions	Aircraft Dimensions			
MTOW		<b>Class II</b>		Subsystem Weights		
		Aircraft Dimensions	<b>Aircraft sizing</b>	Subsystem Positions		
				<b>CG calculation</b>	Subsystem CG	
		Aircraft Dimensions		Lemac Positioning	<b>Stability Analysis</b>	Updated CG
						<b>Landing Gear sizing</b>

Figure 1.3: N2 Chart of python script

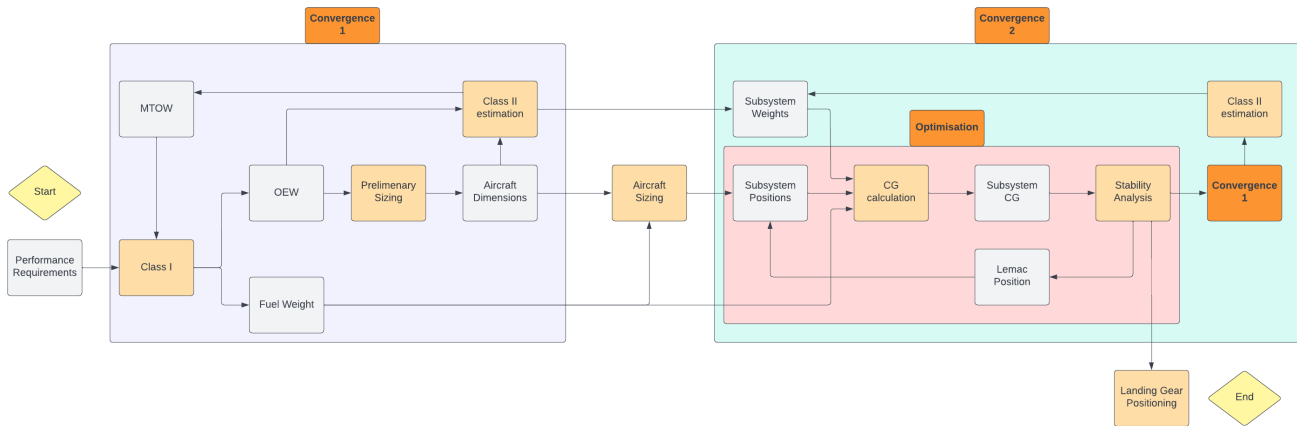
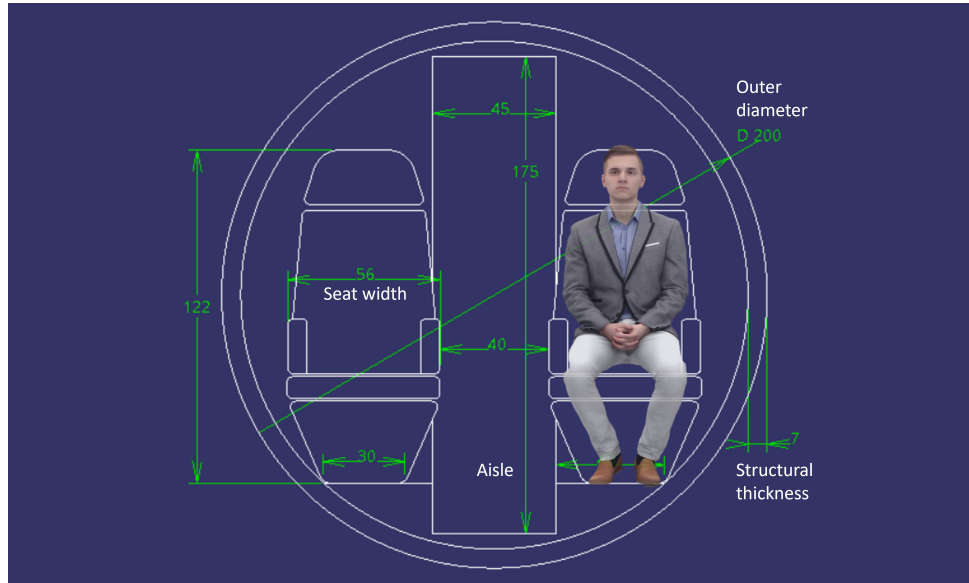


Figure 1.4: Flow Diagram of python script

The Sustainable Air Taxi promises a comfortable experience for its clients. Thus, an analysis of the fuselage is done in order to comply with this statement. The sizing of the fuselage is closely related to the liquid hydrogen tank, because of its size and required storage capacity. To this end, an outer fuselage diameter of 200 cm is deemed acceptable, as well as an aisle height of 175 cm which should be sufficient for a person of average height. A visualisation of the cabin is displayed in Figure 1.5.



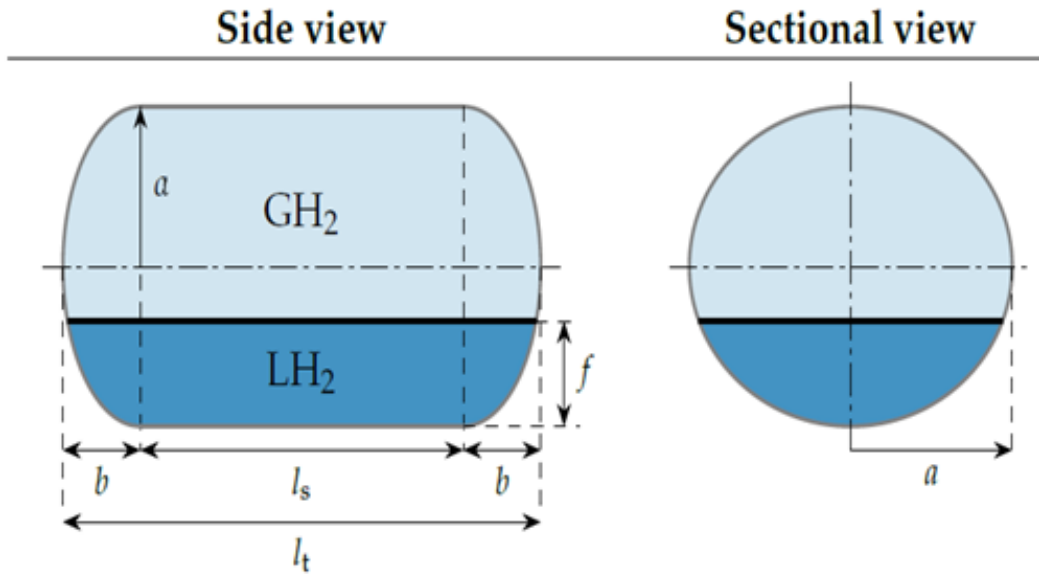
**Figure 1.5:** Cabin cross section dimensions cm with human model for scale

There is more than enough room, not only laterally, but also along the length of the aircraft. The seat pitch and legroom are chosen to be competitive to a modest business class configuration, found on similar aircraft. This is done in order to ensure the passengers are not too restricted in any way. There are 6 seats in the cabin, with 60 cm legroom and a seat pitch of 115 cm. A lavatory is included in the design, as well as two wardrobes for other pieces of luggage.

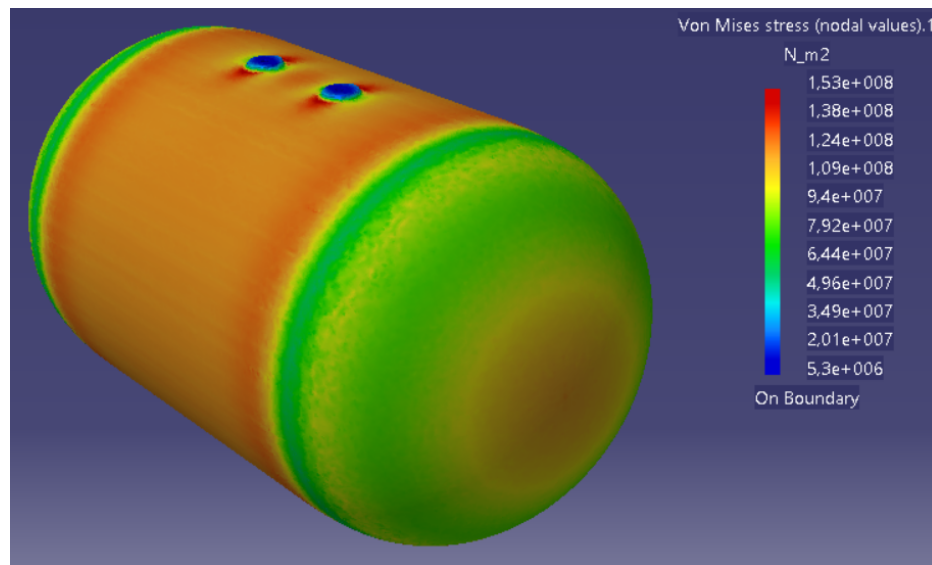
A cargo compartment is also designed for the luggage of the passengers, and it is placed at the end of the aircraft, behind the hydrogen tank. Using the requirement that the payload weight shall be 200 kg, the cargo hold is sized accordingly. It has a volume of 2.1 m<sup>3</sup>, in order to fit bulky pieces of luggage. The landing gear is sized afterwards, and the most notable aspect of this subsystem is its placement. After calculations, it is found that the main landing gear had to be placed right under the hydrogen tank, which poses a challenge for storing the retracted landing gear. For this reason, fuselage mounted pods are chosen to store the landing gear. The aircraft has to also land on any type of hardened runways, and the tyres are chosen as such.

The fuel tank has roughly a length of 3 m, making up a rather large portion of the aircraft. The correct choice of materials for producing it is key in this case, while keeping in mind sustainability as well. The choice for the shell of the tank is Aluminium 2219 because it performs best in terms of thermal conductivity and yield stress. On top of this, because hydrogen has to be kept at cryogenic temperatures of -253 °C, the chosen insulation material is Expanded Polystyrene foam. This is decided by taking into account its density, among other properties. The tank itself is also supported inside the aircraft using tank blocks that are connecting the tank to the airframe. The blocks are made out of foam glass, given its high compressive strength as well as decent thermal conduction properties.

The geometry chosen for the tank is given in Figure 1.6. A cylindrical shape is chosen, and an elliptical option is proposed for the ends of the tank. This option is a good compromise between spatial efficiency and stress concentration. The loads acting on the tank during aircraft operations are also analysed using CATIA and visualised in Figure 1.7.



**Figure 1.6:** Nomenclature for the geometry of the hydrogen fuel tank.



**Figure 1.7:** Finite Element Analysis for the fuel tank.

With the weight and general parameters of the aircraft known, the choice of the propulsion system comes next. With a required  $1021.6 \text{ kW}$  of combined shaft power during cruise, the choice of the electric motor driving the propeller is first. This choice is the *magniX's magni650* motor which is illustrated in Figure 1.8 and can deliver up to  $640 \text{ kW}$  of power. The propeller choice itself comes afterwards. The analysed parameters include the efficiency of the propeller, the rotational speed, the diameter and the blade number which is chosen to be 4, as well as the tip speed of the blades.

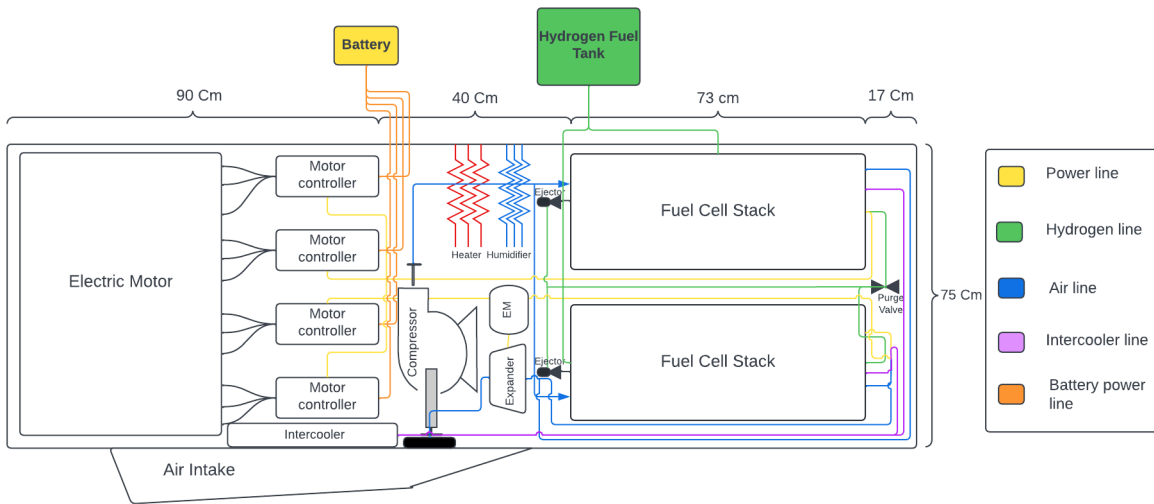
The required power for the electric engines is provided by the fuel cells inside the engine pods. They are responsible for producing sufficient energy using the liquid hydrogen. By consulting literature, it is found that using fuel cells is in fact feasible for aircraft such as the Sustainable Air Taxi. They also provide a green replacement to regular combustion engines, because of the reduction in polluting emissions. The performed research indicates towards fuel cells having an efficiency of 50%, with a power density of  $3000 \frac{\text{W}}{\text{kg}}$ , which are devices that exist using present day's technology. The last component of the propulsion system is a battery, which acts as an



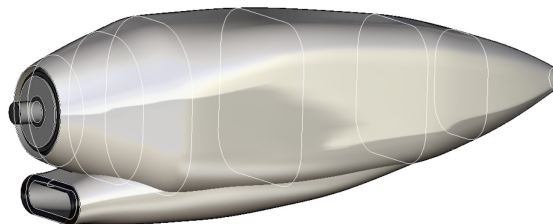


**Figure 1.8:** Demonstration of compatibility between the magni650 motor and a Hartzell 4-blade propeller (actual propeller model is unknown)<sup>1</sup>

Auxiliary Power Unit, for powering up the aircraft, and even act as a back-up in emergency situations. A final internal configuration of the propulsion system is given in Figure 1.9, together with a CATIA model of the engine pod, in Figure 1.10.

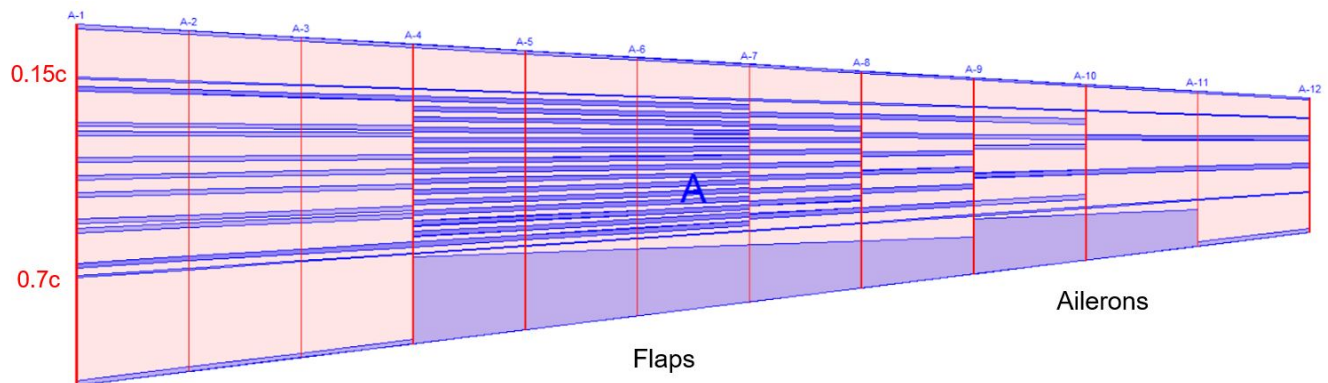


**Figure 1.9:** Diagram of the internal configuration of the propulsion system



**Figure 1.10:** 3D model of engine pod based on Figure 1.9

The first step in analysing the wing of the aircraft is choosing the cross-section of the wing, or the airfoil. The choice is NACA64312, and this is important for the engineering steps taken afterwards. A lift distribution using XFLR5 and structural load analyses are done on the wing to find the final dimensions. Afterwards, the ailerons, which are responsible for making the aircraft roll, are placed on the wing. A final representation of the internal wing box, which withstands all the flight loads, and the flaps and ailerons is given in Figure 1.11.



**Figure 1.11:** Top view of the wing box generated using DevWing.

Furthermore, the final subsystem that is installed on the aircraft is the vertical tail. An aerodynamic analysis, as well as a rough sizing using reference aircraft is done. With the last subsystem to be sized now done, the final configuration of the Sustainable Air Taxi is determined. Renders using CATIA are created and they are provided for visualisation purposes in Figure 1.12 and Figure 1.13.

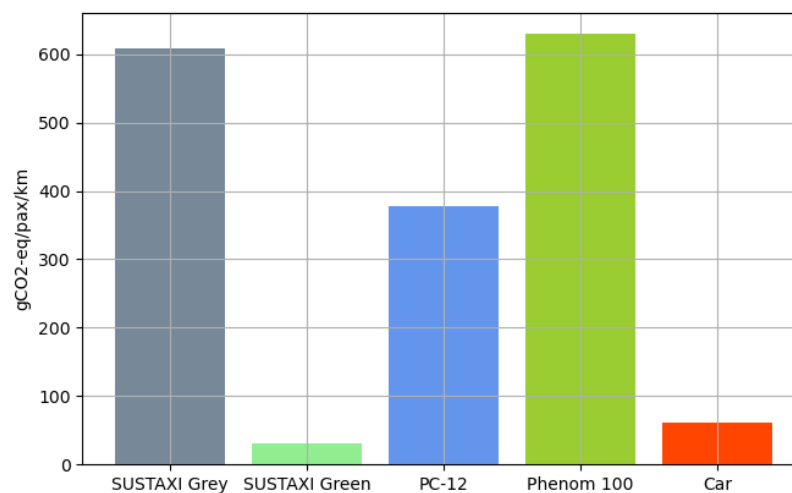


**Figure 1.12:** Render of the Sustainable Air Taxi in flight



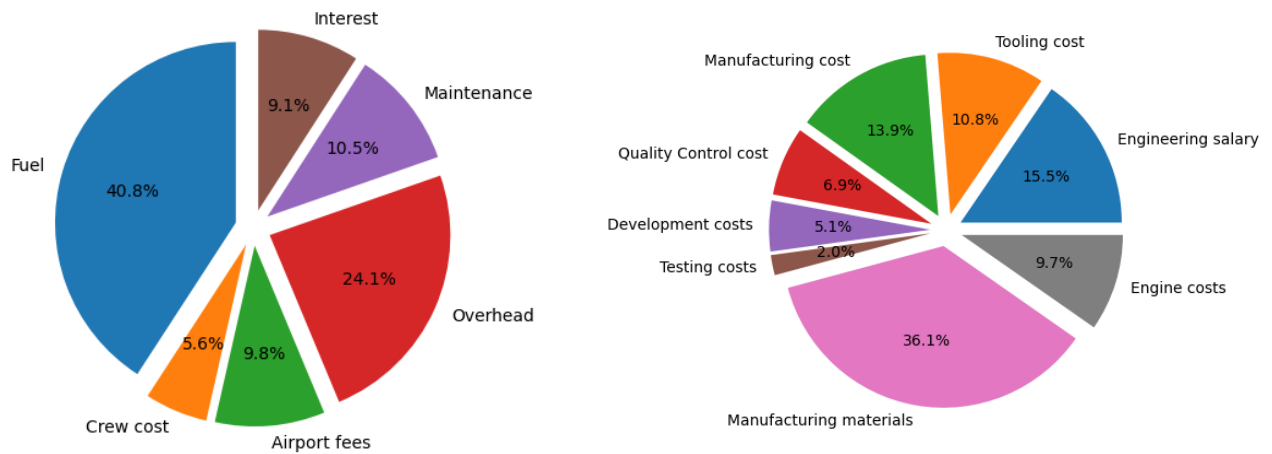
**Figure 1.13:** Cutaway view of the aircraft showing the aft fuel tank

An impact analysis is performed, showing that the Sustainable Air Taxi truly has the potential to reduce the global warming footprint of aviation. Depending on the energy source and projection, various scenarios for the environmental sustainability of the aircraft can be constructed, which sees the Sustainable Air Taxi in different positions regarding environmental competitiveness. Figure 12.3 puts the Air Taxi operational emissions on the map with similar aircraft and an average 2 passenger car when grey and green hydrogen are used.



**Figure 1.14:** The CO<sub>2</sub> emissions per passenger kilometre of the Sustainable Air Taxi and other aircraft as well as an average car.

The last analysis performed is regarding the market of the Air Taxi. This market analysis distinguishes the market for the manufacturer and operator of the Air Taxi. The unit price of the Air Taxi is set at 6.5 million USD because with this price it is competitive within the market and it will be financially viable for both the manufacturer and operator. For both involved parties the costs are analysed and shown in Figure 1.15. With the costs and unit price it is possible to derive the break even moments, which is after 58 months of operation for the operator and after 240 sold Air Taxis for the manufacturer.



**Figure 1.15:** Cost distribution for operator (left) in the first months of operations and for manufacturer (right) producing 325 Air Taxis.

The final production plan of the aircraft is devised, having each of the described subsystems in mind. Firstly, the aircraft is split into systems, and then a production plan is discussed for each of these: aerodynamic surfaces, fuselage, fuel tank and power system. This is done in order to document where each material is used and is also a good way of following whether or not all the materials used lead to an aircraft more than 80% recyclable. The production plan further considers aspects linked to sustainability by attempting to make production processes adhere as closely as possible to the sustainability requirements.

## Introduction

In recent years, more and more effort has gone into the research and development of alternative, greener aircraft, because of the considerable contribution that aviation has to the global emissions of compounds with a high polluting and global warming potential, such as  $CO_2$ ,  $NO_x$ ,  $CO$ , ultra-fine particles etc. The Sustainable Air Taxi is designed with a considerable effort towards sustainability during operations and towards end-of-life solutions. This report aims to present all the taken steps that lead to arriving at a feasible design.

The report covers a variety of topics which are introduced here for the reader. It starts with a discussion about the sustainable development strategy employed by the group during the design process, in Chapter 3. In Chapter 4, an overview of the steps leading to a converged aircraft sizing is given, including the class I and II weight estimations, as well as a stability and control analysis and the flight envelope diagrams. Next, the fuselage and landing gear are discussed in Chapter 5, followed by the design and integration of the liquid hydrogen fuel tank and propulsion system in Chapter 6 and Chapter 7, respectively. The preliminary aerodynamic design and wing design (both aerodynamic and structural design) are included in Chapter 8. The last design-oriented part of this report can be found in Chapter 9, which deals with the sizing and positioning of the horizontal and vertical tail of the Sustainable Air Taxi. Moreover, this chapter ends with an overview of the final aircraft layout and configuration. Additionally, Chapter 10 outlines the Verification and Validation procedures carried out for the technical tools used in the design process. The system-specific production plan is provided in Chapter 11, which focuses specifically on the sustainable approach to producing the Air Taxi. Chapter 12 provides an impact analysis of the Sustainable Air Taxi throughout its lifetime to prove that it, indeed, represents a green alternative to other modes of transportation. In order to make sure that the resulting design is competitive on the market not only from a performance perspective, but also from a financial one, a detailed market analysis is covered in Chapter 13. The logistics and operations related aspects associated with the design are then discussed in Chapter 14, followed by the technical risk assessment in Chapter 15 and by the requirement compliance matrix in Chapter 16. Last but not least, conclusions are drawn and future recommendations are given in Chapter 17, while the updated organisational and project logic diagrams can be found in the appendices.

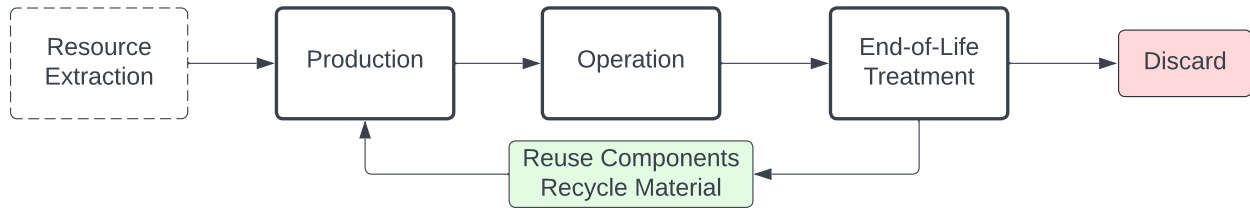
This report is the follow-up deliverable of the midterm report. It enables the reader to follow all the procedures that have been carried out during the last few weeks of the DSE, as well as a summary of the preliminary steps made before this final report. This is thus a standalone document which can be used to reproduce the results obtained by Group 18 during the design of the Sustainable Air Taxi.

# Sustainable Development Strategy

Sustainability is the central aspect of the Air Taxi. In order to deliver a final product that truly upholds the promise of being sustainable, a sustainable development strategy needs to be devised. Previously, in the midterm report, a number of trade-offs were performed which laid the foundation for attaining an environmentally sustainable Air Taxi. In this chapter, the conceptual considerations regarding sustainability are translated into a concrete development strategy for a sustainable Air Taxi. According to that strategy, the Air Taxi's lifetime is to be divided into three clearly separable stages of production, operation and end-of-life treatment, the necessity of which is presented in Section 3.1. Departing from that, Section 3.2 presents the design philosophy that is implemented throughout the final design stages.

## 3.1. Life Cycle Assessment

For the analysis of environmental impacts, life cycle assessment (LCA) methods are used. This facilitates a clear attribution of impacts to certain processes, thereby helping the design team identify and mitigate these issues in a targeted manner. Figure 3.1 visualises the life cycle stages of production, use and end-of-life that serve as partition of processes in the following sections.



**Figure 3.1:** *The general aircraft life cycle followed in the sustainable development.*

Currently, no LCA papers performed on aircraft of a comparable size are available. However, LCA of conventional commercial jet aircraft in the medium to large segment consistently show that the operational stage has by far the largest share of global warming (GWP) impacts among kerosene based aircraft [62] [63]. The production phase has a comparatively small impact, being estimated at 3.5% of the total GWP for an A320 as stated by Tyler Lewis [63]. End-of-life (EoL) of conventional aircraft has little impact and is omitted by most studies. Since generally, aircraft are parked and stripped for useful parts, there are no processes that emit environmental stressors. Nevertheless, this does not put EoL treatment outside the scope of this study as waste management and recycling are part of an environmentally sustainable product. Furthermore, choosing to reuse and recycle components as shown in Figure 3.1 can lead to impact reductions in the production stage. This is not limited to the GWP, but also helps reduce primary resource depletion, land use, particulate matter and possibly, toxicity potentials, which extends the environmental benefits to encompass socially and economically sustainable advancements.

## 3.2. Design Philosophy

The primary objective of the design should focus on reducing operational emissions, as these form the bulk of an aircraft's GWP. This is most effectively done by moving away from internal combustion of aviation fuel and employing electric propulsion solutions instead. Previously performed trade-offs lead to the conclusion that fuel cells, running on hydrogen stored in a liquid state are the most sustainable and achievable alternative. The detailed designs of the propulsion system and liquid hydrogen storage tank to be implemented in the Air Taxi

are described in Chapter 6 and Chapter 7, respectively.

With most modern aircraft using kerosene, production impacts and recycling tend to get neglected as employing lighter but less environmentally friendly materials can reduce the overall lifetime impact of the aircraft. Carbon fibre reinforced polymers, for instance, are badly recyclable but the fact that they lead to weight savings reduces the entire environmental impact of the aircraft. Once the operational impact of the Air Taxi is reduced, the manufacturing stage takes up a larger share of the overall impact. In addition, with a potentially green propulsion system, adding weight in return for a recyclable material becomes more sensible. As such, an environmentally sustainable aircraft should also limit its impact during manufacturing and end-of-life treatment. Using recycled materials goes a long way in reducing the environmental impact of the manufacturing stage. The GWP of recycled aluminium, as an example, is about 10 times smaller than when it is newly sourced [65]. So far, the main reason for why materials in aircraft are not properly separated is that the ordered disassembly procedure is too labour intensive and not economically viable, as different materials or alloys are used. In order to facilitate recycling of the aircraft with the potential of creating a materially circular aircraft, the variety of employed materials should be kept as small as possible and they should be clearly distinguishable from each other. The main goal regarding recyclability should therefore be to remove as many barricades that currently restrict recycling of aircraft. For the purpose of facilitating same level recycling, hence without downcycling, it is decided that the aircraft structure is divided into distinct sections such as the wing, fuselage, propulsion system etc., that each use only one material. For the example of a wing box, elaborated in Chapter 8, this strategy is carried out using aluminium 7050 for every part of the wing structure. That way, the company charged with disassembling the aircraft can simply separate the wing from the remaining structure, cut it into smaller parts and then recycle the material while introducing a minimum of impurities. Furthermore, introducing a system in which the various materials, alloys and grades are labelled accordingly, companies can see which material is used in the parts that they are recycling. Thereby, separation is additionally streamlined and recycling is incentivised.

# Design Tools

This chapter explains every step that was taken as part of the systems engineering involved in the design. This involves creating multiple tools in Python which are linked together to make more iterations possible. The purpose of doing more iterations on the subsystems of the aircraft combined is to create a numerical analysis that converges to one final solution, which produces the final general parameters of the aircraft. The tools' functionalities are explained in logical order, together with how they are called when the code is run. In Section 4.1, the initial parameters of the code are presented and then Section 4.2 shows the first part of any iteration, which is the class I estimation. Afterwards, Section 4.3 explains how preliminary sizing of the aircraft is found. Section 4.4 represents the class II weight estimation and also the next step in any iteration. With the geometry of the aircraft fully known, the center of gravity and stability analysis can be done in Section 4.6. Landing gear position is documented and motivated in Section 4.8 and then the iteration and optimisation technique of the Python program is better explained in Section 4.9. Finally, to comply with CS-23 requirements, a flight envelope is generated in Section 4.10.

## 4.1. Initial parameters

This section is dedicated to storing and presenting all the parameters that are required in order for the code to produce full results. The parameters are found using literature, assumptions, calculations and other explanations. They are not explained in this section, but they refer to the parts of the report relevant for them.

**Table 4.1:** Initial parameters used in estimation tools

General specifications			Mass estimation parameters		
Parameter	Value	Unit	Parameter	Value	Unit
Clean stall speed	46.2	$\frac{m}{s}$	$W_{payload}$	800	$kg$
$C_{Lmax_{clean}}$	1.5	-	$c_p$	90e-9	$\frac{J}{kg}$
$C_{Lmax_{take-off}}$	2.0	-	R	1500	$km$
$C_{Lmax_{land}}$	2.1	-	$n_{ee}$	0.9	-
$e_{clean}$	0.78	-	$n_{pmad}$	0.9	-
$e_{take-off}$	0.83	-	$n_{fc}$	0.5	-
$e_{land}$	0.88	-	$n_{comp}$	0.7	-
$C_{D0_{clean}}$	0.02	-	$n_{fuel_{tank}}$	0.63	-
$C_{D0_{take-off}}$	0.038	-	$\rho_{fc}$	3000	$\frac{W}{kg}$
$C_{D0_{land}}$	0.073	-	$\lambda$	0.4	-
$W_{TO}/W_{land} = f$	0.95	-	$\lambda_h$	1	-
$s_{land}$	1500	$m$	$\lambda_v$	0.8	-
$\eta_p$	0.85	-	$\Lambda$	3.5	$^\circ$
$h_{cruise}$	5000	$m$	$\Lambda_h$	20	$^\circ$
AR	10	-	$\Lambda_v$	20	$^\circ$
$V_{cruise}$	475	$\frac{km}{h}$	$\bar{c}$	1.85	$m$
c	12	$\frac{m}{s}$	$l_{cockpit}$	2.52	$m$
$c_V$	0.083	-	$l_{cabin}$	5.1	$m$
			$l_{insulation}$	2.1	$m$
			$h_{fuselage}$	1.73	$m$



## 4.2. Class I Weight Estimation

The Class I weight estimation is the first step in the aircraft sizing and this is done via one of the tools. The code assumes that the maximum take-off weight is the sum of all other important weights in the plane.

$$W_{TO} = W_{OE} + W_{PL} + W_F \quad (4.1)$$

Equation 4.1 shows the relation between the weights, where  $W_{OE}$  is the operational weight,  $W_{PL}$  is the payload weight, which is taken from requirements to be 800 kg, and  $W_F$  is the weight of the fuel. Their definitions are shown in Equation 4.2 and Equation 4.3.

$$W_{OE} = W_E + W_{crew} \quad (4.2)$$

$$W_F = W_{F_{used}} + W_{F_{reserve}} = (1 - M_{ff}) \cdot W_{TO} + f_{reserve} \cdot W_{F_{used}} \quad (4.3)$$

$$W_F = (1 - M_{ff})(1 + f_{reserve}) \cdot W_{TO} \quad (4.4)$$

In this set of equations,  $W_E$  is the aircraft empty weight,  $W_{crew}$  is the weight of the crew,  $M_{ff}$  is the fuel fraction over the entire mission, found from the fuel fraction method, and  $f_{reserve}$  is the percentage of used fuel which is kept as reserve.  $W_E$  is found using empirical data from other aircraft of the same type. The approach used is according to Roskam's Aircraft Preliminary Design [38]. A least-squares regression is used to find a relation between the empty weight and the take-off weight of the aircraft, exemplified in Equation 4.5.

$$W_E = a \cdot W_{TO} + b \quad (4.5)$$

Afterwards, the fuel fraction method is used in order to find  $M_{ff}$ . This method implies dividing the mission into multiple phases, where cruise and loiter are considered to be fuel-intensive phases. The rest of the fuel fractions are found empirically from other aircraft of the same type [38] where a correction is made for the higher energy density of hydrogen. The fuel intensive phases fractions are found using Breguet's range and endurance equations, and the jet engine variants for this equations are found in Equation 4.6 and in Equation 4.7.

$$\frac{W_{endcruise}}{W_{startcruise}} = e^{\frac{R}{\frac{V}{g \cdot c_j} \cdot L/D_{cruise}}} \quad (4.6)$$

$$\frac{W_{endloiter}}{W_{startloiter}} = e^{\frac{E}{\frac{1}{g \cdot c_j} \cdot L/D_{loiter}}} \quad (4.7)$$

Next,  $M_{ff}$  can be found by using Equation 4.8.

$$M_{ff} = \frac{W_1}{W_{TO}} \prod \frac{W_{i+1}}{W_i} \quad (4.8)$$

Finally, adding everything mentioned previously, the first iteration of the take-off weight is found in Equation 4.9. The last step is using this value of the take-off weight to find the operational empty and the fuel weights using Equation 4.2 and Equation 4.3.

$$W_{TO} = \frac{W_{PL} + b + W_{crew}}{1 - a - (1 - M_{ff}) \cdot (1 + f_{reserve})} \quad (4.9)$$

## 4.3. Preliminary Sizing

In order to start performing the class II weight estimations, some geometrical parameters are required. As a result, a preliminary design has been made including all the necessary geometrical parameters.

### 4.3.1. Wing & Power Loading

Before finding the sizes of different subsystems of the aircraft, a design space is required. The design space uses the required wing loading for many different conditions. Thus, the final plot showing the available design space is a diagram showing different curves for these conditions for power loading ( $\frac{W}{P}$ ) against wing loading ( $\frac{W}{S}$ ). Power loading was chosen as a metric due to the fact the design includes propeller engines.

The first constraint is the landing condition. On the plot, this is represented by a simple vertical line as it is only limited by wing loading. The formula used is empirical, and the landing distance is directly taken from the requirements to be 1500 *m*. The formula used is Equation 4.10:

$$\frac{W}{S} = \frac{C_{L_{max,land}} \rho^{\frac{s_{ground}}{0.5915}}}{2 \cdot f} \quad (4.10)$$

where  $C_{L_{max,land}}$  is the maximum  $C_L$  for landing configuration,  $s_{ground}$  is the landing distance and  $f$  is a fraction represented by the ratio between the landing weight and the maximum take-off weight. This was found using the class I weight estimation.

The next constraint is the stall condition in clean configuration. This also represented by a vertical line on the plot and the formula used is Equation 4.11:

$$\frac{W}{S} = \frac{1}{2} \cdot \rho V_{stall}^2 C_{L_{max,clean}} \quad (4.11)$$

where  $C_{L_{max,clean}}$  is the maximum  $C_L$  in clean configuration of the aircraft.

The third constraint is given by the take-off requirement. This takes the shape of a parabolic curve and it involves more parameters than the previous constraints. The Take-Off Parameter (TOP) is chosen to be 570, because this corresponds to the 1500 *m* take-off length. Then,  $\sigma$  is the ratio between the runway's elevation density and ISA sea level density. The runway elevation is chosen at 2500 *m* by inspecting various airports across Europe. The  $C_L$  for the take-off was taken as  $\frac{C_{L_{max,takeoff}}}{1.1^2}$ . With this information,  $\frac{W}{P}$  in terms of  $\frac{W}{S}$  can be found using Equation 4.12.

$$\frac{W}{P} = \frac{\sigma C_{L_{TO}} TOP}{\frac{W}{S}} \quad (4.12)$$

Cruise is the next limiting condition for the design space. The formula is more complicated, but it involves only parameters that were used previously.  $\frac{W}{P}$  in terms of  $\frac{W}{S}$  is found using Equation 4.13. AR stands for aspect ratio,  $e$  stands for Oswald efficiency factor,  $\rho$  is the density at the chosen cruise altitude and  $\eta_p$  is the propeller efficiency.

$$\frac{W}{P} = \frac{0.9}{0.8} \eta_p \left( \frac{\rho}{\rho_0} \right)^{0.75} \cdot \left[ \frac{C_{D_0} \frac{1}{2} \rho V^3}{0.8 \cdot \frac{W}{S}} + \left( 0.8 \cdot \frac{W}{S} \right) \frac{1}{\pi A R e \frac{1}{2} \rho V} \right]^{-1} \quad (4.13)$$

Climb rate is another condition that is looked at during this analysis. The aircraft has to satisfy certain requirements for both the climb rate and the climb gradient. Thus, Equation 4.14 is used in order to build a curve  $\frac{W}{P}$  in terms of  $\frac{W}{S}$ , to further limit the design space:

$$\frac{W}{P} = \frac{\eta_p}{c + \frac{\sqrt{\frac{W}{S}} \cdot \sqrt{\frac{2}{\rho}}}{1.345 \cdot \frac{(ARe)^{0.75}}{C_{D_0}^{0.25}}}} \quad (4.14)$$

where  $c$  is the climb rate in *m/s*. Finally the climb rate condition is found similarly using Equation 4.15 and is also the last curve added to the wing power loading diagram. In this equation,  $\frac{c}{V}$  is named the climb gradient.

$$\frac{W}{P} = \frac{\eta_p}{\sqrt{\frac{W}{S}} \cdot \left( \frac{c}{V} + \frac{1}{L/D} \right) \cdot \sqrt{\frac{2}{\rho_0 C_L}}} \quad (4.15)$$

Putting all of these curves together on a plot, the design space can be found. Based on the design space illustrated in Figure 4.1, a design point is chosen as a focus for all further procedures. The design point is located at a wing loading ( $\frac{W}{S}$ ) of 1961  $\frac{N}{m^2}$ .

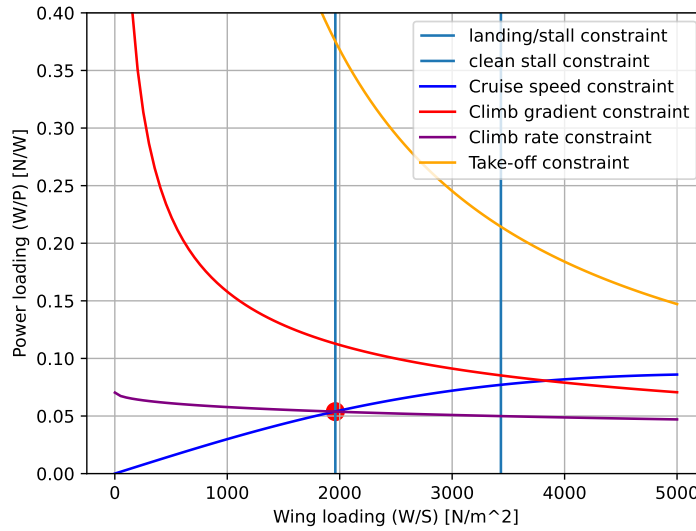


Figure 4.1: Power loading versus wing loading diagram including the design point (red dot)

#### 4.3.2. Wing Sizing

In order to size the wing, a loading analysis has been performed to extract the maximum power loading and wing loading required during the mission of the aircraft. As a result of this analysis, it has been concluded that the aircraft needs to be able to have a  $\frac{W}{S}$  of 1961.02  $\frac{N}{m^2}$ . The wing loading value is then used in order to calculate the surface area of the wing based on the class I estimation. Moreover, the aspect ratio of the wing was estimated to be 10 using statistical data of aircraft that closely represent the aircraft that is being designed.

### 4.4. Class II Weight Estimation

In order to assess the weights of each subsystem, a class II estimation should be performed based on the preliminary design of the aircraft and the class I estimation. Moreover, the Raymer method for general aviation has been used to get weights for each subsystem [15]. However, given that the fuel systems and engines for this design are unconventional, Raymer semi-empirical formulas would not give accurate predictions. Hence, new estimation equations have been developed in order to give a more accurate representation of the mass required by the respective subsystem mass.

#### 4.4.1. Powertrain Mass Estimation

In order to assess the mass of the power train system of the aircraft, it has to be divided into multiple parts. Consequently, the following equation divides the power train into parts which can be calculated separately in order to get a good approximation of the power train subsystem:

$$m_{pt} = (m_{FC} + m_{comp} + m_{coolingsystem} + m_{PMAD} + m_{em}) \cdot 1.2 \quad (4.16)$$

The 20 percent margin accounts for auxiliary components such as the propellers, mounting of the components

and wiring.

The approach for the powertrain mass estimation is to start with the shaft power, as obtained from the powerwing loading design point. Using estimates for component efficiencies, the power of each component is established. Assuming that each system has a constant specific power value indicated by  $\rho_{component}$ , the mass of the component can be estimated based on its power. The masses of the compressor and cooling system include some extra steps that are shown in Equation 4.17 up until Equation 4.23:

$$\dot{m}_{air} = 2.856 \times 10^{-7} \cdot \lambda_{O_2} \cdot \frac{P_{FC}}{\eta_{FC}} \quad (4.17)$$

$$PR_{comp} = \frac{P_{oper}}{P_{alt}} \cdot 1.05 \quad (4.18)$$

$$T_{t2} = T_{t1} \cdot \left( 1 + \frac{1}{\eta_{comp}} \cdot PR_{comp}^{\left( \frac{\gamma-1}{\gamma} \right)} \right) \quad (4.19)$$

$$P_{comp} = \dot{m}_{air} \cdot C_{p,air} \cdot \frac{(T_{t2} - T_{t1})}{\eta_{em}} \quad (4.20)$$

where  $\lambda_{O_2}$  is the excess air supply ratio which is set at 1.75,  $P_{oper}$  is 1 atmosphere,  $P_{alt}$  is the ambient pressure at cruise altitude,  $\gamma$  is 1.4,  $T_{t1}$  is the total pressure at cruise altitude and  $C_{p,air}$  is the specific heat of air. The cooling power is calculated using the following semi-empirical formulas:

$$P_{heat,rejected} = \left( \frac{1}{\eta_{FC}} - 1 \right) \cdot P_{FC} \quad (4.21)$$

$$f(dT) = 0.0038 \cdot \left( \frac{T_{air}}{dT} \right)^2 + 0.0352 \cdot \frac{T_{air}}{dT} + 0.1817 \quad (4.22)$$

$$P_{cooling,system} = (0.371 \cdot P_{heat,rejected} + 1.33) \cdot f(dT) \quad (4.23)$$

where  $dT$  is the difference in input temperatures for a 2-sided heat exchanger set at 25 K,  $T_{air}$  is the ambient air temperature set at 250 K.

The parameters given in Table 4.2 are used for the powertrain sizing and mass estimations.

**Table 4.2:** Parameters related to powertrain sizing and mass estimations

Parameter	Value	Unit
$n_{em}$	0,9	-
$n_{FC}$	0,55	-
$n_{PMAD}$	0,9	-
$n_{comp}$	0,7	-
$\rho_{comp}$	2	$\frac{kW}{kg}$
$\rho_{PMAD}$	10	$\frac{kW}{kg}$
$\rho_{em}$	2.8	$\frac{kW}{kg}$
$\rho_{FC}$	3	$\frac{kW}{kg}$

Here, *em* is short for electric motor, *FC* is short for fuel cell, *PMAD* is short for power management and distribution system and *comp* is short for compressor. The fuel cell specific power and efficiency are estimated based on consulting with an expert from *AeroDelft*. The electric engine specific power is obtained from the *Magni650* electric engine specifications.<sup>1</sup> The remaining parameters are found from Vonhoff's master thesis

<sup>1</sup><https://www.magnix.aero/services> [accessed 01-06-2022]

[32]. Equation 4.24 until Equation 4.26 are also used in the powertrain sizing and mass estimation.

$$P_{electric,net} = \frac{P_{shaft}}{\eta_{PMAD} \cdot \eta_{em}} \quad (4.24)$$

$$P_{FC} = P_{PMAD} = P_{electric,net} + P_{comp} + P_{cooling} \quad (4.25)$$

$$P_{em} = \frac{P_{shaft}}{\eta_{em}} \quad (4.26)$$

#### 4.4.2. Tank Mass Estimation

In order to estimate the mass that the tank will have, a so called tank efficiency is used. The tank efficiency is defined in Equation 4.27.  $\eta_{tank}$  is set to 0.5 as obtained from Vonhoff's thesis [32]. Then for a known fuel mass, the tank mass can be calculated.

$$\eta_{tank} = \frac{m_{fuel}}{m_{fuel} + m_{tank}} \quad (4.27)$$

### 4.5. Aircraft Sizings

This section includes the sizing of the fuselage, of the fuel tank and of the wing area. First the fuel tank length is calculated, then the length of the fuselage and the area of the wing are updated. The fuel tank is assumed to be cylindrical in order to ease the calculations in the iterations. Thereby, the length of the fuselage is calculated using the following formula:

$$l_{fuel} = \frac{V_{fuel}}{0.25\pi D_{fus}^2} \quad (4.28)$$

It is important to note that the required fuel volume used in the previous formula is divided by a factor of 0.85 to take into account the empty volume in the tank and the additional fuel required in future iterations. Moreover, when the fuel tank length is calculated, the fuselage length is updated accordingly. Lastly, the difference in fuselage length causes the class II estimations to be outdated. As a result, class I and class II are ran once again to converge with the updated fuselage length to give a more accurate representation of the weights and surface area of the wing.

### 4.6. Wing and Empennage Sizings

This section covers the sizing and positioning of the wing and empennage subsystems of the aircraft. A center of gravity estimation is described in Subsection 4.6.1. Afterwards, based on the centre of gravity, the empennage and wing positioning are detailed in Section 4.7.

#### 4.6.1. Center of Gravity Extrusion

The first step in the detailed design of the previously mentioned subsystems is locating the center of gravity of the aircraft. This is done using statistical data, assumptions, and an inspection of the aircraft's model. On top of this, an iterative approach is used to find the position of the most forward and aft locations of the center of gravity. This is all put together in a class I loading diagram.

Firstly, to make the procedure possible, the weights of the most important components of the aircraft are required. These are already presented in Section 4.4. Next to the weights, the positions of the centers of gravity of individual components also need to be known and are given in Table 4.3. The aircraft can be divided into a fuselage group and a wing group, hence the difference in reference for some of the components. The fuselage group uses the tip of the aircraft's nose as the datum, and the wing group positions are given in terms of percentage of the Mean Aerodynamic Chord (MAC).

**Table 4.3:** C.G. positions of different aircraft components

Fuselage group					
Component	Fuselage	Crew	Empennage	Fuel Tank	Landing Gear
Center of gravity positions [m]	7.52	1	13.53	13.97	N/A
Wing group					
Component	Engines	Wing	Battery		
Center of gravity position [ % of MAC]	-0.1	0.45	0.45		

In order to find the exact positions, some assumptions are made:

- The fuselage c.g. is placed along the centerline of the fuselage
- The pilots' seats are assumed to be positioned at 40 percent of the cockpit length
- The empennage position is found statistically at 90 percent of the fuselage length.
- The fuel tank c.g. is found by summing the cockpit length, the cabin length, and half of the fuel tank length
- The landing gear is split into main and nose landing gear. It is neglected in the calculation until it is first positioned later on.
- For the wing group, the battery and the wing are assumed to have the same position with regards to MAC (Because the battery will be placed right at the half span the wing, on top of the fuselage)
- The engines are chosen statistically slightly in front of the leading edge.

Now that all the required data is found, the fuselage group and wing group centers of gravity are found using Equation 4.29. The fuselage group is named  $fcg$ , the wing group is named  $wcg$  and  $\bar{c}$  stand for MAC.

$$X_{fcg} = \frac{\sum X_i W_i}{\sum W_i} \quad (4.29)$$

$$X_{wcg} = \bar{c} \cdot \frac{\sum x_j W_j}{\sum W_j} + X_{LEMAC} \quad (4.30)$$

The code works by choosing a location of the leading edge mean aerodynamic chord position, or LEMAC, and then reiterates until it finds the optimum LEMAC positioning as explained in Section 4.9. The initial value for  $X_{LEMAC}$  is 26 [ft] or 7.92 *m*. Using this value for LEMAC, the operational empty weight in terms of MAC is calculated using Equation 4.31:

$$\left(\frac{x}{\bar{c}}\right)_{OEWCg} = \frac{\frac{W_{fcg} X_{fcg} + W_{wcg} X_{wcg}}{W_{fcg} + W_{wcg}} - X_{LEMAC}}{\bar{c}} \quad (4.31)$$

The actual location of the Operation Empty Weight is then found using this fraction. With the operational empty weight c.g. position now known, the class I loading diagram becomes feasible. For this to be possible, the fuel and payload locations on the aircraft are required. These are easy to find, the fuel has the same c.g. location as the fuel tank, and the payload is split into two parts. First, the 600 *kg* of the payload are assumed to be made up by the passengers, with the position in the middle of the cabin, and 200 *kg* of the payload are placed in the aft cargo compartment, which is assumed to be at  $0.9 \cdot \text{fuselage length}$ . Using this split, the moment contribution

of each part of the payload are added up together using a formula similar to the one in Equation 4.29.

The diagram is created by imagining four possible loading sequences/ states of the aircraft: aircraft at OEW, aircraft at OEW with full payload, aircraft at OEW with full fuel tank and aircraft at Maximum Take-Off Weight. This way, the most forward and aft c.g. positions are found, and used in later stability calculations. The results of the first iteration of the center of gravity program are shown in Figure 4.2. The way to compare the positions is by using the MAC as a datum. As expected, the position of the center of gravity is quite aft on the fuselage length, due to the fuel tank, fuel mass and the payload at the rear end of the aircraft. The diamond shape of the diagram is a direct result of this fact. The wing is rather heavy, which is why the center of gravity is pulled towards the tip of the aircraft.

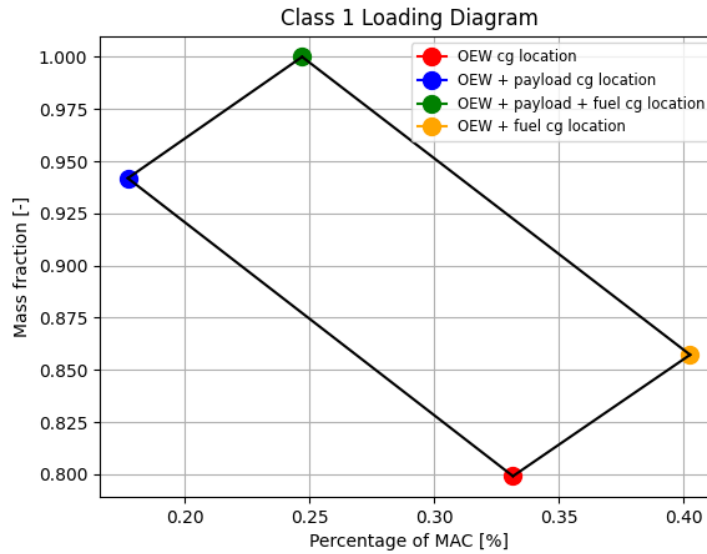


Figure 4.2: Positions of important center of gravity locations

## 4.7. Stability and Control

After performing the Center of Gravity Extrusion, it is not possible to perform the empennage sizings using the CG variation of the aircraft. The methodology involves calculating the aerodynamic characteristics of the wing and using the center of gravity locations to impose stability and controllability constraints on the design. Subsequently, the ratio of horizontal stabilizer surface area to wing surface area is computed.

### 4.7.1. Methodology

In order to analyse the stability and controllability of the aircraft, it is important to first calculate the necessary parameters that are used in the stability and controllability equations. The aerodynamic center is calculated using the contribution of the wing, fuselage and flaps on the aerodynamic center which can be represented in the following equation:

$$\begin{aligned} \left( \frac{x_{ac}}{\bar{c}} \right)_{wf} &= \left( \frac{x_{ac}}{\bar{c}} \right)_w \\ &- \frac{1.8}{C_{L_{\alpha_{A-h}}}} \frac{b_f h_f l_{fn}}{S \bar{c}} \\ &+ \frac{0.273}{1 + \lambda} \frac{b_f c_g (b - b_f)}{\bar{c}^2 (b + 2.15 b_f)} \tan \Lambda_{1/4} \end{aligned} \quad (4.32)$$

Moreover, another important parameter is the lift slope of the tailless aircraft which can be calculated using

Equation 4.47 and the following equation:

$$C_{L_{\alpha_{A-h}}} = C_{L_{\alpha_w}} \left( 1 + 2.15 \frac{b_f}{b} \right) \frac{S_{net}}{S} + \frac{\pi}{2} \frac{b_f^2}{S} \quad (4.33)$$

Lastly, the moment coefficient at the aerodynamic center is calculated using the contributions of the wing, fuselage and flaps on the moment coefficient using the following formulas:

$$C_{m_{ac}} = (C_{m_{ac}})_{wing} + \Delta_f C_{m_{ac}}^{flaps} + \Delta_{fus} C_{m_{ac}} + \Delta_{nac}^{fuselage} \quad (4.34)$$

$$C_{m_{ac_w}} \approx C_{m0airfoil} (A \cos^2 \Lambda (A + 2 \cos \Lambda)) \quad (4.35)$$

$$\Delta_{fus} C_{m_{ac}} = -1.8 \left( 1 - \frac{2.5 b_f}{I_f} \right) \frac{\pi b_f h_f l_f}{4 S \bar{c}} \frac{C_{L_0}}{C_{L_{\alpha_{A-h}}}} \quad (4.36)$$

$$\Delta C_{m_{1/4}} = \mu_2 \left\{ -\mu_1 \Delta C_{l_{max}} \frac{c'}{c} - \left[ C_L + \Delta C_{l_{max}} \left( 1 - \frac{S w f}{S} \right) \right] \frac{1}{8} \frac{c'}{c} \left( \frac{c'}{c} - 1 \right) \right\} + 0.7 \frac{A}{1 + 2/A} \mu_3 \Delta C_{l_{max}} \tan \Lambda_{1/4} \quad (4.37)$$

$$C_{m_{1/4}} = C_{m_{ac}} + C_L \left( 0.25 - \frac{x_{ac}}{\bar{c}} \right) \quad (4.38)$$

After calculating the required parameters, it is now possible to compute the stability and control constraints for a certain ratio of horizontal tail surface area to wing surface area using Equation 4.39 for stability and Equation 4.40 for control.

$$\bar{x}_{cg} = \bar{x}_{ac} + \frac{C_{L\alpha_h}}{C_{L\alpha_{A-h}}} \left( 1 - \frac{d\varepsilon}{d\alpha} \right) \frac{S_h l_h}{S \bar{c}} \left( \frac{V_h}{V} \right)^2 \quad (4.39)$$

$$C_{m_{ac}} + C_{L_{A-h}} \left( \frac{x_{cg} - x_{ac}}{\bar{c}} \right) = \frac{C_{L_h} S_h l_h}{S \bar{c}} \left( \frac{V_h}{V} \right)^2 \quad (4.40)$$

Using those two equations, two lines can be plotted together in terms of the position of the center of gravity referenced to the MAC. This creates the so-called *scissor plot*, shown in Figure 4.3. The scissor plot is important because it describes the stability and the controllability of the aircraft. If the center of gravity of the aircraft which was computed previously fits within the two lines, it means the aircraft is both stable and controllable. This plot is also used to find the lowest possible center of gravity range which still matches the center of gravity shift of the aircraft during different loading plans. From this plot, the  $\frac{S_h}{S}$  ratio is taken and the horizontal tail can be sized accordingly.



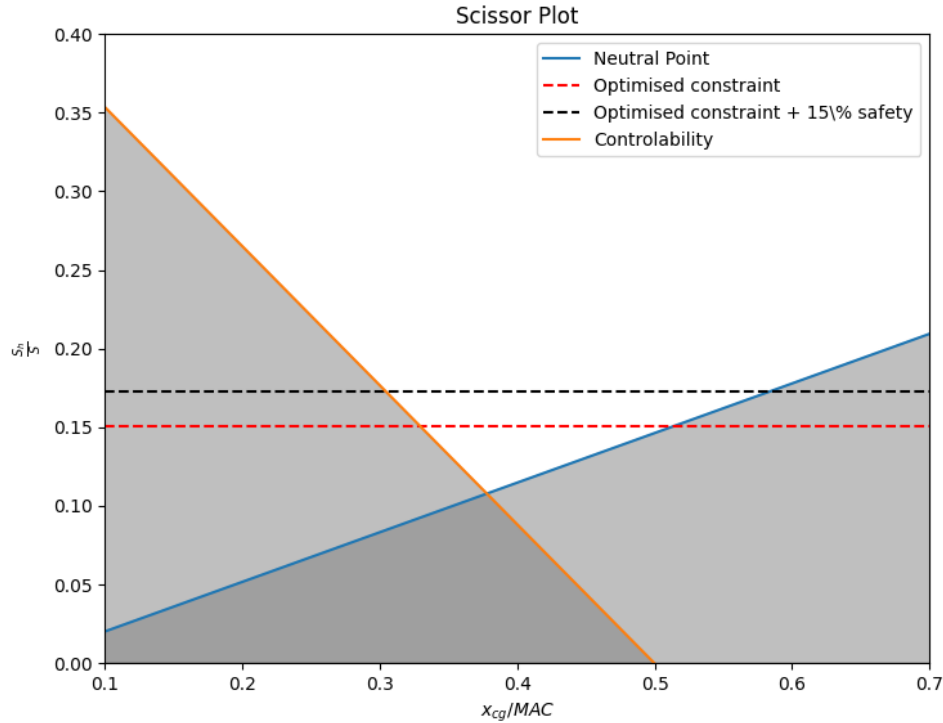


Figure 4.3: Scissor plot showing the computed  $S_h/S$  ratio

## 4.8. Landing Gear Positioning

The landing gear position is computed by first finding out how much load each gear should withstand. Based on literature and reference aircraft, it is decided that the nose gear and main gear will carry 9% and 91% of the MTOW, respectively, to be above the minimum recommended 8% for adequate steering capability [41] and also within a feasible range for the longitudinal position of the nose gear. This is implemented as shown in Equation 4.41.

$$P_{mlg} = 0.91 \cdot MTOW \quad P_{nlg} = 0.09 \cdot MTOW \quad (4.41)$$

Afterwards, some angle constraints are imposed on the location of the main landing gear, which are the tip-back angle and the scrape angle. The tip-back angle is limited to be greater than or equal to  $15^\circ$  from the most aft c.g. position, and the scrape angle is chosen to be  $13^\circ$ , since it must be smaller than the tip-back angle. The latter is implemented as a limit from the tangency point on the tail cone. Detailed information on these angle constraints, further lateral and vertical landing gear positioning, as well as related figures can be found in Chapter 5 Subsection 5.3.2.

## 4.9. Iteration Technique

In order to make sure that the main features of the design converge, every estimation technique used must be congruent with the other estimations that are used. In this case, the estimations used were class I, class II, fuel sizing estimations and stability and control analysis. This analysis is performed using Python scripts which can be portrayed using Figure 4.4 and Figure 4.5.

<b>Class I</b>	OEW	OEW	Fuel Weight	Fuel Weight		
	<b>Preliminary Sizing</b>	Aircraft Dimensions	Aircraft Dimensions			
MTOW		<b>Class II</b>		Subsystem Weights		
		Aircraft Dimensions	<b>Aircraft sizing</b>	Subsystem Positions		
				<b>CG calculation</b>	Subsystem CG	
		Aircraft Dimensions		Lemac Positioning	<b>Stability Analysis</b>	Updated CG
						<b>Landing Gear sizing</b>

Figure 4.4: N2 Chart of Python script

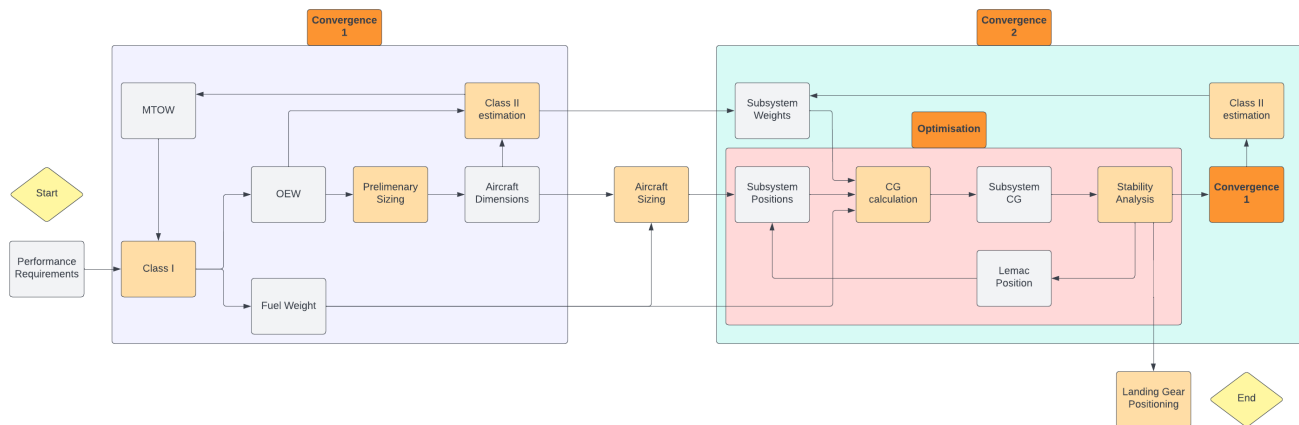


Figure 4.5: Flow Diagram of Python script

In the first iteration loop (convergence 1 in Figure 4.5), the class I and class II weight estimations are iterated until the OEW does not change more than one percent between consecutive iterations. Every iteration of the wing and powertrain sizing is done again. The fuselage is sized after the class I - class II iterations converge, as when it is included in the loop, convergence cannot be reached. After the fuselage is sized, it is verified that it is consistent with the converged design from the class I - class II iterations.

The optimisation block in the second convergence loop includes the procedures taken in Section 4.7. However, every time the procedure takes place, the position of the wing leading edge changes, causing a change in the CG range produced in Subsection 4.6.1. This leads to the position of the constraint in the scissor plot to change depending on whether the aircraft is constrained predominantly by the stability or control. The purpose of the optimisation block is to keep on changing the positioning of the wing with respect to the fuselage such that the aircraft is constrained by both the control and the stability lines. As such, the horizontal stabilizer can have the smallest possible surface area. After the position of the wing leading edge is determined a horizontal stabilizer surface area is set which causes the weight estimations to change, this is the reason why convergence 1 is repeated once again in the script to produce the updated subsystem weights. The aforementioned procedure is repeated such that when the horizontal stabilizer surface area is produced, it has no effect on the weight estimations and cg locations. This way, the aircraft is optimised to have the ideal wing position and horizontal stabilizer surface area with a converged aircraft mass.

## 4.10. Flight Envelope

In order to check if the design complies with the CS-23 requirements, and if it would in fact be allowable to fly this aircraft, a flight envelope is also generated. The flight envelope is constructed using 2 plots that are placed together in the end. The most important value that is found from the diagram is the ultimate loading factor,

which is a value that is used throughout other estimations described previously, for example the class II weight estimation, Section 4.4. The maneuver diagram is presented in Subsection 4.10.1 and the gust loading diagram in Subsection 4.10.3.

#### 4.10.1. Maneuver Diagram

The first part of the flight envelope is the maneuver diagram. The flight envelope is also named the Velocity-Loading factor diagram because it involves the airspeed at certain phases of flight and the loading factor felt by the aircraft at these speeds. The maneuver diagram consists of more elements. The stall curve, where the stall speed of the aircraft can be found by drawing a horizontal line from the loading factor of 1. The curve equation is presented in Equation 4.42.

$$n = \frac{\frac{1}{2}\rho V^2 C_{L_{max}}}{\frac{W}{S}} \quad (4.42)$$

The stall curve goes up parabolically until it reaches the design loading factor, whose value is calculated using Equation 4.43, according to CS-23. The speed respective to this point of the plot is also known as  $V_A$ .

$$n_{des} = 2.1 + \frac{24000}{MTOW + 10000} = 3.17 \quad (4.43)$$

In the above equation, the maximum take-off weight is expressed in pounds. The design load factor is found to be 3.07, illustrated in Figure 4.6. The design factor line becomes horizontal up until the design dive speed, which is the maximum speed achievable by the design. This is found using  $1.25 \cdot V_C$ , where  $V_C$  is the design cruise speed, which was decided to be  $475 \text{ km/h}$  in previous estimations. On the negative part of the maneuver diagram, the curve uses the same equation, the only difference being it uses a negative slope. The curve ends at the design negative loading factor, calculated using another CS-23 relation, given in Equation 4.44.

$$n_{neg} = -0.4 \cdot n_{des} = -1.27 \quad (4.44)$$

Afterwards, the negative loading line goes horizontally up until the cruise speed, or  $V_C$ , specified before. Finally, the line goes back to 0 loading, linearly, at the design dive speed  $V_D$ . On Figure 4.6, the maneuver diagram is drawn in black.

#### 4.10.2. Gust Loading Diagram

The second step in generating the flight envelope is creating the gust loading diagram, which involves finding the three most important loading factors which are caused by gusts during flight. The load factors are computed at three important velocities that occur during flight, which are the design cruise speed, the dive speed and the maximum gust loading for minimum airspeed.

For each of those airspeeds, a similar approach is adopted, according to CS-23. First, a coefficient named the alleviation factor had to be computed, described in Equation 4.45. This is a special relation for subsonic flights, which fits the group's design specifications.

$$K = \frac{0.88 \cdot \mu}{5.3 + \mu} \quad (4.45)$$

In Equation 4.45  $\mu$  is a value found from empirical relations, shown in Equation 4.46. This value is computed using imperial units in order to yield a correct result.

$$\mu = \frac{2 \cdot \frac{W}{S}}{\rho g \bar{c} C_{L_\alpha}} \quad (4.46)$$

In Equation 4.46  $C_{L_\alpha}$  is the slope of the  $C_L$  curve with respect to the angle of attack. This is estimated using the DATCOM method from Equation 4.47:

$$C_{L_\alpha} = \frac{2\pi AR}{2 + \sqrt{4 + \left(\frac{AR\beta}{0.95}\right)^2 \cdot \left(1 + \frac{1}{\beta^2}\right)}} \quad (4.47)$$

where  $\beta$  is the Prandtl-Glauert correction factor, and AR is the aspect ratio of the wing of the aircraft. The aspect ratio was chosen to be a factor of 1.2 higher than the one that was found previously in order to account for winglets placed on the wing. Now that the alleviation factor can be computed, the gust contribution to load factor is determined using Equation 4.48:

$$U = K \hat{u} \quad (4.48)$$

with  $\hat{u}$  being the empirical gust data taken directly from CS-23, the respective values for this are illustrated in  $ft/s$  in Table 4.4.

**Table 4.4:** Different gust speeds for important flight phases

Flight speed	Minimum speed	Cruise speed	Dive speed
Gust speed [ft/s]	66	50	25

From here onward, the contribution to the load factor by the gusts is found using Equation 4.49. For positive loading factors, the difference is added with 1, and for negative loading factors, the difference is subtracted from 1. This way, the y-components of the gust diagram are found.

$$\Delta n = \frac{\rho V C_{L_\alpha} U}{2 \cdot \frac{W}{S}} \quad (4.49)$$

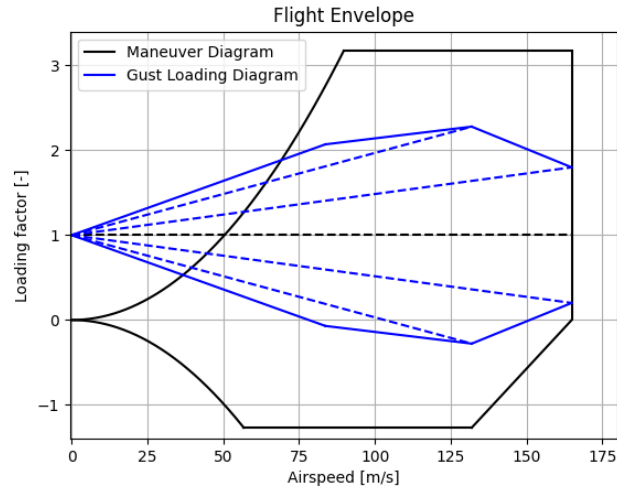
The last component of the gust diagram is assuming the minimum speed for maximum gust loading, or  $V_B$  for short. This one is computed using CS-23 regulations and it has to be higher than  $V_A$  previously computed in Subsection 4.10.1, or higher than  $V_{stall}\sqrt{n_g}$ , whichever of these is lower. The code uses a factor of 1.1 for any of these values it finds to be lower, as a safety margin. In this case  $n_g$  is the load factor found caused by gusts during cruise.

Now all components of the diagram are found, and it becomes simply a matter of plotting. The contour of the diagram is drawn out to make up the shape of a diamond. The important airspeeds are connected using dashed lines starting from a loading factor of 1. The gust loading diagram in Figure 4.6 is drawn in blue for visualisation purposes.

### 4.10.3. Diagram and Conclusions

The third and final step towards building the flight envelope is stacking the maneuver and gust diagrams on top of each other. This is done in order to figure out which one of the two is more critical to the loading factor of the design. The diagram and all the relevant speeds, as well as the stall speed are shown in Figure 4.6. In order to refresh what has been said in previous sections, the maneuver diagram is drawn in black and the gust loading diagram was drawn in blue.

From the envelope, it becomes obvious that the most critical case for this design stems from maneuvering. The loading during reaches a factor of 3, whereas the loading due to gusts only goes as high as 2.4. This was to be expected however, because most of the gusts formulae use wing loading and density as parameters. Because the design is quite sturdy in terms of wing surface and the fact that the aircraft will not fly very high, the gusts turn out to not have such a large impact during any phase, making the design quite stable. The last value to take from this plot is the ultimate load factor, which is a design variable required during other estimations. This is found according to CS-23 in Equation 4.50.



**Figure 4.6:** CS-23 regulated flight envelope of the design

$$N_{ult} = n_{des} \cdot 1.5 = 4.76 \quad (4.50)$$

## 4.11. Results

In this section, the results of the analysis is presented using the procedure outlined in Section 4.9. Table 4.5 shows all the parameters that are computed as a result of the iterations and optimisation that takes place:

**Table 4.5:** Output of the converged analysis

Weights		
$W_{wing}$	435	kg
$W_{fus}$	618	kg
$W_{Vertical}$	54	kg
$W_{Horizontal}$	52	kg
$W_{Avionics}$	505	kg
$W_{Furnishing}$	219	kg
$W_{Icing}$	2.6	kg
$W_{Electrical}$	223	kg
$W_{FuelSystem}$	97	kg
$W_{FlightControls}$	110	kg
$W_{InstalledEngine}$	1932	kg
$W_{Hydraulics}$	4.3	kg
$W_{FuelTank}$	193	kg
$W_{Fuel}$	328	kg
$W_{Battery}$	50	kg
CG Group Positions		
$x_{Fus}$	8.1	m
$x_{Wing}$	6.7	m
$x_{mlg}$	0.18	m
$x_{nlg}$	0.15	m
$\frac{x_{OEW}}{mac}$	0.10	m
Aircraft Dimensions		
$l_{Fus}$	14.5	m
$l_{FuelTank}$	3.0	m
$l_{emac}$	6.4	m
Weight Groups		
$W_{\{OEW\}}$	4495	kg
$W_{\{MTOW\}}$	5623	kg
Power Requirement		
$P_{\{shaft\}}$	1022	kW
$P_{\{Cooling\}}$	630	kW
$P_{\{FC\}}$	2033	kW
$P_{\{Waste\}}$	2033	kW
$P_{\{Compressor\}}$	209	kW
$P_{\{ElectricNet\}}$	1135	kW
Power Mass distribution		
$W_{FuelCell}$	678	kg
$W_{Cooling}$	219	kg
$W_{Compressor}$	104	kg
$W_{PMAD}$	203	kg
$W_{ElectricEngine}$	405	kg

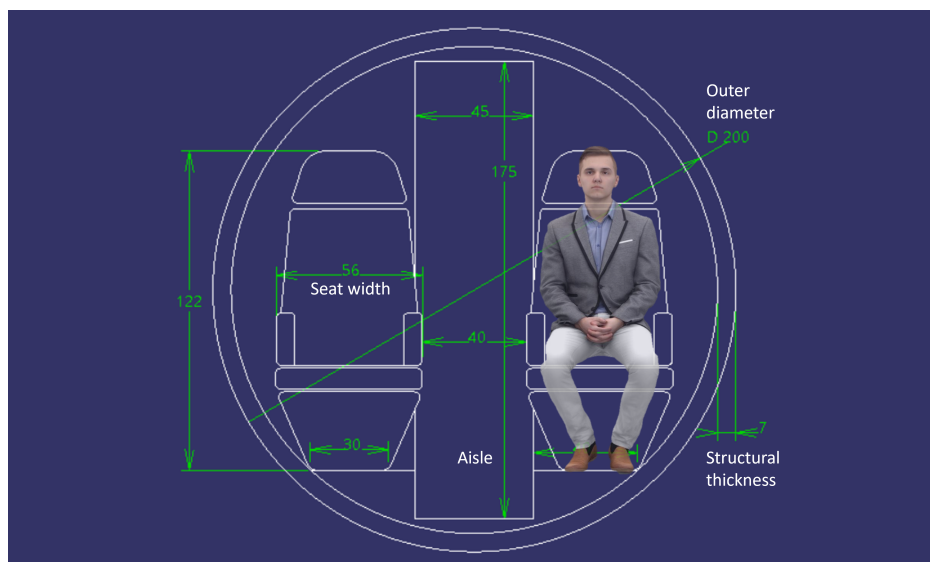
# Fuselage and Landing Gear Design

This chapter contains the cabin design, sizing of the fuselage and the landing gear design. Section 5.1 shows the cross-section design and top view layout of the passenger cabin, including exits and windows. Section 5.2 shows the design of the fuselage shape and layout, with the positioning of the fuel tank and the design of the cargo compartment. Finally, Section 5.3 details the sizing, positioning, and storage of the landing gear.

## 5.1. Cabin Cross-section and Layout

In order to size the cross section on the fuselage, the layout of the passenger cabin needs to be considered, which is also an important input for the sizing of the LH<sub>2</sub> tank in the fuselage. The starting point is the aisle height and width. CS23 regulations require that for less than 10 passenger seats, the aisle width must be a minimum of 38 cm [44]. An aisle width of 45 centimeters was chosen for sufficient comfort and ease of access to seats. Based on similarly sized competitors, and keeping in mind that passengers will not want to duck too low when walking through the cabin, an aisle height of 175 cm is deemed appropriate. This is achievable by a lowered aisle floor since none of the cargo storage, fuel storage, wingbox structure, or landing gear bays are positioned directly under the cabin floor. Next, the seats are sized to accommodate passengers within a 56x122 cm space as recommended in the ADSEE course [40] when seated. The fuselage wall accounts for 40 mm of structural depth and 30 mm of insulation and lining [40], giving a wall thickness of 7 cm and an outer fuselage diameter of 200 cm. This thickness is from the skin to the inner lining panel, meaning it includes wiring and piping. When the seats are positioned with seated passenger comfort in mind, the distance between the edges of two seats decreases the effective aisle width to 40 cm locally, but this is still well within CS23 limitations. It is assumed that the wingbox structure of the high wing will not go through the passenger cabin but be positioned right above it, as is often the case in similar aircraft.

Figure 5.1 shows the cross section view of the passenger cabin, including seat dimensions, aisle width, aisle height, fuselage inner and outer diameters, sketched in CATIA and shown in centimeters. A seated human model<sup>1</sup> is included for visual reference. The resulting inner diameter of the fuselage is 186 cm, which will be a constraint in the design of other subsystems in the aircraft.



**Figure 5.1:** Cabin cross section dimensions in [cm] with human model for scale

<sup>1</sup><https://free3d.com/3d-model/justin-business-sitting-1-3d-human-model-8019.html> [accessed 01-06-2022]

Next, the layout of the cabin as viewed from above is designed. Since the lateral position of the seats is already determined, the leg room and seat pitch need to be computed. The choice was made not to restrict passenger comfort to something comparable to economy class on an airliner, so the seat pitch and leg room were decided to be closer to those of a modest business class configuration, without going overboard with fully reclining seats or other luxuries of widebody business class layouts of course. The final seating configuration consists of six seats with 60 *cm* legroom and 115 *cm* seat pitch, which lies between premium economy class and business class for most airlines. Figure 5.2 shows the top view layout of the passenger cabin with the aforementioned dimensions given in centimeters.

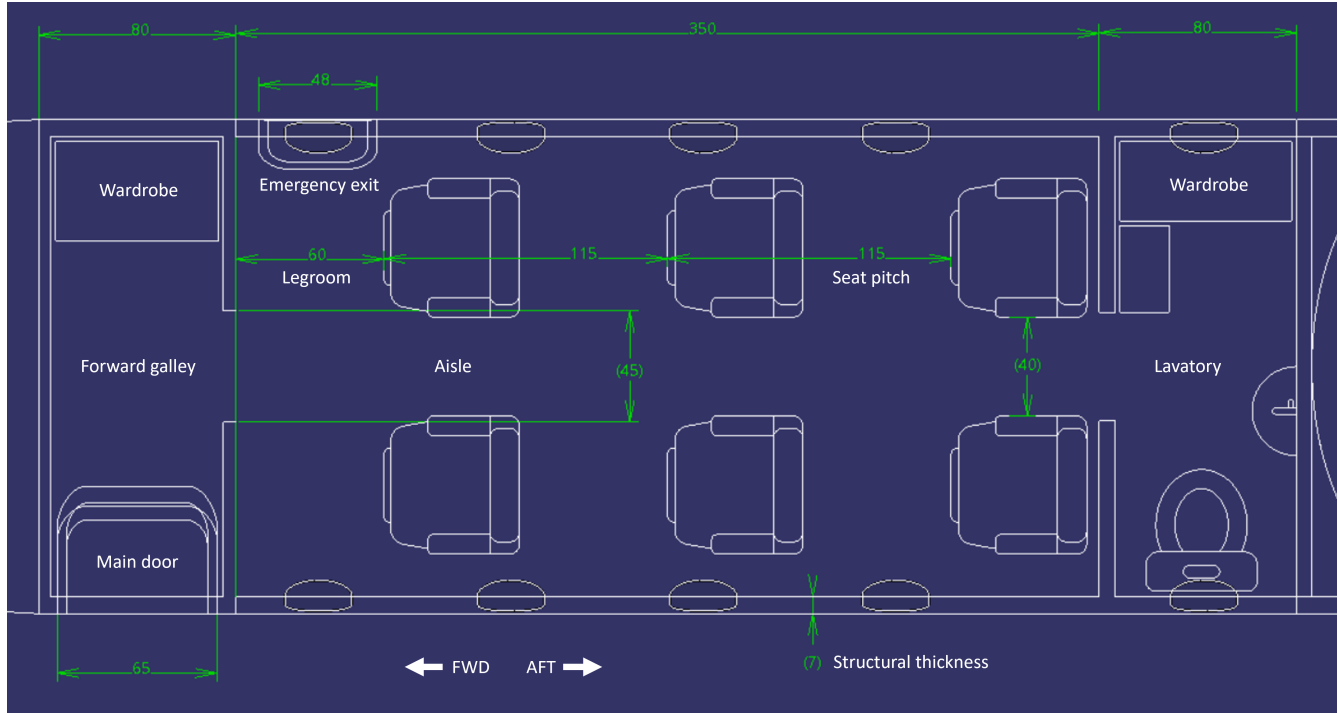


Figure 5.2: Cabin top view dimensions in [cm]

Figure 5.2 also includes several other elements, such as the main door, emergency exit, forward galley, lavatory, and windows. The forward galley is 80 *cm* long and is sized around the main door, which has a width and height of 65x170 *cm* and is not only compliant with CS23 regulations [44] but also taller for ease of boarding since the CS23 minimum is rather low compared to similarly sized aircraft such as the Phenom 300. There is also an emergency exit, sized and positioned on the opposite side of the fuselage as dictated by CS23. This was originally positioned more aft, but was moved forward later in the design when it became apparent that the position of the wing mounted propellers would be hazardous for exiting passengers in an emergency, which would violate CS23 regulations on emergency exits [44]. The aircraft also features a lavatory 80 *cm* long as shown in the figure, as well as wardrobes placed both in the forward galley and in the lavatory for storage of personal items and emergency equipment since there is not enough space in the cabin for overhead bins without seriously compromising on headroom. Finally, the figure shows the number and position of the cabin windows, which is based mainly on reference aircraft in the small business jet category, and depends also on the main door and emergency exit positions as well as the seating layout.

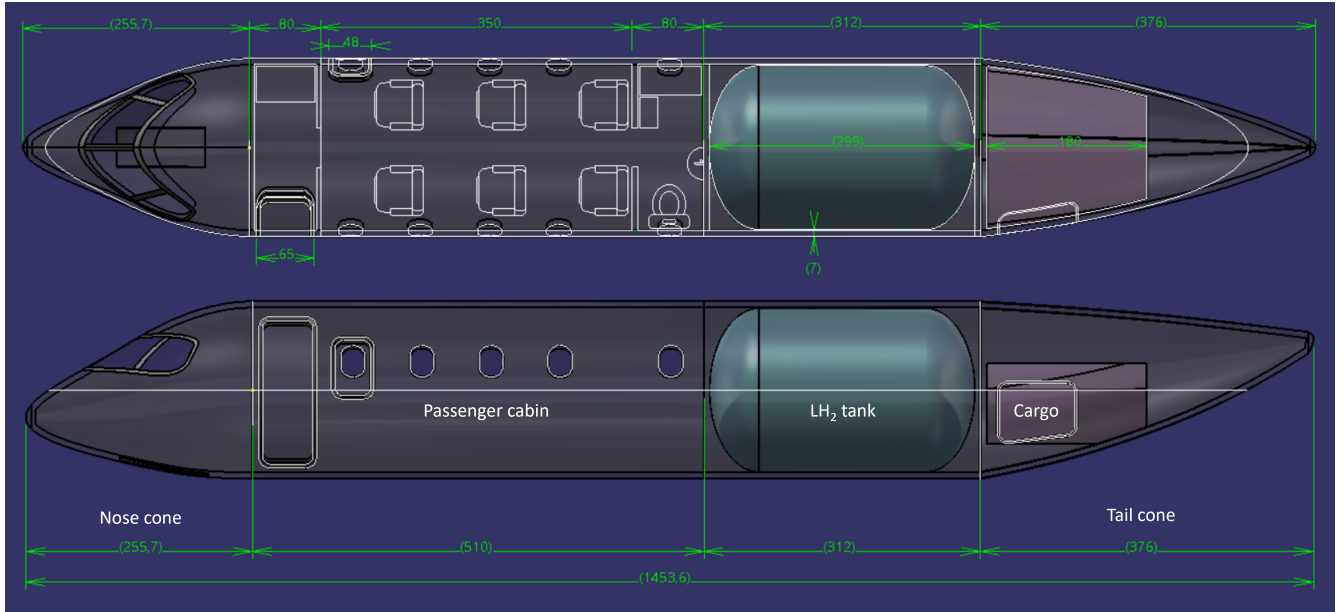
## 5.2. Fuselage, Fuel Tank Placement and Cargo Compartment

Once the cabin layout and fuselage diameter is determined, the rest of the fuselage design, fuel tank positioning and cargo compartment sizing can be done, thereby completing the fuselage design and internal layout.



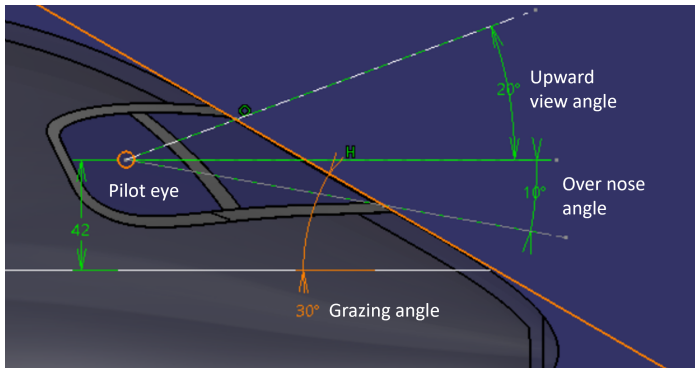
### 5.2.1. Fuselage Layout and Dimensions

The cylindrical section of the fuselage houses the passenger cabin shown in Figure 5.2 as well as the large liquid hydrogen tank in the aft section positioned in between the lavatory and the cargo compartment. This can be seen in Figure 5.3, which shows a top view and side view of the fuselage shape and internal layout. The thermal, structural and shape design of this tank is detailed in Chapter 6. The tank length used is the value of 299 cm from Section 4.11 after the iterations described in Section 4.9, and the section of the fuselage housing the tank is slightly longer to accommodate some structure separating the tank from the passenger cabin and the tail cone. The cargo compartment shown in the figure is described in Subsection 5.2.2.

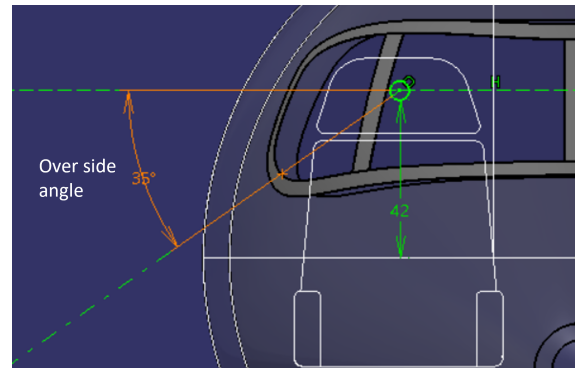


**Figure 5.3:** Top view and side view of the fuselage, dimensions in [cm], single decimal precision

The nose cone and cockpit windows are shaped based on the over nose angle, upward view angle and over side angle from statistical values [40], the minimum 30° grazing angle recommended for an undistorted view [40], and the pilot's line of sight based on Figure 5.1, which are shown in Figure 5.4 and Figure 5.5.



**Figure 5.4:** Pilot visibility, side view



**Figure 5.5:** Pilot visibility, front view

An additional consideration for the nose cone is its length to fuselage diameter ratio (fineness ratio), which is typically in the range of 1.2-2.5 for transport aircraft [40], with slower aircraft at the lower end. The nose cone shown in Figure 5.3 was checked to have a fineness ratio of approximately 1.3, which is appropriate since the cruise speed of  $475 \frac{km}{h}$  puts the sustainable air taxi at the lower end of this range.



For the tail cone, the upsweep angle is an important parameter serving to provide ground clearance during rotation of the aircraft. However, high upsweep angles cause more drag in flight, so the average curvature of the tail cone was limited to  $19^\circ$ , which is the high end of the typical range for regional transports [40].

### 5.2.2. Cargo Compartment

With 6 passengers and the 800 kg total payload requirement, there needs to be a large cargo compartment on the aircraft that can accommodate passenger baggage. For passengers travelling for a long duration business trip or holiday, or travelling with large items such as skis or golf sets, baggage allowance is important. Based on the 200 kg baggage estimation used in Subsection 4.6.1 and an average luggage density of  $170 \frac{\text{kg}}{\text{m}^3}$  [40], the minimum required volume would be  $1.17 \text{ m}^3$ . However, this is very small compared to reference aircraft such as the Embraer Phenom 300, which can accommodate up to  $2.15 \text{ m}^3$  ( $76 \text{ ft}^3$ ) of baggage<sup>2</sup> for its 6-7 passenger capacity. Considering competitor aircraft and passenger needs for spacious storage, the cargo compartment on the sustainable air taxi is sized according to a volume of  $2.1 \text{ m}^3$  and positioned at the aft of the fuselage inside the tail cone. Figure 5.6 shows the cargo compartment with height and width given in centimeters, and enclosed volume measured using CATIA. The cargo door on the left side of the fuselage is also shown highlighted in red.

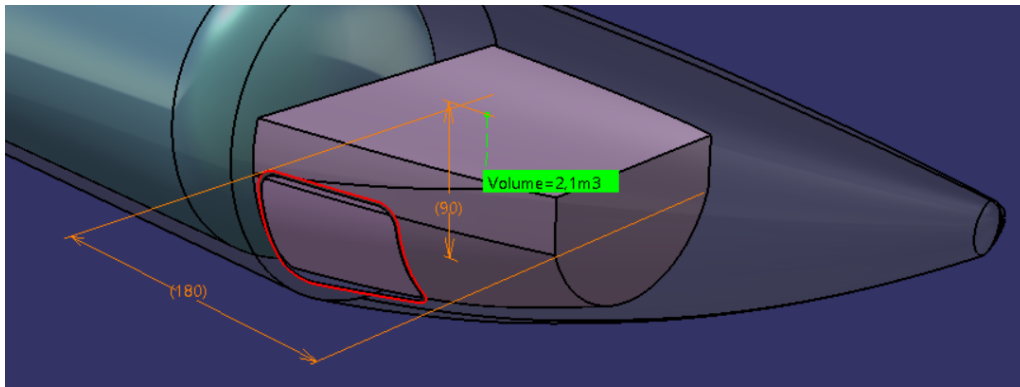


Figure 5.6: Aft cargo compartment of the sustainable air taxi, dimensions in [cm]

### 5.2.3. Structural Considerations

The structural design of the fuselage is not addressed in this report. However, some preliminary calculations can be done for the pressurization loads as considerations for further design and to check feasibility. A cabin pressure altitude of 6600 ft (2011.7 m) is chosen for passenger comfort comparable to the Phenom 300<sup>3</sup> and P180 Avanti<sup>4</sup>, giving a pressure differential between the cabin altitude and the 5000 m cruise altitude for the Sustainable Air Taxi of 25356 Pa. Using  $\sigma_{circ} = \frac{pR}{t}$  [67] with radius  $R = 2 \text{ m}$  and a typical skin thickness range of  $t = 0.002 - 0.004 \text{ mm}$  [40] gives a circumferential stress range of 25.36-50.72 MPa when multiplied by a safety factor of 2 [67]. This is rather low since the cruise altitude of 5000 m is around 2.5 times lower than typical altitudes because of the oxygen requirements of the fuel cells as explained in Chapter 7, so the pressurisation loads will not be limiting for the fuselage structure. With this in mind, aluminium alloys with good fatigue life can be preferred for the fuselage skin, rather than focusing on ultimate strength. Aluminium 2024-T3/T351/T4 are good alloy and temper combinations for this, with a fatigue endurance limit of 140 MPa (based on  $5 \cdot 10^8$  cycles) [68]. One thing to be wary of, however, are stress concentrations at the connections of the forward and aft pressure bulkheads as well as around holes and cut-outs on the fuselage such as doors, windows and hatches which must be locally reinforced. These will need to be taken into account in later design of the fuselage structure.

<sup>2</sup><https://www.flexjet.com/wp-content/uploads/2015/02/14155-phenom-300-aircraft-book.pdf> [accessed 05-06-2022]

<sup>3</sup><https://jetsplus.com/phenom-300/> [accessed 13-06-2022]

<sup>4</sup>[https://www.smartcockpit.com/docs/P180\\_Avanti-Specification\\_and\\_Description.pdf](https://www.smartcockpit.com/docs/P180_Avanti-Specification_and_Description.pdf) [accessed 13-06-2022]

## 5.3. Landing Gear Design and Storage

Landing gear design plays a large role in the configuration of the sustainable air taxi for several reasons: the limited fuselage diameter, the high wing configuration, and the large liquid hydrogen tank in the fuselage. The choice was made in the midterm report to store the main landing gear in external fuselage pods such that it would not interrupt the fuselage structure or the tank when stowed.

### 5.3.1. Tyre Sizing

The tyre selection depends on the load per tyre and the maximum allowable pressure, which depends on the runways the aircraft will operate on. The sustainable air taxi is designed to operate on large, well-maintained concrete runways. However, to stay on the safe side and offer more flexibility to operators when choosing destination airfields, the small tarmac runways with good foundation are also considered. Using the values for recommended maximum tire pressures by Roskam [37], a minimum tyre pressure of  $6.3 \frac{kg}{cm^2}$  is chosen for the tyres to withstand, which corresponds to the high end of small tarmac runways with good foundation. This value is the same for the main and nose landing gear tyres.

Next, the load carried per tire is determined based on the aircraft maximum takeoff weight and the number of wheels. For CS23 aircraft, it is recommended that one wheel per main landing gear strut is chosen [41]. This is also useful for fitting the gear into the fuselage pods compactly because the width of a single large diameter wheel is less than that of two wheels of smaller diameter. For the nose landing gear, the solution for compact storage is the opposite; this time the vertical space under the cockpit is limited rather than the width, so two smaller nose wheels are more advantageous. In addition, two nose wheels are safer in case of a tyre blowout because the aircraft will remain steerable, which is another reason similar aircraft use this configuration often. The nose gear is designed to carry 9% of the aircraft weight, above the minimum recommended 8% for adequate steering capacity [41], and the main gear carries 91%. These values were chosen because they resulted in a longitudinal position of the nose gear that gave a feasible strut height and retracted position. This results in a load per wheel of 253.0 kg for the main wheels and 2558.4 kg for each of the nose wheels using the converged MTOW of 5622.9 kg from Section 4.11. The static load and tire pressure are used in the chart shown in Figure 5.7 which is sourced from Torenbeek [39]. Only the British size chart is shown because the pressure and load do not correspond closely to the tyre sizes in the American chart. The red lines in Figure 5.7 are for the main wheels and the blue lines are for the nose wheels, with the chosen tyre (green) and its dimensions shown for each. One thing to note is that for the nose wheels, the closest tyre on the chart is rated for a higher static load at the same pressure, which is chosen as a conservative estimate and is indicated with the dashed blue line.

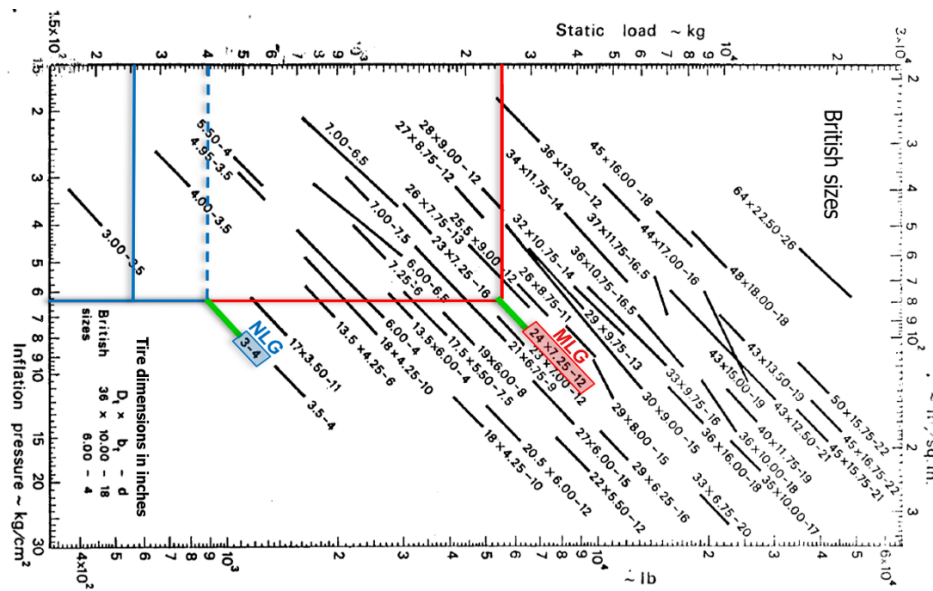


Figure 5.7: Selected main landing gear and nose landing gear tyres [39]

As shown in Figure 5.7, the main wheel tyres have an outer diameter of 24 inches (61 cm), width of 7.25 inches (18.4 cm) and an inner diameter of 12 inches (30.5 cm). The nose wheel tyres have a width of 3 inches (7.6 cm) and inner diameter of 4 inches (10.1 cm). While the dimensions of the main wheel tyres are fully specified, the nose wheel tyres are Type III tyres<sup>5</sup>, for which the outer diameter is not standardized. Using tire data for Type III aircraft tyres from Goodyear<sup>6</sup> and Bridgestone<sup>7</sup> aircraft tyre charts, the outer diameter for the nose wheel tyres was approximated to be 30 cm.

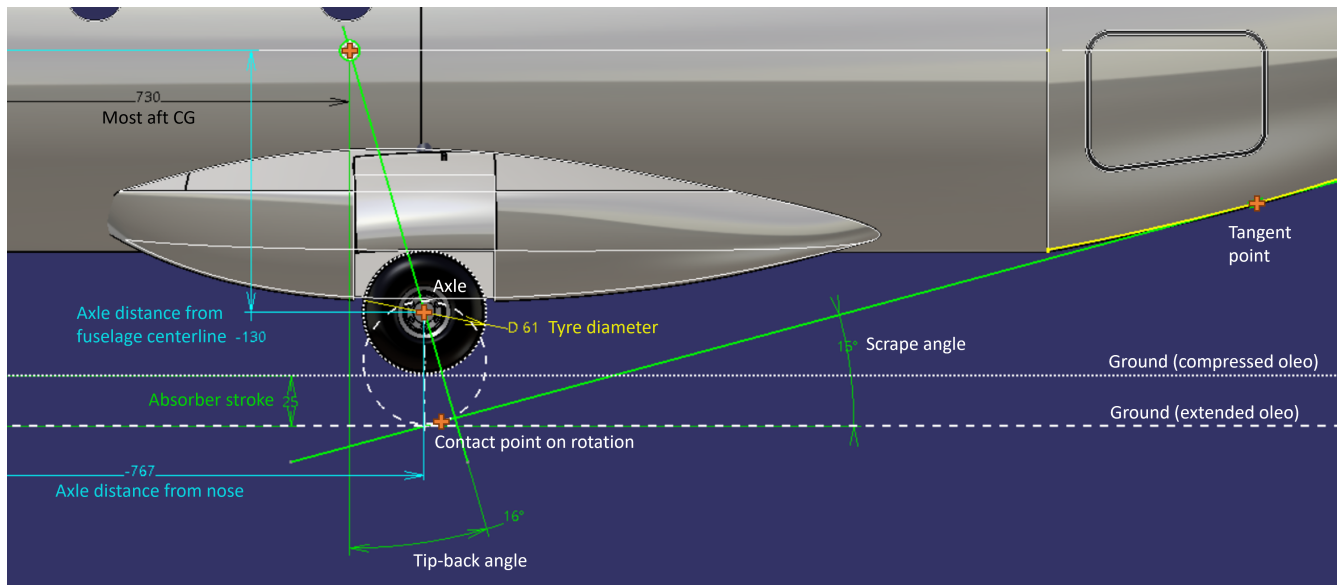
### 5.3.2. Landing Gear Positioning

Once the wheels are sized, the longitudinal, vertical, and lateral positioning is performed based on the the load distribution, tip-back angle, scrape angle, and turnover angle. These calculations are based on the most aft CG position of the aircraft, which is for the case with full fuel and no payload. This CG position is indicated in Chapter 4 Figure 4.2, and is positioned at 7.3 m from the nose. A 15° scrape angle constraint is chosen, going through the tangent point on the tail cone and the contact point of the wheel in its extended position as shown in Figure 5.8, with a shock absorber stroke of 25 cm estimated from the range of 20-50 cm [41]. The tip-back angle going through the most aft CG position and the main wheel axle is set to 16°, which is above the scrape angle [41]. From these constraints and the the 61 cm tyre diameter, the axle location of the wheel is computed and shown in Figure 5.8 in centimeters from the nose and fuselage centerline.

<sup>5</sup><https://www.aircraftsystemstech.com/p/aircraft-tires-and-tubes-aircraft-tires.html> [accessed 02-06-2022]

<sup>6</sup><https://www.goodyearaviation.com/resources/pdf/2021%20Data%20Section.pdf> [accessed 02-06-2022]

<sup>7</sup>[https://www.bridgestone.com/products/aircraft/products/applications/pdf/tire\\_specifications.pdf](https://www.bridgestone.com/products/aircraft/products/applications/pdf/tire_specifications.pdf) [accessed 02-06-2022]

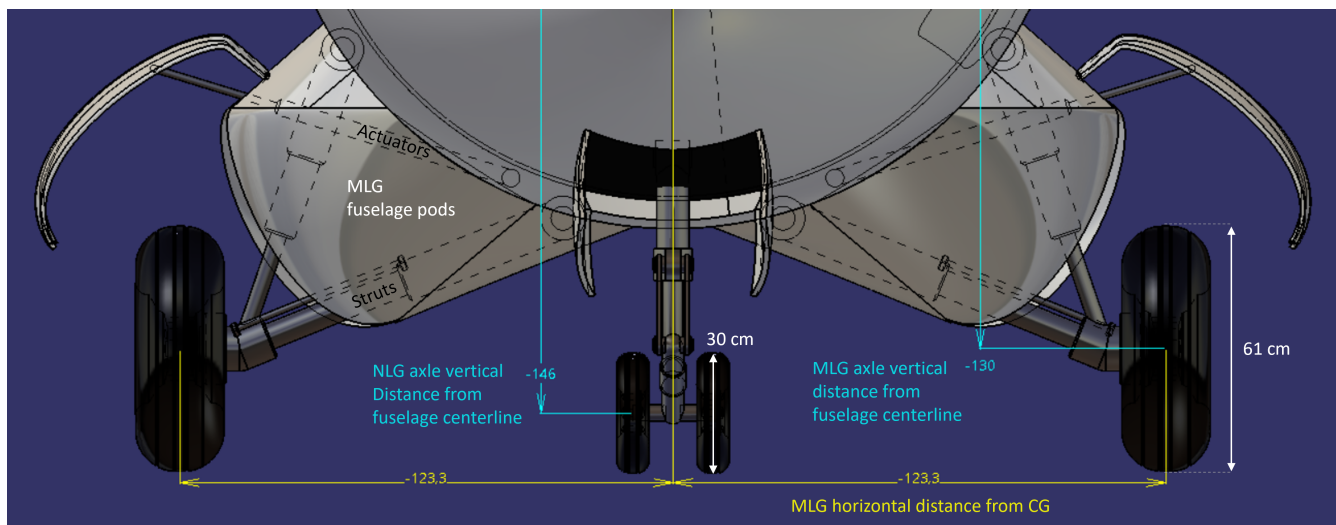


**Figure 5.8:** Longitudinal and vertical positioning in [cm] of the main landing gear with respect to angle constraints

After the main landing gear is positioned, the longitudinal position of the nose gear is determined from the moment equilibrium on ground to comply with the 9%-91% load distribution as mentioned previously. This results in a nose gear positioned 211 *cm* from the nose of the aircraft. The height of the nose gear is based on the main gear height, keeping the fuselage parallel to the ground, and can be seen in Figure 5.9.

The final step in the landing gear positioning is the lateral position  $Y_{LG}$  based on the turnover angle  $\Psi$ , which are given in Equation 5.1 where  $l_n$  and  $l_m$  are the longitudinal distances of the nose gear and main gear from the most aft CG as calculated earlier, and  $z$  is the height of the CG from the ground. With the CG assumed to be on the fuselage centerline and 160.5 *cm* from the ground based on the MLG height, the maximum turnover angle limit of  $55^\circ$  recommended by the ADSEE course [41] yields a lateral position for the main gear of 123.3 *cm* from the centerline. This lateral distance from the fuselage centerline is shown in Figure 5.9 in yellow, along with the vertical dimensions of the MLG and NLG. The wingtip ground clearance and propeller clearance are not limiting here thanks to the high wing [41] and the propeller diameter as discussed in Chapter 7.

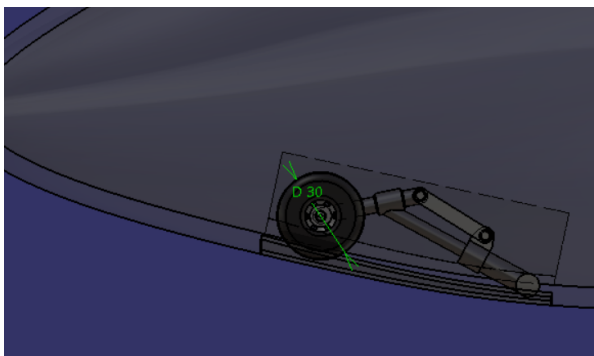
$$Y_{LG} \geq \frac{l_n + l_m}{\sqrt{\frac{l_n^2 \tan^2 \Psi}{z^2} - 1}}, \quad \Psi < 55^\circ \text{ [41]} \quad (5.1)$$



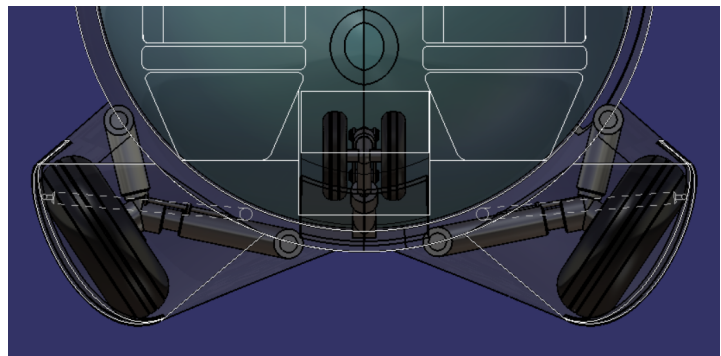
**Figure 5.9:** Lateral and vertical positioning in [cm] of the main and nose landing gear in accordance with Equation 5.1

### 5.3.3. Landing Gear Retraction and Storage

In Figure 5.8 and Figure 5.9 when displaying the gear positioning, the main gear pods and doors, nose gear doors, as well as an estimated configuration for the struts based on reference aircraft are also shown. These are based on the retraction mechanism and available storage for the landing gears. The nose landing gear swivels up and retracts below the cockpit, where it can be accommodated below the central console of the cockpit so as to not restrict the room for the pilots. This can be seen in Figure 5.10 and Figure 5.11 viewed from the side and front respectively. The area shown with dashed lines in Figure 5.10 indicates the nose wheel well. For the struts and retraction mechanism design of the main landing gears into the pods, the mechanism of the Mitsubishi MU-2B-60 Marquise was taken as a reference. The MLG struts (shown extended in Figure 5.9) retract inwards hydraulically and swivel around their connection point to the wheel and the fuselage structure, bringing the wheel to the retracted position shown in Figure 5.11.



**Figure 5.10:** NLG retracted side view



**Figure 5.11:** MLG and NLG retracted front view

As shown earlier in Figure 5.8, the position of the main landing gear is quite far aft due to the CG position and scrape angle constraints, which puts it longitudinally at the same position as the liquid hydrogen tank. The MLG retraction and storage mechanism circumvents this problem, since the tank (shown in blue in Figure 5.11) is not interrupted, with the load path going through the attachment points of the struts to the fuselage frames and being transferred to the fuselage structure. The MLG door actuators from Figure 5.9 are also shown retracted in Figure 5.11 with dashed lines.

#### 5.3.4. Load Transfer and Impact Safety

An important structural consideration when it comes to the landing gear design is how the load is transferred to the fuselage structure. While this report does not address this in detail, it is possible to do a preliminary analysis on the current main landing gear structure to get an idea of the relative magnitudes of the loads on different parts. The connections of the struts to the fuselage and the wheel are treated as ideal pin joints, and the struts are simplified as beams carrying axial loads such that a static truss calculation can be done. The results of this calculation are presented in Figure 5.12 which shows that the greatest reaction forces are in joint A with strut AC under a high compressive load and strut BC under a lower tensile load. In case of a strong impact like a crash landing, if the hydraulics cannot compress enough, this presents the possibility that strut AC could penetrate the fuel tank. To ensure this does not occur, a shear pin can be used in joint A, designed such that it shears off strut AC from the fuselage structure at a critical load, enabling it to slide up and outwards over a reinforced plate as shown in Figure 5.13.

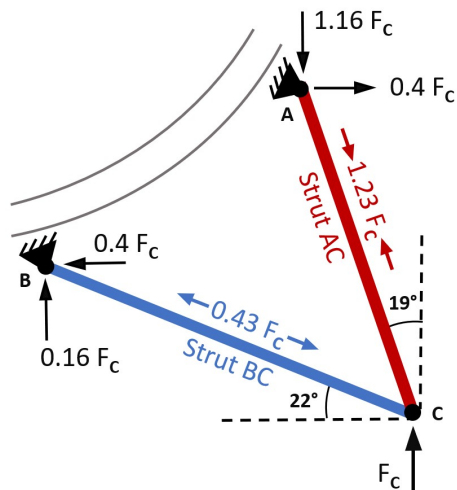


Figure 5.12: Static analysis on simplified MLG structure

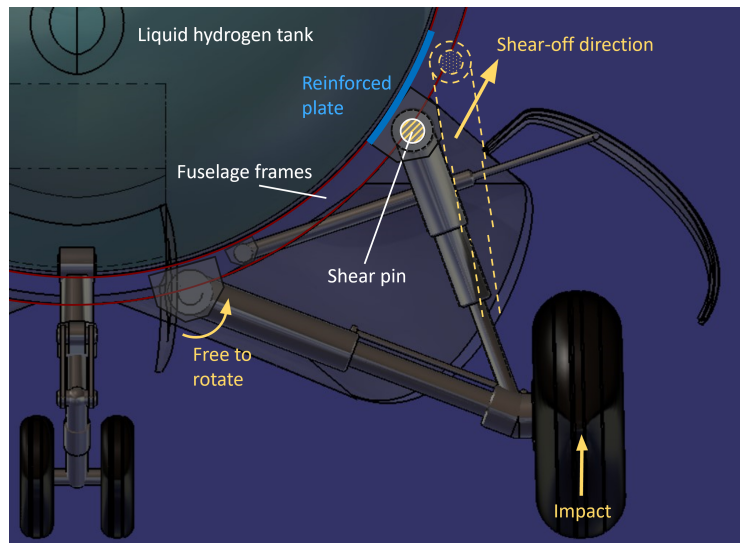


Figure 5.13: Shear-off mechanism of strut AC



# Fuel Tank Design

To store liquid hydrogen, a tank is designed such that the fuel will be kept at cryogenic temperatures. In Section 6.1 the first phase of the design process is described which concerns the material selection for the tank itself. After the materials have been selected, the geometry of the fuel tank is assessed in Section 6.2. Then, in Section 6.3, the operational aspects of the fuel tank are considered. This includes the procedures for when the fuel enters and leaves the tank and miscellaneous concepts that concern the fuel system.

## 6.1. Fuel Tank Material

The tank consists of three different sections which are the shell, the insulation and the supports. The shell is the airtight part which carries the internal pressure loads as discussed in Subsection 6.1.1. The primary function of the insulation material is insulating the tank from heat entering the system as described in Subsection 6.1.2. Finally, the insulation material is not capable of carrying the load of the tank, which is why supporting blocks are required to account for these loads. This supporting material is analysed in Subsection 6.1.3.

### 6.1.1. Shell Material

Currently, stainless steel, titanium, aluminium and composites are good options for the application at hand. The material assessment relies heavily on the hydrogen embrittlement. This concerns the process of introduced cracks and fractures by means of hydrogen molecules diffusing into the material[3]. As a result, composites are not widely used for cryogenic hydrogen storage options. A solution has been proposed by lining the inner wall of the tank with another material that is less likely to experience hydrogen embrittlement. This does, however, impact the overall recyclability negatively because of the added complexity and amount of materials involved. On top of this, the non-uniform expansion coefficient of resin and fibres, make for complex low fracture mechanisms. In combination with other factors, this results in more required research in composites for cryogenic tank applications. As discussed in the midterm report [10], Titanium is a relatively expensive material compared to stainless steel and aluminium. It also appears to have weaker mechanical performance at low temperatures, thus, special low temperature titanium alloys have been created. This specific alloy would again make it harder to be recycled, which is not beneficial for the overall sustainability. Both stainless steel and aluminium show high hydrogen embrittlement resistance. Compared to aluminium, stainless steel can still be developed to improve on this property. In general aluminium has better cryogenic performance than stainless steel and so, for now, it can be concluded that aluminium is the best material concerning cryogenic liquid hydrogen fuel storage. In the field of aerospace engineering, there are still many situations where an aluminium alloy is required. For the use of cryogenic tanks the most used shell material is aluminium 2219[6]. As a result, this alloy will be chosen for the shell of the fuel tank. In Table 6.1 the material characteristics can be found. These properties are analysed at room temperature. However, their strength can be increased at subzero temperatures.<sup>1</sup> Since the strengths are lowest at room temperature, the values in Table 6.1 will be considered in further calculations regarding critical conditions.

**Table 6.1:** Properties aluminium 2219 at room temperature.

	Thermal conductivity [W/m*K]	Yield stress [MPa]	Tensile stress [MPa]
Aluminium 2219 <sup>1</sup>	170	76	170

### 6.1.2. Insulation Material

To keep the liquid hydrogen at cryogenic state, active or passive methods can be used. The active methods rely on adding energy into the system to keep it at a desired temperature. However, due to the extra weight and

<sup>1</sup><https://www.azom.com/article.aspx?ArticleID=6616> [accessed 20-06-2022]

energy this solution will bring along, this option is not looked into any further. Passive cooling can be split up into having a material as insulation or having a vacuum. To first obtain and maintain a vacuum, a large amount of energy is needed [31]. In addition, the installation and maintenance processes will be more complex. As a result, no further research will be invested in this method for now.

For the insulation material thermal conductivity and density are the most important criteria. The thermal conductivity gives an indication on how well heat is conducted by the material. The density is also taken into account since this will give an indication on the mass of the fuel tank system. Since the mass goes hand in hand with the amount of insulation needed, which is proportional to the thermal conductivity, no absolute conclusions on the final mass can be derived from the density alone. In Table 6.2 the material properties are shown for 5 different insulation materials.

From Table 6.2, it can be seen that, EPS foam and PMI foam have a comparable thermal conductivity, but that PMI foam has a worse performance when it comes to density. Glass wool is the best performer on the density criteria, but hands in on the thermal conductivity property. From values alone in the table it can be concluded that MLI has by far the lowest thermal conductivity, but has large density relative to glass wool or EPS foam. As research on a aviation cryogenic liquid hydrogen storage tank points out, a lot of research is still to be done on MLI[31] with it not yet being viable for mass production. MLI is also shown to be less effective around low temperatures since its development was driven on heat rejection. As a consequence, the conclusion of the article led to EPS foam being the lightest and most effective solution for use on a cryogenic liquid hydrogen tank application.

**Table 6.2:** Material properties of insulation layer.

	Thermal conductivity [W/m*K]	Density [kg/m <sup>3</sup> ]
<b>Cork</b> <sup>2</sup>	0.037	116
<b>PMI foam</b> <sup>3</sup>	0.0246	75
<b>Glass wool</b> <sup>4</sup>	0.04	12
<b>EPS foam</b> <sup>5</sup>	0.02594	26
<b>MLI</b> [31]	0.000135	173

### 6.1.3. Supporting Material

The tank itself should be supported within the aircraft while still maintaining its insulating properties. Since EPS foam has too little load supporting properties, the tank can not be directly mounted to the air frame via the insulation. A solution would then be to mount the aluminium tank shell directly on load carrying blocks that connect the tank with the air frame. Because the insulation will be interrupted at the places where the support blocks are mounted, heat can enter the system more easily. Consequently, it is important to still have as good as possible insulating properties while still being able to support the tank structure. As the tank will rest on top of the support blocks, the material will be in compression most of the time, hence compressive strength is one of the assessment criterion. Two possible contenders are XPS foam and Foam Glass. XPS foam is an extruded polystyrene which has increased stiffness and rigidity over normal EPS foam<sup>6</sup>. Foam Glass, also known as cellular glass is the result of a reaction between glass and carbon, made entirely of inorganic material<sup>7</sup>. As can be deduced from Table 6.2, the thermal conductivities of the two materials are almost the same. Due to

<sup>2</sup><https://thermalcorksolutions.com/cork-insulation-faqs/> [accessed 25-05-2022]

<sup>3</sup><https://www.azom.com/article.aspx?ArticleID=16425> [accessed 25-05-2022]

<sup>4</sup><https://www.gamma.nl/assortiment/gamma-glaswol-16-cm-3-0-m2-rd-4-0/p/B431910> [accessed 25-05-2022]

<sup>5</sup>[https://www.isolatiwereld.nl/product/eps-isolatieplaat-60se-20mm-500x1000mm/?gclid=CjwKCAjwp7eUBhBeEiwAZbHwkWRLJBeB7Xa8fAnp3WovssBkPsWQizblp-eGnQoyMLzKmUuiU4baVhoCYMEQAvD\\_BwE](https://www.isolatiwereld.nl/product/eps-isolatieplaat-60se-20mm-500x1000mm/?gclid=CjwKCAjwp7eUBhBeEiwAZbHwkWRLJBeB7Xa8fAnp3WovssBkPsWQizblp-eGnQoyMLzKmUuiU4baVhoCYMEQAvD_BwE) [accessed 25-05-2022]

<sup>6</sup><https://www.progressivefoam.com/eps-vs-xps-vs-gps/> [accessed at 17-05-2022]

<sup>7</sup><https://www.thermal-engineering.org/what-is-foam-glass-cellular-glass-definition/> [accessed at 17-05-2022]



the compressive strength of Foam Glass being way higher than for XPS at almost no loss in thermal conductivity, Foam Glass will be the material for the supporting structure.

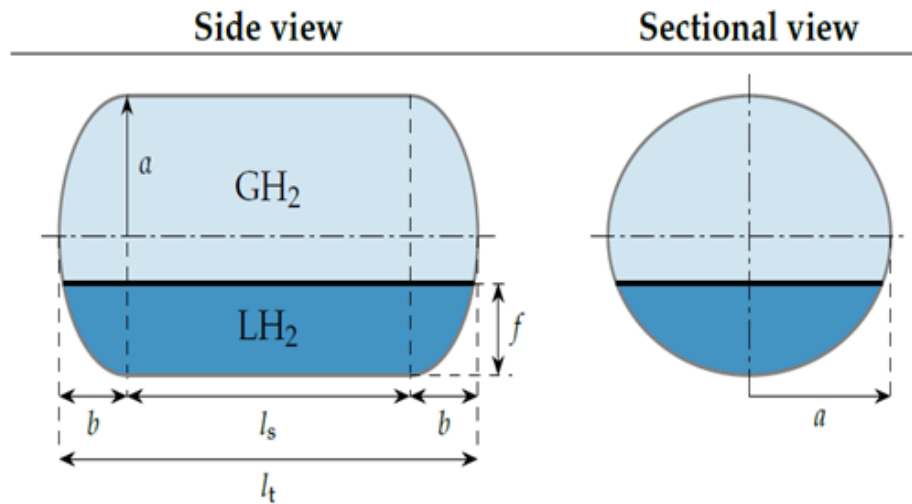
**Table 6.3:** Support material properties

	Thermal conductivity [W/m*K]	Compressive strength [kPa]
XPS	0.034 <sup>8</sup>	690 <sup>9</sup>
Foam Glass	0.035 <sup>10</sup>	2400 <sup>11</sup>

## 6.2. Fuel Tank Geometry

The tank shape flows down from the volume of the liquid hydrogen and the loads it has to carry. The geometry can be limited by certain production process constraints tied to certain material choices. To use the available space as optimal as possible, the crosssectional view will be cylindrical as the fuselage is cylindrical as well. For the ends of the fuel tank, 3 options are considered: Flat, semi-elliptical and semi-spherical. The flat ends are the best option regarding the space they will occupy. The semi-spherical option is the best candidate for eliminating high stresses at the edges since the stresses are equally distributed over the end caps with no stress concentration points. However, this shape takes up more space and has a negative impact on the production process being more complicated and thus being more expensive.<sup>12</sup>

For the preliminary design, the choice is to use the shape displayed in Figure 6.1 with the end caps having an elliptical shape with a ratio of  $\frac{a}{b}$  equals 1.66. This elliptical shape is the best choice for achieving maximum volume and tank length[7]. The elliptical end caps are also the best combination of the advantages of the flat end caps and the spherical end caps. The curved edges make sure stress concentration points are reduced compared to a cylinder with flat ends. From the geometry in Figure 6.1, it is possible to derive the tank volume and surface, shown in Equation 6.1 and Equation 6.2 respectively.



**Figure 6.1:** Nomenclature for the geometry of the hydrogen fuel tank [1]

<sup>8</sup><https://www.building-innovation.co.uk/products/extruded-polystyrene-xps> [accessed at 25-05-2022]

<sup>9</sup><https://www.dupont.com/content/dam/dupont/amer/us/en/performance-building-solutions/public/documents/en/styrofoam-brand-highload-40-60-and-100-pis-43-D100079-enNA.pdf> [accessed at 25-05-2022]

<sup>10</sup><https://www.foamglas.com/en/download> [accessed at 25-05-2022]

<sup>11</sup><https://www.foamglas.com/en/download> [accessed at 25-05-2022]

<sup>12</sup><https://www.wermac.org/equipment/pressurevessel.html> [accessed at 24-05-2022]

$$V_{tank} = \pi \cdot a^2 \cdot l_s + \frac{4}{3} \cdot \pi \cdot a^2 \cdot b \quad (6.1)$$

$$S_{tank} = 2 \cdot \pi \cdot a \cdot l_s + 4 \cdot \pi \cdot \left( \frac{2 \cdot (a \cdot b)^{1.6} + a^{3.2}}{3} \right)^{\frac{1}{1.6}} \quad (6.2)$$

Besides the general shape of the hydrogen tank, the insulation thickness and integration with the airframe structure shall be considered. An interesting alternative consists of combining the tank shape within the load bearing structure of the fuselage as it was proven to be the most volume efficient solution. From Design 1 in Figure 6.2, it can be deduced that, by implementing stringers within the tank structure itself, a significant reduction in overall thickness can be obtained. However, due to the support structure that is needed for the more complicated load path into the tank, the required insulating properties cannot be maintained. This results in too much energy entering the system with unwanted boil off at an early stage. Conclusively, Design 1 in Figure 6.2 is not feasible and the conventional method as in Design 2 of Figure 6.2 will be used.

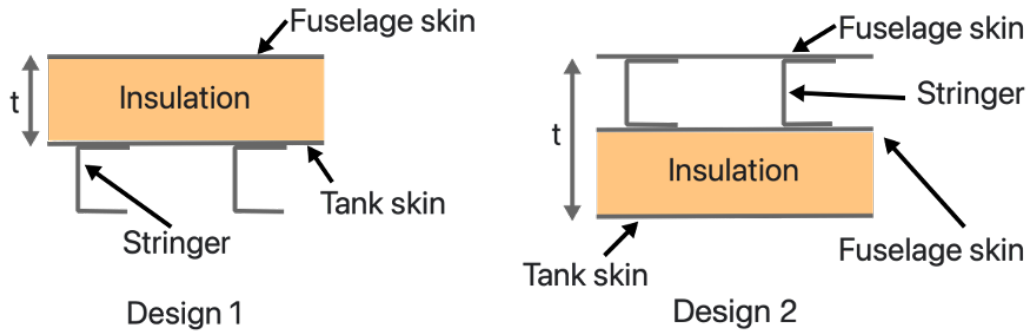


Figure 6.2: fuel tank insulation integration options

### 6.2.1. Geometry Support Blocks

For the load calculations, cylindrical support blocks will be used under an angle of 45 degrees with the horizontal as schematically shown in Figure 6.3a. A cylindrical cross section is used since, for bending moments in multiple directions, this shape proves to be best suitable in this design phase. The 45 degrees is chosen to equally transpose the vertical weight force of the tank into an axial and shear force within the blocks in case of static loading. To distribute the force of the tank more evenly, 4 support blocks will be mounted on the bottom of the tank. To make use of the available space as efficiently as possible, the blocks will have the same height as the insulation thickness. The calculations are based on the following material load properties of Foam Glass shown in Table 6.4 which resemble the worst case loading properties:

Table 6.4: Material properties of Foam Glass

	Compressive strength [MPa]	Tensile Strength [MPa]	Bending Strength [MPa]
Foam Glass	2.4 <sup>13</sup>	0.2 <sup>12</sup>	0.55 <sup>12</sup>

Since the tank will not only undergo static but also dynamic loads, the following ultimate load factors are used determined in Subsection 4.10.3. It should be noted that for the stress calculations an additional safety factor of 2 is used. The ultimate load factors are  $n_{up} = 2$  and  $n_{down} = 4.5$ .

For each load case and load factor the radius of the support block is calculated. The radius based on the axial load is calculated with Equation 6.3 where  $F_{axial}$  is the axial force on the support block,  $sf$  is the safety factor and the material strength is either the compressive or tensile strength depending on the load case. It should be

noted that Equation 6.3, Equation 6.4 and Equation 6.5 are the rewritten results of the stress formulas in order to have the radius as an output.

$$r_{axial-load} = \sqrt{\frac{sf \cdot F_{axial}}{material-strength \cdot \pi}} \quad (6.3)$$

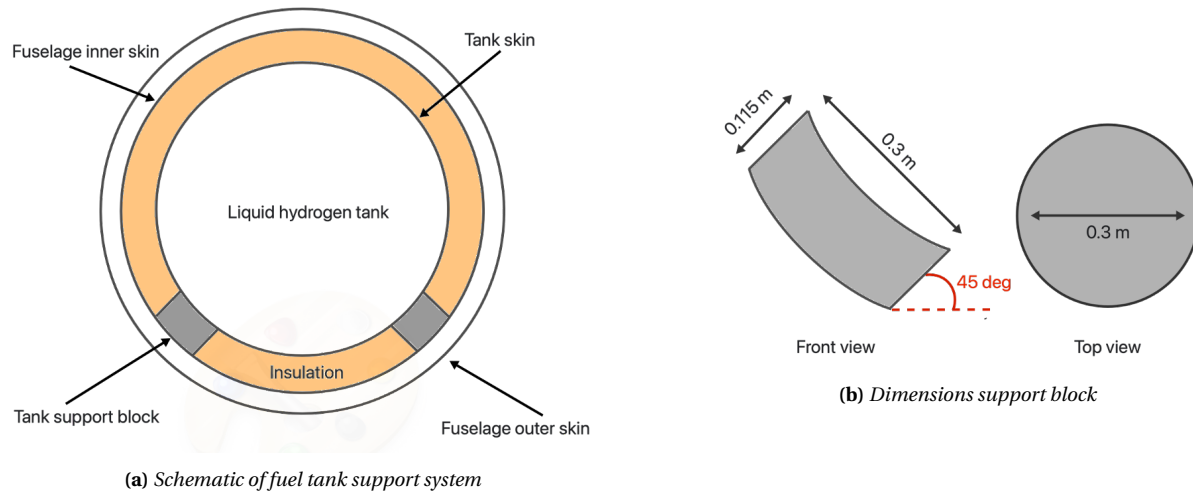
Concerning the radius of the block when calculated for a shear load, equation Equation 6.4 [47] is used. The only new parameter here is  $F_{shear}$  which represents the shear load applied on the block.

$$r_{shear-load} = \sqrt{\frac{4}{3} \cdot \frac{sf \cdot F_{shear}}{material-strength \cdot \pi}} \quad (6.4)$$

The last load that is assessed is the bending stress caused by the sideways loads and the 45 degrees mounting angle of the blocks. The radius followed from this case is calculated with Equation 6.5<sup>14</sup> where  $F_{bending}$  is the bending load applied on the blocks.

$$r_{shear-load} = \frac{1}{2} \cdot \sqrt[3]{32 \cdot \frac{sf \cdot F_{bending}}{material-strength \cdot \pi}} \quad (6.5)$$

After all calculations are performed, the most critical load case is determined to be the bending load. The critical load case is determined based on the largest radius that is needed to safely support the fuel tank under all load cases. This resulted in the largest radius being needed for the downwards load factor with the bending load case.



**Figure 6.3:** Fuel tank support system

<sup>14</sup> <http://www.faculty.fairfield.edu/wdornfeld/ME311/BasicStressEqns-DBWallace.pdf> [accessed at 22-05-2022]  
[accessed at 24-05-2022]

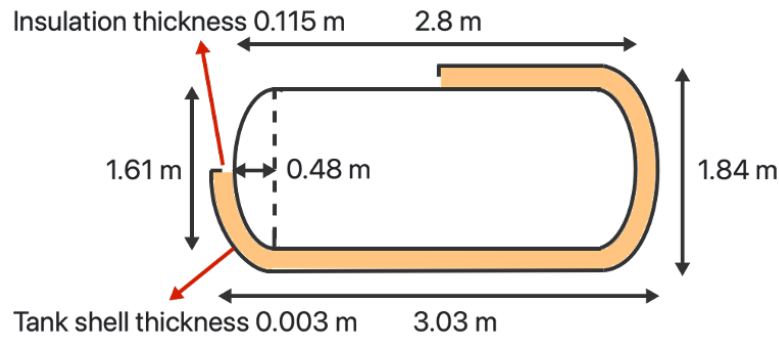


Figure 6.4: Dimensions of fuel tank including insulation

### 6.3. Fuel Tank Operations

Regarding the fuel tank operations, it is important to determine how the fuel enters and leaves the tank. The most challenging aspect of storing fuel at cryogenic temperatures is the increase in pressure when heat enters the tank. This problem can be solved in two ways: Design the tank such that it can handle the high pressures or vent fuel such that the pressure does not build up. An analysis regarding this topic is made in Subsection 6.3.1. In each scenario, the pressure build up results in loads onto the tank which are considered in Subsection 6.3.2. Filling of the tank is a more straightforward aspect and is discussed in Subsection 6.3.3 with some other miscellaneous topics about the tank.

#### 6.3.1. Boil-off Process

The boil-off temperature concerns the temperature at which, in this case, liquid hydrogen starts to evaporate. Since the energy density of gaseous hydrogen is way lower than its liquid phase, evaporation shall be limited. In a closed system, the pressure rises as a function of temperature increase as shown in Figure 6.5. Eventually every cryogenically stored liquid that is not actively cooled, reaches the boiling temperature at which the liquid becomes a gas. For hydrogen, this boiling temperature is at 20.1 degrees Kelvin.<sup>15</sup> For a closed system, this boiling results in an increase in pressure as displayed in Figure 6.5.

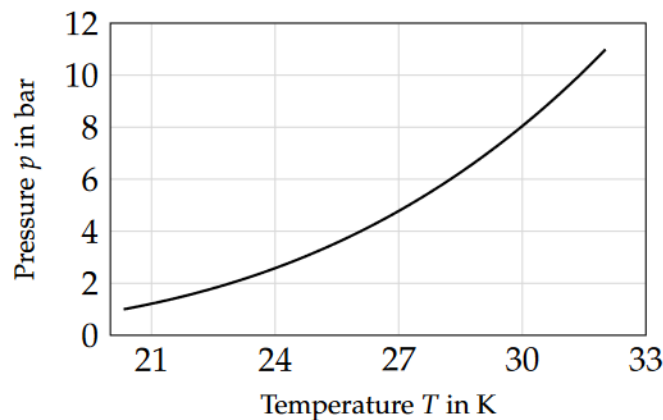


Figure 6.5: Saturation curve for hydrogen [1].

The next issue concerns how quickly the temperature increases over time. For this aspect the thermal conductivity of the system becomes very important and by using Equation 6.6, the amount of heat entering the tank per unit of time can be calculated. In this formula  $\lambda$  is the thermal conductivity,  $A$  is the tank surface,  $t$  is the thickness of the insulating material and at last  $(T_i - T_o)$  is the difference in temperature between inside and outside the tank. When the energy entering the tank is known, it can be used to derive how fast the hydrogen

<sup>15</sup><https://www.nuclear-power.com/hydrogen-melting-point-boiling-point/> [accessed 24-05-2022]

heats up. To make this possible, the specific heat  $c_V$  of hydrogen shall be used, which is  $14.304 \text{ kJ/kg} \cdot \text{K}$ .<sup>16</sup>

With this data and Equation 6.6 it is possible to derive a thermodynamic model analysing the required insulation thickness. For example, if it is allowed to increase fuel temperature with  $X$  degrees in  $Y$  hours, the maximum heat entering the tank is equal to  $C_V \cdot m_{fuel} \cdot X$  and the heat entered is  $Y \cdot 3600 \cdot \dot{Q}$ . These parameters have been inserted in a Python file, such that the numbers can be changed easily.

$$\dot{Q} = \lambda \cdot \frac{A}{t} \cdot (T_i - T_o) \quad (6.6)$$

A hydrogen tank consisting of 100% liquid hydrogen becomes problematic because the liquid can not expand with the result of rapid pressure built up. For this reason, it is important to start with a specific liquid to gas fraction that makes sure the liquid can expand. Furthermore, if venting is required, it is more convenient to vent gaseous hydrogen instead of liquid hydrogen because a much smaller amount can be withdrawn[4]. The reason for this is that one liter of liquid hydrogen is equal to 788 L of gas.<sup>17</sup> To accomplish this buffer for pressure to build up in the tank, 3% of the total content will consist of gaseous hydrogen. This amount of 3% is the required value to be sure that gaseous hydrogen is vented [4]. Figure 6.6 displays the different venting pressures with their corresponding liquid volume fraction. Each line represents how the pressure develops over time till venting starts at a liquid volume fraction of 0.97. It can be seen that venting starts at a volume fraction of 97% since each line ends there, which means that liquid hydrogen can expand until it fills 97% of the total tank volume.

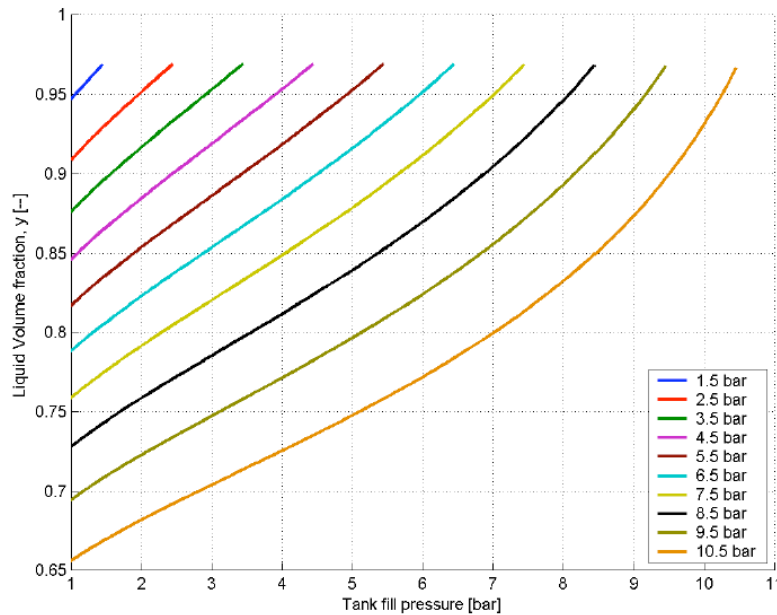


Figure 6.6: Venting pressure as a function of the filling pressure and filling ratio.[4]

### Design for No Boil-off

Avoiding boil off permanently is impossible, since there is always heat entering the tank. When the tank is designed to avoid boil off during operation, an approximation of the duration per flight is required. A rough estimate is 5 hours for the block time when no delays occur. This duration is calculated by adding up 1 hour for boarding and refuelling, 30 minutes for taxiing, 2.5 hours of flight and 1 hour for deboarding and taxiing after

<sup>16</sup><https://www.nuclear-power.com/hydrogen-specific-heat-latent-heat-vaporization-fusion/> [accessed 24-05-2022]

<sup>17</sup><https://keengas.com/gases/hydrogen/> [accessed 15-06-2022]

the flight. Furthermore, an airliner is allowed to keep the aircraft on the tarmac with passenger for a maximum of 5 hours.<sup>18</sup> Conclusively, for this design, boil-off starts 5 hours after refuelling.

The boil-off period is computed using a Python script, in which the tank geometry is combined with the material properties of the tank and Equation 6.6. With the current insulation, the internal temperature of the tank increases by approximately 4°C, which results in 3 *bar* of pressure as can be seen in Figure 6.5. In order to control the pressure built up in the tank, pressure relief valves will be installed that vent the gaseous hydrogen at 3 *bar*. Concerning the refueling phase, the tank will be pressurised at 1 *bar* with the temperature of 20 K.

Since the structure of the tank is designed to carry a load of 3 *bar*, from Figure 6.6 it can be concluded that the maximum liquid volume fraction is approximately 90% liquid hydrogen during refuelling. This means that the tank should be designed to have 10% of extra volume for the liquid hydrogen to expand. If a lower fraction than the 90% would be used during refuelling, the volume is used inefficiently, resulting in an over-designed heavier tank.

After iterating the variables in the Python program, it turns out the shell needs to be 3.0 *mm* thick to withstand the loads and the insulation needs to be 11.5 *cm* thick to keep the pressure low for 5 hours. This results in a shell mass of 140.36 *kg* and insulation which weighs 48.96 *kg*. After 5 hours the boil-off process will start, but then in most cases the aircraft will be at the ground base which means an external system can be connected to collect the boiled-off hydrogen.

### Design for Direct Boil-off

Another option includes direct boil-off. Since the aircraft will be refuelled with a pressure slightly above 1 *bar*, the direct boil-off will be initiated with a pressure relieve valve of 1.5 *bar*. In this scenario the boil-off starts relatively quickly after refuelling. The amount of boil-off can be computed using Equation 6.7 [9], which shows the amount of boiled-off fuel as a fraction of the total amount of fuel. In this formula  $Q_{in}$  is the heat entering the tank,  $V$  the volume of the tank,  $\rho$  the density of the fluid and  $H_{vap}$  the latent heat for vaporising.

$$\text{Boil-off rate} = \frac{Q_{in} \cdot 24 \cdot 3600}{V \cdot \rho \cdot H_{vap}} \cdot 100 \quad (6.7)$$

Equation 6.7 can be inserted in the Python file determining the heat transfer, and it turns out during a period of 5 hours, 36 *kg* of hydrogen will be boiled-off. It shall be noted that the EPS insulation thickness is kept at 11.5 *cm*, because it is similar to the design without boil-off. If the internal pressure is reduced by a factor 2, the thickness of the shell can be reduced by the same factor. As a result, the shell reduces in weight by 70.18 *kg*. Furthermore, when the system starts boil-off directly, the pressure will not increase and there is no additional space required for the liquid to expand. As can be seen in Figure 6.6, the tank can be filled up to 95% with liquid to reach a venting pressure of 1.5 *bar*.

### Boil-off Trade-off

Since there are two options to deal with the increase in temperature, a trade-off is performed between the two options. The trade-off is shown in Table 6.5 and includes the emissions during operation, the liquid filling ratio and the shell mass of the tank. In the trade-off, green colours indicate the best option per criteria, yellow means it is manageable and red becomes unacceptable. As can be seen the emission of 36 *kg* of hydrogen during flight drives the direct boil-off to an unacceptable extent in the perspective of sustainability. The main reason is that emission of pure hydrogen is contributing to the greenhouse effect, as discussed in Chapter 7, but venting hydrogen is also expensive. As a result, the tank is designed to boil-off after approximately 5 hours. This increases the shell mass by 70 *kg*, but that does not weight up against 36 *kg* of extra hydrogen per flight. Furthermore, direct boil-off emits a very explosive gas in the air, which might become dangerous once people

<sup>18</sup><https://www.claimcompass.eu/blog/tarmac-delay-rules/> [accessed 31-05-2022]

are smoking or other vehicles using ignition are close. In terms of sustainability, emitting hydrogen into the air is harmful as it has a global warming potential 11 times larger than carbon dioxide.<sup>19</sup>

	Emission	Liquid filling ratio	Shell mass
Boil off after 5 hours	0 kg $H_2$ during flight	0.90	140 kg
Direct boil off	36 kg $H_2$ during flight	0.95	70 kg

**Table 6.5:** Trade-off regarding the boil off process.

### 6.3.2. Loads Fuel Tank

The next aspect regarding the fuel tank is the loading applied to it. As described during the previous section the maximum operational internal pressure will be around 3 *bar*, since at this pressure the boil-off starts. This subsection analyses if the tank can withstand a load of 3 *bar*. In this case, 3 *bar* is the maximum allowable pressure (MAWP) during operation.

For designing against loads, regulations become important because it includes safety issues. The European aviation authority EASA does not have regulations yet about liquid hydrogen tanks in aviation, because it is a very modern method which is still under development. Despite no aviation laws, there are some general requirements set by the European Commission regarding the storage of liquid hydrogen. In Commission Regulation (EU) No 406/2010 it is specified that a fuel tank storing liquid hydrogen shall be tested at  $P_{test}$ , which can be calculated using Equation 6.8. It shall be noted that in this formula all pressures have *MPa* as unit. When the test pressure is applied to the tank, the induced stresses shall not exceed the ultimate tensile strength.

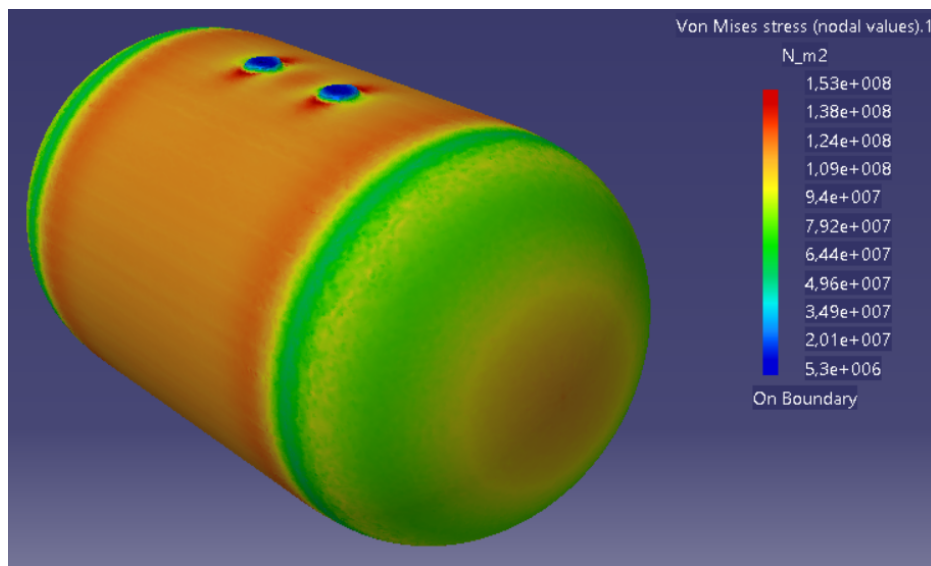
$$P_{test} = 1.3 \cdot (MAWP + 0.1) \quad (6.8)$$

From Equation 6.8 it can be derived that the fuel tank shall withstand an internal pressure of 5.2 *bar* to comply with the regulations. This load was applied to a model of the tank made in CATIA, and the resulting stresses can be found in Figure 6.7. Since it is an ultimate stress test, it is important that every spot faces a stress lower than the ultimate tensile stress of 170 *MPa* (Aluminium 2219), which is true for this case. As a conclusion from this stress test, it is feasible to have a minimal skin thickness of 3 *mm* to remain below the yield stress during operation and below  $P_{test}$  during stress testing. A thicker shell only increases weight and is not necessary, so the shell will be 3 *mm* thick. With this thickness, during operational pressures (3 *bar*) the stress remains below the yield stress and during ultimate pressures (5.2 *bar*) the tensile stress is not exceeded. It should be noted that this stress test includes two holes on top of the tank for two pressure valves to vent gaseous hydrogen and one at the bottom for the transport of liquid hydrogen. These holes are not designed specifically for the optimal load case, but were simply taken into account to observe what the effects on the total structure would be.

In the performed stress analysis some assumptions were necessary which shall be mentioned. At first, the material is assumed to be in perfect conditions, without imperfections, dents or scratches. This assumption is valid since the material can be manufactured and handled with great care. Furthermore, the shell material is not made with one part, which means the assembly will be welded and this might cause weaknesses. To solve this issue the weld thickness can be increased such that the weld would not become the weak link. The last assumption is made within the software of the stress analysis, because in the finite element analysis it is required to specify a mesh size. The mesh size chosen is 5 *mm*, which is a valid choice since the results are almost equal to a mesh of 10 *mm*. Therefore, it is known that at a mesh size of 5 *mm* the results are converging close to the exact values.

<sup>19</sup><https://www.rechargenews.com/energy-transition/hydrogen-twice-as-powerful-a-greenhouse-gas-as-previous-ly-thought-uk-government-study/2-1-1200115?adlt=strict&toWww=1&redig=3744378693EA415DB415CA0667DC81A3> [accessed 14-06-2022]





**Figure 6.7:** Finite Element Analysis for the fuel tank with an internal pressure of 5.2 bar.

### 6.3.3. Miscellaneous Concepts of the Fuel System

Concerning the fuel tank operations, this includes all miscellaneous parts of the fuel system that still need to be addressed but will not be worked out in detail for now. As mentioned before, the liquid hydrogen will be stored at 20 K at 1 bar within the aircraft. Since no liquefaction of gaseous hydrogen will take place on the aircraft itself, pre-cooled liquefied hydrogen has to be fueled at the airport. Because of these cryogenic processing temperatures, all the inlet and outlet pipings of the fuel tank have to be insulated.

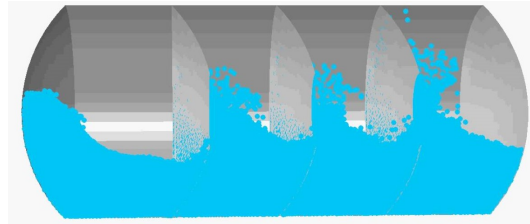
Because the hydrogen tank will not be perfectly insulated, heat will be able to enter the system slowly, heating up the liquid hydrogen. As shown in Figure 6.5, as soon as the temperature of the liquid hydrogen starts to rise the pressure within the tank increases. Because the tank is designed to withstand a nominal pressure of 3 bar, a pressure relief valve of 3 bar will be fitted onto the tank. This valve opens at the specified pressure and thus ensures no further pressure build up in the tank can take place. For redundancy, a second pressure relief valve will be fitted of 4 bar to function as a backup in case of a failure occurring with the first valve. Because gaseous hydrogen is lighter than liquid hydrogen it will move to the top of the tank. As a result, the valves will also be mounted on top of the hydrogen tank and vent the gaseous hydrogen, via some pipelines, outside of the aircraft.

Concerning the internal fuel delivery system to the fuel cells, liquid hydrogen is transported via pipelines with a fuel pump. The amount of fuel and pressure will be regulated with sensors, like flow meters and valves/pressure regulators. A pressure regulator in combination with a heat exchanger[49] will make sure the liquid hydrogen is transformed into gas with the correct temperature to be used within the fuel cell. As mentioned before, the fuel will be taken from a hole at the bottom side of the tank for easy routing to the fueling port of the aircraft and the fact that the liquid hydrogen is heavier than the gaseous hydrogen within the tank.

Another important aspect for the fuel tank operations is the boil-off valve because significant heat leakage may occur in these valves. The pressure release valves (PRV) are complex and often made from metals, which are good thermal conductors. The details of the PRV will not be discussed since that is too much detail for this stage of the design and thus rough estimation of the heat conduction will be considered. As a possible design option for the fuel tank the 'SUS316L' valve from Fujikin is analysed. Fujikin is a company with expertise in cryogenic valves [19]. The 'SUS316L' body, extended bonnet design and hollow stem permit minimal thermal conductivity between the fluid and actuator[19]. The total heat transfer is approximately 2-3 W for the valve, which is included in the thermodynamic model in the Python script.



Finally, it should be mentioned that having a single large fuel tank in the aft fuselage brings up the issue of sloshing. In sudden forward accelerations or deceleration and in case of strong gusts, the fuel in the tank can move around freely. With a 3 m tank carrying more than 300 kg of fuel, this can cause dangerous sudden shifts in CG position in flight, which can destabilize the aircraft. A solution to mitigate this is the use of slosh baffles in the tank, which are thin dividers that limit the movement of the fluid to smaller sections as shown in Figure 6.8<sup>20</sup>.



**Figure 6.8:** *Visualisation of an accelerated fluid in a tank with slosh baffles*

<sup>20</sup><https://i.ytimg.com/vi/hFAyqwGjUc/maxresdefault.jpg>[accessed 15-06-2022]

# Propulsion System

The Sustainable Air Taxi that the team is designing makes use of an electric propeller propulsion system. The electric power is generated in a hybrid manner, using several hydrogen fuel cells as well as a fixed battery that may be used as the APU of the aircraft. This chapter describes how the propeller engine of the aircraft is chosen in Section 7.1. In Section 7.2 the fuel cell type and size are chosen based on the power needed, as well as their efficiency. Finally, in the same section, the air intake of the propulsion system is discussed. It should be noted that in this design process multiple interdependent steps are performed at the same time. What this means for the propulsion system is that the parameters on which the design relies heavily, such as the power requirement resulting from the convergence of the weight estimation methods, will not be available from the beginning. Because of this and the limited available time in the DSE, there is still room for further improvements, as discussed in Chapter 17.

## 7.1. Engine

The first major component of the propulsion system that needs to be carefully chosen is the engine itself, whose main components are the electric motor(s) and the propeller, respectively. In order to know how much fuel is required to be stored on board and how many batteries are required to provide extra power during the take-off and climb it is necessary first to know the required output from the propulsion system. Hence, a start is made from the outcome of the power loading diagram, which resulted in a maximum power requirement of  $1021.6kW$  *shaft power* during *cruise*. It should be noted that this is the required power output after accounting for multiple intermediate efficiencies of the propulsion system's components: fuel cell efficiency, battery efficiency and electric motor efficiency, as described in subsequent sections. This means that the actual required power needed from the electric motor is given by the aforementioned value multiplied by its efficiency. This value leads in turn to the required amount of fuel, by considering the conversion efficiency of the fuel cell, and, finally, to the amount of power required from the batteries. In a simplified form, the power output is given by Equation 7.1.

$$P_{available} = P_{shaft} \cdot \eta_{propeller} \quad (7.1)$$

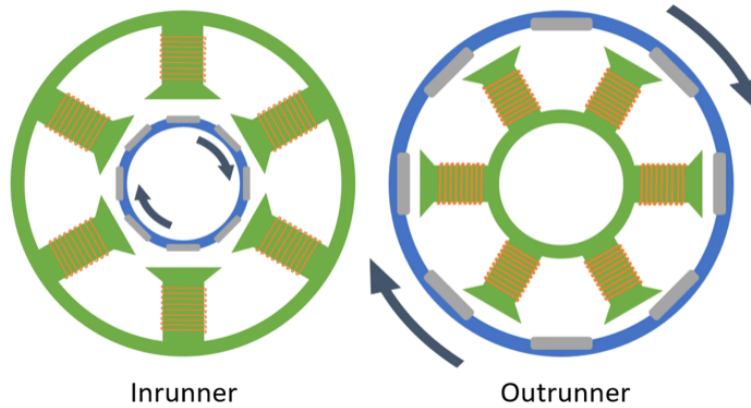
After finding an option which produces the minimum required power, the generated thrust also has to be analysed and a final decision is made based on this aspect. The complete propulsion system has to be able to translate its power into the needed thrust, otherwise it is useless. The engine itself is further broken down in this chapter into the electric motor and the propeller, respectively, and they are both analysed below.

### 7.1.1. Electric Motor Considerations

The electric motor is the component responsible for converting the electric energy to mechanical energy. In this section the working principles of a DC (direct current) electric motor are provided, as well as a theoretical analysis of the governing equations which give the sizing requirements of an electric motor. It should be noted that, for the sake of simplicity, only direct current motors are investigated, as most of the commercially available motors for electric transportation are DC. All electric motors use a combination of permanent magnets and electromagnets which can be activated or deactivated as desired by controlling the flowing current. Firstly, a distinction has to be made between the more classic Brushed Direct Current and the Brushless Direct Current motors. The former use conductive brushes "to connect the power supply with the rotor"<sup>1</sup>, while the latter uses conductive wired coils around a metal instead. When a current is allowed to flow through the coils, an electromagnet is generated and the rotating part (called the rotor) starts its motion around the stator component. The current is controlled across all the electromagnets permanently through the so-called ESC, or Electronic Speed

<sup>1</sup><https://www.tytorobotics.com/blogs/articles/how-brushless-motors-work> [accessed 23-05-2022]

Controller, such that the rotation does not stop because of the alignment of the electromagnet with the permanent magnet. Hence, the induced rotation rotates the drive shaft, to which a propeller can be connected to provide the thrust. There are two typical types of electric motor architectures, namely inrunner and outrunner. The former has the rotor placed on the inside, as compared to the latter, which works the other way around, as depicted in Figure 7.1.



**Figure 7.1:** *Inrunner vs. Outrunner electric motor*<sup>2</sup>

A crucial parameter of the motor is its efficiency, which is defined as the ratio between the output mechanical power and the input electrical power. The difference between the two comes from the heat losses across the motor during the conversion to mechanical energy. In order to simplify the analysis, the latter can be modelled as a resistance.<sup>3</sup> This leads to the following two expressions for the mechanical and electrical power, respectively:

$$P_{mechanical} = T \cdot \omega_{rpm} \quad (7.2)$$

$$P_{electrical} = P_{mechanical} + I^2 \cdot R \quad (7.3)$$

which finally leads to

$$P_{electrical} = T \cdot \omega_{rpm} + I^2 \cdot R \quad (7.4)$$

where  $T$  is the produced torque,  $I$  is the current intensity and  $R$  is the equivalent internal resistance of the motor. The taken approach is to perform a market search for aviation used electric motors and to make a list out of the existing products which have been validated and successfully used in aircraft applications. The results of the search can be seen in Table 7.1.<sup>4</sup>

<sup>3</sup><https://www.tytorobotics.com/blogs/articles/brushless-motor-power-and-efficiency-analysis> [accessed 23-05-2022]

<sup>4</sup><https://www.tytorobotics.com/blogs/articles/brushless-motor-manufacturers-for-evtol-and-aviation> [accessed 29-05-2022]

**Table 7.1:** Available electric motors used in multiple applications including aviation

	Max Power [kW]	Max Torque [Nm]	Max Speed [RPM]	Max Voltage [V]	Peak Efficiency [%]	Max Weight [kg]
<b>magniX</b>	640	3020	2300	800	–	200
<b>Safran</b>	500	–	2200	–	–	–
<b>Emrax</b>	380	1000	6500	800	98	42
<b>H3X</b>	250	120	20000	800	95.7	15
<b>Siemens</b>	204	1500	1300	–	–	49
<b>YASA</b>	200	790	8000	700	95	37
<b>MGM COMPRO</b>	80	300	12000	800	95	22
<b>Pipistrel</b>	57.6	220	2500	400	–	22.7
<b>Thin Gap</b>	44	191	2200	726	–	4
<b>Plettenberg</b>	30	80	7000	140	95	6.5
<b>T-motor</b>	28	56	3134	100	–	5.2
<b>MAD Components</b>	21	67	–	100	–	4.2
<b>ePropelled</b>	16	30	8000	72	94	3.1
<b>KDE Direct</b>	12.8	–	–	69.6	–	0.7
<b>Turnigy</b>	9.8	–	7800	52	–	2.5
<b>Alva Industries</b>	10	37	4000	–	95.4	2.8

Given the power requirement, it appears that magniX's and Safran's motors are the only ones capable of fulfilling it. However, it is not correct to consider the efficiency of only the motor itself, as the overall system also includes the propeller. An important aspect to note is that for such a motor-propeller combination, the torque and the rotational speed influence both of the components' efficiency [13]. In order to have an optimized propulsion system, the optimal combination of torque and RPM has to be found such that the overall efficiency is maximized. Thus, the following subsection presents the most important features of propellers. It should also be noted that the assumed efficiency of the electric motors used for the aircraft sizing iterations and power requirements is 95%, according to the study in [32].

### 7.1.2. Propeller Considerations

Propellers come in many different configurations related to number of blades, airfoil, diameter etc. As a first step towards deriving the sizing and operational requirements of the propellers, it is useful to find a first, crude estimate of their required efficiency. This can be done as presented in [14]. Thereby, if one knows the required engine power and the corresponding needed lift-to-drag ratio for the chosen cruise speed, the following equation can be utilised:

$$\eta_{prop} = \frac{W \cdot V_{\infty}}{(L/D)_{cruise} \cdot P} \quad (7.5)$$

with  $W$  being the aircraft's weight at the beginning of the cruise phase. Since that's the biggest weight during cruise and required efficiency is proportional to the weight making it the critical design point for the cruise phase.  $P$  is the required cruise power,  $V_{\infty}$  the cruise speed and  $(L/D)_{cruise}$  being the lift to drag ratio, as obtained from the wing and power loading diagrams elaborated in Chapter 4. Using the values of 55160.5  $N$  (it is assumed that the mass at the beginning of the cruise phase is equal to MTOW, since the mass of hydrogen is estimated to be very small compared to the total weight), 1021.6  $kW$ , 475  $\frac{km}{h}$  and 13.4, respectively, a propeller efficiency requirement of at least 53.3% is estimated. Hence, in a worst case scenario the propellers would have to be used in a configuration in which they are at least this efficient.

Next, there are certain propeller parameters which are of particular interest in terms of which the efficiency can be expressed, as described in [15].

**Advance ratio - J**

This parameter simply represents the forward distance travelled by the propeller during one full revolution and is given by the following formula:

$$J = \frac{V}{n \cdot D} \quad (7.6)$$

where V is the aircraft speed, n is the rotational speed in revolutions per second and D is the propeller diameter.

**Power coefficient -  $C_P$** 

The power coefficient is given by:

$$C_P = \frac{P}{\rho \cdot n^3 \cdot D^5} \quad (7.7)$$

with P being the shaft power,  $\rho$  the air density and n and D are the same as for the advance ratio.

**Thrust coefficient -  $C_T$** 

The thrust coefficient is given by:

$$C_T = \frac{T}{\rho \cdot n^2 \cdot D^4} \quad (7.8)$$

with T being the thrust and  $\rho$ , n and D are the same as before.

With these parameters, the following analyses can be investigated. Firstly, one can inspect for a certain propeller model its efficiency map, which is a plot containing curves of constant efficiencies against the advance ratio and/or power coefficient [14]. However,  $C_P$  is a function of J, relation which has to be found again in the specifications of a specific propeller model. After a certain desired point on the efficiency map is selected, it is important to also check if at the efficiency associated with that point enough thrust is generated, such that the drag is counteracted. The thrust can be straightforwardly obtained through the following relation containing the propeller efficiency, the engine power in Watts and the aircraft speed in m/s:

$$T = \frac{\eta_{prop} \cdot P_{engine}}{V_{cruise}} \quad (7.9)$$

from which, using the assumed propeller efficiency of 0.85, the cruise speed of  $475 \frac{km}{h}$  and the power requirement of 1021.6 kW in cruise, a required thrust of 6581 N is obtained.

Finally, as stated before, the optimum point between the applied torque and the rotational speed of the propeller has to be found. However, this analysis is deemed too detailed given the time and resources available to the group within the DSE (it requires very specific data which is difficult to obtain from the manufacturers). Hence, another approach will be taken, as a result of which the initial sizing and some performance parameters will be obtained for the required propeller. The discussion covers the propeller diameter and efficiency, the number of blades, the type of propeller (variable/fixed pitch), the blade tip speed and noise, as well as matching the propeller with the electric motor at the end, by choosing a suitable candidate for both components.

**Propeller efficiency**

In order to size the propeller of the aircraft, it is necessary to start by estimating certain parameters, as otherwise there are too many variables and arriving at a converged design without making certain assumptions first would be almost impossible. Hence, in order to perform the initial sizing of the aircraft, as part of the class II

weight estimation the efficiency of the propeller was assumed to be 0.85, which is in accordance with the available literature and current trends.<sup>5 6</sup> The power requirement of 1021.6 kW during cruise is thus based on this efficiency, so this is the final value that the propeller should be designed for.

### Propeller diameter and RPM

As far as finding a suitable diameter and an operating rotation rate is concerned, this is done using the advance ratio, as propellers are designed around this parameter, since it directly affects their efficiency. Hence, first iterations were made on the required rpm of the propeller for a range of values for the diameter and the advance ratio and at the desired cruise speed of  $475 \frac{km}{h}$ , in order to get an estimate of some feasible limits on all the parameters. In the next phase the matching of the propeller with the electric motor is done, which is further discussed in Subsection 7.1.3. In this stage, an electric motor is chosen and its operational rpm limits are used to find a suitable propeller, along with checking whether the investigated propeller(s) would operate within their design space.

### Type of propeller

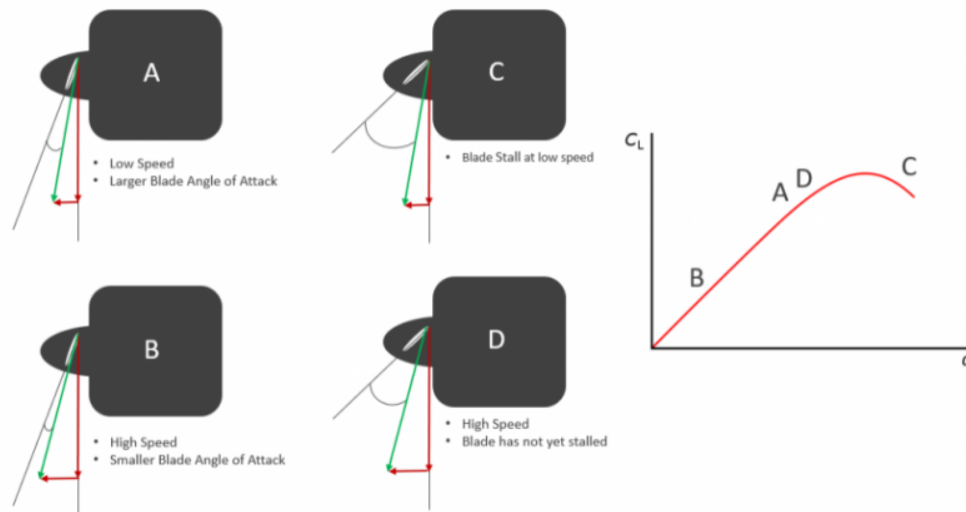
Propellers can generally be divided in four categories: fixed pitch, ground adjustable pitch, variable pitch and constant speed propeller. The first two are pretty self-explanatory, while the latter two bring more complexity to the design. The variable pitch propellers are adjusted in flight to maximize their performance during different flight phases with different requirements. The constant speed propeller makes use of a so-called speed governor to maintain a constant rotation rate irrespective of the airspeed, engine setting and altitude.<sup>7</sup>

As seen in Figure 7.2, the effect of increasing aircraft speed is a reduction in the effective angle of attack seen by the air flow on the propeller blades, for a set pitch. If the pitch is too high at a low speed, the blade will stall. If, on the other hand, the pitch is too fine at a relatively large speed, the effective reduction of the angle of attack causes the blade to shift too much down on the lift curve. Consequently, less thrust is produced with increasing velocity. In the group's case, the design is driven by the cruise power requirement and the cruise speed, so adapting the propeller design decisions to this flight phase is crucial. However, special attention needs to be paid to maintaining a fine balance between all of the operational phases, since the two propellers have a fixed pitch. Hence, a low pitch is required during the take-off phase in order to compensate for the reduced airspeed through a higher rotational speed. In contrast, the cruise phase is characterized by a high airspeed, for which a coarser pitch is needed in terms of efficiency. The climb phase consequently requires a pitch somewhere between the previous two.

<sup>5</sup><https://aerotoolbox.com/thrust-cruise-speed/>[accessed 30-05-2022]

<sup>6</sup>[http://www.epi-eng.com/propeller\\_technology/selecting\\_a\\_propeller.htm](http://www.epi-eng.com/propeller_technology/selecting_a_propeller.htm)[accessed 30-05-2022]

<sup>7</sup><https://aerotoolbox.com/thrust-cruise-speed/>[accessed 30-05-2022]



**Figure 7.2:** Effective blade angle of attack for different pitch and speed configurations<sup>8</sup>

All of the options come with advantages and disadvantages. Both the fixed pitch and the ground adjustable pitch propellers are less complex and require no systems for adjusting the RPM or the pitch, at the cost of reduced performance. While there are many aircraft using fixed pitch propellers, such as Cessna 172, Tecnam P-92 Echo and Piper PA-28-140 Cherokee<sup>9</sup>, these are relatively small aircraft compared to the designed aircraft and their cruise speed is much lower. Hence, their power requirements are considerably smaller and the expected range of conditions (mainly different advance ratios) the propellers have to operate in is relatively narrow. Thus, the decision here is that a variable pitch propeller design (it may also be a constant speed one) is the natural choice for an aircraft flying up to  $475 \frac{km}{h}$ . The propellers need to maintain adequate capabilities across a wider range of advance ratios, which requires constant changes in the pitch until reaching the cruise altitude.

### Number of propeller blades

Another crucial propeller parameter that needs to be estimated at this stage is the number of blades to be used, which, together with the chord of each blade and with the diameter, gives the effective propeller area, which in turn directly affects the conversion of power into thrust.<sup>10</sup> According to the same source, aircraft requiring more power tend to have more blades, which can also be verified by experience. For example, a Cessna 172 only uses 2 blades, like most general aviation aircraft. In contrast, the Piaggio P180 Avanti, which is still a small aircraft, uses 5 blades for each propeller. While this effective area can be increased also by increasing the diameter or the chord of the blades, these options come with limitations, such as ground clearance, (trans)sonic tip speeds and efficiency reduction because of blade interactions. Since most similarly sized twin-engine propeller business aircraft have 4-5 blades per propeller, it is decided to go for a similar blade number for the Sustainable Air Taxi as a preliminary estimate.

### Propeller efficiency vs. Advance ratio

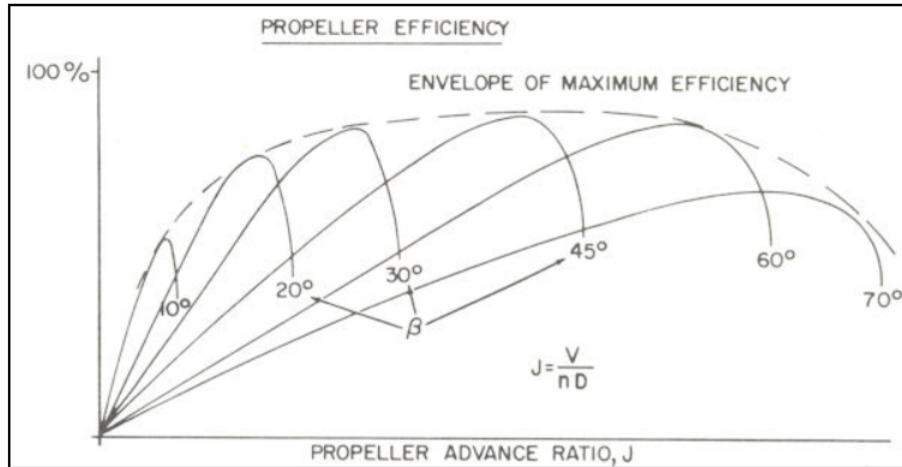
Another crucial aspect to consider is the variation of the propeller's efficiency with the advance ratio  $J$ , introduced above. Typical such curves look like the ones depicted in Figure 7.3, for multiple blade pitch values. As can be seen, there is a peak efficiency for a certain advance ratio, after which further increasing the airspeed or decreasing the rotation speed of the blades results in a sudden loss in efficiency, and thus in thrust. This is why the aircraft should be equipped with propellers with an efficiency of at least 0.85 at an advance ratio obtained at the cruise speed of  $475 \frac{km}{h}$  and the cruise rotation speed. The latter parameter has to be chosen in accordance

<sup>9</sup><https://aerotoolbox.com/thrust-cruise-speed/> [accessed 30-05-2022]

<sup>10</sup><https://aerotoolbox.com/thrust-cruise-speed/> [accessed 30-05-2022]



with the selection of the electric motor, which is further discussed in Subsection 7.1.3.<sup>11</sup>



**Figure 7.3:** Variation of propeller efficiency with advance ratio, for multiple pitch settings (general example for visualisation purposes)

### Propeller tip speed

Another important parameter which could have a negative impact on the efficiency of the propeller if not properly investigated is the speed felt by the blades at their tips. If the tips operate at a speed higher than the one associated with the peak efficiency the sudden loss of efficiency could lead to a big loss of thrust.<sup>12</sup> The tip speed can be obtained via the following equation:

$$V_{tip} = \sqrt{V_{trans}^2 + V_{rot}^2} \quad (7.10)$$

where  $V_{trans}$  is simply the aircraft speed and  $V_{rot}$  is the rotational speed of the propeller, given by:

$$V_{rot} = \pi \cdot D \cdot rps \quad (7.11)$$

with  $rps$  being the revolutions per second. Generally, for metallic or composite propellers using thin airfoils towards the tips a typical limit for the tip speed is  $M = 0.9$ .<sup>13</sup>

### Propeller noise

As far as the noise of the propeller is concerned, this can be analysed qualitatively by comparison with the reference chosen aircraft fitted with the same propellers the Air Taxi will use, as presented in Subsection 7.1.3. A quantitative analysis is not considered in this report because of time and resource limitations concerning the available data on the propeller model.

### 7.1.3. Matching the Propeller with the Motor

As the power requirement of 1021.6 kW (or 511 kW per engine) obtained through the preliminary sizing process is rather high, at least when considering the desired cruise speed of 475  $\frac{km}{h}$  (for example, the Piaggio P180 Avanti has 2 engines producing 634 kW each for a cruise speed of over 700  $\frac{km}{h}$ <sup>14</sup>), the two electric motors have to be very potent from this perspective. A research of the available market, as presented in Subsection 7.1.1, pointed the group in the direction of MagniX's magni650 electrical power unit (EPU). This is capable of producing a maximum of 640 kW and a nominal continuous power of 560 kW, which satisfies the requirement. In total, the two EPU's dry mass is 400 kg.<sup>15</sup> Moreover, the operational limit for the motor's rotational rate is

<sup>11</sup>[http://www.epi-eng.com/propeller\\_technology/selecting\\_a\\_propeller.htm](http://www.epi-eng.com/propeller_technology/selecting_a_propeller.htm)[accessed 30-05-2022]

<sup>12</sup>[http://www.epi-eng.com/propeller\\_technology/selecting\\_a\\_propeller.htm](http://www.epi-eng.com/propeller_technology/selecting_a_propeller.htm)[accessed 30-05-2022]

<sup>13</sup><https://www.kitplanes.com/wind-tunnel-52/>[accessed 30-05-2022]

<sup>14</sup><http://www.avantievo.piaggioaerospace.it/>[accessed 30-05-2022]

<sup>15</sup><https://www.magnix.aero/services>[accessed 30-05-2022]



1200-2300 *RPM*, while the nominal and maximum continuous torque the company claims are 2820 and 3020 *Nm*, respectively. The motor's capabilities were demonstrated through flights of aircraft converted to electric propulsion, in which the slightly less powerful magni500 motor was used on both a DHC-2 Beaver and a Cessna Grand Caravan.<sup>16</sup> Moreover, Eviation's Alice aircraft will feature the group's chosen model of electric motor.<sup>17</sup>

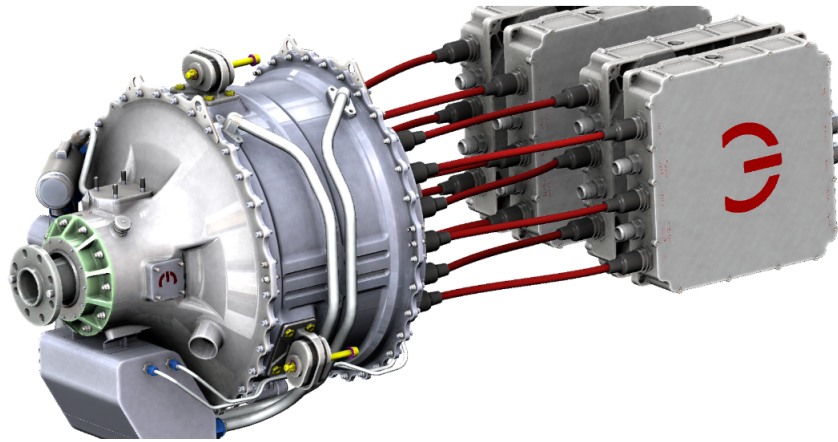


Figure 7.4: magni650 electric motor

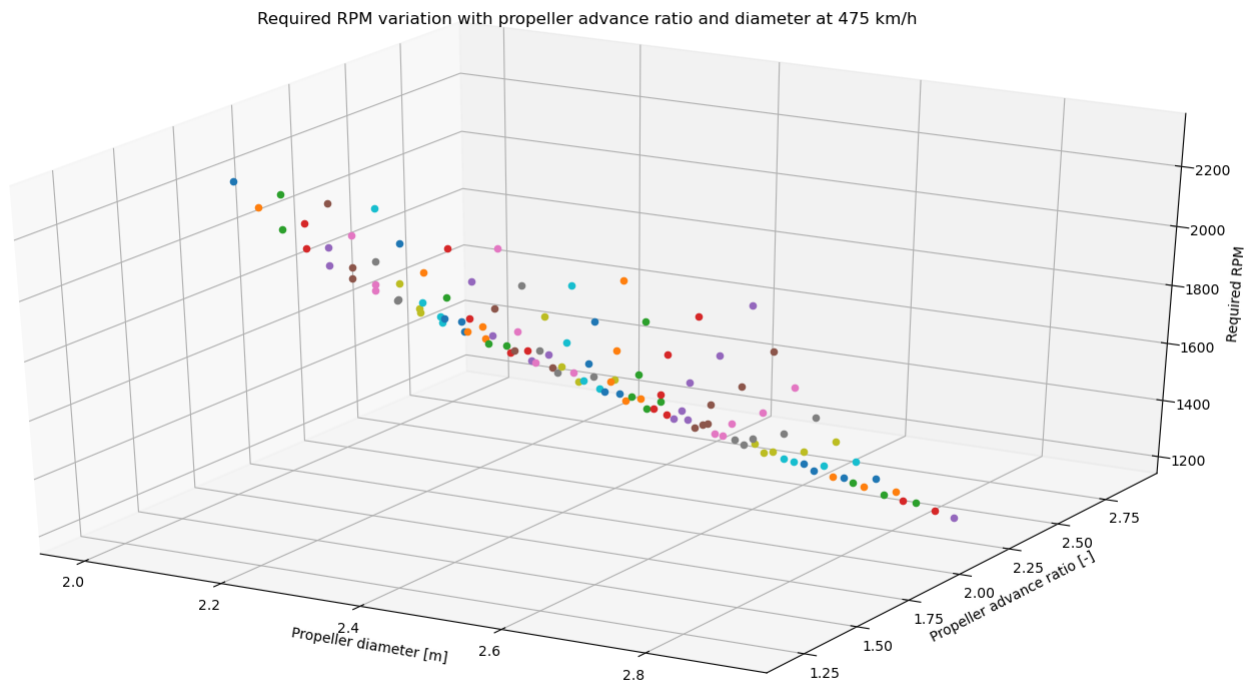
One aspect which should be further taken into consideration in the future is the fact that, according to the capabilities of the magni motor and the shaft power requirement of 511 *kW* per engine, the motors would operate at a lower power output than the nominal one of 560 *kW*. However, generally motors are not damaged if they operate at a lower voltage than the rated nominal one.<sup>18</sup> Hence, the magni650 motor remains a feasible option as long as no other electric motor exists on the market which is better tailored to the Air Taxi's requirements.

As a result, this choice imposes some limits within which the propellers should operate. Firstly, the propellers should operate within the specified rotational rates while maintaining the necessary efficiency of at least 0.85 at speeds up to the cruise speed. Moreover, the torque range at which the motors operate must translate into an appropriate torque in the propeller, such that they generate enough thrust at the given aircraft speed and *RPM*. In order to make a start, some parameters need to be estimated. These are the propeller diameter and the advance ratio, as explained in Equation 7.1.2, in order to find a realistic range of values for which rotational rates between 1200 and 2300 *RPM*, as dictated by the electric motor. After having consulted the aircraft catalogue available on the website of Hartzell Propeller Inc. [51] for aircraft with similar power capabilities, the range between 2 and 3 metres is chosen for the iteration on the propeller diameter. Moreover, the advance ratio is also iterated using values between 1 and 3, which is a rather large range which is chosen in order to have a complete overview of how the required rpm scales with this parameter. The iteration is performed using a step of 0.1 for both the propeller diameter and the advance ratio (as no additional value was added for smaller steps, since the variations were too small between two consecutive steps), using the specified cruise speed. The analysis yields the results presented in Figure 7.5.

<sup>16</sup><https://www.futureflight.aero/news-article/2021-06-18/magnix-expands-power-options-350-kw-and-650-kw-electric-propulsion-units>[accessed 02-06-2022]

<sup>17</sup><https://www.eviation.co/aircraft/>[accessed 02-06-2022]

<sup>18</sup><https://www.motioncontroltips.com/faq-can-dc-motors-run-lower-than-nominal-voltage/>[accessed 02-06-2022]



**Figure 7.5:** Required RPM vs. propeller advance ratio and diameter at 475  $\frac{km}{h}$

As can be seen from Figure 7.5, there is a wide range of plausible operating points for the propeller for the given RPM range from the motor. The next step is to perform a search for existing propeller aircraft whose propellers' diameters are within the specified range and operate within the specified range of advance ratios. An interesting option is found in Beechcraft's Super King Air 350 aircraft, which uses a constant-speed, feathering, 4-blade aluminium propeller with a diameter of approximately 2.67 m (propeller model as given by manufacturer is HC-B4MP-3C), as described in the same aircraft manual used before, weighing in total approximately 160 kg. It should be noted that Hartzell Propeller Inc. are currently offering new propellers with better performance for their clients, such that some King Air 350 may already have composite blades. However, as the goal of this DSE is to design a highly recyclable aircraft, the old aluminium option is preferred, since composites prove to be impossible to recycle without too much downcycling with current technology. Also, the chosen propeller is certified for 6000 operational hours (lower than the general lifetime of an aircraft), so it is expected that they will be changed multiple times during the operational life of the Air Taxi, making the aluminium a suitable feature. Given the King Air's cruise speed of 560  $\frac{km}{h}$  and the propeller RPM of 1500 at cruise<sup>19</sup> it is easily calculated through Equation 7.1.2 that this propeller should be operated in cruise conditions under an advance factor of 2.3. Therefore, by inspecting Figure 7.5 once again, one can find a suitable point which lies at this advance ratio. It is found that a combination between a diameter of 2.67 m (the dimension of the analysed propeller model) and 1270 RPM gives the desired advance ratio.

To check whether this propeller satisfies all of its requirements, it is also crucial to check the thrust it produces and the tip speed. Starting off with the most straightforward one, the tip speed is easily computed using Equation 7.10 and Equation 7.11, which yield a tip velocity of 221.2  $\frac{m}{s}$ , which, at the cruise altitude of 5000 m is equivalent to  $M = 0.69$ . Being far below the sonic and transonic regions, no negative effects are expected because of this. Hence, because of this low tip speed, the noise produced by the interaction of the propellers with

<sup>19</sup><http://krepelka.com/fsweb/learningcenter/aircraft/flightnotesbeechkingair350.htm> [accessed 02-06-2022]

the flow is expected to be reduced, as the propeller noise is a function of this parameter [48]. The average cabin and cockpit noise levels of the King Air 350 are 81 dB and 85.5 dB, respectively<sup>20</sup>, but this corresponds to the 1500 RPM propeller rating. Because of the lower operational rotation speed expected for the Air Taxi, these values are expected to be lower. Furthermore, another contributing factor to the noise reduction is the electric motor design, which is inherently quieter than the King Air's combustion engines.

As far as the produced thrust is concerned, first the required thrust in cruise conditions has to be estimated, followed by a calculation of the thrust this propeller produces in the cruise conditions of the King Air 350. The former was computed already in Subsection 7.1.2 and has a value of 6581 *N* for the assumed propeller efficiency of 85%. The latter can be obtained from the same equation using the specifications of the reference aircraft. According to the company's website<sup>21</sup>, the flat-rated shaft power of each engine is 1050hp, or 783 *kW*. Assuming the same 85% efficiency and using a cruise power setting of 66% with the propeller operating at 1500 RPM and  $560 \frac{km}{h}$ <sup>22</sup> this results in a thrust of 5647 *N*. Hence, it can be seen that the thrust required for the Air Taxi is considerably higher. However, the thrust is the result of the combination of RPM, thrust coefficient, air density and propeller diameter, according to Equation 7.8. Plugging the values for the King Air's and the Air Taxi's cruise thrust (using the corresponding air densities for 9144 *m* -  $0.46 \frac{kg}{m^3}$  - and 5000 *m* -  $0.736 \frac{kg}{m^3}$  -, respectively, and the aforementioned required rotational speeds of the propellers) one gets required thrust coefficients of 0.194 and 0.196, respectively. This is a very good result, because this means that the Hartzell 4-blade propellers would have to operate at almost the same thrust coefficient. This also make sense from the perspective in [17], which states that the thrust coefficient is a function of the advance ratio and the Reynolds number, with the latter's effects usually being neglected. Thus, this proves the statement, considering the very tiny difference between the two obtained coefficients.

In a similar manner, the power coefficient can be obtained through Equation 7.7, using the corresponding cruise power requirements per engine for the King Air and the Air Taxi of  $0.66 \cdot 783 \text{ kW} = 517 \text{ kW}$  and 511 *kW*, respectively. The obtained results are a power coefficient of 0.531 for King Air 350 and 0.539 for the Air Taxi. Again, these values are very close to each other, reconfirming the statements made above.

However, the analysis made above assumed that the propeller of the Super King Air 350 can deliver the required thrust at 1270 *RPM*. This is because the  $C_T$  value was obtained assuming that this propeller has an efficiency of 85% at the King Air 350's cruise advance ratio of  $J = 2.3$ . This value for the efficiency can be somewhat validated through the results obtained in [36], even though much lower advance ratios are considered in this paper (the values obtained in the paper are around 90%, meaning that the assumption on the efficiency is actually conservative). Consequently, the propeller must have a thrust coefficient of approximately 0.19 and a power coefficient of 0.53 at the same specified advance ratio of 2.3. In absence of any additional data, such as an efficiency map like the one in Figure 7.3, it is impossible to tell with the available resources whether this assumption is valid or not. Additionally, the pitch angle for which this efficiency would be achieved at the cruise advance ratio is an unknown, but these aspects are considered part of a future, more in-depth analysis, at a later design stage, which is outside the scope of this report.

<sup>20</sup><https://kingairmagazine.com/article/technically-29/> [accessed 03-06-2022]

<sup>21</sup><https://beechcraft.txtav.com/> [accessed 02-06-2022]

<sup>22</sup><http://krepelka.com/fsweb/learningcenter/aircraft/flightnotesbeechkingair350.htm> [accessed 02-06-2022]



**Figure 7.6:** *Demonstration of compatibility between the magni650 motor and a Hartzell 4-blade propeller<sup>23</sup>*

## 7.2. Fuel Cells

The main power for the electric propeller propulsion will be provided using hydrogen fuel cells. Based on the power needed for powering the electric engine and creating sufficient thrust for the Air Taxi, stated in Section 7.1, the fuel cells are chosen.

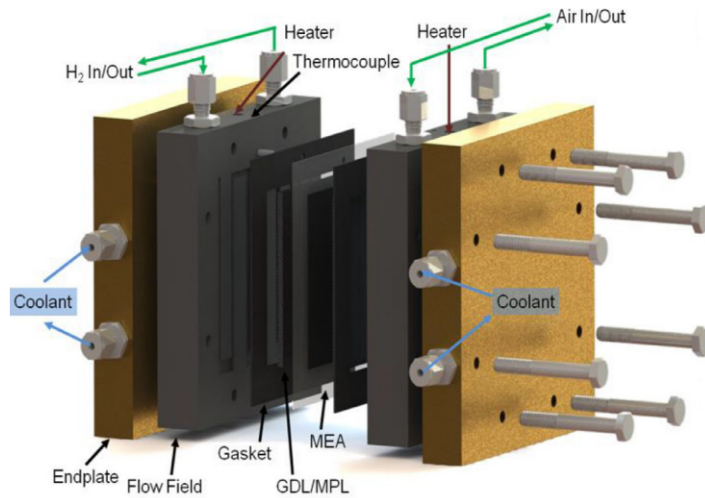
Hydrogen fuel cells are not a new technology and they have been known to work since even the 1800's. The fuel cells found use in the automotive industry since the 1960's as well as in the space industry, being used on small satellites and other space vehicles. Although, they were being used and developments were being made constantly, their efficiency was not enough to solely power an aircraft. This was the case until the late 2000's, when it was demonstrated that it can be used for manned aircraft with the development of the Boeing Fuel Cell Demonstrator.<sup>24</sup> The development of the fuel cells has lead to several types of technologies to be used in different industries<sup>25</sup> such as polymer electrolyte membrane fuel cells, direct methanol fuel cells, alkaline fuel cells, solid oxide fuel cells. Out of these types, the one that was proven to be the most suitable for transportation is the polymer electrolyte membrane fuel cell (PEMFC).

### 7.2.1. Fuel cell operation

Polymer electrolyte membrane fuel cells usually contain the following elements: membrane electrode assembly (MEA), a catalyst layer (CL), a gas diffusion layer (GDL) with a micro-porous layers (MPL) on the catalyst layer side, gas flow channels (GFC) and finally bipolar plates (BP). The whole structure of the PEM fuel cell can be observed in Figure 7.7.

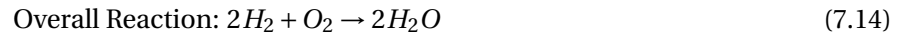
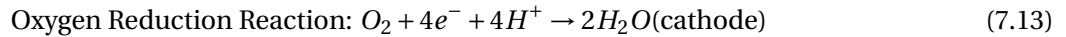
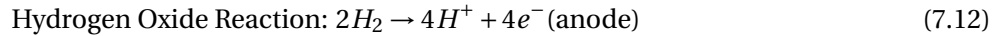
<sup>24</sup>[https://www.boeing.com/news/frontiers/archive/2008/may/ts\\_sf04.pdf](https://www.boeing.com/news/frontiers/archive/2008/may/ts_sf04.pdf) [accessed 23-05-2022]

<sup>25</sup><https://www.energy.gov/eere/fuelcells/types-fuel-cells> [accessed 20-05-2022]



**Figure 7.7:** Structure of a PEMFC [5]

In PEM fuel cells, the usual oxidizer is ambient air. In addition, hydrogen gas is used because of its rapid reactivity. In the fuel cell structure, the hydrogen represents the anode part, while the oxygen from the ambient air is the cathode. Inside the fuel cell, the following electrochemical reactions occur:



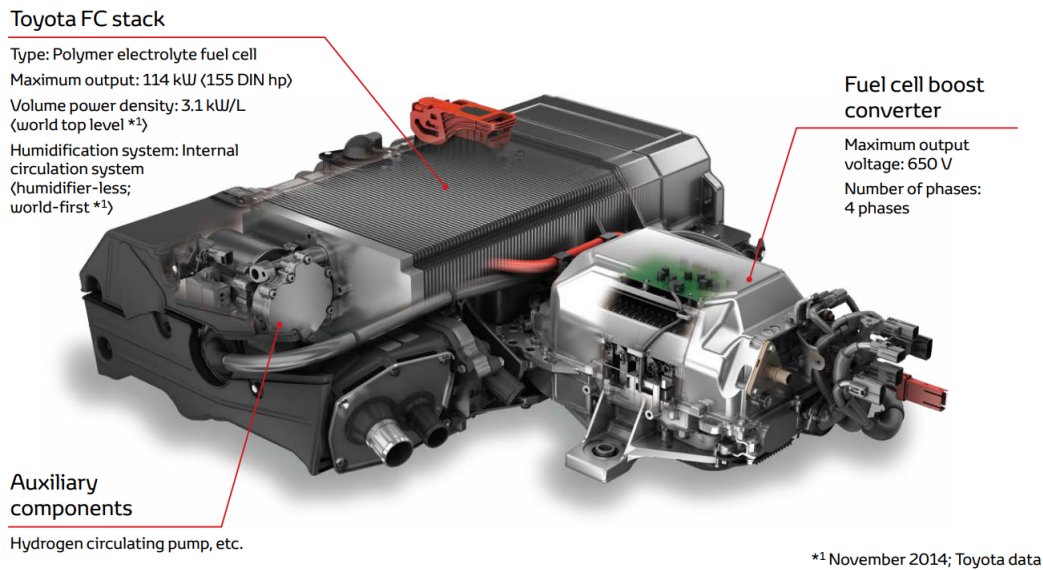
The theoretical maximum efficiency of this reaction comes out at  $\eta_{FC,max} = 83\%$ . This efficiency considers a perfectly reversible process, but in reality this cannot happen, so the real efficiency, for automobile fuel cells comes down to around  $\eta_{FC} = 60\%$ , while using high purity hydrogen. In real life integration however, the efficiency as of 2022 sits around 45 – 50%, and it can be used approximately at 50%.

As fuel cell technology is advancing, more and more development is being done towards increasing the efficiency and the power output compared to the fuel cell's mass and volume. Companies such as Toyota, want to implement hydrogen based propulsion systems on their cars and have already done that.<sup>26</sup> As of right now, the average fuel cell power density is approximately  $2000 \frac{W}{kg}$  and  $3100 \frac{W}{L}$  Figure 7.8[12] with state-of-the-art fuel cells sitting at more than this. Companies are making steady progress towards more efficient fuel cells and further information from an expert working for the propulsion department of Technical University of Delft showed that the stack specific power may increase up to approximately  $4000 \frac{W}{kg}$  and  $5000\text{-}5400 \frac{W}{L}$  in the next 5 to 10 years[45].<sup>27</sup> This proves that a  $3000 \frac{W}{kg}$  and  $4150 \frac{W}{L}$  is a good future approximation for the power density of the fuel cell that will be used.

<sup>26</sup><https://www.toyota-europe.com/world-of-toyota/feel/environment/better-air/fuel-cell-vehicle> [accessed 23-05-2022]

<sup>27</sup><https://fuelcellworks.com/news/horizon-automotive-pem-fuel-cells-to-set-300kw-benchmark/> [accessed 01-06-2022]

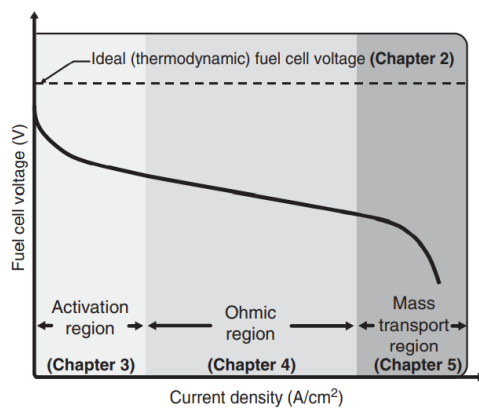




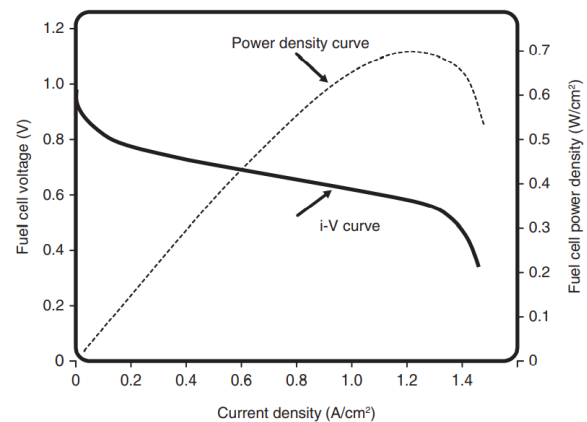
**Figure 7.8:** Toyota Mirai engine design as of 2014<sup>28</sup>

Engines as the one presented in Figure 7.8 lead the market for fuel cell powered electric vehicles in which Toyota is a leader. Thus, similar numbers can be considered for implementation in aviation, but a more detailed discussion shall be performed regarding, operating temperature, fuelling, air intake and performance of this type of fuel cells.

Besides the efficiency and power densities of the fuel cells, other aspects have to be discussed and analysed such as the current-voltage characteristics. In an ideal system from a thermodynamic point of view, the fuel cells can generate any current at a constant voltage dictated by thermodynamics. In reality this phenomenon does not happen as in the fuel cell operations voltage drops appear. This idea is graphically represented in Figure 7.9[33].



**Figure 7.9:** Ideal and real i-V curve for a generic PEMFC[33]



**Figure 7.10:** Combined i-V curve and power density curve for a generic fuel cell[33]

In Figure 7.9 three different regions can be observed; they correspond to the three major types of fuel cell voltage losses. These losses give the characteristic shape of the i-V curve and can be defined as such:

- Activation losses (losses due electrochemical reaction)
- Ohmic losses (losses due to ionic and electronic conduction)

- Concentration losses (losses due to mass transport)

The real output voltage for a fuel cell is defined by Equation 7.15

$$V = E_{thermo} - \eta_{act} - \eta_{ohmic} - \eta_{conc} \quad (7.15)$$

where  $E_{thermo}$  is the thermodynamically predicted fuel cell voltage output and the three  $\eta$  are the losses defined earlier[33].

In a general manner, the maximum voltage output of a fuel cell is limited to 1 V, but accounting for the efficiencies and losses, in a real life operation sweet spot for the PEMFC cell voltage is around 0.6 V with an efficiency of 50%. As it is seen in Figure 7.10, this voltage corresponds to a current density of approximately  $1 \frac{A}{cm^2}$  and a power density of  $0.6-0.65 \frac{W}{cm^2}$ . However, if for the fuel cell system a state-of-the-art architecture that may be developed in the next 5 years is considered, such as the one that the Wright Electric company plans to construct[46], then this further implies that the voltage and current will also increase and they can be considered at 0.7 V with around  $1.2 \frac{A}{cm^2}$  resulting in a power of  $0.84 \frac{W}{cm^2}$ .

### 7.3. Air compressor

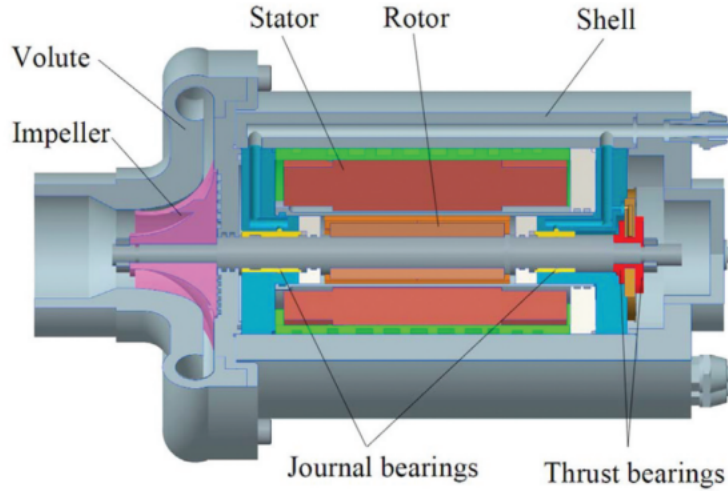
As stated in the Section 7.2, the PEMFC also needs an air intake such that Equation 7.12 and Equation 7.13 are satisfied. The designed aircraft will fly at an altitude of 5000 m, where the air density is lowered to around 50% compared to sea level. This means that in order to provide the necessary oxygen to the fuel cell systems, compressors have to be used.

#### 7.3.1. Air supply system

The air for the fuel cell will be provided by means of a fuel cell air supply (FCAS). The FCAS contains several elements that aid with the air supply, such as a compressor, a compressor engine, an air filter and optionally an expander system. The use of a compressor is needed as the atmosphere contains less oxygen when increasing the altitude. Such, the altitude was chosen to 5000 m as at this altitude the aircraft can fly efficiently with a relatively light weight compressor system.

The fuel cells are sensitive systems that do not allow for impurities such as solids, oil or even some chemical substances to enter. Getting rid of the solid particles from the air can be done via a filtering system, while for the latter, oil free compressors may be used. Some examples of such compressors are: the scroll compressor, the screw compressor, and the centrifugal compressor. The first two compressors are positive displacement compressors while the latter represents a dynamic one[21]. These compressors were tested for the PEMFC application and several aspects were found.

For the scroll and screw compressors, water can be used, which would satisfy the humidity needed for the fuel cell membrane, but this implies that their rotational speeds should decrease and such their volume and mass increase. This would not be suitable for an aircraft application. The centrifugal compressor is characterized by high speeds that can get up to 100,000 RPM[21], which further decreases the volume and mass needed for an efficient compression. Additionally, it also has low noise, high efficiency and high reliability, which makes it a splendid candidate for the aircraft design. The centrifugal compressor has: high rotational speed, high mass flow, high pressure ratio, small volume/weight



**Figure 7.11:** Centrifugal Compressor [21]

Several aspects related to the centrifugal compressor have to be calculated. From literature, the following formulas were found[23]:

$$\text{Air usage} = 3.57 \cdot 10^{-7} \lambda \frac{P_c}{V_c} [\text{kg} \cdot \text{s}^{-1}] \quad (7.16)$$

where  $\lambda$  represents the stoichiometric ratio of air,  $P_c$  is the power that the fuel cell should generate and  $V_c$  the voltage that each cell in a fuel stack produces.

$$\text{Compressor power} = c_p \frac{T_1}{\eta_c} \left( \left( \frac{P_2}{P_1} \right)^{\frac{\gamma-1}{\gamma}} - 1 \right) \dot{m} [\text{W}] \quad (7.17)$$

where, for air  $c_p = 1004 \text{ J} \cdot \text{kg}^{-1} \cdot \text{K}^{-1}$  and  $\gamma = 1.4$ ,  $\eta_c$  is the compressor efficiency,  $P_1$  the atmospheric pressure,  $P_2$  the pressure at the outlet, and  $\dot{m}$  is the air mass flow.

In addition to these equations, the oxygen and hydrogen mass flows may also be calculated based on Equation 7.18 and Equation 7.19.

$$\dot{m}_{O_2} = \frac{M_{O_2} P_{elec} \lambda}{4 V_c F} \quad (7.18)$$

The oxygen mass flow may be divided by 0.235, which is the relative percentage of oxygen in air based on the molar masses for an altitude of 5000 *m*, such that the air mass flow may be found.

$$\dot{m}_{H_2} = \frac{M_{H_2} P_{elec} \lambda}{2 V_c F} \quad (7.19)$$

Based on the power that the fuel cell should generate, the air flow and compressor power requirement will be calculated and further sized. As a preliminary sizing, usually, this type of compressor uses around 20% of the power generated by the fuel cell stack.

The centrifugal compressor is the most efficient type for a mobile application such as the Sustainable Air Taxi. The high rotational speed allows for low volume and weight compared to other types. In addition its operation does not require oiled components, working on magnetic or gas bearings. Finally they can be very energy efficient especially in combination with an expander system. It's efficiency can be considered to be in the range  $\eta_c = 0.65 - 0.7$  and it can compress the air up to the needed pressure for the fuel cell operation. As the atmospheric pressure for the flight conditions is equal to approximately 0.5 *bar*, a higher pressure ratio can be considered, in the range of 2 to 3, resulting in an outlet pressure between 1 and 1.5 *bar*[35].



### 7.3.2. Compressor power requirement

The compressor that will be used for pushing air in the fuel cell is a centrifugal compressor. For this type of compressor Equation 7.16 and Equation 7.17 are used. In this case a compressor efficiency of 0.68 are used with a cell voltage of 0.7. Further, the atmospheric temperature,  $T_1$  is  $-20\text{ }^\circ\text{C}$  or  $253\text{ K}$  and the atmospheric pressure is around  $0.5\text{ bar}$  at  $5000\text{ m}$  altitude[23]. With a fuel cell power requirement of  $2034\text{ kW}$ , the compressor power comes out to  $98\text{ kW}$  per fuel cell so  $196\text{ kW}$  in total. This comes out to around 10% of total power generated by one fuel cell stack.

### 7.3.3. Expander system

The compressor system consumes a relatively big proportion of the power generated by the fuel cell, and this can further decrease the overall efficiency of the stack. This requirement can get up to 20% of the total power so a method of making the compressor more power efficient has to be considered. The main solution for this issue is the addition of a system that can recycle the exhaust generated by the fuel cell stack. This system represents a type of turbine that makes use of the output gasses and an expander system that further powers the compressor. A diagram for the implementation of such a system can be observed in Figure 7.12

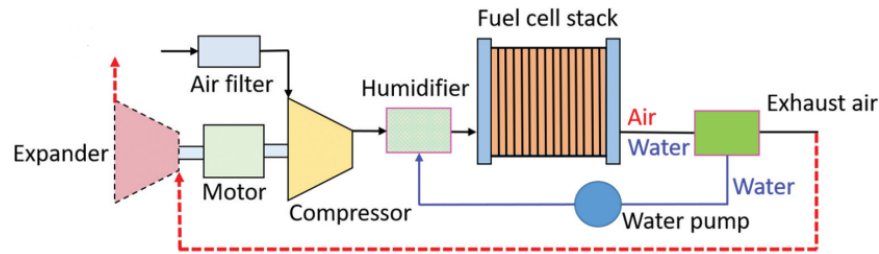


Figure 7.12: Diagram of implementation of an expander system [21]

As it can be seen, the expander system makes use of the exhaust air to power the smaller compressor engine. The efficiency improvement coming from this system can decrease the power usage by up to 14% [21]. The expander may add a more complicated structure and weight, but this will be balanced by the extra power created and the overall improvement to the efficiency.

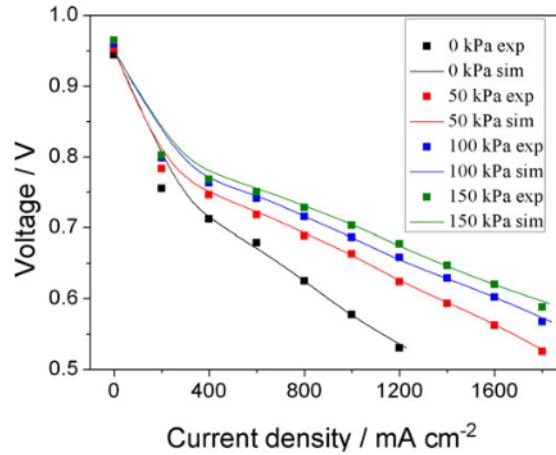
The exhaust air can be assumed to have the a mass flow close to the input at  $\dot{m} = 1.07\text{ kg} \cdot \text{s}^{-1}$ . In addition the input and output pressures can be considered as  $P_1 = 1\text{ bar}$  as stated in Subsection 7.3.1 and  $P_2 = 0.5\text{ bar}$  and the output temperature at around  $T_1 = 90\text{ }^\circ\text{C}$  [43]. Further, the heat capacity can be approximated as  $\gamma = 1.3$  and the specific heat capacity at  $c_p = 1100\text{ J} \cdot \text{kg}^{-1} \cdot \text{K}^{-1}$ . These values can be used in Equation 7.17 to calculate the recycled power that the expander system provides. The exist air flow rate can be calculated using Equation 7.20[23].

$$\text{Exist air flow rate} = (3.57 \cdot 10^{-7} \lambda - 8.29 \cdot 10^{-8}) \frac{P_e}{V_c} [\text{kg} \cdot \text{s}^{-1}] \quad (7.20)$$

## 7.4. Operational Pressure of Fuel Cells

Proton exchange membrane fuel cells work on the basis of the redox reaction of hydrogen. This reaction may be accelerated by use of different operational pressures inside the FC stack. In addition, the conductivity of the membrane can be improved by this pressure. As stated in Subsection 7.3.1 the inlet pressure if the fuel cell provided after the compressor is  $1\text{ bar}$ , thus research has been made to find the performance parameters of the fuel cell at this pressure. The efficiency of the fuel cell has been found to be strongly dependent on the operational pressure, influencing parameters such as the voltage and current outputs. Experimental values were found for the current density and the voltage of fuel cells based on several pressures ranging from  $0\text{ kPa}$  up

to 150 *kPa* and the graphical interpretation can be observed in Figure 7.13. It has to be noted that the exhaust temperature was 80 *C*°.



**Figure 7.13:** Experimental and simulated data for the current and voltage of a fuel cell operating at different internal pressures [34]

It is clear from Figure 7.13 that the difference between the pressures in the range 50-150 *kPa* is not massive, but it is still significant. Further research was found on the influence of pressure on the conductivity of the membrane electrode assembly. The membrane conductivity improvement is a bigger influence on the productivity of a fuel cell than the acceleration of the reaction. It was further found that for a low density ( $\leq 1000 \frac{mA}{cm^2}$ ) a pressure of 50 *kPa* has to be used while for high current density ( $\geq 1000 \frac{mA}{cm^2}$ ) a higher than 100 *kPa* pressure is needed [34]. Further, taking into consideration the humidity requirements and aspects of the fuel cell, and the power consumption of the other subsystems such as compressor or heating unit, it is found that the optimal pressure is placed higher at around 2-2.5 *bar* [35].

## 7.5. Humidifier

As stated before, the membrane in the PEMFC has to have a certain level of humidity to have sufficient proton conductivity for stable power generation and the necessary water can be provided from the outputs of the fuel cell stack, as a byproduct of this reaction is water, as observed in Equation 7.13. In case the quantity of water turns out to be insufficient for the humidity requirements of the membrane, a liquid water injector can be used, but this can prove to be difficult because of its complexity [22]. The water produced by the fuel cell can be calculated based on Equation 7.21 [23]

$$\text{Water production} = 9.34 \cdot 10^{-8} \frac{P_e}{V_c} [kg \cdot s^{-1}] \quad (7.21)$$

Several humidifying methods exist at the moment and are divided into internal and external humidification. The internal part can be implemented by using physical methods where the internal structure of the fuel cell can be changed or the operating conditions of the stack can be optimized; to have a fully efficient membrane humidification, these two methods can be combined. In addition to the internal physical methods, there are also chemical solutions, where the compositions of the membrane or the electrode can be changed and optimized. Finally, external humidification methods can be implemented into the fuel cell stack by gas bubbling humidifier methods, direct water injection, enthalpy wheel humidifier method or membrane humidifier method [29].

As the fuel cells that were presented until now are based on the information and design of the Toyota Mirai PEMFC, the same humidification solution can be further discussed. This design implements an internal humidification method that combines the physical stack structure improvements with the operating conditions optimization [30]. This concept works by recirculating the water generated in the cathode to the anode and distributing it on the membrane. This system has been created and optimized for the driving conditions of a

car, but the same concepts can be applied to the system to be implemented on the design of the sustainable air taxi. The team recommends that more solutions should be analysed and tested for implementation in aircraft, as this is outside the scope of the current design strategy.

## 7.6. Hydrogen re-usage

In addition to the water output that can be reused, some hydrogen will also be an output from the fuel cell stack. This happens because the reaction is not entirely perfect and some particles may not react at all, becoming an "exhaust" of this system. This unused hydrogen can be recycled and reused as input to the fuel cell. The diagram for this system can be seen in Figure 7.14.

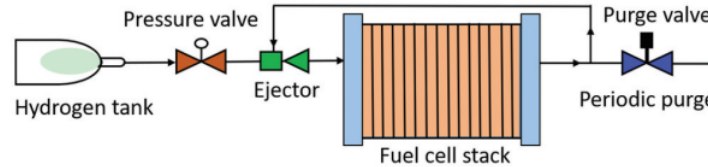


Figure 7.14: Hydrogen capturing and re-usage system [21]

In Figure 7.14 it can be seen that a purge valve is used after the fuel cell stack. This creates a system that is not too complex and also gives the necessary hydrogen pressure without making use of another compressor system. The purge will happen periodically after the exhaust hydrogen has reached the necessary pressure and thus it will automatically be added to the hydrogen fuel line. Further optimizations and calculations may be done in subsequent design stages that focus on more details of this subsystem.<sup>29</sup>

## 7.7. Temperature Control

When using the polymer electrolyte fuel cell system, the chemical reaction between the hydrogen and oxygen is not completely reversible which is why some energy will escape. This energy is transferred into latent heat of exhaust water vapour and in conventional heat. This heat can represent an issue for the effective functioning of the fuel cells and thus a cooling system is needed. The exhaust heat generated by the fuel cell stack can be calculated using Equation 7.22 and Equation 7.23. These equations already take into account the cooling effect of water evaporation[23].

$$\text{Heat rate} = nI(1.25 - V_c)[W] \quad (7.22)$$

$$\text{Heat rate} = P_e \left( \frac{1.25}{V_c} - 1 \right) [W] \quad (7.23)$$

In addition to the heat generated by the fuel cells, other temperature control systems may be needed such as heating for intake air; this has to be implemented as the air the fuel cells operate with has to have a certain temperature. This means that a heater system shall be placed after the compressor to prepare the air for entering the fuel cell system. The heater system can be a simple heating resistor as its temperature can be exactly controlled and the assembly is not too complex. In addition to this, the power needed to heat up this system is insignificant compared to the total power generated within the fuel cell stacks.

When considering cooling of the fuel cell system it has to be noted that the aircraft will be generating a relatively high power and such, it will also output a high quantity of heat. In order for the fuel cell stack to properly and efficiently function, this heat has to be controlled and kept around the 80 °C temperature. The cooling system of a PEMFC can be passive or active, the first one making use of natural convection of air against the

<sup>29</sup>[https://repository.lboro.ac.uk/articles/conference\\_contribution/A\\_fuel\\_cell\\_system\\_sizing\\_tool\\_based\\_on\\_current\\_production\\_aircraft/9221111](https://repository.lboro.ac.uk/articles/conference_contribution/A_fuel_cell_system_sizing_tool_based_on_current_production_aircraft/9221111) [accessed 01-06-2022]

external surface area or via the convection of the reactant and/or product gasses in the fuel cell[33]. A passive temperature control system cannot be adopted because the fuel cell stack to be used in the Sustainable Air Taxi generates a high quantity of power.

The active control system makes use of a different fluid than the reactant and products to regulate the temperature via forced convection or enhancing the passive forced convection by increasing the flow of reactant and product in the fuel cell. The active control system will be adopted for the fuel cell stack and such, auxiliary devices such as fans, blowers or pumps will be needed to recirculate the extra fluid[33]. As noted before, the active temperature control system makes use of an additional fluid. If the fuel cell was to generate power under 50 kW then air could have been used for the convection, but in this case, a deionized water-glycol mixture will be used. The water has to be deionized as to not be an electric conductor[33]. The efficiency of the cooling system can be defined using Equation 7.24[33]:

$$\text{Effectiveness} = \frac{\text{heat removal rate}}{\text{electrical power consumed by fan, blower, or pump}} \quad (7.24)$$

Usually, this efficiency is in the range of 20-40 for a well designed system, thus, it can be assumed that the effectiveness is equal to 40.

## 7.8. Numerical values

The above sections have been written to present an overview of the theory and objectives of using fuel cells. In addition to this, the issues that may appear have been raised and solutions were found for each of them. The scope of this section is to present the relevant numerical values corresponding to the performance and sizing of the fuel cell stacks.

### 7.8.1. General subsystem values

Numerous formulas were used to find the numerical values of the parameters and they will be given in this section in the form of Table 7.2. The values in the table have been generated for one fuel cell stack.

**Table 7.2:** Numerical values for one fuel cell stack

Sub-system	Numerical Value	Unit
Air Usage	1.21	kg/s
Required Compressor Power	98	kW
Oxygen mass flow	0.281	kg/s
Hydrogen mass flow	0.0354	kg/s
Exit air flow rate	1.07	kg/s
Recycled power by expander system	48.6	kW
Water production	0.158	kg/s
Heat rate	1101	kW

### 7.8.2. Fuel cell sizing

One of the aspects that was not touched upon by now is the sizing of the fuel cell stack and especially the sizing of the individual cells of the stack. It was found that the needed power to be generated by the fuel cell is 2034 kW. With a voltage cell of  $V_c = 0.6 \text{ V}$ , a current of  $1 \frac{\text{A}}{\text{cm}^2}$  this comes out to a power per area of  $0.6 \frac{\text{W}}{\text{cm}^2}$ . Assuming that the fuel cells will be place in the nacelle of the engine pods, and a diameter of 75 cm it can be approximated that a surface area of  $360 \text{ cm}^2$  can be used to place the fuel cells. To solve cooling and humidification issues, the fuel cell may be divided into 4 stacks that are connected in series. Each of the stacks can have be have a area of

$28 \times 28 = 784 \text{ cm}^2$ , yielding a power density of  $470 \frac{W}{\text{cm}^2}$ .

With  $1017 \text{ kW}$  needed to be produced by each fuel cell system, the stack power comes out to  $\frac{1017}{4} = 254.25 \text{ kW}$ , which further leads to a number of 541 cells. Considering that the fuel cells from Toyota have an average thickness of  $1.34 \text{ mm}$ , the total length of the fuel cell stacks is  $725 \text{ mm}$ . All values calculated above are summarized in Table 7.3.

**Table 7.3:** Numerical values for fuel cell stack characteristics

Element	Numerical Value	Unit
Cell voltage	0.6	V
Cell current	1	$\frac{A}{\text{cm}^2}$
Cell power density	0.6	$\frac{W}{\text{cm}^2}$
Cell area	784	$\text{cm}^2$
Power per cell	470	W
Number of cells	541	-
Stack length	725	mm
Stack mass	339	kg

## 7.9. Materials

Considering the operational characteristics of the fuel cell and the requirements for safety, durability and sustainability for the mission of the Sustainable Air Taxi the materials composing the different parts of the fuel cell have to be analysed and clearly defined. Thus, this section will present each segment of the fuel cell stack and the materials that will be recommended for their design.

### 7.9.1. Electrolyte Materials

The electrolyte material of the fuel cell has various requirements for an efficient functioning of the fuel cell. First of all, the electrolyte must conduct ions, but not electrons. In addition, it has to be gas impermeable such that the anode and cathode gasses do not mix. Finally, the electrolyte has to be as thin as possible to minimize the resistance[33].

The most popular material used for the electrolyte of a PEMFC is Nafion<sup>30</sup>, which is a perfluorinated polymer. Nafion is based on the structure of polytetrafluoroethylene (TEFLON), but it also includes sulfonic acid ( $\text{SO}_3^- \text{H}^+$ ) functional groups. The first part of the structure, that is a TEFLON-like polymer provides mechanical strength, while the sulfonic acid provides charge sites for proton transport. Because of these structures, the Nafion based electrolyte is extraordinarily stable and durable and exhibits high ionic conductivity[33]. There are also some disadvantages of this polymer, such as that, it needs to be fully hydrated with liquid water and that it cannot function at high temperatures ( $>100 \text{ C}^\circ$ ) and that it requires noble metal catalysts such as platinum[33]. The hydration part means that the cell system must implement efficient water management architectures, as explained in Section 7.5. Finally, Nafion can be extremely costly with more than  $400 \frac{\$}{\text{m}^2}$ .<sup>31</sup>

Even with the disadvantages stated above, the perfluorinated polymer (Nafion) is still the best candidate for this type of fuel cell and the operational characteristics that are needed (low temperature). In addition, for an aircraft implementation, the stability and durability are especially important both from an operational and a sustainable point of view.

<sup>30</sup><https://www.nafion.com/en> [accessed 03-06-2022]

<sup>31</sup><https://www.fuelcellstore.com/naflon-117> [accessed 03-06-2022]

### 7.9.2. Electrode/Catalyst Materials

The fuel cells electrodes are implemented for two reasons. The first reason is that they have to efficiently deliver/collect electrons from the fuel cell, while the second one is that they must deliver/collect reactant/product species. These reasons imply that the electrode must present high conductivity and porosity while high catalytic activity is also desired. Usually, the electrode is based on expensive metals such as platinum and they can get quite expensive, so as little catalyst as possible should be used[33].

In order to follow this requirement a dual-layer approach is followed. Firstly, a thin (10-30  $\mu m$ ) thick, but highly active catalyst layer is placed on the surface of the electrolyte. This layer is made out of a mixture of platinum-carbon catalyst and electrolyte material. The second layer is a much thicker (100-500  $\mu m$ ) thick, inexpensive porous and electrically conductive electrode layer used on top of the first layer for protection and current collection. The dual layer approach is the most implemented method for this type of fuel cells[33]. The two layers are the catalyst layer (CL) and the gas diffusion layer (GDL). For the catalyst layer, to combat the expensive price, particles of the catalyst are spread on a carbon powder, such as Vulcan XC-72. This is done to increase the surface efficiency of the catalyst. The GDL represents the protective layer of the electrode; it should permit gas to diffuse into the catalyst layer, hence its name, and it should also provide protection and electrical connectivity[33].

The GDL usually employ carbon-fiber-based materials, where the two most used materials are carbon fiber cloths and carbon fiber papers. The carbon fiber materials present good electrical conductivity and high porosity while having excellent stability, corrosion resistance and mechanical properties which go hand in with the integration in an aircraft such as the Sustainable Air Taxi. In the case of this design, the carbon fiber cloths are preferred as they can highly compress (30-50 %) when installed in the fuel cell stack, while still presenting high performance characteristics[33]. A hydrophobic treatment has to be employed as to avoid the phenomenon known as "flooding". The hydrophobic layer is usually created by treatment of the GDL layers with polytetrafluoroethylene (PTFE, or TEFLON)[33]. Finally, a modern solution that is implemented more and more into the GDL is to apply a microporous layer between the layers of the GDL. This microporous layer provides an efficient transition between the different thicknesses of the GDL, by improving the wicking of liquid water from the CL, while also decreasing the electrical contact resistance between the layers. The addition of the microporous layer results in a "seven-layer" MEA or "Electrode Los-Alamos Type" (ELAT). The seven layers are: anode GDL, anode microporous layer, anode catalyst layer, electrolyte, cathode catalyst layer, cathode microporous layer and cathode GDL[33].

### 7.9.3. Anode/Cathode Catalyst

For both the anode and the cathode in a PEMFC using hydrogen, the most efficient catalyst is platinum. Even though this is an expensive material, it still presents properties that are beneficial for the PEMFC system and thus its integration has been optimized as to use as little material as possible. In the case of the anode, the quantity of platinum has been reduced down to 0.05  $mgPt/cm^2$  while for the cathode, the quantity is around 8-10 times higher at 0.4-0.5  $mgPt/cm^2$ [33].

## 7.10. Hydrogen Environmental Impact

Besides discussing the materials of the fuel cells it is also crucial to discuss how the used hydrogen is produced and what possible environmental impacts the hydrogen use and production comes along with. According to [33], emissions are split in two categories: those influencing global warming and those affecting the air pollution. A much more detailed impact analysis is performed in Chapter 12, comparing the Air Taxi to other aircraft. First of all, hydrogen could end up in the atmosphere in much higher concentrations than today if the use of hydrogen-powered vehicles increases in the future. According to [33], since the start of the industrialisation, the concentration of hydrogen in the atmosphere has increased by 200 parts per billion by volume. Since hydrogen



molecules are relatively smaller compared to other known pollutants, their dispersion rates are as much as four time higher than those of natural gas. On top of that, some liquid hydrogen tanks need to release some of the stored hydrogen to avoid pressure build ups [33]. The hydrogen in the lower atmosphere reacts in time with hydroxyl radicals (OH), producing atomic hydrogen and water vapors. Had the hydroxyl radicals not been used in this reaction, they would have further reacted with methane in the atmosphere and diminish its concentration via the reaction:



As far as hydrogen contribution to air pollution is concerned, in time the released hydrogen in the atmosphere may increase  $\text{O}_3$  concentrations in the atmosphere [33] via a series of reactions. Thus, the aforementioned reaction of hydrogen with hydroxyl radicals leads to further reactions between the atomic hydrogen and oxygen ( $\text{O}_2$ ), to which the photon energy of light is added to arrive at the final reaction product:



M "represents any molecule in the air that is neither created nor destroyed during the reaction but that absorbs energy from the reaction". It should also be noted that in Equation 7.26 the hydroxyl radical should not be confused with the diatomic anion  $\text{OH}^-$  called hydroxide. Consequently, the resulting hydrogen in the right hand side is neutral, not the hydrogen anion [77].

One of the most widely used production techniques for hydrogen is called steam methane reforming and is based on heating up methane from natural gas to get a mixture of carbon monoxide and hydrogen.<sup>32</sup> Carbon monoxide is toxic for humans and is also a greenhouse gas. For each type of fuel or even product, a life cycle analysis has to be performed. In the case of hydrogen fuel, the supply chain, containing the energy input as well as the outputs of each step and the flow between the phases can be observed in Figure 7.15.

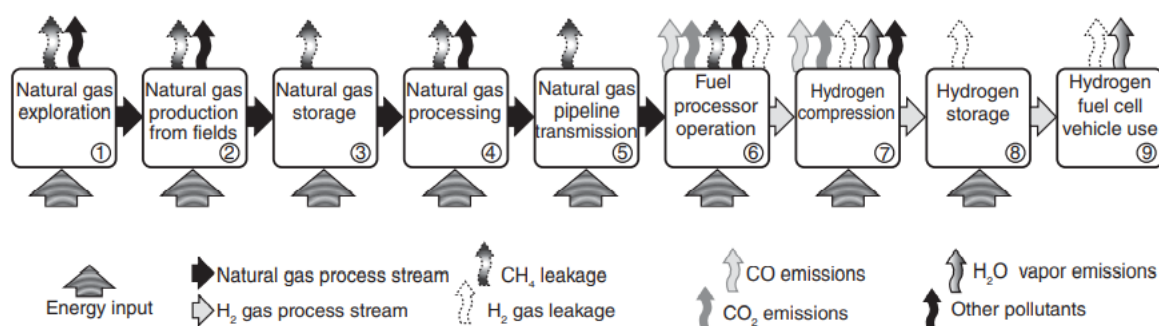


Figure 7.15: Life Cycle Analysis for the hydrogen fuel supply chain [33]

In spite of all the aforementioned potentially harmful impacts hydrogen use and production might have on the environment, it is still an overall better solution to current fuels with high carbon footprints. This can be visualised in Figure 7.16, which shows a comparison between the carbon contents produced by multiple typical fuels and hydrogen-based fuels.

<sup>32</sup><https://studentenergy.org/production/steam-methane-reforming/> [accessed 08-06-2022]

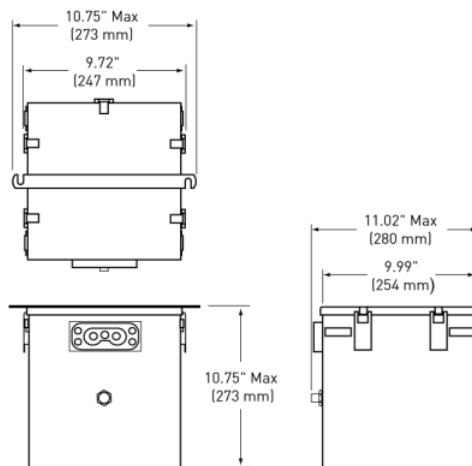
Fuel	Chemical Formula	Carbon Content of Fuel		
		LHV Fuel Energy (MJ/kg)	Per Unit Energy of Fuel	Per Unit Mass of Hydrogen
			Mass of Carbon per Unit of Fuel Energy (kg carbon/GJ fuel)	Mass of Carbon per Unit Mass of Hydrogen (kg carbon/kg atomic hydrogen)
Coal	$C_nH_{0.93n}O_{0.02n}O_{0.14n}S_{0.01n}(s)$	26.7	28.5	12.8
Gasoline	$C_nH_{1.87n}(l)$	44.0	19.6	6.5
Ethanol	$C_2H_6O(l)$	26.9	19.4	4.0
Methanol	$CH_4O(l)$	20.0	18.7	3.0
Natural gas	$C_nH_{3.8n}N_{0.1n}(g)$	45.0	15.5	3.1
Methane	$CH_4(g)$	50.0	15.0	3.0
Hydrogen	$H_2(g)$	120.0	0.0	0.0

*Note: Coal and gasoline have among the highest carbon contents per unit energy. Natural gas, methane, and hydrogen have among the lowest carbon contents per unit energy. Assuming a constant efficiency in energy conversion, the higher carbon content fuels will produce more CO<sub>2</sub> emissions than the lower carbon content fuels:*

**Figure 7.16:** Comparison of carbon content of different fuels [33]

## 7.11. Battery

The final component that needs to be added to the propulsion system is the battery. Even though, initially the chosen configuration featured a heavy battery responsible for aiding the fuel cells during the more demanding flight phases, the actual concept proved that this is not necessary. The performed analysis showed that the fuel cells are capable of operating alone during the whole flight. Hence, the only need for a battery comes in the form of an APU, with the battery performing its functions. Because of this, a small battery relative to the initial estimations is needed. For this purpose, the Beechcraft 300 series aircraft are used, since these have MTOWs very similar to the Air Taxi.



**Figure 7.17:** Dimensions of Meggit SLA battery



A Meggit 41.28 kg sealed lead-acid (SLA) battery was found (part number 9750W0370-8)<sup>33</sup>, which is certified for replacing the existing Nickel-Cadmium and SLA batteries on King Air 100, 200, 300 and 90 series aircraft. Moreover, it could be used for other applications, such as Cessna Citation I, II, V, Bravo, Ultra, Encore, Encore+, 560XLS, 56XLS+, as well as for the Boeing 747 100, 200 and 300 series.<sup>34</sup> However, SLA batteries have an enormous impact on the environment, with 44% - 70% of the lead in lead-acid batteries in China ends up as waste in the environment.<sup>35</sup> At the same time, the lead in lead-acid batteries has a high recyclability potential, with a 99% rate of recycling and around 90% of batteries being collected in North America, Europe and Japan.<sup>36</sup>

However, Li-Ion batteries are preferred in this case because of their higher specific energy of up to 265 Wh/kg and up to 670 Wh/L<sup>37</sup> and overall better performance, reason why they have been leading the market for a few decades now. As far as Li-Ion batteries' recyclability is concerned, it is expected that 374000 tonnes of such batteries are expected to enter the global waste stream by 2025 [52]. In spite of continuous recycling efforts, the materials in these batteries continue to find their way into the soil and damage the environment. An optimistic study in the US showed the projected lithium demand until 2090 [53], as shown in Figure 7.18.

Even though the study is optimistic in the sense that the demand is assumed to stop increasing at some point, it shows that it would not be impossible to achieve a market in which most of the materials in batteries can be recovered and reused. However, some time would need to pass in order for the first batches of batteries to reach end-of-life and virgin material would have to be used in the meantime. Hence, Li-Ion batteries seem a better option both from the perspective of performance and from the perspective of sustainability. Because these are the currently most used batteries in many industries, such as the automotive, one could also expect that more research is being made on the recycling opportunities of Li-Ion batteries.

Besides the APU function the battery needs to perform, it should also act as back-up in emergency situations. Because fuel cells are not very effective when it comes to instantaneous big power requirements [54], the battery is supposed to help the cells. This is only considered for an aborted landing and not for the take-off run and climb, as the requirement on the required runway length is of more than 1500 m, which is quite a large distance for such an aircraft. Hence, it is concluded that this distance allows the fuel cells to work on their own and ensure a safe take-off and climb. Thus, the only requirement from the batteries is to provide the necessary power to maintain the stipulated climb rate at sea level, which, according to the power loading diagram, is of 0.054 N/W. Using the maximum take-off weight of the aircraft and assuming that the batteries provide 100% of the required power during the go-around for 60 seconds and using the best available energy densities, one gets a required battery Li-Ion battery mass 64 kg and volume of and 25.4 L, respectively. Adding a margin to the Meggit battery previously found such that some extra 50 kg are added to the battery results in a 114 kg battery occupying approximately 45 L (after adding the Meggit battery volume to the calculated one, as taken from Figure 7.17. It should be noted that the dimension and weight of the Meggit battery could have been scaled down, considering that a Li-Ion battery is more weight and volume efficient than an average SLA battery, but in order to allow for some safety margin in the design, this was not done.

## 7.12. Propulsion System Integration

With all the components of the propulsion system discussed and/or chosen, it is important to treat the integration and positioning of this subsystem with respect to the other subsystems. Thus, this section deals with the lateral positioning of the propellers on the wings, according to CS 23 guidelines, as well as with the integration of the electric motors, fuel cells and battery within the aircraft.

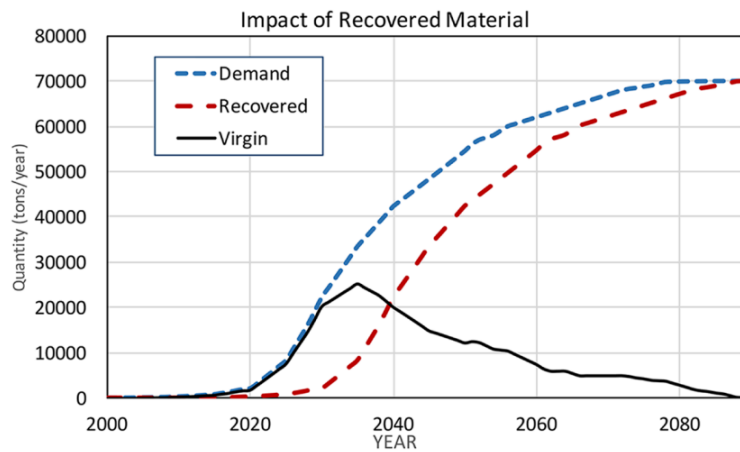
<sup>33</sup> <https://www.meggitt.com/wp-content/uploads/2019/09/King-Air-SLA.pdf> [accessed 07-06-2022]

<sup>34</sup> <https://www.meggitt.com/> [accessed 03-06-2022]

<sup>35</sup> <https://www.adb.org/> [accessed 03-06-2022]

<sup>36</sup> <https://blog.se.com/datacenter/2016/03/03/are-lithium-ion-batteries-greener-than-lead-acid/> [accessed 03-06-2022]

<sup>37</sup> <https://www.cei.washington.edu/education/science-of-solar/battery-technology/> [accessed 08-06-2022]



**Figure 7.18:** Projection of lithium demand and recovery in US on a 80 year timespan

To begin with the propeller lateral placement, the following CS 23.925 applicable requirements have to be complied with [44]:

- Ground clearance. There must be a clearance of at least 18 *cm* (7 *in*) (for each aeroplane with nose wheel landing gear) or 23 *cm* (9 *in*) (for each aeroplane with tail wheel landing gear) between each propeller and the ground with the landing gear statically deflected and in the level, normal take-off, or taxiing attitude, whichever is the most critical. In addition, for each aeroplane with conventional landing gear struts using fluid or mechanical means for absorbing landing shocks, there must be positive clearance between the propeller and the ground in the level take-off attitude with the critical tyre completely deflated and the corresponding landing gear strut bottomed. Positive clearance for aeroplanes using leaf spring struts is shown with a deflection corresponding to 1.5g.
- Structural clearance. There must be – (1) At least 25 *mm* (1 *in*) radial clearance between the blade tips and the aeroplane structure, plus any additional radial clearance necessary to prevent harmful vibration. (2) At least 12.7 *mm* (½ *in*) longitudinal clearance between the propeller blades or cuffs and stationary parts of the aeroplane; and (3) Positive clearance between other rotating parts of the propeller or spinner and stationary parts of the aeroplane.

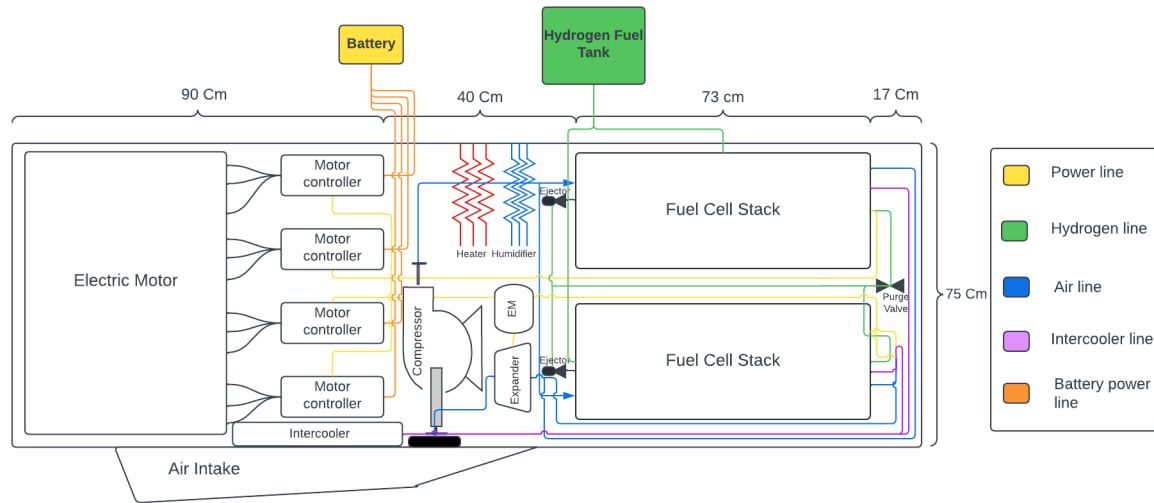
While the ground clearance requirement does not pose a problem considering the high-mounted wings and the diameter of the propeller of 2.67 *m*, the structural clearance is something which has to be carefully kept in mind. Due to that, the closest the propellers can be fitted to the fuselage is with their center located at the propeller radius plus 25 *mm* from the fuselage outer surface point closest to the propeller blades. Also, because the blades are made of aluminium, some extra safety margin is considered in order to account for the possibility of thermal expansion during hot days. At the same time, the propellers should be placed as inboard as possible, so as to minimize the required vertical tail size for the one engine inoperative condition. However, according to [40], the propeller clearance from the fuselage should be between 0.5-1 *m*, such that acoustic fatigue on the fuselage is avoided. Hence, the propellers will be placed 50 *cm* horizontally from the closest point on the fuselage. This way, the CS 23 requirements are also met. The electric motors are placed within the nacelle of each engine, but their dimensions are yet unknown. Hence, the initial sizing of the nacelles is based on estimates made by the group, as visualised in Figure 7.19.

The integration in the engine of the fuel cells has to make up for the positioning of all its other subsystems such as compressor, radiator, humidifier, ejector etc. It was calculated in Section 7.8 that the dimensions of one fuel cell stack would be 72.5 x 28 x 28 *cm*, leading to 227.36 *L* usable for 1021 *kW* of power, leading to a volumetric

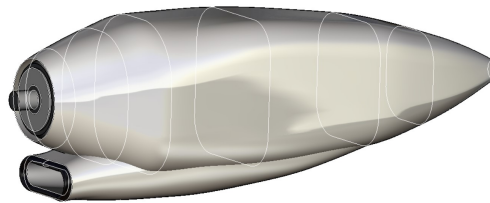
density of  $4.47 \frac{kW}{L}$ , resulting in a less efficient volumetric density than what it was assumed. This, however is acceptable, as it would mean that the individual cells should not be improved to such a high level.

The cell stacks will be connected in series, as to provide the necessary current and voltage and the other systems will be placed in front of them as shown in Figure 7.19. Their dimensions were assumed to fit into a rectangle with a length of  $2.2 \text{ m}$ , and a square cross section of  $75 \times 75 \text{ cm}$ . Several lengths were unknown and thus, these dimensions have been assumed based on experience and comparing to literature.

Finally, the battery can be fitted in the region where the wings join the fuselage, since its weight and volume are not big enough to pose any problems to the structure of the fuselage. Furthermore, that area is also generally reinforced because of the increased loads induced by the wing mounting. Figure 7.20 is designed to hold the system in Figure 7.19



**Figure 7.19:** Electrical Block Diagram of the internal configuration of the propulsion system



**Figure 7.20:** 3D model of engine pod based on Figure 7.19

# Wing Design

This chapter discusses the design of the wing in combination with some basic aerodynamic properties. First, an airfoil is selected and the planform is designed in Section 8.1, while also providing some initial aerodynamic parameters on the wing. In Section 8.2 the inside of the wing is designed in more detail. Afterwards the ailerons and high lift devices are sized in Section 8.3 and Section 8.4. At last, an overall layout of the wing is presented in Section 8.5 and the basic aerodynamics of the entire aircraft are discussed in Section 8.6.

## 8.1. Airfoil Selection and Planform Design

The initial design of the wing consists of determining the size and shape of the wing in combination with selecting an airfoil. The wing surface area is obtained from the wing power loading in Subsection 4.3.1. Furthermore, an aspect ratio is determined from reference aircraft by setting up a database. This database consists of the Dornier 228, Mitsubishi MU-2, Beechcraft 1900D, Beechcraft king air C90, 690B Twin Commander, The C212-200 Aviocar, Fairchild SA227-CC and -DC Metro 23.<sup>1</sup> Note that this database mostly consists of aircraft which are able to carry more than 6-8 people because it is based on similar MTOW and wing surface area. Now, using the wing surface area in combination with the aspect ratio, a wing span is determined along with an initial taper ratio estimated based on the reference aircraft. With these parameters, an initial planform can be designed but before actual aerodynamic analysis can start, the airfoil has to be selected.

The airfoil selection is the first step in the aerodynamic analysis of an aircraft. The airfoil library "Airfoil Tools"<sup>2</sup> provides a broad database for airfoil shapes and enables users to review an airfoil's performance with integrated Xfoil aerodynamic analysis. An initial lineup of 6 airfoils is taken based on a visual estimation regarding manufacturability and the thickness of the airfoil. Accordingly, extremely cambered and thin airfoils are less suitable in production than moderately thick (10% -16% of chord) airfoils and are therefore not taken into consideration. Furthermore, since the aircraft flies at subsonic speeds (cruise velocity at 475 km/h), there is no need to employ supercritical airfoils. The 6 initial airfoils come from different series, such as the NACA 4 and 6 series, the Clark and Wortmann series and the airfoil used on the Dornier 228.

In order to make a well founded choice on the airfoil, certain criteria first need to be established that cover the entirety of aspects influenced by the airfoil selection. This is done in four steps. Firstly, the thickness to chord ratio of the airfoil is considered. Thereby, a thicker airfoil is beneficial towards the structural resistance of the wing to bending and torsion loads. At the same time, unlike during the design of the aircraft where fuel is stored in the wing, there is no volumetric requirement on the airfoil in the given case, as the tank is in the fuselage. Secondly, in order to minimise drag, it is beneficial if the design lift coefficient  $C_{l_{des}}$ , which occurs at an angle of attack close to  $\alpha = 0$ , is as close as possible to the cruise lift coefficient  $C_{l_{cruise}}$  and that the  $C_d$  at  $C_{l_{des}}$  is close to  $C_{d_{min}}$ . With Equation 8.1, the average  $C_{l_{cruise}}$  during the cruise phase can be determined [24]. Note that the factor of 1.1 at the beginning of the formula is there to compensate for possible downforce of the horizontal tail during flight.

$$C_{l_{cruise}} = 1.1 \frac{1}{\frac{1}{2} \rho V_{cruise}^2} \frac{1}{2} \left( \left( \frac{W}{S} \right)_{start} + \left( \frac{W}{S} \right)_{end} \right) \quad (8.1)$$

Equation 8.1 results in a design lift coefficient of 0.29. Hence, it is important that the chosen airfoil has a  $C_l$  at  $C_{d_{min}}$  close to 0.29 and that the drag bucket stretches around this  $C_l$ . Thirdly,  $C_{l_{max}}$  and stall of the airfoil are

<sup>1</sup><https://customer.janes.com/janes/home> [accessed 30.05.2022]

<sup>2</sup><http://www.airfoiltools.com/?adlt=strict&toWww=1&redig=6ED17BA035B74C428BCF666DFECA2E31> [accessed 30.05.2022]

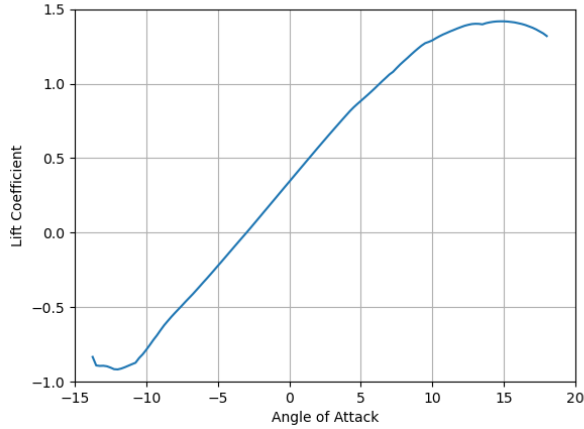


Figure 8.1: The lift polar of the NACA 63-412 airfoil

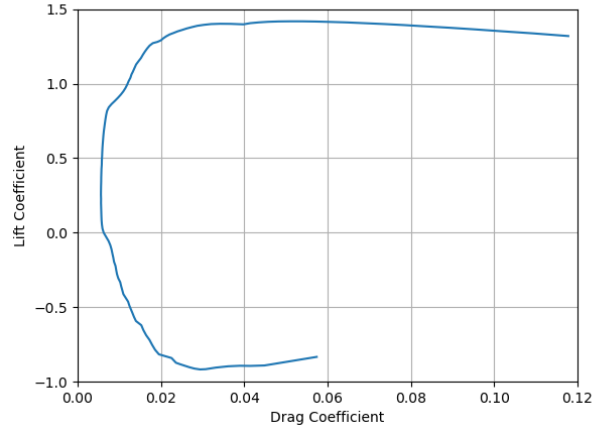


Figure 8.2: The drag polar of the NACA 63-412 airfoil

considered. For  $C_{l_{max}}$  a high value is preferred as this will decrease the amount of high lift devices required in a later stage. Preferably, an airfoil with smooth stall characteristics is chosen, since a sharp drop in  $C_l$  at maximum  $\alpha$  can result in dangerous handling problems. Fourthly, the final step is to look for an airfoil which has a low  $C_m$  at  $C_{l_{des}}$ . This will decrease the torsion moment in the wing and help design a lighter wing box. A variety of properties of the selected airfoils are documented in Table 8.1. These properties are used too select an airfoil according to the considerations mentioned above.

Table 8.1: Parameters of airfoil line up, at  $Re = 10^6$ 

	NACA 2414	NACA 642 415	CLARK YM-15	Dornier A5	NACA 63415	FX 38-153	NACA 63412
Thickness ratio $(t/c)_{max}$	14	15	15	16.2	15	15.5	12
$C_l$ for $\alpha = 0$	0.24	0.35	0.4	0.42	0.35	0.48	0.34
$C_{l_{max}}$	1.54	1.43	1.65	1.5	1.47	1.56	1.42
$\alpha$ at $C_{l_{max}}$	16.5	17.5	16	18.5	15.5	16	14.5
$C_{d_{min}}$	0.0062	0.0063	0.0063	0.0059	0.0063	0.0056	0.0056
$C_l$ at $C_{d_{min}}$ (pref close to cruise)	0.38	0.14	0.5	0.42	0.26	0.42	0.26
$\alpha$ at $C_{d_{min}}$	1.3	-1.8	1.3	0	-1.5	-0.5	-0.8
$(C_l/C_d)_{max}$	104	120	108	78	120	90	115
Cruise $C_m$	-0.05	-0.08	-0.075	-0.09	-0.08	-0.1	-0.08
Drag bucket length	-	9	-	5	10	3	7
Is $C_{l_{cruise}}$ inside the drag bucket	-	Y	-	Y	Y	Barely	Y
Stall characteristics	normal	normal	abrupt	abrupt	normal	normal	normal

Following the previously mentioned design criteria, the NACA63412 is chosen. Most importantly, this airfoil has a  $C_l$  at  $C_{d_{min}}$  which is close to the design lift coefficient of 0.29 and this  $C_l$  point lies right in the middle of the drag bucket (Figure 8.2). Moreover, the angle of attack at  $C_{d_{min}}$  is close to 0 which also makes it easier to incorporate the wing on the fuselage as it does not have to be mounted at an angle. The  $C_{l_{max}}$  of this airfoil is not as high as the other airfoils in the line-up. However, the benefits of lower drag outweigh the lower  $C_{l_{max}}$  in this case and the lift discrepancy can be fixed using high lift devices. Another favourable aspect of the selected airfoil is the behaviour at stall as it happens in a gradual manner (Figure 8.1). Lastly, as previously mentioned there is no real requirement on the  $t/c$  ratio as long as it is manufacturable, which is the case for the NACA64312 airfoil.

With the airfoil selected, the initial planform can be designed and afterwards the aerodynamic analysis can be performed. The aspect ratio and the taper ratio are obtained from the reference aircraft. The initial wing surface area is obtained from combining the wing power loading of  $1920 \text{ N/m}^2$  with the MTOW of  $5623 \text{ kg}$ . This results

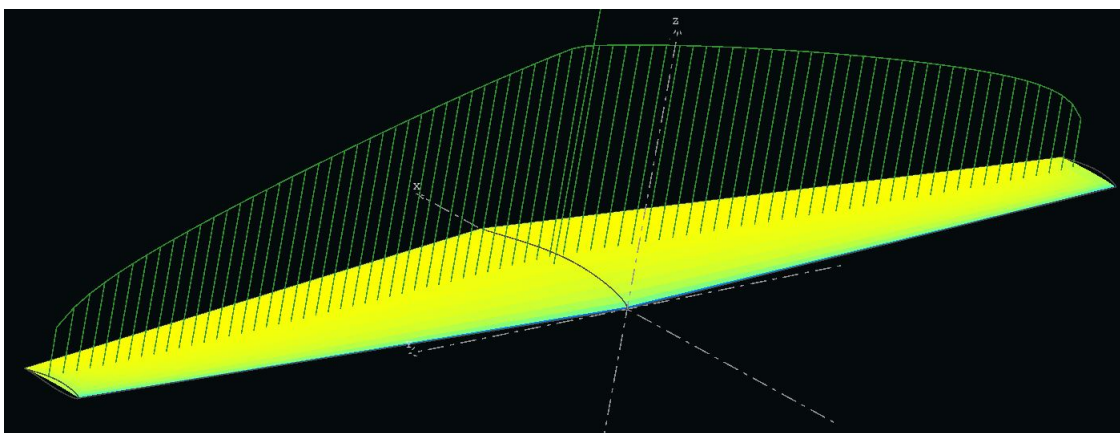
in a wing surface of  $28.06 \text{ m}^2$ . Other parameters can be found in Table 8.2. Furthermore a small leading edge sweep angle of  $3.4^\circ$  is implemented to make the quarter chord straight. Other geometric parameters can be found in Table 8.2.

**Table 8.2:** *Wing geometry*

Wing Area [ $\text{m}^2$ ]	Wing Span [ $\text{m}$ ]	Taper ratio, $\lambda$	Root chord [ $\text{m}$ ]	Tip chord [ $\text{m}$ ]	MAC [ $\text{m}$ ]	Aspect Ratio, AR	Sweep angle [ $^\circ$ ]
28.06	16.7	0.371	2.45	0.9	1.80	9.94	3.4

The wing is modelled and analysed in XFLR5 (version flow5 v7.01), shown in Figure 8.3.<sup>3</sup> It is split up into 40 equally spaced panels in spanwise direction and 13 panels along the chord with a cosine distribution so that the leading edge and trailing edge have a higher panel density than the centre. The wing is modelled for different angles of attack and velocities, using the vortex lattice method. The chosen range of angles of attack is limited from  $-6$  to  $17^\circ$  since outside of this range, the airfoil stalls and XFLR5 data becomes unreliable. Effectively, the data is applicable to the linear part of the  $C_L/\alpha$ -curve.

The output is a  $C_L$  distribution along the span of the wing for the modelled angles of attack and velocity. In order to get the lift along the span, this  $C_L$  distribution has to be integrated over the wing area. A python program is set up to read the output file and integrate the  $C_L$  over the panels. This results in a lift distribution along the wing like the one seen in Figure 8.4. This distribution is at a velocity of  $46 \frac{\text{m}}{\text{s}}$  and an  $\alpha$  of  $15^\circ$ , which is the stalling point of the aircraft. This distribution is used and scaled later on to calculate the internal structure of the wing box. The stall speed is determined from the database of reference aircraft and the stall angle is set at  $15^\circ$  as this is close to the stall angle of attack of the airfoil deduced from Xfoil. It should be noted that in Table 8.1, the stall angle of the airfoil is at  $14.5^\circ$ . However, this is at a Reynolds number of  $10^6$ . When increasing the Reynolds number to the scale of  $10^7$ , which is reached in the flow over the airfoil, the stall angle increases beyond  $16^\circ$ . Hence a stall angle of  $15$  is used. Other aerodynamic parameters that are important for the design of the wing and that were obtained from XFLR5 in combination with the code are found in Table 8.3. For cruise, 3 angles of attack are listed. This is to show at what angle of attack the wing should be positioned during cruise. The lift generated at  $\alpha = 0$  is lower than MTOW ( $55160 \text{ N}$ ) and also the landing weight ( $51940 \text{ N}$ ). This means that during cruise the wing has to be at a small angle of attack, preferably between  $0.5$  and  $1$ . At this angle, the wing will provide sufficient lift and still be at an angle which lies within the drag bucket of the airfoil. This can be achieved by flying at this angle of attack or mounting the wing at a small angle with respect to the fuselage, so that fuselage can be level during cruise. It was opted to mount the wing at a small angle, to keep the fuselage levelled for comfort reasons.



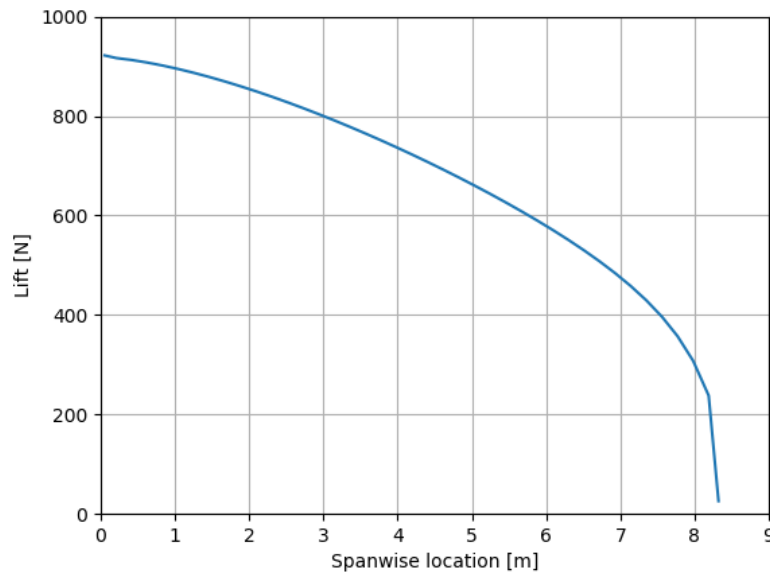
**Figure 8.3:** *model in XFLR5*

<sup>3</sup><http://www.xflr5.tech/xflr5.htm> [accessed 03.06.2022]



**Table 8.3:** Aerodynamic characteristics of the 3D wing

Condition	Cruise ( $\alpha = 0$ )	Cruise ( $\alpha = 0.5$ )	Cruise ( $\alpha = 1$ )	stall, clean	stall, flapped
Density [ $\frac{kg}{m^3}$ ]	0.736	0.736	0.736	1.225	1.225
Velocity [ $\frac{m}{s}$ ]	132	132	132	46	40
$\alpha$ [°]	0	0.5	1	15	15
$C_L$ [-]	0.25	0.30	0.34	1.53	1.97
$C_D$ [-]	0.006	0.007	0.008	0.089	-
$C_M$ [-]	-0.16	-0.19	-0.20	-0.57	-0.57
Lift [N]	46500	54500	62518	55400	41900

**Figure 8.4:** Lift distribution

## 8.2. Wing Box Design

This section is concerned with analysing the steps taken in designing the wing box, the structure inside of the wing. The first step consists of identifying the functions that the wing box shall fulfill. The wing box shall withstand extreme loads while being as light as possible. It shall also be made out of a recyclable material, and capable of supporting the engines and other movable surfaces. In the case of this design, the wing box does not necessarily have to be water or airtight, since fuel is not stored within the wing.

### 8.2.1. Sustainable Design Philosophy

As is already explained in Chapter 3 an environmentally sustainable aircraft should limit its impact during manufacturing and end-of-life treatment. Using recycled materials goes a long way in reducing the environmental impact of the manufacturing stage. In order to, at the same time, facilitate recycling of the aircraft with the potential of creating a materially circular aircraft, the variety of employed materials should be kept as small as possible. So far, the reason for why materials in aircraft are not properly separated is that the ordered disassembly procedure is too labour intensive and not economically viable, if different materials or alloys are used. For the purpose of facilitating same level recycling, hence without downcycling, it was decided that the wing box should be made from only one material. That way, the company charged with disassembling the aircraft



can simply separate the wing from the remaining structure, cut it into smaller parts and then recycle the material while introducing a minimum of impurities. One material that has suitable properties and is proven in aerospace engineering is aluminium. The fact that it is easily manufacturable and recyclable makes it perfectly applicable for the wing box of the Sustainable Air Taxi. Aluminium 7050 is chosen as it is produced in sheets as well as rivets, which means that the removal of small parts and connectors can be circumvented when disassembling the wing. Furthermore, there already exists a well established stream for aluminium recycling, into which the Sustainable Air Taxi can tap. The mechanical properties of aluminium 7050 are summarised in Table 8.4.

**Table 8.4:** *Properties of aluminium 7050<sup>4</sup>*

Al-7050		
Young's Modulus, $E$	70-80	GPa
Ultimate Tensile Strength, UTS	515	MPa
Yield Strength, $\sigma_y$	455	MPa
Shear Modulus, $G$	26.9	GPa
Shear strength, $\tau$	303	MPa
Poisson's ratio, $\nu$	0.33	-
Density, $\rho$	2.6-2.8	g/cm <sup>3</sup>

### 8.2.2. Structural Design

In order to create a structurally resistant wing box, it needs to be tested for various failure modes under different load cases. The purpose of this section is to prove to the reader that constructing a wing box out of a single material, namely Al-7050, is practically feasible. Sheet and stringer failure was assessed while rivet failure was omitted, due to the limited time available for this analysis. Additionally, it is assumed that any failure mitigation related to rivet failure would not majorly change the wing box layout. The analysed failure modes therefore are sheet yield failure, sheet buckling, stringer crippling and shear as well as torsion failure.

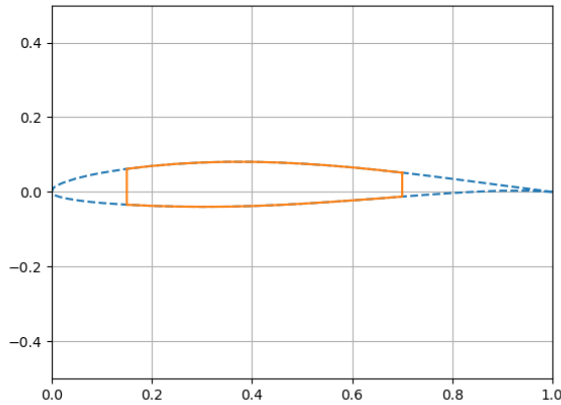
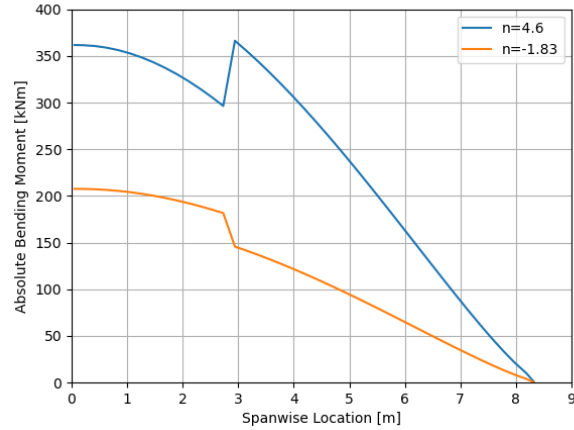
Before entering the assessment of failure modes, certain parameters on the wing are preliminarily determined and simplifications are made to facilitate the calculations behind the design. The front and rear spars are fixed to be at 15% and 70% of the chord as shown in Figure 8.5 and thicknesses for the spars and sheets are taken to be  $t_{spar} = 5 \text{ mm}$  and  $t_{sheet} = 3 \text{ mm}$ . Moreover, dimensions of the stringers are set before their number and placement can be calculated. L-stringers are placed in each corner which helps join the sheets to the spars. Their base and web are  $L_{base} = L_{web} = 25 \text{ mm}$  wide and high. In reality, the L-stringers won't have exactly a right angle, since the sheets and spars meet at angles slightly larger than  $90^\circ$ , but this detail is considered small enough to be omitted during this analysis. Z-stringers are used as stiffening elements on the upper and lower sheet. The base and top of the Z-stringers is  $Z_{base} = Z_{top} = 15 \text{ mm}$  and its height is  $Z_{web} = 20 \text{ mm}$ . Both stringer types have a thickness of  $t_{str} = 3 \text{ mm}$ . The stringer dimensions are such that interference of stringers is avoided by, for instance, the top and bottom stringers touching or stringers overlapping. The thinnest height of the wing box is found at the tip trailing edge spar and is  $57.8 \text{ mm}$ , leaving enough space for stringers to be placed without touching.

For the placement of stringers, it is assumed that their distance from the centroid is constant along the cross section, hence the wing box is rectangular rather than curved. This distance is calculated as the average height of the top and bottom sheet to the centroid. This simplification is acceptable, as taking the average height cancels out the difference in distance from the centroid that the stringers on one sheet have, when they are equidistantly laid out.

Sheet yield failure occurs due to the stresses introduced into the wing box by the lift induced bending moment. The highest stress is found at the point farthest away from the cross section's centroid  $z_{max}$ , located in the top

**Table 8.5:** Part dimensions in mm

	Base	Web	Top	Thickness
Top&bottom sheet	-	-	-	3
Front&rear spar	-	-	-	5
Z-stringer	15	20	15	3
L-stringer	25	25	-	3

**Figure 8.5:** The NACA 63-412 airfoil with the basic wing box outline set between 15% and 70% of the chord.**Figure 8.6:** The moment distribution along the wing from root to tip for the ultimate load factors of  $n_{ult} = 4.76$  and  $n_{ult} = -1.905$ 

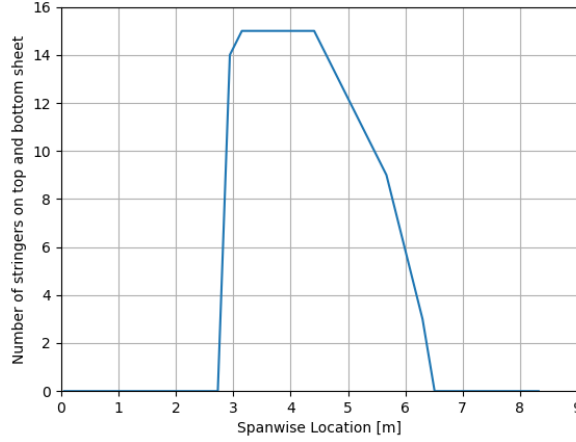
sheet. Reducing the stress at that point along the span is done by adding stringers to the top and bottom sheet, which increases the second moment of area  $I_{xx}$ . Equation 8.2a shows how the stress  $\sigma$  can be determined along the span for a given moment distribution  $M_x(y)$  at the positive ultimate load factor  $n_{ult} = 4.76$  as plotted in Figure 8.6. In the present case, the wing box is to be designed according to a certain maximum stress that shall not be surpassed, namely the material's yield stress  $\sigma_y = 455 \text{ MPa}$  combined with a preliminary safety factor of 1.5. This safety factor is there to account for potential changes in the design space and may be reduced as the design progresses to a fully converged state. As such, a required  $I_{xx}$  is calculated along the span using Equation 8.2b.

$$\sigma(y) = \frac{M_x(y) \cdot z_{max}(y)}{I_{xx}(y)} \quad (8.2a)$$

$$I_{xx}(y) = \frac{M_x(y) \cdot z_{max}(y)}{\sigma_y} 1.5 \quad (8.2b)$$

At each position, the required number of stringers is calculated in order to increase the local  $I_{xx}$  to the required value. The distribution of stringers needed to mitigate sheet yield failure is displayed in Figure 8.7. Note that for the sake of simplicity, it is assumed for bending stress mitigation that the upper and lower sheets carry the same number of stringers. At the tip and the root, no stringers are needed for support as the bending moments produced near the tip are not large enough to require additional support for the bending stress reduction. Additionally, the weight of the propeller and fuel cell system relieve the inner section of the wing to a considerable extent as can be seen in Figure 8.6. At the same time, the wing cross section is larger near the root which increases the base  $I_{xx}$  of the wing box without stringers.

The next failure mode that is analysed is sheet buckling. The analysis for sheet buckling needs to be done on the top sheet for the positive ultimate load factor ( $n_{ult} = 4.76$ ) and on the bottom sheet for the maximum negative load factor of  $n_{ult} = -1.905$ . With Equation 8.3, the critical buckling stress  $\sigma_{cr}$  can be determined for each section. To avoid buckling,  $\sigma_{cr}$  should be maximised and be above the actual stress in the sheet. This can

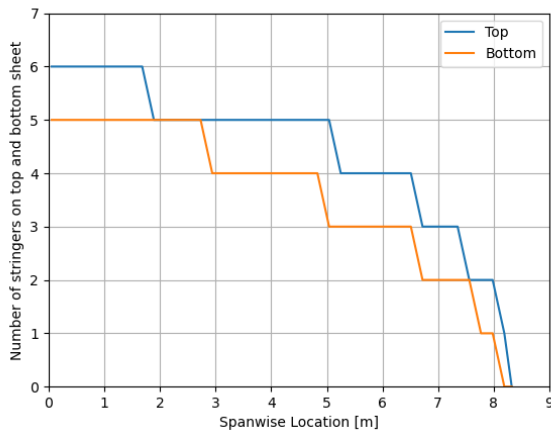


**Figure 8.7:** The span wise distribution of stringers due to the bending moment stress.

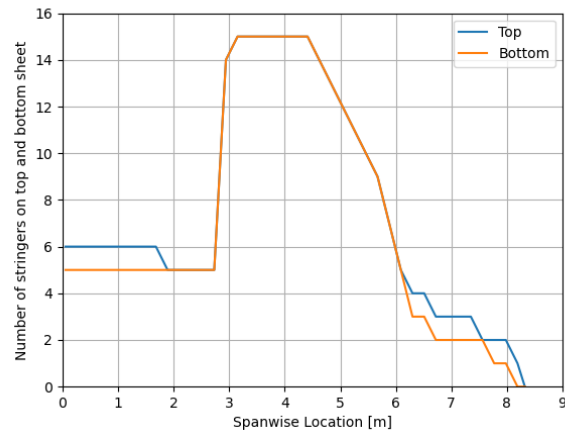
be done by increasing the sheet thickness  $t$  and reducing the effective sheet width  $b$  by adding stringers. The included buckling coefficient can be set to  $C = 4$ , considering the sheet boundary conditions [56]. The modulus of elasticity of Aluminium 7050 is estimated at  $E = 75GPa$ , being the average of the range contained in Table 8.4 and the poisson's ratio is  $\nu = 0.33$ .

$$\sigma_{cr} = C \frac{\pi^2 E}{12(1 - \nu^2)} \left(\frac{t}{b}\right)^2 \quad (8.3)$$

Assuming that the wing box has no supporting stiffeners, the required number of stringers to prevent the sheets from buckling under the moment distributions in Figure 8.6 is shown in Figure 8.10. Laying this new stringer distribution over the results found in Figure 8.7 yields the final distribution contained in Figure 8.11.



**Figure 8.10:** The required stringer distribution to prevent buckling alone.



**Figure 8.11:** The stringer distribution when combining the sheet yield stress and buckling constraint.

The assessment of stringer buckling is done by a derivative of the sheet buckling formula 8.3, given in Equation 8.4a.  $\frac{\sigma_{cc}}{\sigma_y}$  is the ratio of crippling stress over yield stress of a stringer section. Using Equation 8.4b, the

overall crippling stress of a stringer can be determined. The coefficients are given as  $\alpha = 0.8$  and  $n = 0.6$  and  $t$  and  $b$  now refer to the thickness and width of stringer sections. It is important to keep in mind that the buckling coefficient  $C$  is not the same for sections of the stringers. For the sections of the L-stringers and the top and bottom flanges of the Z-stringers, hence, sections that have no support on one side,  $C = 0.425$ . The vertical web of the Z-stringer, however, uses  $C = 4$  due to it being supported on all sides [56].

$$\frac{\sigma_{cc}}{\sigma_y} = \alpha \left[ \frac{C}{12(1-\nu^2)} \frac{\pi^2 E}{b} \left( \frac{t}{b} \right)^2 \right]^{1-n} \quad (8.4a)$$

$$\sigma_{cc} = \frac{\sum \sigma_{cc}^i A^i}{\sum A^i} \quad (8.4b)$$

The  $\frac{\sigma_{cc}}{\sigma_y}$  ratios of the L- and Z-stringers are 2.86 and 1.61, respectively. Since the wing box is designed such that no point of the cross section surpasses the yield stress of Al-7050, the buckling, and failure in general, of stringers is of no risk.

The torsional loads on the wing box are also modelled. The maximum shear stress can be calculated using the shear flow and the minimal thickness of the wing box Equation 8.5. The shear flow is caused by torsion of the wing box and the lift, which includes the engine weight. Shear flow due to torsion is modelled using Equation 8.6, where  $A$  is the area of the cross section of the wing box at a span-wise location and  $T$  the torsion along the span.  $T$  is calculated with Equation 8.7 where the  $C_M$  is obtained from XFLR5,  $c$  is the chord at that span location and  $S$  is the area of the wing from the tip to that spanwise location. The shear flow caused by the lift is calculated using Equation 8.8, which comes from the idealized structures theory in structural analysis and design [56]. It assumes that all the shear load is taken up by the stringers. In Equation 8.8,  $r$  represents the number of stringers,  $I_{xx}$  is moment of inertia of the cross section of the wing box,  $L$  is the lift multiplied by the ultimate load factor including the weight of the engine,  $B_r$  is the area of the stringer and  $z_r$  is the distance of that stringer to the x-axis. Combining the shear flow due to lift and torsion, a maximum shear flow is obtained along the span. Divided by the minimal skin thickness, the maximal shear stress along the span can be found to be 44 MPa, which is far below the allowable shear stress of aluminium 7050 Table 8.4. It should be noted that the torsion due to the offset of the engine in y-direction is not taken into account. This is justifiable, because in order for the shear stress to exceed the maximum allowable shear stress, the engine's center of gravity has to be 3 m in front of the wing. Which is larger than the actual chord of the wing. Thereby, it is concluded the wing box is properly designed for shear stress.

$$\tau_{\max} = \frac{q_T + q_L}{t_{\min}} \quad (8.5) \quad q_T = \frac{T}{2A} \quad (8.6)$$

$$T = C_M \frac{1}{2} \rho (V_{\text{stall, clean}})^2 S c \quad (8.7) \quad q_L = \frac{L}{I_{xx}} \sum_{r=1}^r B_r z_r \quad (8.8)$$

### 8.3. Aileron Design

The ailerons of the wing will allow the aircraft to control the roll. The roll regulations for the aircraft are set by EASA in CS23.157 for the approach phase [16]: "It must be possible using a favourable combination of controls, to roll the aeroplane from a steady 30° banked turn through an angle of 60°, so as to reverse the direction of the turn within, for an aeroplane of over 2722 kg (6 000 lb) maximum weight,  $\frac{W+1300}{1000}$  seconds, but not more than 7 seconds, where  $W$  is weight in kg." For take-off, these numbers are less strict (at most 10 seconds) due to the assumption that the moment of inertia is much larger due to fuel storage in the wing. Since the Air Taxi does not store any fuel in the wing, the moment of inertia is approximately constant and the critical phase is found during approach. Furthermore, the Air Taxi will weigh more than 6000 lb such that the 60° roll time is set to a maximum of 7 seconds.

Assuming that the roll rate  $P$  is be constant during the required maneuver,  $P$  can be calculated in radians per second using Equation 8.9. In this equation  $\Delta\phi$  is  $\frac{\pi}{3}$  radians and  $\Delta t$  is 7 seconds. The required constant roll

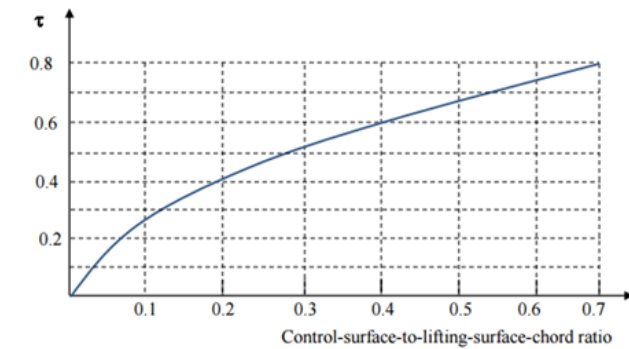
rate  $P$  is  $0.149 \frac{rad}{s}$ . Since a constant roll rate is an invalid assumption at the start and end of the rotation due to accelerations, a safety factor of 1.5 is included such that the required  $P$  becomes  $0.224 \frac{rad}{s}$ . This safety factor also ensures that the design is not on the edge of regulations. The safety factor of 1.5 is not only compensating for the assumption of constant roll rate. In fact, there are also other aspects reducing the efficiency. Deflecting the aileron, for instance, results in a twist of the wing box, reducing the difference in angle of attack created by the aileron. This phenomenon is called aileron reversal and is also accounted for by the safety factor. Finally, in the current aileron design both ailerons are assumed to deflect an equal amount of  $20^\circ$  ( $\frac{\pi}{9}$ ). In practise, this will cause adverse yaw. Deflecting the upgoing aileron a little bit more than  $20^\circ$ , while deflecting the downgoing wing less than  $20^\circ$  can solve this problem. Adverse yaw shall be analysed in a more detailed design stage of the aileron, but is outside the scope of this report.

Another expression for the roll rate is established in Equation 8.10, derived during an aircraft design course at the TU Delft [24]. In Equation 8.10,  $C_{l_{\delta a}}$  is the aileron control derivative and can be calculated using Equation 8.11.  $C_{l_p}$  is the roll damping coefficient, which can be computed with Equation 8.12.  $V$  is the true air speed during the approach phase ( $60 \frac{m}{s}$ ) which is obtained by multiplying the stall speed ( $46 \frac{m}{s}$ ) by 1.3.  $\delta a$  stands for the aileron deflection ( $\frac{\pi}{9} rad$ ) and  $b$  is the wing span ( $18 m$ ).

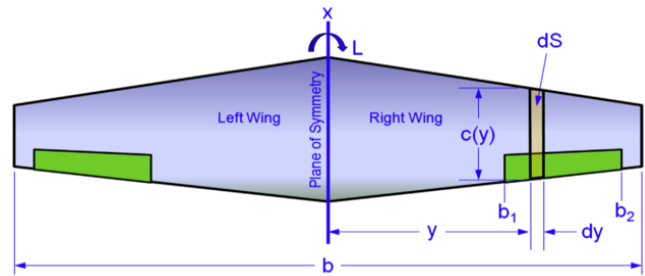
$$P = \frac{\Delta\phi}{\Delta t} \quad (8.9)$$

$$P = -\frac{C_{l_{\delta a}}}{C_{l_p}} \cdot \delta a \cdot \left( \frac{2 \cdot V}{b} \right) \quad (8.10)$$

There are many variables required to compute the aileron control derivative with Equation 8.11. The lift slope  $C_{l_\alpha}$  of the NACA 63412 is approximately 5.37 per radian.  $\tau_a$  is the aileron effectiveness, which is a function of the ratio of the aileron chord length to the total chord at a certain spanwise location as shown in Figure 8.12a. Since the aft spar is at 70% of the chord, the aileron will be approximately 20% of the chord. The remaining 10% of the chord are allocated to actuators, hinges and other aileron related systems. This chord ratio of 0.2 results in an aileron effectiveness of 0.4, as can be seen in Figure 8.12a.  $S_{ref}$  is the surface area of the wing and  $b$  is the wing span. Furthermore,  $y$  is the spanwise location and  $c(y)$  is the chord length at this specific spanwise location. For the roll damping coefficient in Equation 8.12 one other parameter needs to be known, which is  $C_{d_0}$ . According to simulations in XFLR5, this value is 0.0063 for the NACA 63412.



(a) Aileron effectiveness as a function of the control surface to lifting surface chord ratio.



(b) Geometry parameters for the sizing of the aileron.

Figure 8.12: Aileron parameters

$$C_{l_{\delta a}} = \frac{2 \cdot c_{l_\alpha} \cdot \tau_a}{S_{ref} \cdot b} \int_{b_1}^{b_2} c(y) \cdot y \cdot dy \quad (8.11)$$

$$C_{l_p} = -\frac{4 \cdot (c_{l_\alpha} + C_{d_0})}{S_{ref} \cdot b^2} \cdot \int_0^{\frac{b}{2}} y^2 \cdot c(y) \cdot dy \quad (8.12)$$

$b_1$  and  $b_2$  in Equation 8.11 are still unknown and arbitrary, so these parameters will determine the roll perfor-

mance and can be adapted until the roll rate converges to the required value of  $0.224 \frac{rad}{s}$ .  $b_1$  and  $b_2$  are the spanwise locations where the aileron starts and ends, as can be seen in Figure 8.12b. All equations are inserted in a Python file, such that the iterations can be done easily. The ailerons are preferably placed as close as possible to the tips, which provides them with the longest arm to create a rolling moment. For that reason,  $b_2$  is set to  $7.5 m$ , leaving  $80 cm$  for the design of wing tips. Then,  $b_1$  needs to be  $6.1 m$  from the centre to meet the required roll rate of  $0.224 \frac{rad}{s}$ , yielding an aileron width  $1.4 m$ . An aileron which is a little bit smaller would also meet the roll requirement. Nevertheless it is convenient to build the aileron between two ribs. Later on, Section 8.5 shows that there is a rib present at  $6.1$  and  $7.5 m$  in chordwise direction.

## 8.4. High Lift Devices

The high lift devices should increase the  $C_{L_{max}}$  of the wing. In order to determine the size and type of the high lift devices an estimation of the required  $C_{L_{max}}$  and the clean  $C_{L_{max}}$  of the wing is made. The clean  $C_{L_{max}}$  of the wing is calculated using XFLR5 and can be found in Table 8.3. The required  $C_{L_{max}}$  is calculated with Equation 8.13, where  $W$  is the maximum take-off weight,  $\rho$  the air density,  $S$  the wing surface area and  $V$  the stall speed of the aircraft in flapped condition, which was determined from reference aircraft. This results in a required  $C_{L_{max}}$  of 1.97, as can also be observed in Table 8.3 meaning that the high lift devices should increase the  $C_{L_{max}}$  by a minimum of 0.45. Taking into account a safety margin, the high lift devices were designed to increase the  $C_{L_{max}}$  by 0.5.

$$C_L = \frac{W}{0.5V^2\rho S} \quad (8.13)$$

With the  $\Delta C_{L_{max}}$  known, the type of high lift device and sizing of the high lift devices can be performed. This is done using Equation 8.14 [24], where  $\Delta C_{L_{max}}$  is a parameter dependent on the chosen high lift devices,  $S_{wf}$  is the wing area depicted in Figure 8.13,  $S$  is the wing area,  $\Lambda_{hinge-line}$  is the angle of the hinge line of the high lift devices, which is set equal to the angle of the trailing edge. Being a simple high lift device which should be sufficient for an aircraft of this size, a single slotted flap is selected. The positioning on the wing is determined by setting a starting point and an end point of the flaps. Using this the  $S_{wf}$  is obtained. The result is a flap that starts at  $b/2 = 2.3m$  and ends at  $b/2 = 6.1m$ .

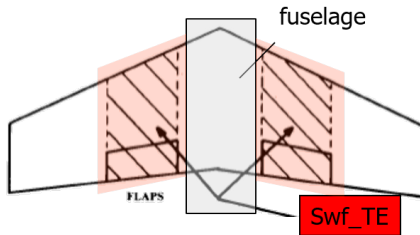


Figure 8.13: Visualisation of the required area for the flap [24]

$$\Delta C_{L_{max}} = 0.9 \Delta C_{l_{max}} \frac{S_{wf}}{S} \cos \Lambda_{hinge-line} \quad (8.14)$$

## 8.5. Wing Box Layout

With the minimum number of stringers determined and the moving surfaces sized, a planform for the structure can be created. That way, it can be shown that the wing box design is feasible and ribs can be placed conceptually. Figure 8.14 shows the wing box lay-out generated in DevWing as seen from the top. It shows the front and rear spars at 15% and 70% of the chord, respectively and the Z stringers in-between. The Z-stringers are modelled as boxes which have the width of the top and bottom flanges added,  $Z_{base} + Z_{top} = 30mm$ , and the height of the web,  $Z_{web} = 20mm$ . Keep in mind that Figure 8.14 shows the stringers on both the top and bottom sheet,

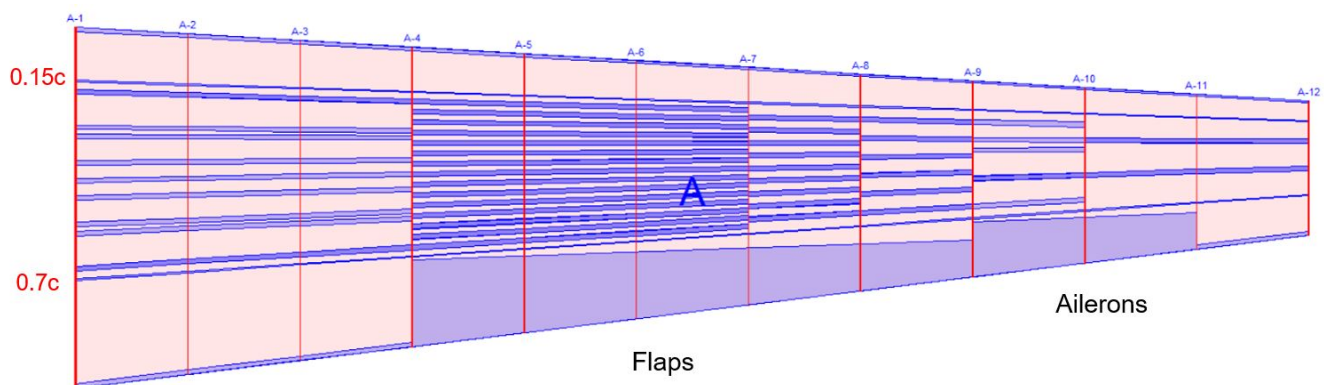


which leads to some sections misleadingly appearing to have overlapping stringers, such as the part from the root rib until the beginning of flaps. The main spot of interest is located at the seventh rib from the root where both sheets bear 15 stringers each. As can be deduced from the figure, this leads to the cross section being very cramped, but nonetheless a feasible design, since some space is left between stringers.

The ribs are placed such that the flaps and ailerons are clearly separated from the rest of the structure and can be supported along with hydraulic lines, actuators and hinge mechanisms that they require. With the objective of avoiding stress concentrations along the span of the wing, the ribs should contain holes for the stringers to fit through. Optionally, a solution is proposed where continuous stringers are connected to ribs on both sides, thereby transferring the load through the rib, rather than the less resistant sheet. This could be done by riveting or bolting the rib and stringer flanges to each other or bonding of the two parts, although the latter is discouraged, as the involvement of adhesives should be avoided due to problems that they pose in recycling. Figure 8.15 also conceptually depicts how lightening holes can be included in the ribs to decrease the wing weight.

Comparing Figure 8.11 to Figure 8.14, it is apparent that the stringer distribution modelled in DevWing is a simplified version of the one yielded by calculations. As the design evolves to a more concrete stage, factors beyond the structural resistance of the wing box need to be taken into account. Being linked to cost and sustainability, manufacturability makes up a large share of these considerations. In order to decrease the variety of parts that need to be produced, it is smarter to have similar and even identical parts. As such, stringers of the same length are favourable as they decrease the complexity of parts production, delivery and storage. By using more stringers of the same length as suggested in Figure 8.14, as opposed to Figure 8.11, larger batch sizes are enabled, sorting of parts during transport and storage is simplified and it gets easier for labourers to figure out, which part needs to be installed where. Keeping a set of spares for the case that a part is deficient is also easier when the variety of parts is decreased.

Calculating the total volume of the material used in the wing box, a mass of 440 kg for the core wing structure is attained. Considering that flaps and ailerons will further increase the wing mass, the class II estimate for wing weight (430 kg) will be exceeded. However, further improvements yielding weight savings can be made when the design proceeds to further stages. For instance, a variable sheet thickness and stringer size should be implemented which would make the design more weight efficient.



**Figure 8.14:** Top view of the wing box generated using DevWing.



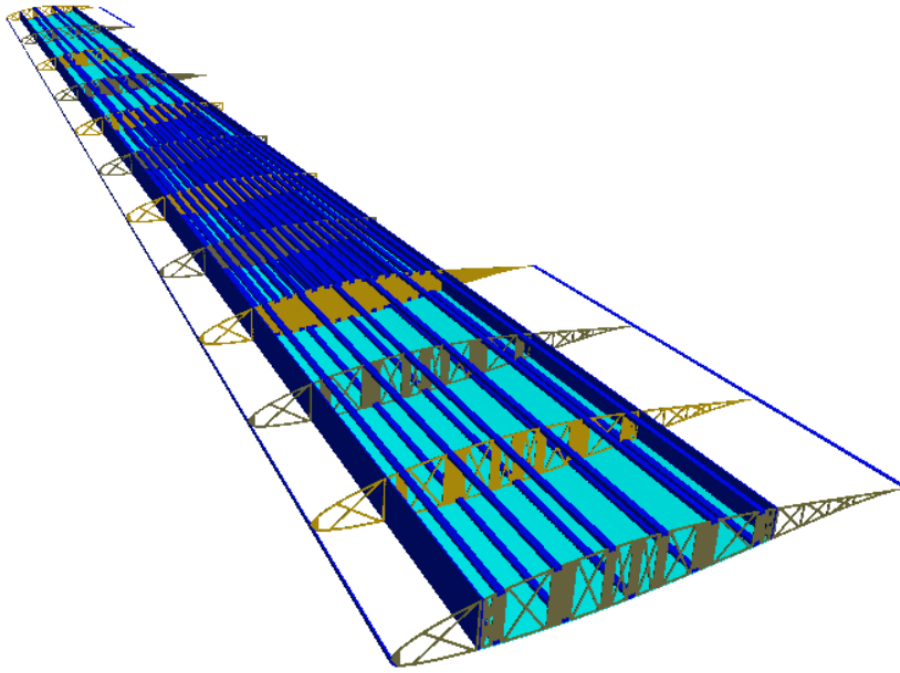


Figure 8.15: Isometric view of the wing structure

## 8.6. Drag Calculations

So far, only the drag of the wing has been considered. In order to give a good estimation of the lift and drag of the aircraft, also the effect of other components has to be taken into account. The total drag of the aircraft can be calculated with Equation 8.15, where  $C_{D_0}$  is the zero lift drag of the aircraft and  $\frac{C_L^2}{\pi A e}$  is the drag due to lift.

$$C_D = C_{D_0} + \frac{C_L^2}{\pi A e} \quad (8.15)$$

### Zero Lift Drag

The zero lift drag of the aircraft can be estimated using a statistical method [24], which uses the reference area of the aircraft components and an estimation of the drag of different components. The reference area of the wing is the wing surface area, for the fuselage the reference area is the maximal frontal area, the nacelle reference area is the maximal frontal area of the nacelles and for the tail it is the tail surface area [24]. Then, the total zero lift drag is estimated using, Equation 8.16, with the values from Table 8.6. The multiplication factor of 1.15 is used to account for the miscellaneous drag. This resulted in a zero lift drag coefficient of 0.025 for the entire aircraft.

$$C_{D_0} = 1.15 \left( \frac{1}{S_{ref}} \sum_c C_{Dc} S_{wet\ c} \right) \quad (8.16)$$

Table 8.6: Reference drag estimation values

Aircraft component	CDc [ $\frac{1}{m^2}$ ]	Reference area [ $m^2$ ]
Wing	0.0070	28.06
Fuselage: multi-engine	0.0800	3.14
Nacelles	0.0600	1.36
Tail (both horizontal and vertical)	0.0080	4.84 + 5.35

### Drag due to Lift

The drag due to lift is dependent on the Oswald efficiency factor, aspect ratio and lift generated by the wing.

The Oswald efficiency factor is attained with Equation 8.17. Here, the effective aspect ratio was used, which is the normal aspect ratio together with the effect of winglets, which are added in the following chapter. These increase the effective aspect ratio by 0.61 using Equation 8.18. Furthermore, the Oswald efficiency factor can be increased, when flaps are used, due to the airflow from the engine interacting with the flow over the flap. This  $\Delta e$  is equal to 0.003 [24].

$$e = 1.78(1 - 0.045AR^{0.68}) - 0.64 + \Delta e \quad (8.17)$$

$$\Delta AR = 1.9(h/b)AR \quad (8.18)$$

Finally, the total drag of the aircraft can be calculated using Equation 8.15, which results in drag coefficient of 0.029 in cruise. The relevant results and parameters can be found in Table 8.7.

**Table 8.7:** Drag and relevant parameters

Parameter	Value
Effective Aspect Ratio	10.55
Oswald efficiency factor	0.75
$S_{ref} [m^2]$	28.06
$C_L$ (cruise)	0.3
$C_D$ (cruise)	0.029

# Empennage Design and Final Aircraft Layout

The Sustainable Air Taxi has a T-tail configuration to avoid downwash from the high wing and propwash from the wing-mounted propellers. The sizing and planform design of this T-tail is explained in Section 9.1. Once the tail is designed, the final layout of the aircraft with the integration of the wing and propulsion system is detailed in Section 9.2.

## 9.1. Tail Sizing and Positioning

As explained in Section 4.7, stability and controllability constraints are applied to calculate the iterated tail surface area to wing area ratio  $\frac{S_h}{S}$ . As given in Section 4.11, this results in a horizontal stabilizer surface area of  $4.84 \text{ m}^2$ , with its area centroid positioned at  $14.508 \text{ m}$  from the nose. For the planform design of the horizontal tail, the sweep angle at 75% chord is set to zero such that the elevator hinge line remains straight for the best control surface efficiency [41]. The aspect ratio and taper ratio of the horizontal stabilizer are selected from statistical values with the twin propeller Beech Super King Air 200 as a reference. This is because the design MTOW of  $5622 \text{ kg}$  and wing area of  $28 \text{ m}^2$  very closely match those of the Super King Air 200, which weighs  $5670 \text{ kg}$  and has a wing area of  $28.15 \text{ m}^2$ . Its normal cruise speed is also  $503 \frac{\text{km}}{\text{h}}$  compared to the  $475 \frac{\text{km}}{\text{h}}$  cruise speed of the Sustainable Air Taxi. Based on Figure 9.1, an aspect ratio of 5.2 and a taper ratio of 0.5 are chosen for the horizontal stabilizer. These parameters yield the tail planform shown in Figure 9.2, which shows the root and tip chords, tail span, and the location of the 25%MAC in  $\text{cm}$ .

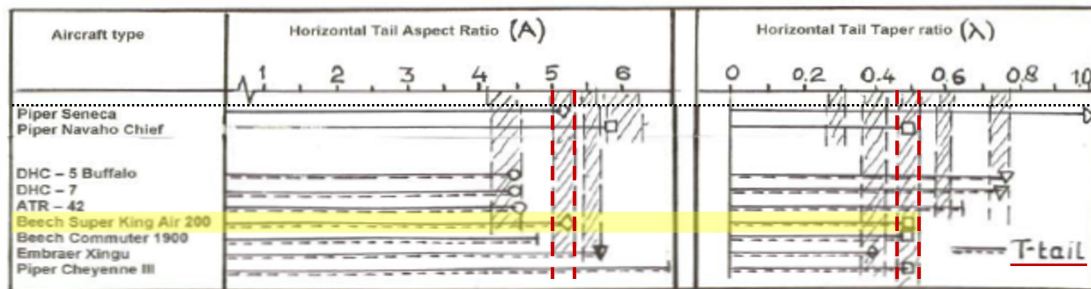


Figure 9.1: Horizontal stabilizer aspect ratio and taper estimation from reference aircraft [41] (cropped and marked)

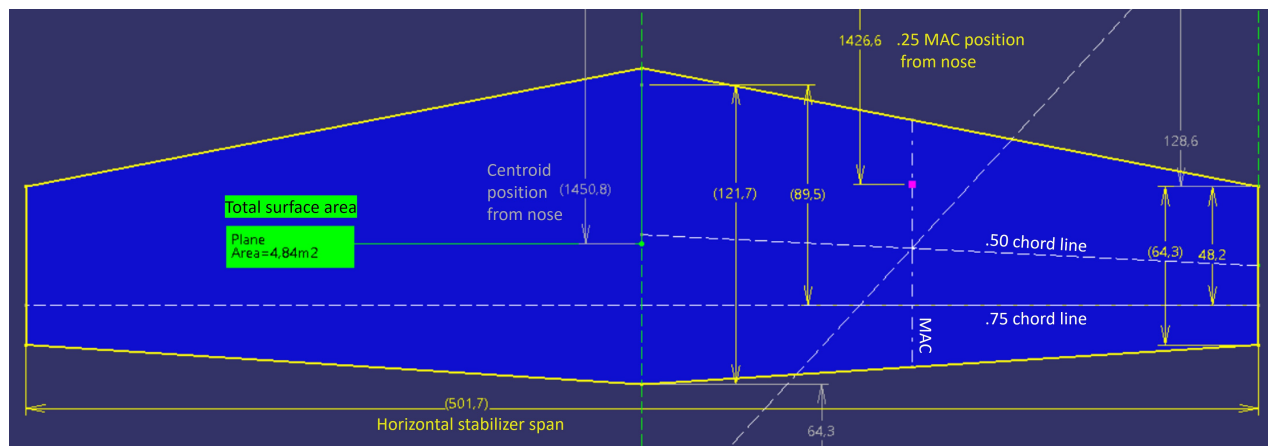


Figure 9.2: Horizontal stabilizer planform, dimensions in [cm]

<sup>1</sup><https://www.globalair.com/aircraft-for-sale/Specifications?specid=52> [accessed 09-06-2022]

Unlike the horizontal tail surface, the vertical tail surface calculation is not included in the design iterations. Therefore, the vertical tail volume coefficient  $\bar{V}_v$  is estimated using Figure 9.3, with again the King Air 200 as reference. It is important here that this reference aircraft also has a T-tail, because the planform of a vertical stabilizer in a T-tail configuration is influenced significantly by the horizontal stabilizer installed on top of it.

**Table 8.6b) Regional Turboprop Airplanes: Vertical Tail Volume, Rudder and Aileron Data**

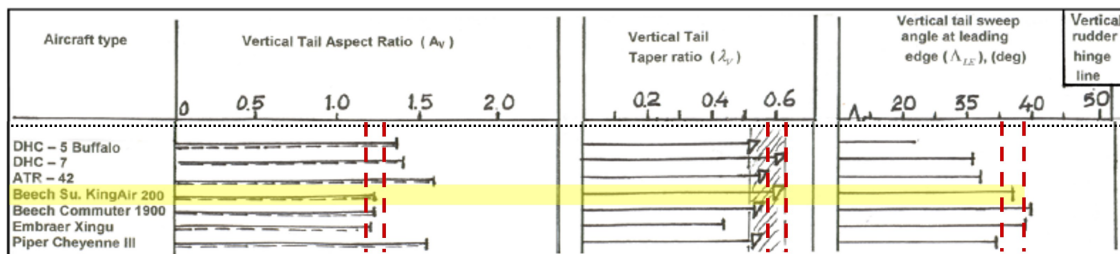
Type	Wing Area $S$ ft <sup>2</sup>	Wing Span $b$ ft	Vert. Tail Area $S_v$ ft <sup>2</sup>	$S_r/S_v$	$x_v$ ft	$\bar{V}_v$	Rudder Chord root/tip fr.c <sub>v</sub>	$S_a/S$	Ail. Span Loc. in/out fr.b/2	Ail. Chord in/out fr.c <sub>w</sub>
CASA C-212-200	431	62.3	77.5	0.41	24.8	0.072	0.41	0.061	.69/1.0	.24/.26
SHORTS 330	453	74.7	93.1	0.26	27.3	0.073	0.41	0.061	.70/.95	0.27
360	453	74.7	91.4	0.37	33.9	0.091	.39/.36	0.074	.69/.98	0.27
BEECH 1900*	303	54.5	47.5	0.35	26.5	0.076	.40/.38	0.064	.60/1.0	0.21
B200	303	54.5	52.3	0.29	20.5	0.065	.47/.41	0.059	.60/1.0	0.21
CESSNA CONQUEST I	225	44.1	41.3	0.38	17.1	0.071	.46/.38	0.060	.61/.86	.29/.28
II	254	49.3	43.5	0.37	18.7	0.063	.48/.33	0.058	.62/.89	.30/.32

**Figure 9.3:** Vertical tail volume coefficient estimation from reference aircraft [41] (cropped and marked)

The tail volume (which is dimensionless) is chosen to be 0.065, from which the surface area of the vertical stabilizer can be calculated using Equation 9.1 once the tail arm from the most aft cg location to the quarter chord of the MAC on the vertical tail is known.

$$\bar{V}_v = \frac{(X_v - X_{aftcg})S_v}{Sb} \quad [41] \quad (9.1)$$

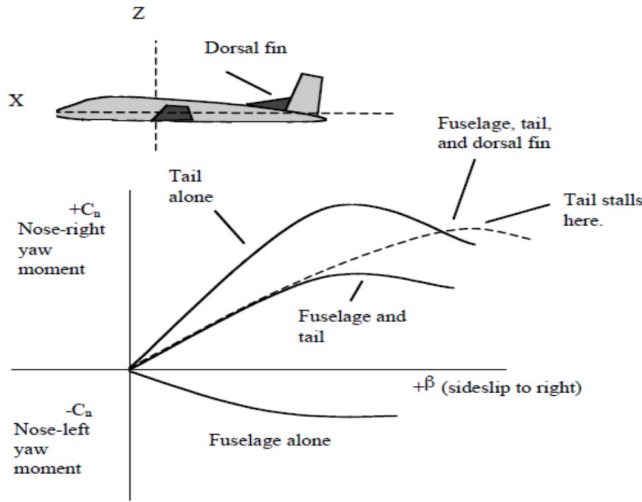
Because of the T-tail configuration, it is assumed at this stage that the tip chord of the vertical stabilizer coincides with and is equal to the root chord of the horizontal stabilizer. Since both the length and position of the horizontal stabilizer root chord are known, this is used as a starting point for the location of the vertical tail. From there, two other parameters need to be decided, which are the aspect ratio and the tail arm. An aspect ratio of 1.2 is chosen based on Figure 9.4, and the tail arm is chosen to be 13 *m* from the nose.



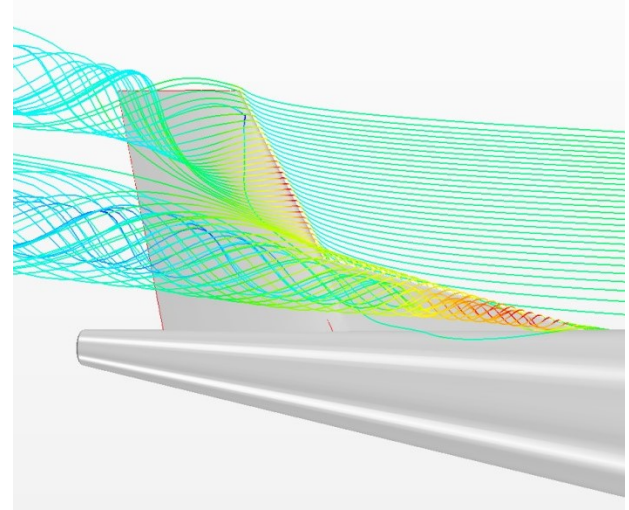
**Figure 9.4:** Vertical stabilizer aspect ratio estimation from reference aircraft [41] (cropped and marked)

The 13 *m* tail arm gives a vertical tail area  $S_v$  of 5.35 *m*<sup>2</sup> when used in Equation 9.1, which in turn gives a tail height of 2.534 *m* based on the aspect ratio. Using the trapezoidal area rule, the root chord of the tail is sized at 2.93 *cm*, and when the 25% MAC is lined up with the 13 *m* point, the leading edge sweep is 43.3°. The resulting surface geometry is shown in Figure 9.8 highlighted in blue. It is worth noting that compared to the values for the King Air 200 in Figure 9.4, the resulting taper ratio is smaller, and the leading edge sweep is higher. This is a result of using the assumption that the vertical stabilizer tip chord is equal to the horizontal stabilizer root chord for the planform design.

In addition to the vertical stabilizer, it is decided that the Sustainable Air Taxi will also have a dorsal fin. Dorsal fins serve to delay the stall of the vertical stabilizer at high sideslip angles and extend the yawing moment coefficient-sideslip curve as shown in Figure 9.5 with the dashed line. This is important because a vertical stabilizer stall can cause "rudder lock," rendering the rudder stuck in the fully extended position and with the pilot unable to center it, which can be dangerous. The dorsal fin accomplishes by generating a vortex slightly before the tail, energizing the flow and delaying separation from the vertical stabilizer as illustrated in Figure 9.6. In addition, since its structure is lightweight and usually separate from that of the vertical stabilizer, a dorsal fin is a convenient way to add vertical surface area without significant weight increase [58].

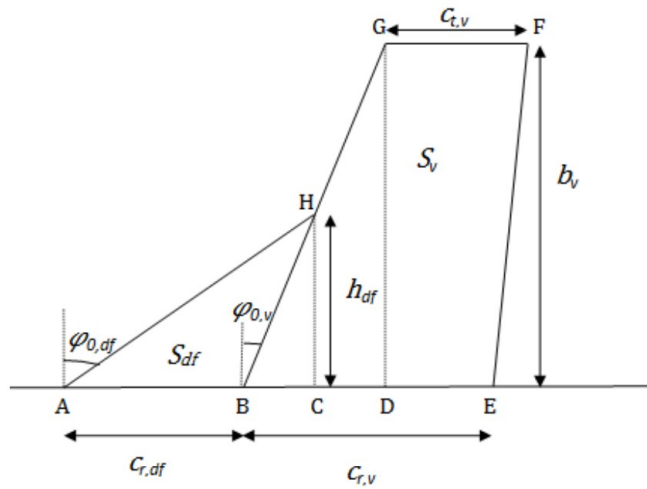


**Figure 9.5:** Effect of dorsal fins on yawing moment with increasing sideslip [58]



**Figure 9.6:** Vortex generation by the dorsal fin at high sideslip angles [59]

In order to size the dorsal fin, the method presented by Barua et al. [58] is used. The method uses statistical regression on reference aircraft to find a relationship between the leading edge sweep angles and surface areas of the dorsal fin and vertical stabilizer, which result in Equation 9.2 and Equation 9.3. It should be noted that the method used separate analyses for propeller and jet aircraft, and the equations presented here are the ones based on propeller aircraft. Finally, Equation 9.4 gives the height of the attachment point between the vertical tail and the dorsal fin using the previously calculated parameters, all of which are defined in Figure 9.7.



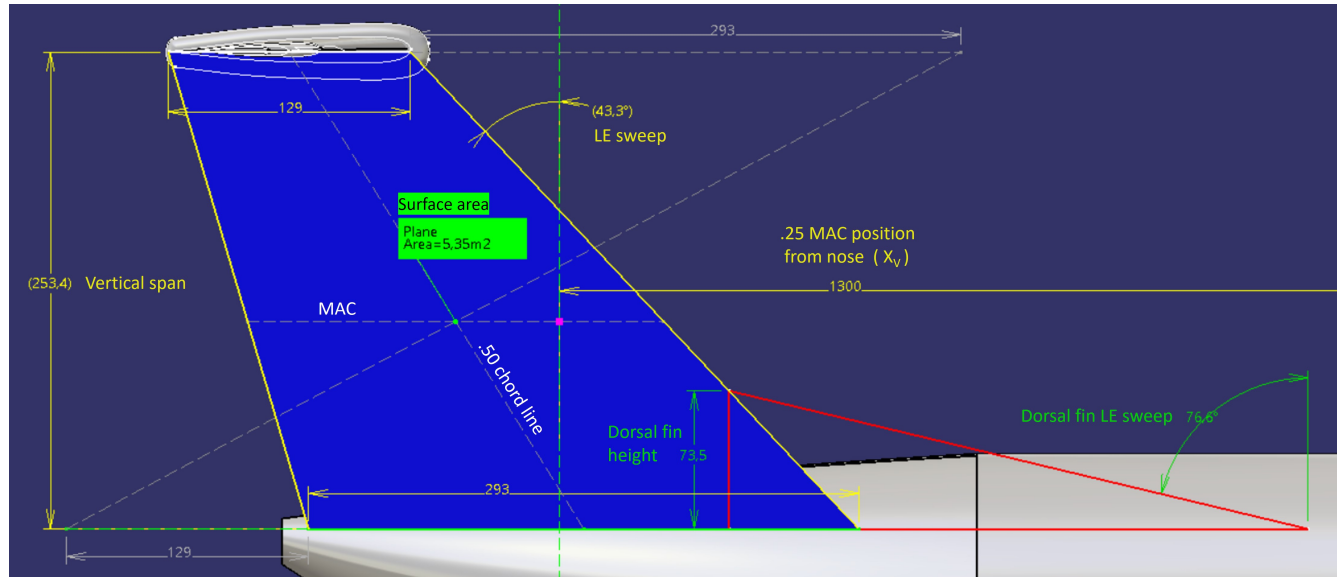
**Figure 9.7:** Definitions of dorsal fin geometric parameters [58]

$$\phi_{o,df} = 70.49^\circ + 0.141\phi_{o,v} \quad [58] \quad (9.2)$$

$$S_{df} = 0.164S_v \quad [58] \quad (9.3)$$

$$h_{df} = \sqrt{\frac{2S_{df}}{\tan\phi_{o,df} - \tan\phi_{o,v}}} \quad [58] \quad (9.4)$$

Using this method with the vertical stabilizer area and leading edge sweep yields a dorsal fin with a leading edge sweep of  $76.6^\circ$  and an attachment point  $73.5\text{ cm}$  above the vertical stabilizer root. The resulting geometry is shown in Figure 9.8 with red lines, alongside the vertical stabilizer planform shown in blue as mentioned earlier. Note that a large portion of the dorsal fin does not actually protrude above the fuselage (shown in white-grey in the figure). This is because the root of the dorsal fin is on the same line as the vertical stabilizer root as shown in Figure 9.7, which is defined not at the fuselage surface, but on a plane slightly below it such that the root remains horizontal.



**Figure 9.8:** Vertical stabilizer planform, dimensions in [cm]

There are a few considerations to address in further design of the tail not included in this report. Firstly, an airfoil selection for the tail should be made. This will typically be a symmetrical airfoil with a thickness between 9-12% (e.g. NACA 00-series) or a negatively cambered airfoil (e.g. NACA 23012 inverted) for improved stall behaviour [39]. Another consideration is the "deep stall" problem that T-tail aircraft face, which is when at high angles of attack near or beyond stall, the airflow to the horizontal stabilizer can be completely blanketed by the wing, making it very difficult to recover. This issue can be addressed by the implementation of a stick pusher, which detects a stall condition from the airspeed, angle of attack, flap settings etc. and forces the nose down automatically. This feature is commonly used, but safety considerations such as enabling a pilot override option and redundancy in sensors are important. In addition, the control surfaces of the tail need to be sized based on stability derivatives and required control forces to have good handling characteristics. The design of the rudder also needs to account for a one engine inoperative scenario, but this is not within the scope of this design stage since it requires difficult-to-obtain lateral stability and control derivatives. Recommendations for further steps in the design are discussed in Chapter 17.

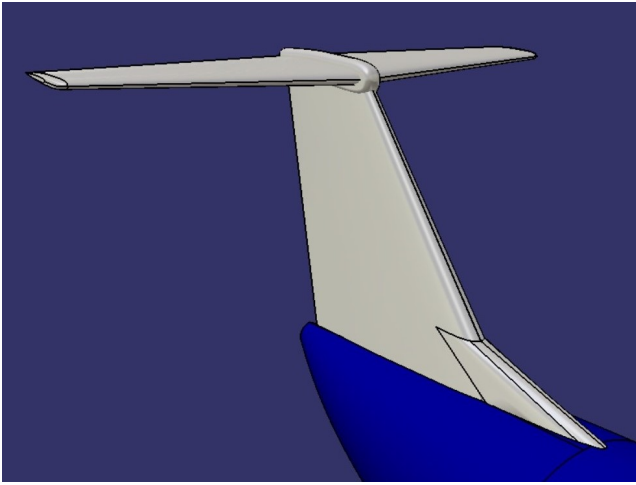
The complete empennage layout based on the sizing and positioning done in this section can be seen in Section 9.2, along with the integration of the propulsion system and wings to the fuselage and the complete aircraft model.

## 9.2. Final Layout of Aircraft

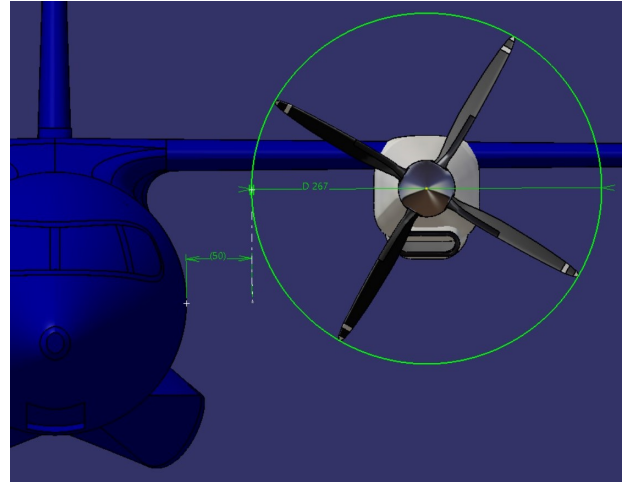
With all main elements of the aircraft sized and positioned, this section briefly shows how they all come together. Figure 9.9 shows the CAD model of the horizontal and vertical stabilizers and the dorsal fin positioned on the tail cone. A small fairing is visible at the top of the vertical stabilizer, the purpose of which is to reduce aerodynamic interference at the right angles between the vertical and horizontal tailplanes.



Figure 9.10 shows the positioning of the propeller and engine pod assembly on the wing, with fuselage clearance detailed in Section 7.12. The engine pod is blended onto the wing without a pylon as is seen in reference aircraft, which is also visible in Figure 9.13. Since it is interrupted by the wing structure, the engine pod is sized slightly wider than required by the internal layout shown in Figure 7.19 to ensure that all systems fit inside.



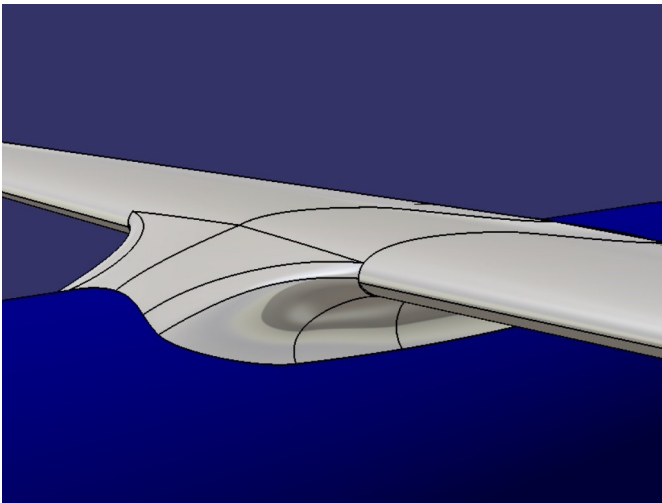
**Figure 9.9:** CAD model of empennage with planform parameters from Section 9.1



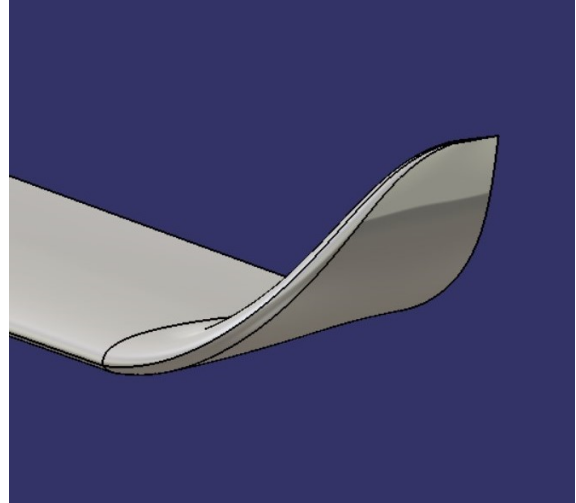
**Figure 9.10:** Positioning of engine and propeller assembly with horizontal fuselage clearance

As mentioned earlier in Section 5.1, the wing structure does not intersect the fuselage since there is limited room in the cabin, and more importantly, the longitudinal wing position from Section 4.11 means that the wing coincides partially with the fuel tank as seen in Figure 9.14. This results in a high vertical position of the wing, and in order to merge it to the fuselage without causing high interference drag, an aerodynamic lofting is required. This is visible in Figure 9.11, and is modelled based on similar high-wing aircraft.

Finally, a simple winglet design to reduce lift-induced drag is shown in Figure 9.12. The height of the winglet is kept short so as to not induce a significant bending moment on the wing structure.



**Figure 9.11:** Wing-fuselage lofting for reduced interference drag



**Figure 9.12:** Winglets for lower lift-induced drag

A render of the complete aircraft model is shown in Figure 9.13, as well as a cutaway view in Figure 9.14 showing the position of the aft liquid hydrogen tank with respect to the wing, landing gear, and the rest of the airframe.





**Figure 9.13:** *Render of the Sustainable Air Taxi in flight*



**Figure 9.14:** *Cutaway view of the aircraft showing the aft fuel tank*

# Verification and Validation

In order to create the design of the aircraft, several tools have been created. Consequently, the tools should be verified and validated in order to ensure that they perform their required functions and deliver the required results. The verification of the tools is categorized into subsystem and system types of verification. Each category has its own verification tests. Moreover, for validation, the whole model is validated against other aircraft that are representative of our design.

## 10.1. Sizing Tools Verification

In this section, the verification of the Python tools that are responsible for the sizing of the aircraft is made. The verification of the sizing tools consists of unit tests, convergence tests, extreme value test and finally a sensitivity test.

### 10.1.1. Unit Tests

**test\_regress()** This unit test verifies the correct implementation of the regression of the OEW-MTOW relation from existing aircraft. An alternative regression on the same data is done with the *numpy.linalg.lstsq* method, compared to the actual method that is used, namely the *scipy.stats.linregress* method.

**Result:** Pass.

**test\_fuel()** This unit test verifies the part of the code that calculates the fuel mass by manually computing the fuel fractions and the MTOW. Then, the value from the code is compared with the manually calculated value.

**Result:** Pass.

**test\_flightcontrols()** In this unit test, similar to **test\_fuel()**, a calculation is worked out manually for arbitrary inputs on the flight controls mass estimation formula. Then it is verified that this manual calculation yields the same answer as the Python program.

**Result:** Fail.

The code is inspected closely and a small mistake is found as indicated in Listing 1. Hence, prior to correcting this mistake, the flightcontrols system mass was over estimated.

```

1      self.w_flightcontrols = 0.053 * self.length_fus[-1] ** (1.536)
2      * self.b_w ** (0.371) * (self.limit_factor * self.limit_load * self.w_design *
    ↪ 10e-4) ** 0.8

```

**Listing 1:** By mistake 10e-4 was written instead of 10 \*\* -4

**test\_powertrain()** In this unit test it is verified that if the required shaft power is zero, the electric motor power is also zero. Subsequently it is verified that the fuel cell power is correctly given by the sum of the cooling power (according to the semi-empirical formula) and the compressor power. It should be mentioned that this is not a physical situation: if no power is required, all power values are zero. The only reason to verify this scenario is to make sure the implementation of the equations is correct.

**Result:** Pass

**test\_stability()** In this unit test it is verified that the stability constraint is correct with respect to any given ratio of horizontal tail surface area to wing surface area.

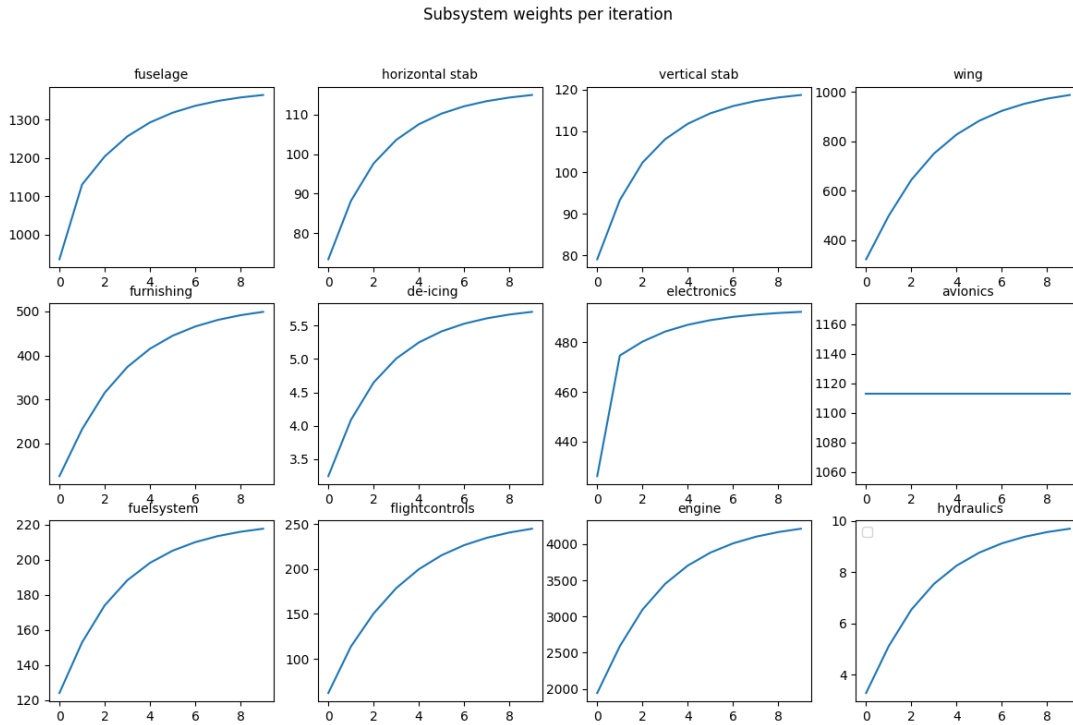
**Result:** Pass

**test\_controlability()** In this unit test it is verified that the controlability constraint is correct with respect to any given ratio of horizontal tail surface area to wing surface area.

**Result:** Pass

### 10.1.2. Convergence Test

**Subsystem Convergence:** As shown in Figure 4.5, to have a final design, the parameters used initially for the aircraft undergo two main iteration loops. However, the condition for the iteration loop to break is that the operating empty weight in the previous iteration is equal to the operating empty weight after the iteration. Therefore, on a subsystem level it is important to analyse the masses of all the subsystems and check if they converge.



**Figure 10.1:** Subsystem weights per iteration in kg

Figure 10.1 shows how the subsystem weights converge after each iteration to a certain value, this verifies the fact that the weights do converge (avionics weight stays constant due to the fact that it was assumed to be a value that is independent of the aircraft parameters).

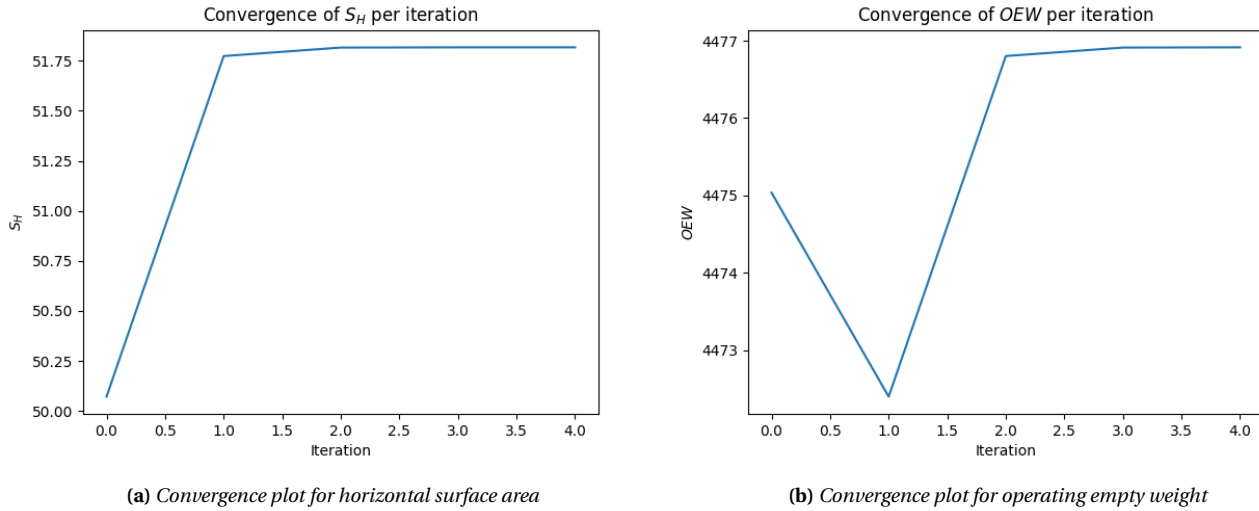
**System Convergence:** In order to assess the whole system for convergence, the operating empty weight of the aircraft is recorded every time the stability optimisation occurs (from Figure 4.5). As a result, the plots in Figure 10.2 show the convergence of the parameters with respect to the optimisation and iteration of the aircraft.

### 10.1.3. Extreme Value Test

Extreme value testing is required in order to test if the code gives realistic results for unrealistic inputs. As an extreme test, all the efficiencies used in the code have been changed to values of 0 and 1 as they represent the extremes of that parameter. Consequently, the output value corresponding to the parameter is checked to see whether or not the output is consistent with the corresponding efficiency. As a result of the analysis, it is safe to conclude that the code outputs the expected results when an extreme value is used.

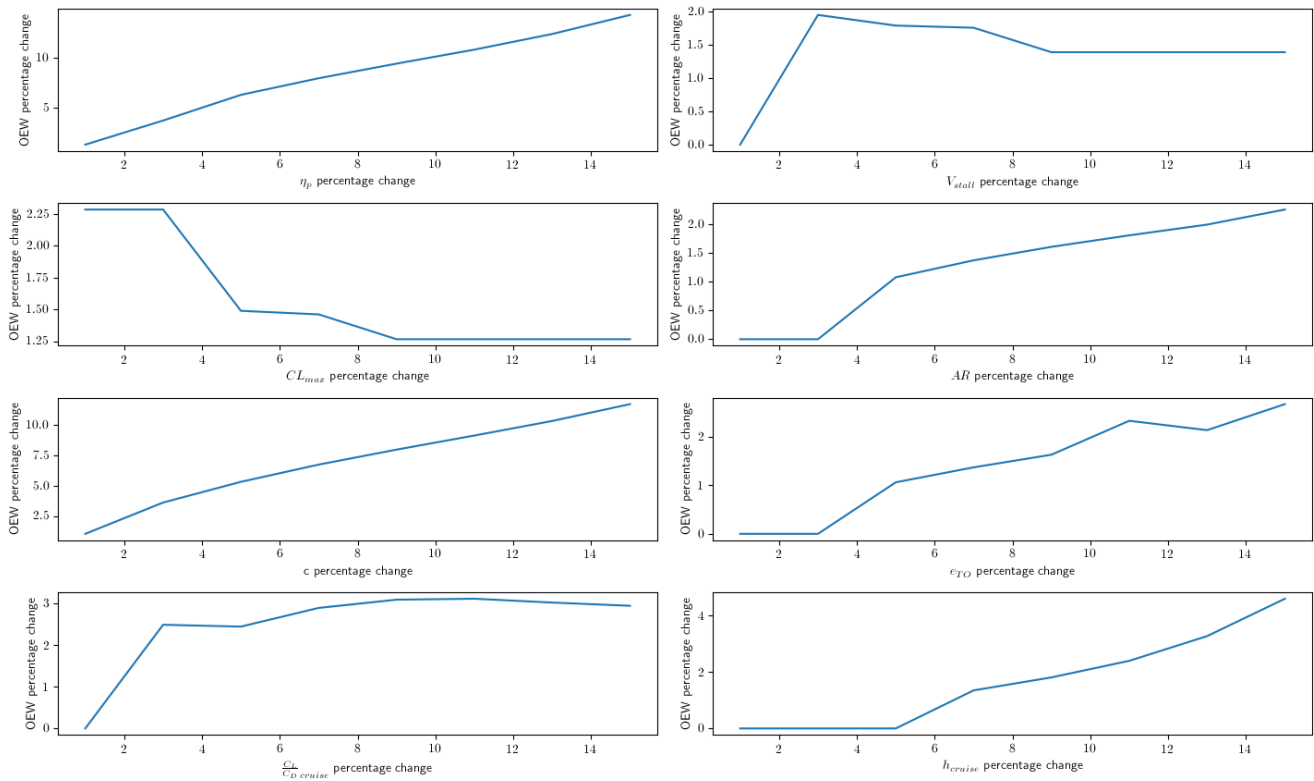
### 10.1.4. Sensitivity Test

To perform a sensitivity analysis, the integrated Python script (including all estimation and sizing tools) is used in a loop where the change caused by changing each parameter is measured. Subsequently, given a certain



**Figure 10.2:** Convergence tests for the stability analysis and the class I and class II tools

input percentage, the algorithm is made in such a way that if the parameter percentage change is more than 1% and the change in operating empty weight caused by the change is less than 1%, then the parameter is excluded from the analysis and the design is considered to be insensitive with respect to that parameter. If the change in the parameter causes a change of more than 1% in the operating empty weight, then the name of the parameter is recorded as shown in Figure 10.3.



**Figure 10.3:** Output of Current tools analysis vs Literature [32]

As shown in Figure 10.3, the output of the analysis is very sensitive to the propeller efficiency and the climb rate

( $c$  and  $\eta_p$ ) with a relationship between the input percentage change being almost linear to the output percentage change. On the other hand, the relationship between the input percentage change to the output percentage change for the other parameters seems to be represented by a non linear relationship (e.g:  $C_{Lmaxclean}$  changes 2 percent of the output when the parameter change is 1 or 3 percent). However, when the parameter change is more than 3 percent then the change in the operating empty weight is around 1 percent, which means that the relationship between the variable and the final result is non linear.

## 10.2. Aero-tools verification

Aero-tools consists of all the code that was used in the design of the wing. This includes calculating the lift distribution, bending moments and stress, buckling, torsion, stringer placement and wing box weight. There are multiple ways in which this code is verified.

### Check by plotting

This test relies on plotting the different outputs of the code and checking whether the distribution is the same as expected. For example, the bending stress is expected to increase with the span and show a dip at the location of the engine. Moreover, it should also be zero at the tip and largest at the root. If these things are not the case something is wrong and the code has to be checked. This was done for all tested loads and the test succeeded every time.

### Extreme value testing

Some parameters have a big effect on the outcome of the program. In order to test if the code works as expected extreme values can be inserted into these parameters. The tested parameters are: velocity and load factor. For both 0 and a large value were inserted and the program acted accordingly.

### Analytical comparison

The total lift can also be calculated analytically. This can be done using the normal formula for lift and using the  $C_L$  from XFLR5. It should be equal to the lift calculated by the program. This was checked and the program passed.

## 10.3. Python Tools Validation

In order to check if the values produced by the Class I, Class II, stability and control analysis are valid, a comparison to a similar aircraft has to be made. Moreover, based on the analysis performed by G. L. M. Vonhoff [32], the input parameters used to produce a hydrogen powered aircraft is presented in Table 10.1. Furthermore, the input parameters from Table 10.1 were used in our tools and the output of the results were compared to the output of the results produced by G. L. M. Vonhoff [32] in Table 10.2.

**Table 10.2:** Output of Current tools analysis vs Literature [32]

Output Parameter	Thesis Results	Tools Results	Unit	Difference [%]
MTOM	4907.2	5010.39	$kg$	2.1
OEM	3736.3	3647.43	$kg$	2.4
$m_{fuel}$	166.1	132.96	$kg$	20
$\frac{W}{S}$	1323.7	1102.50	$\frac{N}{m^2}$	17
$\frac{P}{W}$	15.2	17.2	$\frac{W}{N}$	13

As shown in Table 10.2, the created model produces accurate results when used to compute the operating empty mass and maximum take off mass. However, for the fuel,  $\frac{W}{S}$  and  $\frac{P}{W}$  the outputs are considerably different (even though the order of magnitude is fine). This could be explained by the fact that the paper in [32] did not include the difference in  $C_{Lmax}$  when full flaps are on and when the aircraft is in cruise, which has an effect on the value of power loading and wing loading. Additionally, G. L. M. Vonhoff did not include the value used to take into

**Table 10.1:** Input Parameters used to produce results produced by G. L. M. Vonhoff [32]

Parameter	Value	Unit
R	317	$km$
$V_{cruise}$	93	$ms^{-1}$
c	6.27	$ms^{-1}$
$V_{stall}$	30	$ms^{-1}$
Take-Off distance	800	$m$
$h_{cruise}$	3000	$m$
$n_{passengers}$	10	-
$m_{payload}$	300	$kg$
$C_{D_0}$	0.028	-
$C_{L_{max}}$	2.2	-
$m_{passenger}$	93	$kg$
$\frac{t}{c}$	0.2	-
taper ratio	0.8	-
Tail fineness ratio	1.5	-
Nose fineness ratio	2	-
Seat pitch	0.8	$m$
Door length	1	$m$

Parameter	Value	Unit
$AR_{ht}$	5	-
$AR_{vt}$	5	-
$\rho_{FC}$	2000	$Wkg^{-1}$
$\rho_{PMAD}$	10000	$Wkg^{-1}$
$\rho_{em}$	5000	$Wkg^{-1}$
$\rho_{comp}$	2000	$Wkg^{-1}$
$\eta_{fc}$	0.5	-
$\eta_{PMAD}$	0.9	-
$\eta_{ee}$	0.9	-
$\eta_{volumetric}$	0.5	-
$\eta_{comp}$	0.7	-

account loitering and the fuel fractions that were used for the flight mission. This explains the difference in fuel mass. Overall, since the results were sufficiently similar to the ones produced in the same paper and given the lack of aircraft that can be used as reference for the Sustainable Air Taxi, the Python code can be considered to be verified, as far as the purpose of this report goes.

# Production plan

Since the aircraft should be transformed from an engineering design to an actual physical object, a production plan is made. This plan describes how specific systems are manufactured and the approaches used. At first the general production plan is outlined in Section 11.1. Then, Section 11.2 concerns the specific production plan for each system. At last, for the whole design and production process, a sustainable approach should be maintained with a lean manufacturing philosophy, ensuring that limited waste is generated. Moreover, sustainable manufacturing, joining and assembly methods should reduce the aircraft's environmental impact. A general outline for how the sustainability goals may be achieved during production is given in Section 11.3.

## 11.1. General Production Plan

The aircraft will be divided into distinct systems and subsystems, including the main wing, the horizontal and vertical tail surfaces, the fuselage, the propulsion system and the undercarriage. Within this division, the fuselage for instance, will be further separated into the cockpit, main cabin and tail cone. These divisions are made in order to enable concurrent manufacturing of parts and assembly of subsystems, which allows for a higher production efficiency, better accessibility and ease of production. Furthermore, dividing the aircraft this way allows for a clearer separation of systems in the preceding design process. Additionally, expensive and complex parts (e.g. engines) are mounted at a later stage as will be explained below.

The production process starts with obtaining the material stock for the production of parts. These parts will be manufactured in batches to ensure time and cost are efficiently spent. Not all parts or systems will be manufactured in house and thus, some will be obtained from third party sources. After the necessary first order parts and components have been either manufactured or obtained, they can be assembled into subsystems. This production and assembly will take place within a production and assembly line consisting of several stations. The created subsections will already include the necessary cables, lines and sub components that cannot be accessed after subsections have been joined together. The joining method for these parts relies on what joint properties are desired. This can imply permanent or removable, stiff or movable and external or internal (etc.) joints. This choice is also influenced by the materials incorporated in the joining section as well as the required accessibility or removability of parts and components. For the removable joints, bolts or rivets will be used, whereas for the permanent joints adhesive or welding may be implemented. For assembly of systems such as the fuselage and aerodynamic surfaces, assembly jigs should be used to ensure accurate alignment and support for heavy assemblies during the manufacturing stage. Next to that, adequate jigs will still allow workers to access relevant parts during assembly. One of the final steps of the assembly usually consists of mounting the engines to the aircraft since they are expensive, heavy and prone to performance hindering damage. Mounting them earlier would complicate subsequent assembly stages, requiring stronger support structures and needing more attention towards not damaging the engines, hence, having to be implement larger clearances when moving the aircraft from one stage to another.

## 11.2. System specific production plan

In subsequent sections each main system is discussed in terms of its specific production steps. Subsection 11.2.1 discusses the manufacturing of the aerodynamic surfaces, whereas Subsection 11.2.2 concerns the fuselage. Then, Subsection 11.2.3 explains the fuel tank production and Subsection 11.2.4 includes the manufacturing of the engine system. At last, Subsection 11.2.5 discusses how all systems are joined together to form the complete aircraft.



### 11.2.1. Aerodynamic Surfaces

The wing is one of the largest systems of the aircraft that needs to be manufactured. As mentioned in Chapter 8, the wing will be made exclusively out of 7050 aluminium sheets which will be taken from stock. Because of this design choice, the complete production line for the wing can make use of the same material stock. Since the wing consists of multiple subsystems, a division is made of main wing, flaps and skin panels. Because of the high wing configuration, the wing and thus wingbox are essentially installed on top of the fuselage. As a result, the wingbox for the entire wing can be made in one piece. For this to work, the design should include continuous stringers and spars with large assembly jigs. An example of a wingbox skeleton is shown in Figure 11.1<sup>1</sup>. The spars, ribs and stringers are created in separated production lines for concurrent manufacturing. The spars are created from thicker aluminium beams where holes are drilled into and cutouts cut out of. Then, with the use of a bending machine the final shape will be given to the spars. For the ribs, a similar process is utilised for creating the shape of the ribs together with the holes and cutouts. After this, the ribs will get their final shape by means of a press and die combination. The stringers are cut into shape after which they are bent to obtain the needed shape. After the previously mentioned parts have been created, they will be joined together by means of riveting and supported by a assembly jig. As the wings and wingbox are still a skinless assembly, everything is still accessible within the structures itself. As a result, all required hydraulic lines, actuators and electronics can now be installed within the wing structure.

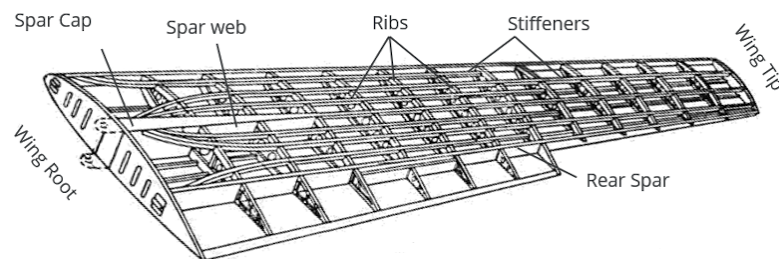


Figure 11.1: Schematic wingbox

Another assembly line will produce the flaps, as schematically shown in Figure 11.2, which follows the same production process as the wings themselves. One of the last steps left is to install the flaps and install the skin panels, except for the access panels to mount the engine pods and the mounting points to the fuselage. It should be noted that the same manufacturing principles apply to the empennage system. However both the vertical and horizontal tail are created in a separate production line for efficiency.

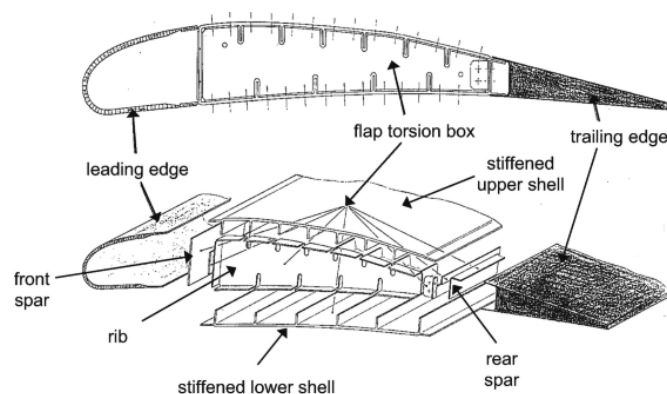


Figure 11.2: Schematic flap wingbox[60]

<sup>1</sup><https://aerotoolbox.com/wing-structure/>

### 11.2.2. Fuselage

As mentioned before, the fuselage will be separated into the nosecone, main fuselage and tailcone. The fuselage will be entirely made from aluminium acquired from stock. The production processes rely on the same principles as explained in Subsection 11.2.1. First, the hoop frames are stamped to form their shape and all the holes or cutouts after which the final shapes are pressed into the part. After all the holes and cutouts have been created by a press, the stringers and floor beams are bent into shape. Now, the hoops will be aligned with help of an assembly jig after which the stringers, hoop frame be riveted for joining. At last, the skin, together with the windows, will be applied to the airframe. The tail cone and cockpit are both manufactured in a different assembly line for efficiency, however, the manufacturing techniques still rely on the same principles as for the rest of the fuselage. It should be noted however that special care has to be put into the instrumentation installation within the cockpit after the structure is finished.

### 11.2.3. Fuel Tank

As discussed in Subsection 6.1.1, the tank will be manufactured from 2219 aluminium. Sheets of aluminium will be taken from stock and transformed into the desired shapes to build the fuel tank. As depicted in Figure 11.3 the tank will be made from 3 different sheets of aluminium. It should be noted however that the current production plan does not take into account margins or deformations, like springback, which might result in small deviations in the measurements being needed. The domed sections indicated with number 1 are circular sheets, blanked from 3 mm thick sheets of 2219 aluminium with a punching machine. The cylindrical section, indicated with number 2, will be made from a 1.8 m by 10.12 m sheet of the same aluminium as mentioned before. It will be formed into a cylindrical shape by making use of a roll bending machine. Then, to form a continuous loop, the ends of the sheets are friction stir welded (FSW) together. Because of the high thermal conductivity of aluminium a lot of energy is required to weld with conventional MIG, TIG, MAG and electric arc techniques. This high amount of energy might result into deformation of the part with the addition of degradation of properties. FSW has a joining efficiency between 70-100% while conventional MIG welding has an efficiency of around 40-50%. At last, FSW will make it possible to weld high performance aluminium parts in the 2000 and 7000 series. To join the 2 domed ends to the cylinder, again FSW is used after the parts have been aligned making the tank one complete structure.

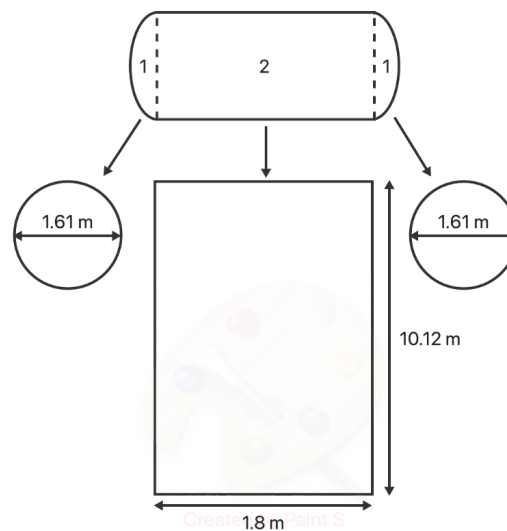


Figure 11.3: Schematic tank sheet parts

After the tank is one solid piece, all required holes are drilled and the support blocks are fitted. The support blocks are made from Foam Glass, as mentioned in Subsection 6.1.3, consisting of cellular glass and carbon. These blocks will be in stock and cut into the desired shapes before installation. As mentioned in Subsec-

tion 6.1.2, the tank will be insulated by a shell of EPS foam. The insulation will be formed by a similar process as depicted in Figure 11.4 which is based on injection molding. For assembly, the actual EPS insulation will be divided in 2 halves to ease the installation of the tank within the insulation.

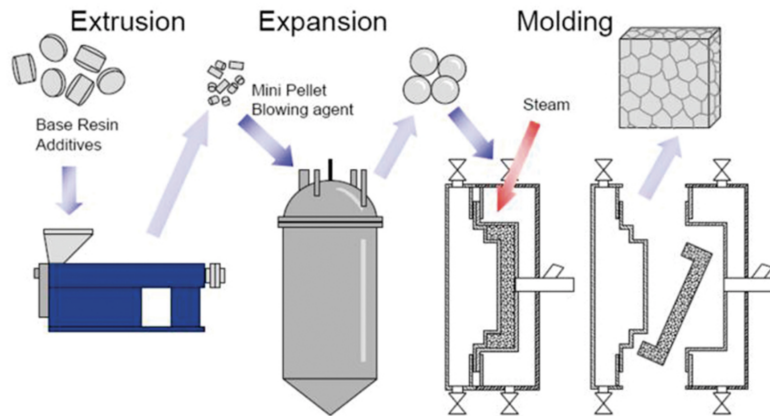


Figure 11.4: Eps forming process[61]

#### 11.2.4. Power System

For the production of the propulsion system a division is made into internal components, as seen in Figure 7.19 and external propulsion system. The external systems include the propellers and the propeller cone as seen in Figure 11.5. It should be noted that all subsystems needed for the propulsion unit are acquired from 3rd party manufactures. These subsystems include the electric motor, motor controller, inter-cooler, compressor, heater, humidifier, fuel cell stack, propellers and propeller cone. The components that are produced in-house are the frame of the engine and the nacelle panels. After the internal parts are acquired, they will be mounted to the frame of the engine and connected to the other subsystems. Then, all nacelle panels will be riveted to the frame to form one engine pod. The propeller assembly is created separately from the internal system and will be installed at the very end of the whole aircraft assembly process for safety and damage mitigation reasons. This postponement does result in a greater use of connectors for the systems. However, having connectors is a convenient solution for testing and replacing systems concerning maintenance and thus a specific design choice made.



Figure 11.5: Exploded view engine system

### 11.2.5. Total Assembly

After all systems have been manufactured in separate production lines, they are joined together in the final production line. After all fuselage sections are finished, the fuel tank will be mounted to the main fuselage before the tailcone is installed. After the tank is put into place, both the cockpit and tailcone are aligned with the main fuselage, with the help of an assembly jig, and bolted together to create one complete fuselage. Both the main wing and empennage will be installed on the fuselage now that the whole fuselage has been put together. The wing will be installed by means of a crane to reach the needed height. It should be noted regarding the T-tail, that the horizontal and vertical stabilizers will be joined together before mounting the empennage to the fuselage. After all systems are installed, they can at last be connected to form one whole functioning system. Since the whole structure is now able to support itself, the undercarriage is installed. To limit the dependence on our own resources, the undercarriage components are produced by a third party manufacturer and then assembled within our assembly line.

## 11.3. Sustainable Production

As a key factor of the air taxi, sustainability also has to be considered during production. This section aims at giving guidance for how to achieve an environmentally sustainable cradle-to-gate production by briefly looking at joining methods, manufacturing techniques and supply chain considerations.

When it comes to joints, it is generally advised to avoid current adhesives from a sustainability standpoint [74]. For one, during the production and application of adhesives, toxic substances are emitted. While these may not contribute to global warming, they are main contributors to impact categories that affect human health and ecosystems. In terms of global warming, adhesives have an elevated impact, since their production and application is energy intensive and as a result entails indirect carbon dioxide emissions. Next to that, being made from crude oil, they contribute to the depletion of finite resources. Lastly, once applied they complicate recycling as separation of components at end-of-life again uses plenty of energy and sticks to the components. In case bolted or riveted joints are used, it would be beneficial to choose the same material as the joined elements or make the employed materials clearly distinguishable through colour coding or engraving. That way, materials can be recycled as efficiently as possible. For the fuel tank, friction stir welding is used which does not produce harmful gasses and does not make use of consumables. From a sustainability point of view, friction stir welding is the best solution for permanently joining metals together.

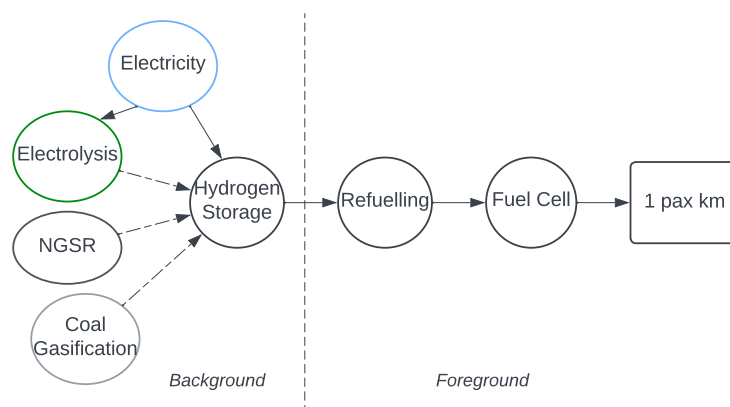
The next point concerns manufacturing processes, which are highly dependant on the chosen material. Processes that require large amounts of energy should be circumvented, since they will lead to high indirect emissions. Furthermore, lean philosophies should be implemented where possible. When machining a part, for example, the dimensions of the pre-fabricate should be such that the removed volume is kept as small as possible to reduce waste. Chipped material should also be recycled if suitable (e.g. aluminium). The supply chain that leads up to the final assembly should be assessed regarding transport and resource extraction. A lean manufacturing philosophy suggests that the transport distances for components and assemblies should be as short as possible, reducing waste as time and carbon emissions, since transport is heavily reliant on hydrocarbons as fuel. Although long transport routes should be avoided, the environmental impacts of resource extraction depending on location should be kept in mind. Luckily, acquiring aluminium from countries within the EU is favourable from a sustainability standpoint. For one, transportation routes are shortened and moreover, EU countries have the least carbon intensive production processes in the world [65].

## Impact Analysis

With the design being completed, one can recall the concept of Life Cycle Assessment (LCA) outlined in Chapter 3. This chapter seeks to assess the environmental impact of the operations (Section 12.1), production (Section 12.2) and end-of-life (Section 12.3) stages.

### 12.1. Operational Impact

Figure 12.1 represents a simplified flowchart from hydrogen production to the functional unit of one flown passenger kilometer. As the total impact of the operational stage is heavily dependent on the hydrogen production process, three alternatives for hydrogen production are considered. Those are natural gas steam reforming (NGSR), coal gasification, and water electrolysis. Furthermore, electrolysis is modelled using different sources of electricity and future scenarios. As a starting point in the impact analysis, the Air Taxi's hydrogen consumption is put at  $35.78 \frac{gH_2}{pax.km}$ , reached at a range of 1500 km carrying 6 passengers. From here on, the operational GWP can be assessed for foreground and background processes and compared to that of similar aircraft.



**Figure 12.1:** A simplified impact analysis of the operational processes.

#### 12.1.1. Foreground Emissions

As depicted in Figure 12.1, the foreground emissions can be traced back to the fuel cell operation and refuelling. Since the propulsion system contains a system that captures unreacted hydrogen and only emits water vapour, the GWP of the reaction process during flight is disregarded. Regarding the refuelling process, it is assumed that 1.5 % of the fuel is lost through leaking and spilling.<sup>1</sup>  $H_2$  having a climate change potential 11 times greater than  $CO_2$ , the GWP of refuelling amounts to  $5.9 \frac{gCO_2-eq}{pax.km}$ , if leakage is assumed.

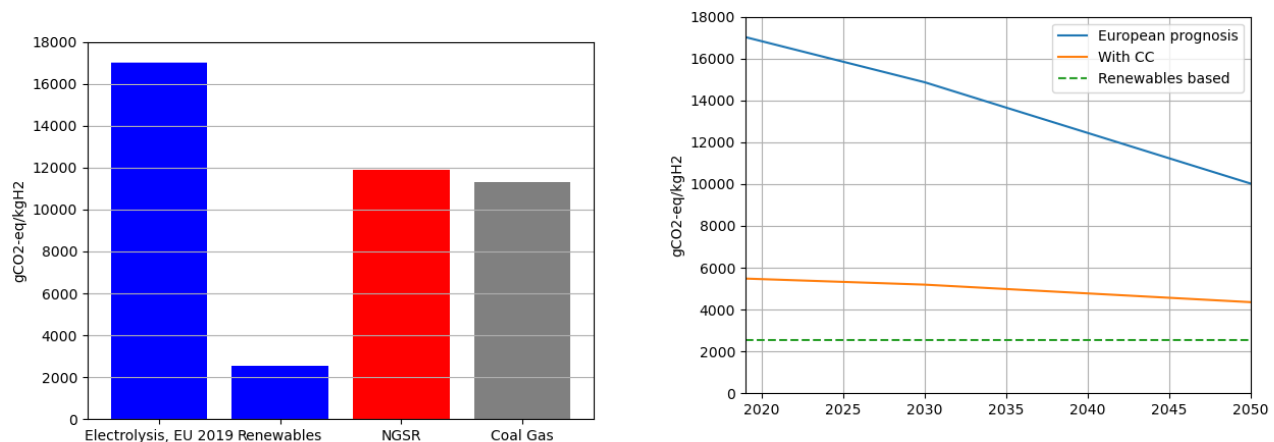
#### 12.1.2. Background Emissions

For the quantification of background emissions, hydrogen production and storage are considered as the leading processes. Impacts stemming from storing can be traced back to cooling the hydrogen to the required cryogenic temperature. Using a specific heat of  $1.304 \frac{J}{gK}$ , the required energy to cool down  $H_2$  to 20 K (from standard atmospheric 288 K) at a cooling efficiency of 60 % results in  $0.162 \frac{kWh}{kg}$ . Doing this by drawing electricity from the

<sup>1</sup><https://www.climatecentral.org/news/limiting-methane-leaks-critical-to-gas-climate-benefits-16020> [accessed 14-06-2022]

average European grid, adds only  $1.7 \frac{gCO_2-eq}{pax.km}$  to the GWP.

By far, the largest share to the operational GWP can be traced back to the production of hydrogen. Figure 12.2a displays the GWP of water electrolysis, natural gas steam reforming (NGSR) and coal gasification in  $\frac{gCO_2-eq}{kgH_2}$ . As the GWP of water electrolysis is strongly linked to the electricity source, the GWP is given for two scenarios. The first one uses electricity from the average EU energy mix produced in 2019 (pre-pandemic) that is derived from an annual statistical report conducted by BP [73] in combination with numbers from Gibon [72], that are both found in Table 12.1. Next to that, a renewable energy mix that is composed mostly of wind, photovoltaic and hydro energy is provided for comparison, clearly showing the benefits of green hydrogen. Figure 12.2b models the production impact from water electrolysis for three scenarios: The regular European commission prognosis [71], the same but using carbon capture technology for hydrocarbon fuel plants and one scenario where the electricity grid is based on renewable energy sources, where fluctuations in energy demand are covered by battery storage and gas plants. The energy demand of electrolysis is set at  $5 \frac{kWh}{m^3}$  at 288 K equivalent to  $59.5 \frac{kWh}{kg}$ . [75]



(a) A comparative impact analysis of hydrogen production methods [70].

(b) The impact of water electrolysis for the normal EU energy prognosis, with carbon capture and using mainly renewables.

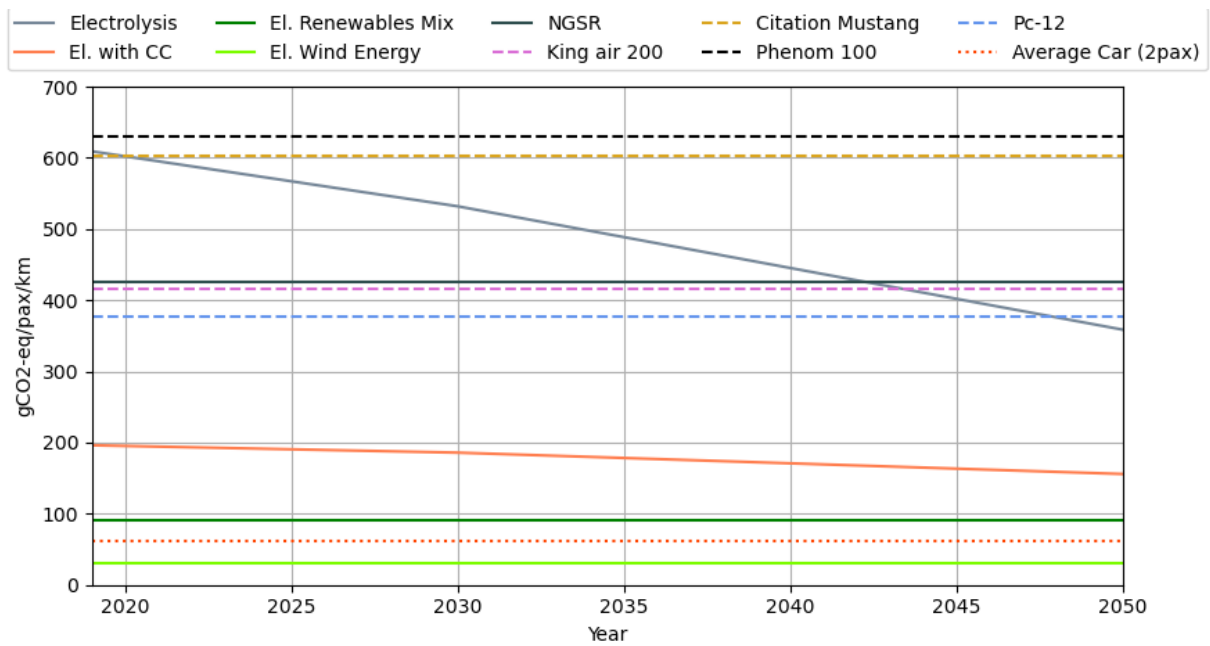
**Figure 12.2:** The impact of producing hydrogen with different production methods and electricity production prognosis

Finally, the  $CO_2$  equivalent emissions per  $kg H_2$  are translated to the passenger kilometre specific GWP  $\frac{gCO_2-eq}{pax.km}$  and can be compared to that of reference aircraft in the same segment. Figure 12.3 shows the GWP of the Sustainable Air Taxi for the different electricity mixes and compares it to that of conventionally propelled reference aircraft. The impacts per passenger kilometre of reference aircraft were estimated by calculating their fuel consumption and taking into account that kerosene production has a GWP of  $500 \frac{gCO_2-eq}{kg}$  and that its combustion leads to an additional  $3160 \frac{gCO_2-eq}{kg}$ .

While the regular energy mix currently makes hydrogen fuel cell aircraft non-competitive with other propeller aircraft, it compares to the GWP of jets in that passenger segment. If, however, renewable energy is used to produce the hydrogen, the Sustainable Air Taxi becomes very environmentally competitive. Using carbon capture technology leads to the same conclusion. In order to lower the Sustainable Air Taxi's carbon footprint below that of a regular car with 2 passengers (GWP =  $61.15 \frac{gCO_2-eq}{pax.km}$ ), even more renewable energy needs to be employed. If the hydrogen for the Air Taxi was to be produced using only wind energy, that goal would easily be reached

<sup>2</sup><https://www.offsetguide.org/understanding-carbon-offsets/air-travel-climate/climate-impacts-from-aviation/co2-emissions/#:~:text=Carbon%20dioxide%20%28CO2%20%29%20is%20emitted%20during%20the,of%20jet%20fuel%20combusted%20%28%20ICA0%2C%202017%20%29.?adlt=strict&toWww=1&redig=B8D15E604C184FCCB8A177219179EB0F> [accessed 14-06-2022]





**Figure 12.3:** The  $CO_2$  emissions per passenger kilometre of the Sustainable Air Taxi (solid lines) and other aircraft (dashed Lines) as well as an average car.

**Table 12.1:** GWP per energy source and the energy mix predictions.

Energy source	GWP [g CO <sub>2</sub> -eq/kWh] [72]	Euro Mix 2019 [73] [%]	2030 Prognosis [71] [%]	2050 Prognosis [%]	Renewables Based [%]
Onshore wind	12.4	-	-	-	-
Offshore wind	14.2	-	-	-	-
Mixed wind	13.3	12	18	25	50
Hydro	5.6	16	11	11	11
Solar ground	11.4	4	7	11	33
Other Renewables	10.1	6	-	-	-
Biopower	64	-	8	9	-
Nuclear	4.7	24	22	18	-
Coal (CC)	930 (200)	18	15	5	-
Gas (CC)	530 (250)	20	19	21	6
Oil (CC)	951 (204.5)	1	-	-	-

with  $30.2 \frac{gCO_2-eq}{pax.km}$ . Note, that the impact of NGSR stems mostly from processes directly emitting greenhouse gases during the chemical reaction needed for production. Thereby, it may currently be a better alternative than water electrolysis but its impact is more or less invariable and largely outperformed by water electrolysis from a green electricity source. Additionally, it can be assumed that with current geopolitical developments, the European union will direct more effort towards energy independence by a swifter move towards renewable energy sources. This would further reduce the projections for the Sustainable Air Taxi's GWP.

## 12.2. Manufacturing

The operational impact of the Sustainable Air Taxi is much lower compared to regular aircraft. The employment of green hydrogen during operations already helps decrease the environmental impact over the operational lifetime by 90 % [11]. As such, the manufacturing process of the aircraft takes up a larger share of the relative impact. In this section, an estimation is made on the environmental impact of the manufacturing process of the aircraft in  $CO_2$  equivalence. It will focus on the impact of the raw materials, since these have large footprints in extraction and processing. Because most systems have not been designed in detail, it is difficult to address the actual raw material input in the systems. Nevertheless, some systems have been designed and in other cases, it can be estimated how much of which raw material goes into manufacturing. In Table 12.2 the



$CO_2$  equivalent in kilograms of manufacturing the raw new material per subsystem is listed. Producing 1 kg of aluminium produces 6.7 kg  $CO_2$ , when produced in Europe<sup>3</sup> and 2.8 kg  $CO_2$  for Copper.<sup>4</sup> However, when using recycled aluminium the direct  $CO_2$  impact is divided by 4<sup>5</sup> with more optimistic estimates going up to a 90%  $CO_2$  reduction, as suggested in the Ecoinvent 3.6 database [65]. The  $CO_2$  impact of copper is decreased by 85% when using recycled material.<sup>6</sup> In Table 12.2 the total impact of the materials used is decreased by more than 9000 kg of  $CO_2$ , when using recycled material. The remaining 57.4 % of the OEW includes all the systems which are not predominantly built from a single material and are therefore difficult to quantify. This includes: furnishing, avionics, fuel cells, APU, cooling system and other small systems. The impact of the other systems is listed in Table 12.3.

**Table 12.2:** *Environmental impact of various subsystems*

Subsystem	Mass [kg]	OEW Percentage	Material	Material as percentage of subsystem mass	Raw CO2 eq [kg]	Recycled CO2 eq [kg]
Wing	430	8.9	Al	100	2,881	720
Fuselage	622	13.7	Al	100	4,167	1,042
Tail (horizontal + vertical)	105	2.3	Al	100	703	176
Propeller	160	3.5	Al	100	1,072	268
Electronics	223	4.9	Cu	90	617	93
Tank	191	4.2	Al	75	1,280	320
Flight controls	109	2.4	Al	100	730	183
Fuel system	97	2.1	Al	75	650	162
Total	2,337	42.6	-	-	12,101	3,914

**Table 12.3:** *Environmental impact of further subsystems*

Component	Component Mass [kg]	OEW Percentage	CO2 eq [kg]
Electric motor <sup>7</sup>	400	8.9	2,946
Fuel Cell <sup>8</sup>	677.8	14.9	67,767
Avionics <sup>9</sup>	505	11.1	7,272
Cooling system <sup>9</sup>	219	4.8	3,153
Battery <sup>10</sup>	114	2.5	2,205
Furnishing <sup>9</sup>	219	4.8	3,153
Misc	473	10.3	6,811
Total	2,212	57.4	93,307

Table 12.3 shows the equivalent  $CO_2$  emissions produced by each subsystem that was not mentioned in Table 12.2. Subsequently, given that the subsystems mentioned in Table 12.3 are made out of compound materials and not just one main material, the way of calculating the equivalent  $CO_2$  produced during manufacturing is different. For the Fuel Cell, Electric motor and Battery, the  $CO_2$  emissions were calculated using sources that indicate the  $CO_2$  emitted per kilogram of the certain system.<sup>78</sup> For the rest of the subsystems in Table 12.3, the emissions were calculated based on the  $CO_2$  emitted per kilogram of a conventional aircraft, then using the

<sup>3</sup><https://european-aluminium.eu/media/3261/european-aluminium-environmental-profile-report-2018-executive-summary.pdf> [accessed at 13-06-2022]

<sup>4</sup>[https://www.winnipeg.ca/finance/findata/matmgt/documents/2012/682-2012/682-2012\\_Appendix\\_H-WSTP\\_South\\_End\\_Plant\\_Process\\_Selection\\_Report/Appendix%207.pdf](https://www.winnipeg.ca/finance/findata/matmgt/documents/2012/682-2012/682-2012_Appendix_H-WSTP_South_End_Plant_Process_Selection_Report/Appendix%207.pdf) [accessed at 13-06-2022]

<sup>5</sup><https://www.aluminium.fr/en/stake/climate-and-carbon-footprint/> [accessed at 18-06-2022]

<sup>6</sup><https://roanemetals.com/benefits-of-copper-recycling/> [accessed at 17-06-2022]

<sup>7</sup>[https://www.researchgate.net/publication/312087454\\_Lifecycle\\_Analysis\\_of\\_Different\\_Motors\\_from\\_the\\_Stand\\_point\\_of\\_Environmental\\_Impact](https://www.researchgate.net/publication/312087454_Lifecycle_Analysis_of_Different_Motors_from_the_Stand_point_of_Environmental_Impact) [accessed 21-06-2022]

<sup>8</sup><https://www.sciencedirect.com/science/article/pii/S0959652620351301> [accessed 21-06-2022]

<sup>9</sup><https://arc.aiaa.org/doi/pdfplus/10.2514/6.2022-1028>

<sup>10</sup>[https://www.transportenvironment.org/wp-content/uploads/2021/07/2019\\_11\\_Analysis\\_CO2\\_footprint\\_lithium-ion\\_batteries.pdf](https://www.transportenvironment.org/wp-content/uploads/2021/07/2019_11_Analysis_CO2_footprint_lithium-ion_batteries.pdf) [accessed 21-06-2022]

mass of the subsystem to calculate the equivalent emissions.<sup>9</sup>

For the purpose of proving that recycling and reusing components of the Sustainable Air Taxi in fact has major environmental benefits, a simplified impact analysis can be performed. If one assumes that due to facilitated recycling, close to 100% of materials in Table 12.2 are recycled in a second generation of Sustaxis, and that 50% of components that can be considered rotatables in Table 12.3 are actually reused, a promising result is obtained. Parts that are considered rotatables can be used as second hand and are, for instance, avionics, switches or even engine parts. Furnishing, on the other hand, is not reused. Then, a first generation of Sustaxis, using no recycled or rotated components emits 105.4 *tonsCO<sub>2</sub>* whereas a second generation Sustaxi emits merely 52.144 *tonsCO<sub>2</sub>* in the material acquisition.

### 12.3. End of life

After the operational life of the aircraft is over, the end of life phase starts. As one of the main focuses is on recycling at least 80% of the aircraft, this represents an important phase to discuss. However, first a substantial note has to be made: If something is recyclable, it does not mean that it will be recycled. There has to be an economic incentive for it to be recycled or reused and it has to be suitable for recycling or reuse. This results in the following issues:

- If it costs more to recycle a certain material than to make that material from scratch, then an End-of-Life company will not make the effort of recycling it.
- Parts are only reusable if they can be removed without damaging them.
- Parts can only be reused if proper maintenance and proper book keeping has been performed. It has to be known in what state the part is.
- Recycling materials is only viable if there is an existing recycling stream. It is not economically viable to set up a recycling company, which focuses on a specific material or type of material, unless there is a constant (large) inflow of material. This means that for the scale of the Sustainable Air Taxi, materials have to be used which can be processed in an existing recycling chain.

Thus, a better focus would be to have an aircraft, of which at least 80% is economically viable to recycle or to reuse. As mentioned, most of the OEW will consist of aluminium. This is beneficial for recyclability, as a large majority of aluminium is recycled in Europe.<sup>11</sup> Recycling aluminium is not only cost effective, it is also more environmentally friendly, because of the large energy requirement of producing virgin aluminium. The *CO<sub>2</sub>* equivalence of recycled aluminium is up to 10 times lower than for producing new aluminium.<sup>12</sup> So when the air taxi has reached its EOL the aluminium content can be easily recycled. There is one major drawback, which is that the high-end aerospace aluminium will be mixed with lower grade aluminium from other sectors and the resulting product will be lower level scrap aluminium. So quality of the aluminium is lost, but it is recycled. In the future there might be companies which will focus on recycling higher end aluminium, giving the aluminium employed in the Sustainable Air Taxi a fully circular life.

In addition to recovering raw material from the aircraft, parts can also be recovered and reused as spare parts in aircraft. If the parts are in a proper condition, they can be reused. Whether a part is in good condition for resale depends on how well it is maintained and if the history of the part is known. This is the job of the operator and is therefore hard to control. Moreover, it is hard to figure out if there is market demand for a certain part, before the aircraft is actually operational. Usually, aircraft parts are reused in the same type or family of aircraft. At this point in time it is difficult to assess which parts in the Sustainable Air Taxi would need frequent replacing.

<sup>11</sup><https://www.european-aluminium.eu/policy-areas/recycling-circular-economy/#:~:text=Aluminium%20recycling%20rates%20in%20Europe,in%20important%20savings%20in%20CO2>. [accessed at 13-06-2022]

<sup>12</sup><https://www.aluminum.org/aluminum-carbon-footprint-cut-half-over-30-years#:~:text=Increased%20Recycling%20Reduces%20Carbon%20Impact&text=Improving%20the%20end%2Dof%2Dlife,1%2C000%20kg%20of%20aluminum%20produced>. [accessed at 14-06-2022]

Therefore, no hard numbers can be given for parts that will be reused. This does not mean that parts can not be reused, it is a matter of if they will be reused. Because any part that is included in maintenance is removable and reusable, according to D.J. van Heerden.

Lastly, one major aspects of the Sustainable Air Taxi differentiates it from regular aircraft, especially in the EOL: Fuel cells. All the materials presented in Section 7.9 are hard or even impossible to recycle, considering current technology. However, they are indispensable and such the fuel cells have to contain them. Nonetheless, studies have shown experimentally, that the materials that the fuel cells consist of, can be recycled using various methods. [55] showed that all the materials inside the MEA can be recycled using an acid treatment, and some parts, such as the Nafion may even be reused, having properties close to virgin Nafion. In addition, the casing and the cooling systems may be recycled as they are built out of metal, but this can be fully considered in later detailed design stages.

## Market Analysis

In order to decide if it is worthwhile to develop a specific product or service, market research should be conducted in order to identify if there is potential demand for the product. First, in Section 13.1 the market situation is analysed such that a competitive unit price can be set for the Air Taxi. In Section 13.2, the costs are analysed regarding the production and operation of the Air Taxi. Furthermore, in Section 13.3 the costs and revenues are estimated for both the manufacturer and the operator to see if profits can be made such that the business model becomes commercially viable. Then, in Section 13.4 the return on investment is calculated for both the manufacturer and the operator, which is an important parameter to see if an investment is worth the risk. Finally, in Section 13.5 the operator business model is re-evaluated for the year 2040 to see how much the hourly rate can be decreased.

Most of the aspects mentioned above are analysed for both the operator and the manufacturer. The business model of the manufacturer of the aircraft is assessed to see when manufacturing the product is profitable. Then the business model of the operator is assessed since this will in the end determine if the manufacturer will have clients.

### 13.1. Market Situation Air Taxi

The most important parameters to estimate the market situation consists of the price and market space, which are discussed in Subsection 13.1.1 and Subsection 13.1.2 respectively. In the next sections the business plans, based on these price and amount of sales, for the manufacturer and operator will be discussed to see if the unit price is financially viable for both parties.

#### 13.1.1. Unit Price Air Taxi

For the unit costs, values are shown in Table 13.1 for different reference aircraft. It is important to notice that these prices are equipped prices, which means the interior of the aircraft is included. The total unit price is reduced to the price per passenger, since not every aircraft has the amount of 6 passengers. As can be seen, the average price per passenger is 990,000 USD. If this amount is multiplied by 6, which is the designed amount of passengers for the Air Taxi, then the Air Taxi shall cost less than 5,940,000 USD to be competitive within the market.

**Table 13.1:** Market prices of competitive products.

Aircraft Type	Unit Cost (million USD)	passengers	Unit price passenger (million USD)
Cessna Citation Mustang	3.35 (2015) [26]	4	0.8375
Embraer Phenom 100	4.25 (2021) [25]	4	1.0625
HondaJet Elite HA-420	5.3 (2021) [25]	4	1.325
Beechcraft King Air C90	4.2 (2019) [27]	6	0.7
Citation M2 Gen2 CE-525	5.855 (2022) [28]	7	0.836
Pilatus PC-24	11.8 (2022) [28]	10	1.18
<b>Average</b>			<b>0.990</b>

The unit price below 5,940,000 USD is aiming to be competitive, but it shall be considered that the Air Taxi has advantages compared to other aircraft. Namely the sustainability consisting of additional recyclability and

mitigation of harmful emissions. For these aspects, the customer is willing to pay more nowadays<sup>1</sup>, so the price can be increased by a decent amount. For that reason, it is not necessary anymore to remain below 5,940,000 USD with the unit price. Conclusively, the unit price will be set at 6,500,000 USD, including a sustainability premium which is estimated to be 500,000 USD.

### 13.1.2. Market Space for the Air Taxi

With knowledge about the market space of the Air Taxi it is possible to estimate how many Air Taxis can be sold. From this data, it can be derived if the business plan seems reasonable. From the baseline report it is analysed that within Europe there is available market space for approximately 130 Air Taxis [11]. There are 5 other continents, but the highest market share is covered by only Europe and North America, combined these continents provide 90% of all global business aviation.<sup>2</sup> Due to this big market share of 2 continents, the Air Taxi will be sold in these continents such that global sales can be calculated by doubling the estimated European sales. Since the market in America is bigger than in Europe, this multiplication factor will be increased to 2.5 for the best estimation of the worldwide demand. Conclusively, the global demand for Air Taxis is approximated at 325.

The production rate of the Air Taxi is estimated at 40 Air Taxis per year. Including holidays, this amount is equivalent to approximately one Air Taxi per week. This production rate results in a period of 8.125 years to produce 325 Air Taxis. This duration is important when approaching investors, because it is roughly equal to the duration when they can not access the invested money.

## 13.2. Cost break-down Structure

The estimation of costs is an important aspect to make the Air Taxi financially viable. In Figure 13.1, a general cost breakdown structure is shown and as can be seen the three most important costs are development, manufacturing and operations.

### 13.2.1. Cost break-down Manufacturer

The first market analysis in the baseline report estimated the break even point at 100 aircrafts with a total accumulated cost and accumulated revenues of 425 million [11]. In this design phase, more parameters of the Air Taxi are known and a more elaborate analysis regarding the costs can be performed.

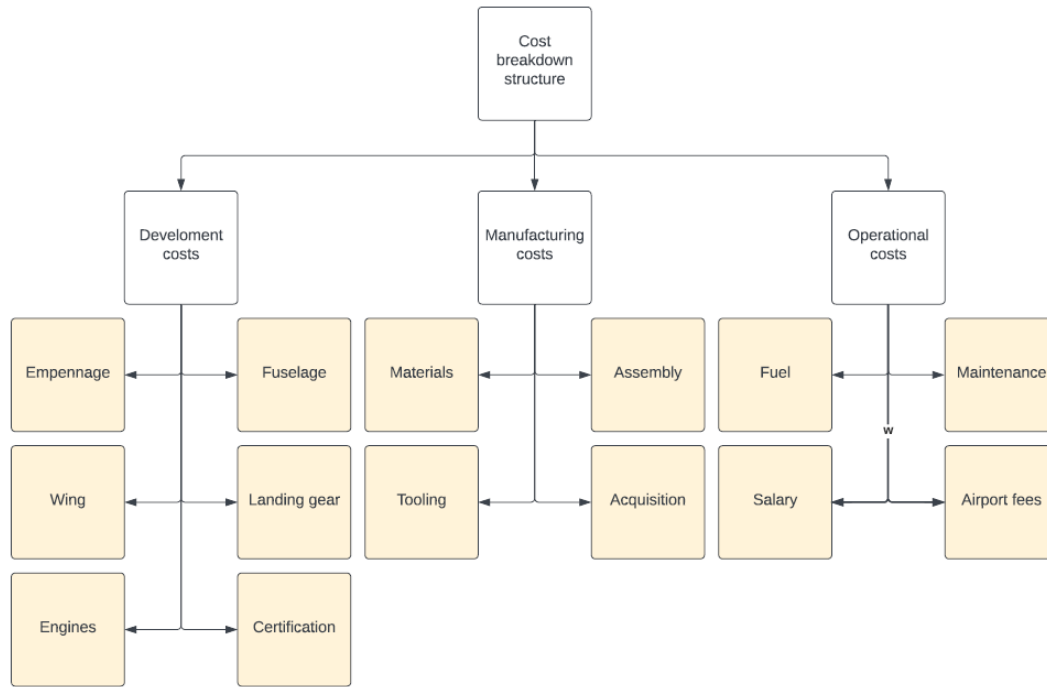
A detailed cost analysis is the DACPA IV method, which was published by Raymer [50]. In this method, many different design aspects are estimated in amounts of money and hours as a function of the operating empty weight, batch size and maximum flying velocity. The method calculates the total costs for research, development and testing (RDT) such that all produced Air Taxis can fly away. This is done using Equation 13.1, in which  $H$  refers to working hours,  $R$  to rates per working hour and  $C$  to the costs in dollars.

$$C_{RDT+flyaway} = H_E \cdot R + H_T \cdot R + H_M \cdot R_M + H_Q \cdot R + C_D + C_F + C_M + C_{eng} \cdot N_{eng} \quad (13.1)$$

Regarding the subscripts of each variable in Equation 13.1, other formulas are established by Raymer [50].  $H_E$  stands for the engineering hours,  $H_T$  for tooling hours,  $H_M$  for manufacturing hours and  $H_Q$  for the quality control hours. Furthermore,  $C_D$  represents the development costs additional to working hours,  $C_M$  stands for the manufacturing costs and  $C_F$  is the cost for testing. The last parameter is the engine cost  $C_{eng}$ , which is harder to estimate since the DACPA IV method considers conventional convention engines. Regarding the engine cost, a division can be made between the the propeller, the engine and the fuel cells, which are the most

<sup>1</sup><https://www.statista.com/statistics/934176/share-of-consumers-willing-to-pay-extra-for-sustainable-products-in-the-netherlands/> [cited 21-6-2022]

<sup>2</sup><https://www.privatefly.nl/inspirational-jet-flights/private-jet-market-in-europe-vs-usa.html> [cited 21-06-2022]



**Figure 13.1:** Cost breakdown structure of the sustainable Air Taxi.

important elements for the cost. The propeller is estimated at 74,000 dollars<sup>3</sup>, excluding a hub of 8,000 dollars.<sup>4</sup> Next the costs of the engine are harder to estimate, since there is little financial data available on high power electric engines. As reference a smaller engine is considered, which costs approximately 15,000 dollars and outputs 315 kW of shaft power<sup>5</sup>, so approximately 3 of these engines are required. As a result, the engine cost is roughly 45,000 dollars assuming as an initial estimate a linear relation. Finally, the fuel cells need to deliver a power of 1016.65 kW per engine, and experts assessed the median 2017 automotive cost to be 75 dollars per kW for fuel cells [57]. Conclusively, the fuel cells will cost 76,249 dollars per engine. If the prices of these elements are summed up, the total engine price  $C_{eng}$  is approximately 203,249 dollars per engine. Modern aircraft propulsion systems nowadays represent around 20% of the acquisition cost of the aircraft [69]. By taking a look at Figure 13.2, one can see that the estimated powertrain cost of the Sustainable Air Taxi represents only about 10% of the total unit cost. This might be due to the lower complexity of the electric powertrain employed by the Air Taxi concept, which comprises a lot less moving parts than a conventional propulsion system. Another interesting comparison to make is the price of the Air Taxi's propulsion system with current prices for the PT6A engine of around 300000\$-400000\$<sup>6</sup>, which is very common for similarly sized aircraft. The Sustainable Air Taxi's powertrain is thus very comparable to the PT6A engine family.

In the calculations of the parameters in Equation 13.1 the 7 equations below are important. In these formulas,  $W_e$  is the operating empty weight,  $V$  is the maximum flight velocity and  $Q$  is the quantity of Air Taxis scheduled to be produced. Lastly,  $FTA$  is the amount of flight tests executed. Finally,  $R$  is the general cost per working hour, while  $R_M$  is the cost per manufacturing hour.

<sup>3</sup><https://ottosenprop.com/products/b4p10015-hartzell-propeller-hc-b4mp-3c-m10476nsk-1> [accessed 09-06-2022]

<sup>4</sup><https://aeroyal.com/ref/1253093/HC-B4MP-3C/> [accessed 09-06-2022]

<sup>5</sup><https://www.js-technik.de/en/products/electric-motors/cast-iron-electric-motors/?p=1&o=7&n=12&f=199%7C34%7C150> [accessed 10-06-2022]

<sup>6</sup><https://www.pwc.ca/en/landing-pages-folder/pt6a-smart-solutions> [accessed 14-06-2022]

$$H_E = 5.18 \cdot W_e^{0.777} \cdot V^{0.894} \cdot Q^{0.163} \quad (13.2)$$

$$C_D = 48.7 \cdot W_e^{0.630} \cdot V^{1.3} \quad (13.6)$$

$$H_T = 7.22 \cdot W_e^{0.777} \cdot V^{0.696} \cdot Q^{0.263} \quad (13.3)$$

$$C_F = 1408 \cdot W_e^{0.325} \cdot V^{0.822} \cdot FTA^{1.21} \quad (13.7)$$

$$H_M = 10.5 \cdot W_e^{0.82} \cdot V^{0.484} \cdot Q^{0.641} \quad (13.4)$$

$$H_Q = 0.133 \cdot H_M \quad (13.5)$$

$$C_M = 22.6 \cdot W_e^{0.921} \cdot V^{0.621} \cdot Q^{0.799} \quad (13.8)$$

The next question concerns the exact values of the parameters in the equations of this section. From the design chapters it is known that  $W_e$  is equal to 4494 kg and the maximum velocity  $V$  is 594 km/h. From Subsection 13.1.2 the expectation is to sell 325 Air Taxis within the first 8.125 years. The amount of flight tests is set at 3, which means 3 flights will be performed to test all flight systems. It should be clarified here that since there has not been done extensive research on the topic of production quality assurance so the number of test flights is only estimated here in order to find a manufacturing price. Finally, the salary per working hour is set at 70 dollars per hour, except for the manufacturing salary since most manufacturing process are automated nowadays. It shall be noted that this is only true for high production volumes and not when 300 parts are created, but many parts occur multiple times within the Air Taxi. As a result, certain parts are manufactured over a thousand times for only 300 Air Taxis. It is important to notice that the set up of these automated machines still require a lot of effort, but this is calculated within the tooling cost, not manufacturing cost. Inserting all these values in the equations result in a cost division as shown in Figure 13.2.

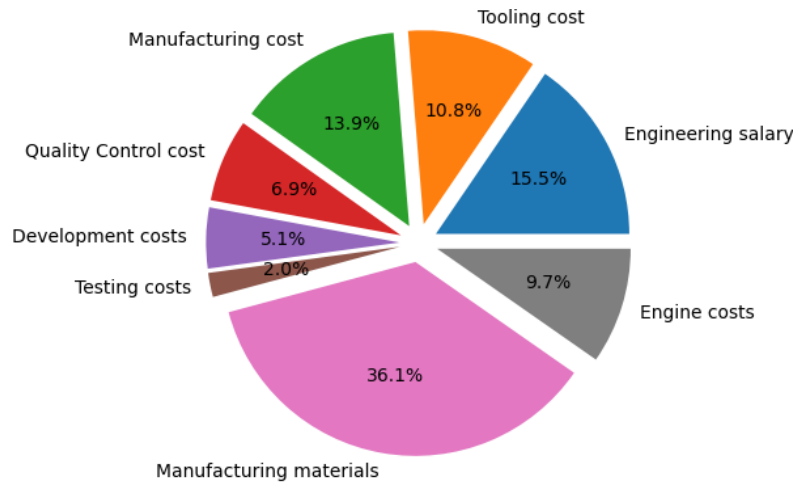


Figure 13.2: Cost distribution for manufacturer producing 325 Air Taxis.

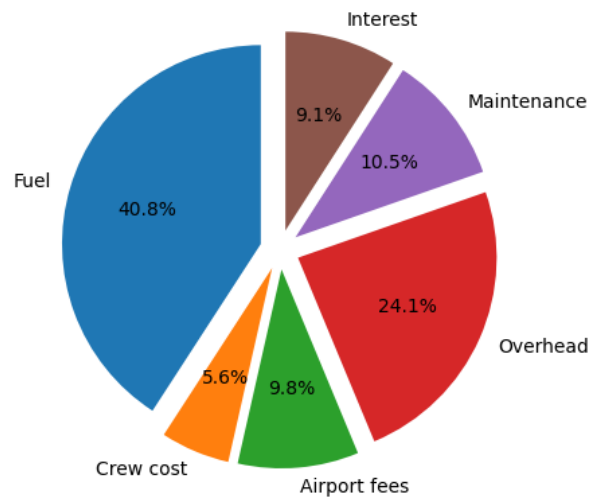
### 13.2.2. Cost Break-down Operator

In order to compute the cost distribution for the operator, the direct and indirect costs for the operator should be taken into account. The direct costs are costs that are directly related to the operations of the aircraft, this includes fuel, crew pay (if crew is paid hourly), maintenance and airport fees. On the other hand, indirect costs are costs that have to be paid even if the aircraft is not operating, this includes crew cost (if it is a fixed monthly allowance), overhead fees (business administration, marketing, ground staff and storage) and interest rates.

After analysing the direct and indirect costs from financial reports of other airlines<sup>7</sup>, Figure 13.3 shows the distribution of the costs for the first month of operation.

<sup>7</sup><https://investor.ryanair.com/results-centre/> [accessed 13-06-2022]





**Figure 13.3:** Cost distribution for operator in the first month of operations of the Air Taxi.

It is noticeable from Figure 13.3 that the Fuel costs dominate the cost distribution for the operator, this is mainly due to the fact that the flights per month is calculated based on a fleet size of 325 aircraft where each aircraft operates on average 3 flights per day. Additionally, it has been decided that the crew will be paid a monthly salary of 9000\$ per staff member and the interest rate is estimated to be five percent yearly. The fixed cost which were derived from the Ryanair annual report are scaled by income to the Air Taxi operation.

### 13.3. Operational profit

In this section the predicted profit for both the manufacturer and the operator is discussed.

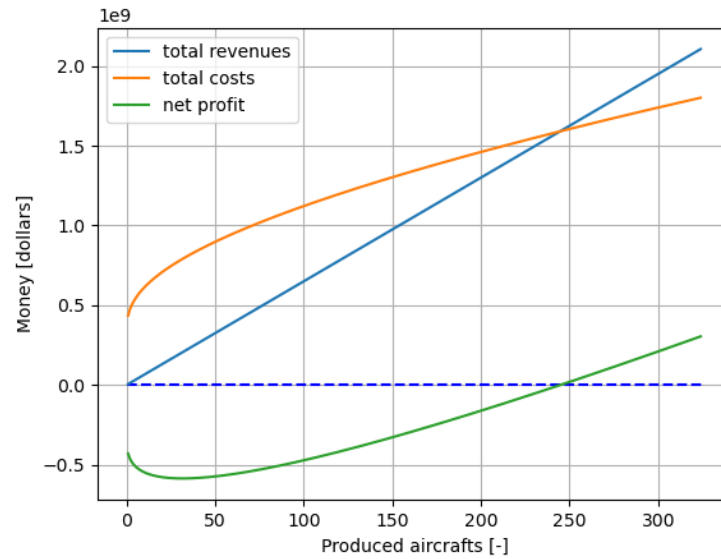
#### 13.3.1. Operation Profit Manufacturer

Regarding the operational profit of the manufacturer, it is necessary to establish the total revenues and total costs of the entire project. Using the cost model DACPA IV from Section 13.2 and the unit price from Section 13.1, it is possible to derive the costs and revenues. The total revenues can be calculated by multiplying the unit price with the amount of sales, which is equal to  $Q$ . For the total cost Equation 13.1 it is assumed the operating empty weight is 4494 kg and the maximum velocity is  $594 \frac{km}{h}$ , these values are taken from previous design chapters.  $Q$  depends on the market analysis, so it is kept variable and plotted in Figure 13.4. As you can see, the point of break even is approximately at 240 sold aircraft.

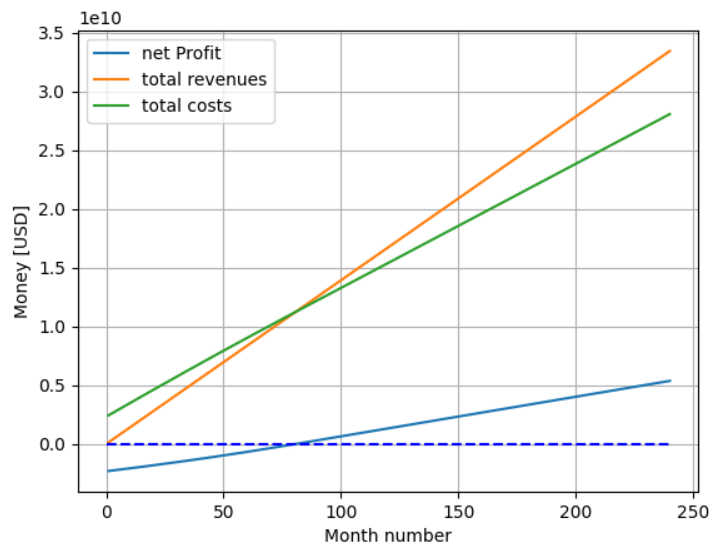
Producing more than 240 sustainable Air Taxis will lead to profits, which increase rapidly when the sales continue. It shall be noted that the first years high debts occur, which means some big investments need to be made. Luckily, after passing the break even point the profits grow fast, so the risk of the investment will be rewarded.

#### 13.3.2. Operation Profit Operator

The operation profit for the operator is calculated by finding the difference between the monthly revenue and the monthly costs. The monthly revenue is the income that the airline receives from its operations and the monthly costs are the payments that the operating business has to pay in order to legally fly and maintain the aircraft. Based on previous analysis [10], the price per hour for the Air Taxi has been decided to be 2350 USD. As a result, the following plot shows the profit made by the airline business as a function of time (months):



**Figure 13.4:** Total cost and revenues for the manufacturer of the sustainable Air Taxi.



**Figure 13.5:** Profit of operator as a function of time

From Figure 13.5, it can be deduced that the break even point of time is 58 months, which is a reasonable time frame for an aircraft to pay off the money spent on purchasing the aircraft. After the period of 58 months the operator starts to make profit for the lifetime of the aircraft.

### 13.4. Return on Investment

The Return on Investment is a parameter which indicates if the investment is financially viable. The ROI can be calculated using Equation 13.9. In this section both the ROI of the manufacturer as for the operator are discussed.

$$\text{Return on investment (ROI)} = \frac{\text{Net profit}}{\text{Cost of investment}} \cdot 100 \quad (13.9)$$

### 13.4.1. Return on Investment manufacturer

The manufacturer of the Air Taxi needs to do a big investment before the sales can start. This investment shall be approximately 590 million USD, as can be seen in Figure 13.4 by the minimum of the net profit. Another observation from Figure 13.4 is the net profit of 310 million dollars after selling 325 Air Taxis. With a production rate of approximately 40 Air Taxis per year, this point is reached after 8.125 years. After these 8.125 years the further development of the air taxi depends on the success, so this phase will not be discussed in this phase. Inserting the above numbers in Equation 13.9, results in a ROI of 52%.

A ROI of 52% seems reasonable for a project with long duration and relatively many uncertainties. Lower ROI values are more common when you invest in more certain projects, like real estate. The production of an aircraft faces more challenges, which means a higher ROI is deserved.

### 13.4.2. Return on Investment operator

In order to calculate the return on investment for the operator it is important to know the operational lifetime of each aircraft. Given an operational life time of 20 years for the aircraft, the profit at the end of the 20 years becomes 5.3 billion USD as shown in Figure 13.5, and for a cost of investment of 2.34 billion USD, the return of investment after 20 years is 122% for the operator.

## 13.5. Future Prospects

The price of hydrogen is now considered to be expensive, however, it is expected that within the next years the price of hydrogen will decrease a drastic amount. The Clean Sky 2 study<sup>8</sup> specifies that in 2040 the price of hydrogen could decrease to 3 USD per kg. For that price of hydrogen, the cost distribution for the operator is updated to have the following distribution:

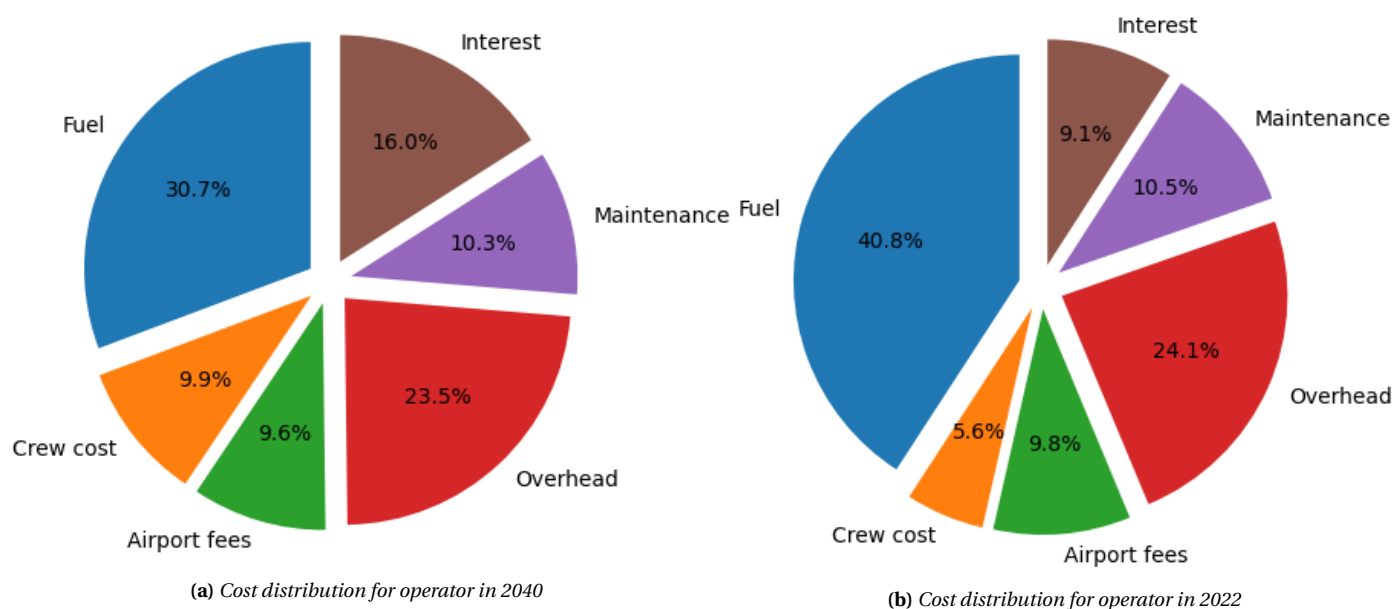


Figure 13.6: Comparison of Cost distributions in the year of 2022 to the year 2040

As Figure 13.6 shows, the fuel occupies 30.7% of the cost distribution as opposed to 40.8% for the year of 2022. Furthermore, given that the price of fuel decreased a significant amount from 7 USD per kg CITE to 3 USD per kg, in 2040 it is possible to decrease the flight hourly rate to 1650 USD instead of 2350 USD and keep the same profit margin per month (The prices used for 2040 do not take into account effects of inflation).

<sup>8</sup>[https://www.fch.europa.eu/sites/default/files/FCH%20Docs/20200507\\_Hydrogen%20Powered%20Aviation%20report\\_FINAL%20web%20\(ID%208706035\).pdf](https://www.fch.europa.eu/sites/default/files/FCH%20Docs/20200507_Hydrogen%20Powered%20Aviation%20report_FINAL%20web%20(ID%208706035).pdf)

# Operations and Logistics

This chapter offers the relevant details concerning the operations and logistics of the Sustainable Air Taxi, as expected to occur during its operational life. On top of that, aspects related to reliability, redundancy, availability maintainability and safety are covered in this chapter.

## 14.1. Operations

Ground operations include all operations of the aircraft from parking up to take off. This section will go through the stages of the operations on the ground. First, the aircraft is towed from its parking place to the spot where it can be refuelled. Then, the aircraft has to be refuelled, the amount of fuel will be based on the distance that will be flown. Refuelling can be done from the bottom of the aircraft. The airport worker can connect the hose to the tank. Currently, there are not a lot of cases where liquid hydrogen refueling is done. A company that is currently working on projects regarding refueling hydrogen vehicles is Linde Engineering.<sup>1</sup> They have developed a refuelling system for a liquid hydrogen powered train in Nedersaksen.<sup>2</sup> This system is able to provide a fuel flow of  $190 \frac{\text{kg}}{\text{hour}}$  per pump. This would result in a refueling time of 1 hour and 40 minutes, when using a single fuel inlet. In the future this time should decrease as hydrogen infrastructure improves. Moreover, it should be taken into account that boil-off starts after 5 hours, so the aircraft should be filled up as close to departure as possible in order to prevent having to vent hydrogen. Except the passengers cannot be on board during refuelling so the refuelling should be done prior to that.

After the aircraft is refuelled, it can be towed around the airport towards the gate, which is used for the air taxi. Usually for chartered flights and other premium services a different gate is used, compared to normal flights. Also, depending on the airport, the passengers who booked the taxi do not have to go through normal security and do not have to check in their luggage.<sup>3</sup> As a result they will have a much smoother and faster travel experience. Depending on the airport, the passengers can walk to the aircraft themselves or they are brought by a small bus, with their luggage. When arriving at the aircraft, the pilot or an airport employee puts their luggage into the cargo hold. The cabin door is opened and the stairs come out so that the passengers and pilots can get on board and take their seats.

When the passengers and pilots are in place, the aircraft will taxi to the take-off area, during this time the fuel cells will warm up and start providing power to engine. Thus, when the actual take-off starts they are ready to provide take-off power. For the take-off itself a runway of at least 1500 meters is required, as this is the minimal take-off distance. Furthermore, the runway should be made from well maintained tarmac or concrete. The general flying profile of the aircraft looks like Figure 14.1, with a range of 1200 km. When the aircraft arrives at the destination it will land on a similar runway.

<sup>1</sup><https://www.linde-engineering.com/en/plant-components/hydrogen-refueling-technologies/index.html> [accessed 10.06.2022]

<sup>2</sup><https://cryostar-hydrogen-solutions.com/mobility-hrs-2/> [accessed 10.06.2022]

<sup>3</sup><https://l33jets.com/what-is-it-like-to-fly-private#:~:text=TSA%20regulations%20state%20that%20for,inspection%20as%20commercial%20flight%20passengers>. [accessed 10.06.2022]

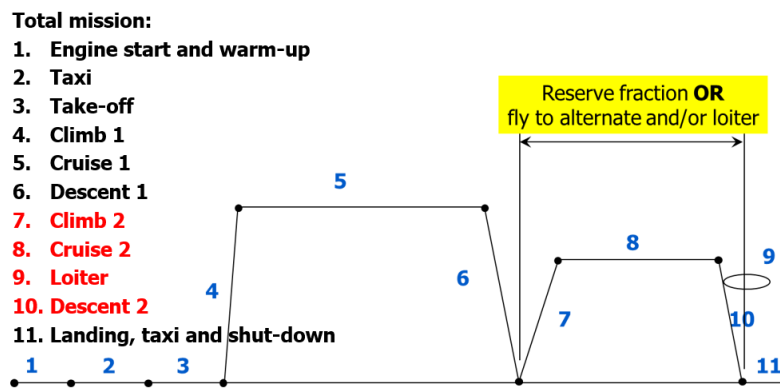


Figure 14.1: Aircraft flight operations [76]

Subsequently, the passengers will get out of the aircraft after it taxied to its temporary parking place. Next, the luggage is taken out of the cargo hold and, if needed, the aircraft is towed to its parking spot where it is stowed until its next use. Meanwhile, inspection can take place and, if necessary, maintenance as well. It is important for the durability of the aircraft that it is properly inspected and maintained. The aircraft consisting mostly from aluminium should help maintainability.

## 14.2. RAMS

In order to evaluate the operations of the aircraft it is important to analyse the Reliability, Availability, Maintainability and Safety. This chapter gives an overview of how the aforementioned points are taken into account in the design of the Sustainable Air Taxi.

### 14.2.1. Reliability

Given that the design procedures used on the Air Taxi were similar to conventional methods used to size and design usual aircraft, it is safe to say that the aircraft is designed with sufficient reliability for the fuselage, wing, engine and empennage. However, for the fuel systems the design procedure strays from the conventional ways of designing an aircraft, as a result, in order to account for the reliability in our fuel systems, the fuel tank contains 2 vents for pressure buildup in case one vent gets clogged. Since the Technology Readiness Level of a liquid hydrogen powertrain is not fully developed, at around 7. and high reliability generally is achieved through a high TRL like 9, this is not favourable for reliability. However the individual parts of the powertrain have a reasonable technology readiness level. For example electric motors is a very mature technology. Fuel cells, however, are less mature technology and issues may appear in the long term, especially in aircraft use. This can be safely implemented though, by using redundancy solutions and extended analysis using computations.<sup>4</sup>

### Redundancy philosophy

Any engineering design should account for unforeseen circumstances and issues. This is usually done by detailed design and close inspection both in the production and operation phases. However, issues can appear during the operations that may place the product and passengers in immediate danger. To account for this risk, redundancy elements have to be implemented into the design of the Sustainable Air Taxi. This is done both in a general manner regarding the systems, such as the propulsion of the aircraft working properly with only one side functional, as well as for subsystems. The aircraft features giving redundancy to the subsystem assemblies are explained below.

The fuel cell systems that are implemented in the propulsion unit of the sustainable air taxi are divided into four smaller stacks per engine. This introduces a redundancy solution as if one of the stacks would encounter issues, a switch would come on and continue the circuit with three out of four fuel cells. Thus, in the event of

<sup>4</sup><https://www.ati.org.uk/uncategorised/flyzero-concepts-and-technology-roadmaps-land/> [accessed 14-06-2022]

one fuel cell malfunctioning, the stack would still generate  $\frac{3}{4}$  of the power.

As explained before, the electric motors are off the shelf components. The magni650 electric motor features a 4x3 phase architecture which "allows for redundancy and increased reliability", according to the company's description of the product.<sup>5</sup> Consequently, should a short-circuit happen, one of the 3-phase sections can be switched off, while still having 75% of the total available power. Moreover, the motors also come with an integrated advanced cooling system, so the risk of overheating is transferred to the motor manufacturer. Lastly, the motor is isolated on both ends from the environment, adding to the design's overall redundancy by reducing the risk of debris entering the motors.

As the objective of this report is only to present the design synthesis of the Sustainable Air Taxi, the reliability can only be considered as an approximation based on several projects that have a related theme or from aircraft comparable to the proposed design. The fuel cell stacks have a lifespan of around 12000 operation hours, while the propellers have around 6000 operational hours. Regarding the fuel tank, further analysis has to be performed as its design is specially made to fit the design of the aircraft and not comparable to any real life model. The aircraft is expected to be operational for 20 years with six flight hours per day.

#### 14.2.2. Availability

Availability is the amount of time the aircraft is available for use, which depends on the operational aspects that are necessary to support the flight. Major aspects include refuelling and airport logistics. Additionally, an aspect of availability is the fuel accessibility at airports. As of 2022, there is not an existing liquid hydrogen distribution infrastructure on airports.

For routes over 600 km, the aircraft has to be able to refuel at its destination airport. The infrastructure for delivery of liquid hydrogen to airports as well as storage in airports is currently not existing. Most likely the creation of this infrastructure would start at a selection of airports. One potential problem in the early phase of hydrogen aviation is diversions to airports that do not have hydrogen refuelling infrastructure. Implementing this infrastructure is not an easy thing to do, as it implies lots of aspects to consider, such as the very high power required for producing hydrogen through electrolysis, which would require enormous power plants and/or surfaces filled with solar panels in the airport vicinity<sup>6</sup>, which might not be a feasible solution for most airports.

#### 14.2.3. Maintainability

##### Powertrain

The maintainability of an hydrogen powertrain is relatively simple compared to a conventional combustion engine. A fuel cell has no moving parts, which makes the fuel cell more reliable than a combustion engine. In particular, a stationary fuel cell requires detailed maintenance only every one to three years.<sup>7</sup> Nonetheless, care has to be taken and constant maintenance is needed to ensure the working and efficiency of the fuel cells. In addition to this, the fuel cell stack durability assessments can be approximated at 12000 hours of operations.<sup>8</sup> As far as the propeller and electric motor are concerned, the former is certified for 6000 hours of operation, which is guaranteed by the manufacturer, Hartzell Propeller Inc. Maintaining the propeller implies following the guidelines of the manufacturer when operating and handling it on the ground. Once the propeller reaches its end of life, it can easily be recycled since it is made of aluminium and a new one can be bought and fitted on the aircraft. Concerning the latter component, there is not a lot of available data from the manufacturer, but since this is a new, high-performance product designed specifically for aircraft, it is safe to assume that it has a high reliability and maintainability. As explained in Chapter 7, there are two types of electric motors,

<sup>5</sup><https://www.magnix.aero/services> [accessed 14-06-2022]

<sup>6</sup><https://www.kearney.com/transportation-travel/article/-/insights/aviations-hydrogen-the-airport-challenge> [accessed 14-06-2022]

<sup>7</sup><https://www.eesi.org/papers/view/fact-sheet-fuel-cells> [accessed 13-06-2022]

<sup>8</sup><https://www.pnas.org/doi/10.1073/pnas.1804221116> [accessed 13-06-2022]

brushed and brushless. The new magni650 electric motor is also most probably a brushless motor, making it require even less maintenance work, as the brushes need to be replaced every once in a while, when they degrade.

### **Hydrogen Storage**

Because of the cryogenic temperatures, all lines and tank should be inspected, on an interval, if the insulation is still up to standard. Another important part for the hydrogen storage safety are the pressure relief valves. These valves should be checked during maintenance to ensure proper functioning. Also all the concerning pumps and valves that are included in the fuel system should be maintained to ensure proper functioning of the whole system. At last, the fuel lines, as for normal kerosene systems, should be checked for liquid and gas leakage.

### **Structures**

Because the Sustainable Air Taxi is designed using the philosophy of having only one material used as much as possible (see Chapter 8) in various subsystems, the maintainability of the structure is expected to be easier than for usual aircraft. That is because a stock of reserve parts can be easily created due to a relatively low variety of parts used as explained in Section 8.5. Furthermore, maintenance work can be performed more straightforwardly, since assembling and disassembling the aircraft should take considerably less time than for a similarly sized aircraft which generally are not as simple as the Sustaxi design.

## **14.2.4. Safety**

### **Powertrain**

Regarding the safety risks associated with the propulsion system, these are transferred to the propeller and electric motor manufacturers, on one hand, and to the fuel cell manufacturer, on the other. The electric motors come with an integrated cooling system, according to MagniX, while the used propeller model is already operation certified by the airworthiness authorities. Moreover, the technology behind the motors was already validated through test flights of converted existing aircraft, as discussed in Chapter 7.

For the fuel cell stack, the safety aspects can be mitigated by ensuring constant maintenance of the fuel cell stack and the surrounding subsystems. Risks of contamination, overheating, flooding or low humidity can be detrimental to the operation of the fuel cell, but these issues can be closely monitored and careful design can help mitigate them.

### **Hydrogen Storage**

The storage of hydrogen is always combined with risks that shall be analysed, since hydrogen is a very explosive gas. When heat is entering the fuel tank the pressure will build up and when this pressure reaches 3 bar hydrogen shall be released in gaseous form. This is done using a pressure release valve, but if it is clogged the high pressure might form a risk. To maintain a safe situation, a second pressure release valve is included. Another safety issue is the released hydrogen, because outside the aircraft the hydrogen is a potential fire hazard. Additionally hydrogen acts as an indirect greenhouse gas as explained in Subsection 12.1.1. With regards to the fire hazard: fortunately hydrogen in gaseous form is lighter than air and since it will be released on top of the aircraft, it will immediately climb such that it does not cause any risks on ground level.

### **Structures**

As described in Chapter 8, the structure of the wing box is designed using an additional 1.5 design safety factor since at this stage there is still uncertainty about the design specification, on top of the 1.5 factor included by default in the ultimate load (which is 1.5 times the design load factor, leading to a wing box able to withstand up to 225% of its design load factor). Other structural features were not discussed in too much detail at this stage of the design, as the available time did not permit. However, the design philosophy behind the rest of the structures would be in line with the one employed for the wing box, proving the safety of the aircraft concept, including critical and demanding situations during its operational life.



## Technical risk assessment

During the detailed design stage, several new risks relevant to the operation and development of the aircraft were identified in addition to the ones already assessed in the baseline and midterm reports. The new risks identified are few in number, but they are more specific in terms of the details of the newly designed subsystems.

### 15.1. Assessment of Previously Identified Technical Risks

The previous technical risks during operations and during development, as identified in the baseline and midterm reports, are compiled in Table 15.1 and Table 15.2, respectively. As before, the *L* and *S* scores signify pre-mitigation likelihood and severity, with a likelihood score of 1 being very unlikely and 5 being very likely, and a severity of 1 being acceptable and 5 being intolerable. These categories are shown on the risk matrices in Table 15.7 and Table 15.8.

**Table 15.1:** Technical risks during operations (from baseline and midterm reports)

Risk	Code	Cause	Consequences	L	S
Propulsion system failure	RISK-PROP-01	Propeller fatigue failure	Damage to engine, possible damage to fuselage, loss of thrust	1	4
	RISK-PROP-02	Partial loss of thrust due to engine malfunction	Thrust asymmetry, risk of insufficient thrust and stall	3	3
	RISK-PROP-03	Total loss of thrust due to engine malfunction	Gliding flight scenario, risk of deadly crash after takeoff	2	5
	RISK-PROP-04	Engine/motor fire	Risk of fire spread, loss of thrust	2	4
	RISK-PROP-05	Battery fire		3	5
	RISK-PROP-06	Fuel pump failure	Partial or total loss of thrust	2	4
	RISK-PROP-07	Icing on propeller/nacelle	Reduction in propulsion efficiency	4	2
Uncontrolled increase of tank pressure	RISK-PROP-08	Tank insulation and relief valve failure	Risk of catastrophic explosion	3	5
Landing gear failure	RISK-GEAR-01	Gear retraction/extension mechanism failure	Aerodynamic inefficiency, emergency or possibly crash landing	3	4
	RISK-GEAR-02	Misaligned retraction/extension of landing gear	Damage to wheel bays, emergency landing	2	4
	RISK-GEAR-03	Landing gear collapse	Structural damage to fuselage, risk to passengers and crew	2	4
	RISK-GEAR-04	Nose gear steering fault	Difficulty or inability to taxi	3	3
	RISK-GEAR-05	Tire blowout	Damage to wheels, rejected takeoff or unstable landing, FOD	2	3
Braking failure	RISK-BRAK-01	Loss of wheel brakes	Large increase of landing distance and distance required for rejected takeoff, possible runway excursion	3	4
	RISK-BRAK-02	Loss of aerodynamic braking		3	3
Severe weather conditions	RISK-WTHR-01	Poor visibility	Increased reliance on instruments and digital landing aids	5	2
	RISK-WTHR-02	Severe turbulence	Disturbance to passengers, risk of small injuries	4	2
	RISK-WTHR-03	Strong crosswind/wind shear	Unsteady approach, hard landing	4	2
	RISK-WTHR-04	Lightning strike	Failure of electrical systems, local surface damage	4	3
	RISK-WTHR-05	Heavy rain	Reduced aerodynamic efficiency and stall angle, water ingestion	5	3
Structural and material failure	RISK-STRC-01	Polymer degradation	Wire degradation, damage to paint and coating layers	3	4
	RISK-STRC-02	Metal fatigue cracking		4	5
	RISK-STRC-03	Composite delamination	Decreased life of components, reduced load capacity	3	5
	RISK-STRC-04	Corrosion of metals	of structure, risk of catastrophic failure	4	5
	RISK-STRC-05	Incorrect production of joints		2	5
	RISK-STRC-06	Reduced material properties in production	Decreased life of components, decreased load carrying capacity	2	4
External damage to aircraft	RISK-DAMG-01	Bird strike to radome	Increased drag, possible loss of radar	5	2
	RISK-DAMG-02	Bird strike to cockpit windows	Reduced visibility, possible injury or incapacitation of pilots	5	3
	RISK-DAMG-03	Bird strike to wing leading edge	Loss of hydraulic lines, increased drag, loss of high-lift devices	5	3
	RISK-DAMG-04	Bird strike to propeller/fan/nacelle	Reduction or loss of thrust, increased drag	5	3
	RISK-DAMG-05	Hard landing on runway	Damage to landing gear, structural damage to fuselage	5	2
	RISK-DAMG-06	Crash landing on runway		2	4
	RISK-DAMG-07	Emergency landing on soft ground	Damage to landing gear, structural damage to fuselage, risk of injury or death to passengers and crew	2	4
	RISK-DAMG-08	Attempted landing on aircraft carrier		1	5
	RISK-DAMG-09	Runway excursion	Damage to landing gear, structural damage to fuselage	3	3
	RISK-DAMG-10	Ditching	Complete loss of aircraft, mortal risk to passengers and crew	2	5
Reduction/change in flight characteristics	RISK-FLGT-01	Icing on wing leading edge	Decreased aerodynamic efficiency, higher stall speed	4	4
	RISK-FLGT-02	Shift of loose payload	Sudden change of center of gravity, risk of instability and stall	2	4
	RISK-FLGT-03	Failure of high-lift devices		2	3
Failure of flight instruments	RISK-FLGT-04	Overweight aircraft due to excess loading	Increased minimum approach speed and takeoff speed	3	4
	RISK-INST-01	Icing on external sensors		4	4
	RISK-INST-02	Faulty mechanical flight instruments	Pilots provided incorrect or insufficient information, possibility of wrongful software intervention, risk of deadly crash	2	4
	RISK-INST-03	Loss of electronic flight instruments		2	4

Loss of control of aircraft	RISK-CTRL-01	Incorrect electronics installation/wiring	Faulty flight controls, risk of deadly crash	1	5
	RISK-CTRL-02	Flight computer failure	Possible catastrophic results due to software intervention	2	5
	RISK-CTRL-03	Aircraft in stall	Mortal risk to passengers if not recovered by pilots or software	2	4
	RISK-CTRL-04	Aircraft in spin		2	4
	RISK-CTRL-05	Icing on control surfaces	Control surfaces less effective or partially inoperative	4	3
	RISK-CTRL-06	Hydraulic system malfunction (if applicable)	Control surfaces inoperative, risk of deadly crash	2	5
	RISK-CTRL-07	Pilot error/misconduct	Mortal risk to passengers if not recovered by software	2	4
	RISK-CTRL-08	Pilot incapacitation		1	4
Endangerment of passengers and crew	RISK-DNGR-01	In-flight cabin fire	Mortal risk to passengers + catastrophic failure of flight	2	5
	RISK-DNGR-02	In-flight cargo fire	Mortal risk to passengers + catastrophic failure of flight	2	5
	RISK-DNGR-03	Cabin pressurization failure	Risk of hypoxia, need for emergency descent	2	4
	RISK-DNGR-04	Emergency exit malfunction	Hindrance of evacuation, mortal risk to passengers	2	5
	RISK-DNGR-05	Encounter with air traffic	Possibility of deadly collision in air or on ground	1	5
	RISK-DNGR-06	Hostile actions against aircraft	Mortal risk to passengers and crew	1	5
Cryogenic fuel causes injury	RISK-DNGR-07	Tank failure or valve failure during handling	Cryogenic burns and lung damage to maintenance or refuelling personnel	3	5
Fuel cells catch fire	RISK-DNGR-08	Improper temperature control on cells	Catastrophic in-flight fire	3	5
Battery capacity degrades	RISK-DEGR-01	Many charge/discharge cycles during operational life	Batteries have to be replaced, which adds to the maintenance costs	5	2
Other technical and operational hazards	RISK-MISC-01	Ground imbalance due to uneven payload	Possibility of tip-over	3	3
	RISK-MISC-02	Improper maintenance by operators	Possible risk hazard during flight/flight cancellation	3	5
	RISK-MISC-03	Long holding/diversion to alternate airport	Insufficient range, possible need for emergency landing	5	3
	RISK-MISC-04	Loss of landing/navigation/taxi lights	Hard landing, traffic risk to other aircraft	3	3
	RISK-MISC-05	Loss of radio communications	Possibility of deadly collision in air or on ground	2	5

Table 15.2: Technical risks during development (from baseline and midterm reports)

Risk	Code	Cause	Consequences	L	S
Final product does not meet client expectations	RISK-CLNT-01	Acquisition cost is unacceptably high	Client is not interested in buying the aircraft as it is incompetent	2	5
	RISK-CLNT-02	Operational cost is unacceptably high		2	5
	RISK-CLNT-03	Aircraft looks unappealing		3	2
	RISK-CLNT-04	Maximum range not sufficient		2	5
	RISK-CLNT-05	Insufficient payload capabilities	Less competitive aircraft and bad company image	2	4
	RISK-CLNT-06	Does not reach defined lifetime		1	2
	RISK-CLNT-07	Inconvenient end-of-Life treatment		2	2
Final product does not meet passenger expectations	RISK-PASS-01	Insufficient passenger space	Passengers dislike aircraft and might choose airlines with aircraft from competitors	1	2
	RISK-PASS-02	Unacceptable cabin noise levels		1	2
	RISK-PASS-03	Not sufficient luggage weight/space		3	2
	RISK-PASS-04	Too high ticket cost	Passengers opt not to use air taxi	3	5
	RISK-PASS-05	Travel time too long		1	4
Final product does not meet the overarching customer	RISK-CUST-01	Insufficient environmental sustainability	The air taxi fails to meet sustainability goals	3	5
	RISK-CUST-02	Insufficient recyclability of aircraft		2	5
Final product does not meet airfield operators expectations	RISK-OPER-01	Unsafe ground operations	Systems need to be redesigned for operational readiness	1	5
	RISK-OPER-02	Tower unable to communicate with airplane		1	5
	RISK-OPER-03	Aircraft lights not according to regulations		1	4
	RISK-OPER-04	Aircraft exceeds noise levels	Restrictions to flight paths and operation hours	1	4
	RISK-OPER-05	Complicated and lengthy refuelling/ recharging process		3	3
	RISK-OPER-06	Incompatibility with existing airport infrastructure		1	5
Ground operations difficult (storage, refuelling etc.)	RISK-OPER-07	Airport infrastructure underdeveloped or improper improvement prospects for hydrogen based propulsion	Increased operational costs and long times for performing them	3	4
Aircraft configuration does not allow for easy maintenance		Unconventional propulsion, for which little experience is available			
Final product is not sustainable	RISK-SUST-01	The propulsion system has high direct emissions	The aircraft is not marketable as "sustainable" and the company image is damaged	2	5
	RISK-SUST-02	The propulsion system has high indirect emissions		4	4
	RISK-SUST-03	The aircraft is less than 80% recyclable by mass		1	5
	RISK-SUST-04	Recycling is disincentivised due to cost aspects		3	4
	RISK-SUST-05	End-of-Life treatment methods are ecologically unsustainable		3	3
	RISK-SUST-06	Manufacturing methods are ecologically unsustainable		3	3
Schedule overrun	RISK-SCHD-01	Aircraft redesign due to noncompliance with aircraft regulations	Technology and demand outdated by roll-out, customer might cancel orders	2	3
	RISK-SCHD-02	Time constraint is unrealistic for expected design complexity		3	3
Cost budget exceeded	RISK-BDGT-01	Implemented design tool cost too high	Not competitive in market, break-even point delayed	1	2
	RISK-BDGT-02	production cost very high		3	4
	RISK-BDGT-03	Additional labour costs due to schedule overrun		2	2
Inadequate Flight characteristics	RISK-CHAR-01	Dynamic eigenmodes are unstable beyond safety standards	Redesign of aircraft before market entry	3	5
	RISK-CHAR-02	Statically unstable Aircraft		3	4
	RISK-CHAR-03	Strong aerolastic flutter during testing		3	4
	RISK-CHAR-04	Strong Vibrations during testing		3	3
Final product deviates from Model	RISK-MODL-01	Model inaccuracies	Unexpected performance characteristics (Can either exceed or subceed expectations)	4	3
	RISK-MODL-02	Calculation errors		1	3

In addition, the risks from Table 15.1 and Table 15.2 with risk levels in red or orange categories were each given a mitigation strategy and quantified reduction in the likelihood and severity scores. These mitigation strategies are described in Table 15.3 and Table 15.4, which include the risks identified in the midterm report and in the baseline report.

**Table 15.3:** Mitigation strategies for the operational risks (from baseline and midterm reports)

Risk code	Mitigation strategy	$\Delta L$	$\Delta S$
RISK-PROP-05	Install a firewall in the battery compartment. / Transfer the risk to a trustworthy battery manufacturer. / Opt for a propulsion method without batteries.	-2	-1
RISK-WTHR-05	Transfer pilot training regarding weather avoidance and mitigation procedures to operators. / Transfer the risk of water ingestion into the engine to the engine manufacturer.	-1	-2
RISK-STRC-02	Design components according to the fail safe or safe life philosophy so that the components are either redundant or can safely be maintained. / Composites are not used in the structure for ease of recycling, so composite delamination is no longer applicable.	-1	-3
RISK-STRC-03		-1	-3
RISK-STRC-04		-1	-3
RISK-DAMG-02	Strengthen the cockpit windows and test the resistance to impacts. / Transfer bird avoidance to airport operations.	-2	-2
RISK-DAMG-03	Reinforce the leading edge structure, do not run critical flight control lines through the leading edge. / Transfer bird avoidance to airport operations.	-2	-2
RISK-DAMG-04	Transfer the risk to the engine or propeller manufacturer. / Transfer bird avoidance to airport operations.	-2	-2
RISK-MISC-02	Design the aircraft and documentation for ease of maintenance for ground personnel. / Transfer maintenance responsibility to operators.	-2	0
RISK-MISC-03	Design the aircraft to have adequate endurance for holding and diversions. / Transfer pilot training for following procedures to operators.	0	-2
RISK-PROP-02	Reduce the severity of an engine malfunction by following the CS-23 guidelines on one engine inoperative situations. / Transfer engine malfunction risk to the engine manufacturer.	-1	-2
RISK-PROP-03	The aircraft should adhere to CS23 requirements relating to total engine loss. / Transfer engine malfunction risk to the engine manufacturer.	-1	-1
RISK-PROP-04	Install a firewall around the engine or motor to protect the fuselage or wings. / Transfer risk of engine fire to the engine manufacturer.	-1	-2
RISK-PROP-06	Transfer the responsibility for proper fuel pump functioning to the supplier.	-1	0
RISK-PROP-07	Install anti icing systems on critical parts. / Transfer de-icing to airport operations.	-2	-1
RISK-PROP-08	Implement redundancies in the cooling system and regulate tank pressure by venting to avoid dangerous gas buildup so that the aircraft could fly to the nearest airport and make an emergency landing.	-1	-2
RISK-GEAR-01	Test gear for reliability. / Incorporate gravity extension. / Design structure to keep passengers as safe as possible during emergency landing. / Design for RISK-MISC-03.	-1	-1
RISK-GEAR-02	Design nose gear strut to remain as straight as possible during (emergency) landing. / Design nose gear steering mechanism with redundancy.	-1	-1
RISK-GEAR-03	Design landing gear struts for high load cases. / Design aircraft structure to keep passengers as safe as possible during emergency landing.	-2	-1
RISK-GEAR-04	Design nose gear steering mechanism with redundancy. / Test nose gear steering in limit cases. / Transfer loading and pushback risks to airport operations.	-2	0
RISK-BRAK-01	Test mechanical brakes and aerodynamic braking surfaces with respect to reliability. / Design mechanical brakes to have enough power to stop the aircraft despite an aerodynamic brake failure during landing.	-1	-1
RISK-BRAK-02		-1	-1
RISK-WTHR-01	Transfer weather avoidance to pilots. / Include proper instrumentation for IFR. / Incorporate ILS capability into design.	-2	-1
RISK-WTHR-02	Transfer weather avoidance to pilots. / Design cabin interior (seatbelts, overhead bins, etc.) for passenger safety in turbulence.	-1	-1
RISK-WTHR-03	Transfer pilot training regarding avoidance and flying skills to operators. / Design aircraft for stability under such conditions.	-1	-1
RISK-WTHR-04	Transfer weather avoidance to pilots. / Design aircraft such that it conducts and discharges electricity while keeping it away from passengers and critical systems.	-1	-2
RISK-STRC-01	Ensure critical polymer coated parts are not exposed to a damaging environment. / Transfer responsibility of checks to operators.	-1	-1
RISK-STRC-05	Ensure that the production plan is clear and complete. / Transfer the responsibility of making sure workplace procedures are the production plant to the responsible employees and authorities.	-1	0
RISK-STRC-06		0	-1
RISK-DAMG-01	Keep critical systems out of radome. / Transfer bird avoidance to airport operations.	-1	-1
RISK-DAMG-05	Design the landing gear and its structural integration to the aircraft to be resistant to impacts. / Transfer pilot training to operators.	-1	-1
RISK-DAMG-06	Strengthen the structure to some extent so that it does not collapse/ break apart on survivable impacts.	0	-1
RISK-DAMG-07	Accept that the health of passengers cannot be assured for impacts that exceed a certain severity.	0	-1
RISK-DAMG-09	Design structurally resistant landing gear and fuselage.	0	-1
RISK-DAMG-10	Design fuselage in order to withstand impacts on water. / Include suitable emergency exits and life vests.	0	-2
RISK-FLGT-01	Install anti icing systems on critical parts. / Transfer de-icing to airport operations.	-1	-2
RISK-FLGT-02	Design cabin interior to have no heavy loose parts. / Design with safety margin in CG range. / Install compartments for cargo that restrict movements.	-1	-1
RISK-FLGT-04	Correctly relay aircraft maximum weights to the operators. / Transfer loading responsibility to pilots and airport operations.	-2	0
RISK-INST-01	Include multiple redundancies for critical sensors. / Transfer de-icing to airport operations. / Transfer visual inspection and checks to pilots.	-3	-2
RISK-INST-02	Transfer risk to a reliable instrument manufacturer. / Transfer checks and procedures to pilots. / Include redundancies for critical flight instruments.	-1	-2
RISK-INST-03	Transfer maintenance of electrical systems to operators. / Include redundant mechanical instruments for the pilots.	-1	-2
RISK-CTRL-02	Limit control authority of computer and enable pilot override. / Include redundant flight computers that can take over in case of failure.	-1	-2
RISK-CTRL-03	Design the aircraft to be recoverable from a stall condition by avoiding deep stall and adding wing twist to maintain control at the stall limit. / Install cockpit stall warnings like a stick shaker or alarms.	-1	-1
RISK-CTRL-04	Design the aircraft such that the pilot can recover from it using the conventional procedures. / Design for RISK-CTRL-03.	-1	-1
RISK-CTRL-05	Transfer de-icing to airport operations. / Add de-icing systems for the control surfaces.	-1	-1
RISK-CTRL-06	Add separate redundant hydraulics systems or servos that can take over in case of a failure. / Transfer malfunction risk to component suppliers.	-1	-2
RISK-CTRL-07	Install cockpit warnings such as bank angle or terrain warnings. / Give the flight computer authority to correct certain pilot decisions. / Transfer pilot training and mental health to operators.	-1	-1
RISK-DNGR-01	Design cabin to offer accessible space for instruments against fire (fire extinguisher, cover blankets). / Use fire-resistant materials inside the cabin.	-1	-1

RISK-DNGR-02	Incorporate firewall in cargo compartment. / Use fire-resistant materials. / Transfer risk of dangerous cargo to operators and airport operations.	-1	-1
RISK-DNGR-03	Regular maintenance and testing of pressure seals. / Include oxygen masks in cabin.	-1	-1
RISK-DNGR-04	Add redundant emergency exits in compliance with CS23.	0	-2
RISK-DNGR-07	Simulate and test tank in operational environment / Add high accuracy hydrogen detection sensors and safety margins for structure.	-2	-0
RISK-DNGR-08	Ensure proper functioning of the intercooler. Install a firewall around the fuel cells and consider extinguishing capabilities.	-1	-2
RISK-DEGR-01	Replacable modular batteries and sensors for monitoring the performance of the battery.	0	-1
RISK-MISC-01	Incorporate margins in loading diagram. / Supply operators with loading charts. / Transfer remaining risk to ground staff.	-1	0
RISK-MISC-05	Transfer risk to reliable manufacturers for communication systems and to the operators regarding pilot training.	-1	0

**Table 15.4:** Mitigation strategies for the developmental risks (from baseline and midterm reports)

Risk code	Mitigation strategy	$\Delta L$	$\Delta S$
RISK-PASS-04	Reduce operational costs by ensuring efficiency and ease of maintenance, and reduce the purchase cost of the aircraft for operators by keeping the development and manufacturing costs low.	-2	0
RISK-CUST-01	Ensure that the focus on environmental sustainability and emission footprint of the aircraft is maintained during the design.	-2	0
RISK-CHAR-01	Run detailed simulations later in the design to predict eigenmodes and perform verification and validation on the simulations. / Design on-board control systems to damp oscillations in flight.	-2	-2
RISK-BDGT-02	Assess materials and manufacturing methods with the goal of keeping the associated production costs low.	-2	0
RISK-CLNT-01	Reduce the purchase cost of the aircraft for operators by keeping the development and manufacturing costs low.	-1	-1
RISK-CLNT-02	Reduce operational costs by ensuring efficient propulsion and flight performance, and design for ease of maintenance.	-1	-1
RISK-CLNT-04	Use maximum range requirement as a driving requirement in the design and ensure that it is fulfilled by iterating calculations.	-1	-2
RISK-CUST-02	By driving the assessment of the materials according to the recyclability requirement the risk can be mitigated.	-1	-2
RISK-SUST-01	Assess propulsion system options with the ecological impacts of direct emissions and emissions due to acquisition of the energy source as key factors in the design. / Accept that design influence on indirect emissions is small.	-1	0
RISK-SUST-02	Use ease and affordability of recycling methods as a driving requirement in the material selection during the design.	-1	-1
RISK-SUST-04	Use payload and maximum weight as driving requirements in the design.	-1	-2
RISK-CLNT-05	Use payload and maximum weight as driving requirements in the design.	-1	-2
RISK-OPER-05	Opt for a propulsion technology that does not imply extreme effort for ground staff to refuel/recharge. / Incentivise airport operators to suitably equip their airports for the Sustainable Air Taxi.	-1	-1
RISK-SUST-05	Ensure that the processes used for recycling aircraft components are sustainable. Design for RISK-SUST-04 to incentivise recycling.	-1	-1
RISK-SUST-06	Ensure sustainable development approach is followed for manufacturing aspects and when creating the production plan.	-1	-1
RISK-SCHD-02	Focus the scope of the performed work in the next 9 weeks on the essential elements of the air taxi development. / Use concurrent engineering to raise the design group efficiency	-1	-1
RISK-CHAR-02	Ensure that static stability calculations are iterated when changes are made throughout the design.	-2	-1
RISK-CHAR-03	Run detailed simulations in later design stages to predict aeroelastic behaviour and vibrational modes of the aircraft. /	-1	-1
RISK-CHAR-04	Perform verification and validation to ensure model accuracy.	-1	-1
RISK-MODL-01	Perform proper verification and validation to reduce and take into account model inaccuracy.	-2	-1
RISK-OPER-07	Take into account the implications of the design on the ground operations while designing, such that these will be easily dealt with during operations and make sure that adequate documentation of the required procedures is made	-1	-2
RISK-MODL-08	Take into account the implications of the design on the ground operations while designing, such that these will be easily dealt with during operations and make sure that adequate documentation of the required procedures is made	-1	-2

## 15.2. Identification and Mitigation of New Technical Risks

With the detailed design of the subsystems in the final design phase, several new technical risks are identified and assessed. These risks are presented with their pre-mitigation likelihood and severity scores in Table 15.5. These risks are given mitigation strategies in Table 15.6, as well as the reduction in likelihood and severity scores which are used to position them in the post-mitigation risk matrices in Section 15.3.

**Table 15.5:** *Newly identified risks*

Risk description	Risk code	Cause	Consequence	L	S
Sloshing within the fuel tank	RISK-FLGT-05	The fuel is free to move within the fuel tank	Sudden change of center of gravity, risk of instability	4	3
Insufficient space in wingbox for the amount of stringers needed	RISK-STRC-07	Faulty assumptions during structural design	Need for redesign due to inadequate load capacity	3	3
The wingbox fails during operation	RISK-STRC-08	Inadequate structural design or underestimation of flight loads	Catastrophic failure, mortal risk to passengers and crew	2	5
Main landing gear penetrates fuel tank	RISK-GEAR-03	Landing gear collapse in crash landing	Rapid release and expansion of hydrogen, mortal risk to passengers and crew	2	5
Fuel cells lose efficiency over time	RISK-PROP-09	The catalyst and electrode degrade throughout use	Decrease in power output over time	3	2
Too much water entering the fuel cells	RISK-PROP-10	Regulator valve failure	Loss of power in flight	2	3
Membrane dehydration in the fuel cells	RISK-PROP-11	Regulator valve failure	Loss of power in flight	2	3
Propulsion system overheats	RISK-PROP-12	Cooling system malfunction	Lower fuel cell efficiency, reduced power	2	3
Too high structural weight after detailed design of components	RISK-STRC-09	All-aluminium airframe results in weight increase beyond accepted margins	Need for major redesign	2	4

Table 15.6 gives the mitigation strategy and risk-level reduction for the new risks. Contrary to the risk mitigation in the baseline and midterm reports where the red and orange risk categories were mitigated, this time the yellow risks are also mitigated since there are not that many of them.

**Table 15.6:** *Mitigation strategies for the developmental risks (from final report)*

Risk code	Mitigation strategy	$\Delta L$	$\Delta S$
RISK-FLGT-05	Install aluminum slosh baffles in the fuel tank will as mentioned in Subsection 6.3.3.	-1	-2
RISK-STRC-07	During the design process, iterate and verify the wingbox design until it allows for the stringers required.	-2	0
RISK-STRC-08	Within the design process the wingbox design shall be specifically designed to account for all possible loading cases including a safety factor.	-1	0
RISK-STRC-09	Take the possible weight issues of the all-aluminium airframe into account in the mass budget, optimize component geometry for best performance to weight ratio.	-1	0
RISK-GEAR-03	Implement shear pin and reinforced plate at strut joint as described in Subsection 5.3.4.	-1	-1
RISK-PROP-09	With proper maintenance, the degradation is kept an eye on and if needed fuel cells are replaced.	-1	0
RISK-PROP-10	Implement a second regulator valve for redundancy within the propulsion system.	-1	0
RISK-PROP-11	Implement a second regulator valve for redundancy within the propulsion system.	-1	0
RISK-PROP-12	Accept cooling system malfunction risk but implement temperature sensors to reduce power and warn the pilots when an overheat is detected.	-1	0

### 15.3. Updated Risk Matrices

Based on the mitigation strategies and reduction in likelihood and severity scores in Table 15.6, the newly identified risks from Table 15.5 are placed in the post-mitigation risk matrices in Table 15.7 and Table 15.8, together with all the previous risks. These risk matrices provide a complete view of the post-mitigation risk levels of all the risks assessed during the design phase.

**Table 15.7: Post-mitigation risk matrix for the operational risks**

Likelihood/ Severity	Acceptable	Tolerable	Considerable	Undesirable	Intolerable
Very unlikely			RISK-DNGR-03 RISK-PROP-04 RISK-GEAR-01 RISK-GEAR-04 RISK-INST-01 RISK-INST-02 RISK-INST-03 RISK-CTRL-03 RISK-CTRL-02 RISK-CTRL-04 RISK-CTRL-06 RISK-CTRL-07 RISK-FLGT-02 RISK-STRC-07 RISK-PROP-10 RISK-PROP-11 RISK-PROP-12	RISK-PROP-01 RISK-CTRL-08 RISK-PROP-05 RISK-PROP-06 RISK-DNGR-01 RISK-DNGR-02 RISK-FLGT-04 RISK-STRC-09 RISK-GEAR-03	RISK-DAMG-08 RISK-CTRL-01 RISK-DNGR-05 RISK-DNGR-06 RISK-MISC-05 RISK-STRC-05 RISK-DNGR-04 RISK-MISC-02 RISK-DNGR-07 RISK-STRC-08
Unlikely	RISK-PROP-02 RISK-PROP-07 RISK-GEAR-03	RISK-STRC-01 RISK-BRAK-02 RISK-STRC-03 RISK-CTRL-05 RISK-FLGT-01 RISK-PROP-09	RISK-FLGT-03 RISK-GEAR-05 RISK-STRC-02 RISK-GEAR-01 RISK-MISC-01 RISK-STRC-06 RISK-DNGR-02 RISK-BRAK-02 RISK-DAMG-06 RISK-DAMG-07 RISK-DAMG-09 RISK-DAMG-10 RISK-PROP-08 RISK-DNGR-08		
Plausible	RISK-WTHR-02 RISK-DAMG-02 RISK-DAMG-03 RISK-GEAR-02 RISK-WTHR-01 RISK-WTHR-03 RISK-WTHR-04 RISK-FLGT-05	RISK-STRC-02 RISK-STRC-04 RISK-BRAK-01			
Likely	RISK-WTHR-05 RISK-DAMG-01 RISK-DAMG-05				
Very Likely	RISK-DEGR-01 RISK-MISC-03				

**Table 15.8: Post-mitigation risk matrix for developmental risks**




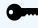
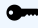
Likelihood/ Severity	Acceptable	Tolerable	Considerable	Undesirable	Intolerable
Very unlikely	RISK-OPER-08	RISK-CLNT-06 RISK-PASS-01 RISK-PASS-02 RISK-BDGT-01 RISK-SCHD-02	RISK-MODL-02 RISK-CHAR-01 RISK-CLNT-04 RISK-CUST-01 RISK-CLNT-05	RISK-PASS-05 RISK-OPER-03 RISK-OPER-04 RISK-BDGT-02 RISK-CLNT-01 RISK-CLNT-02	RISK-OPER-01 RISK-OPER-02 RISK-SUST-03 RISK-PASS-04 RISK-CUST-02 RISK-SUST-01
Unlikely		RISK-CLNT-07 RISK-BDGT-03 RISK-OPER-05 RISK-SUST-05 RISK-SUST-06 RISK-MODL-01 RISK-CHAR-04 RISK-OPER-07	RISK-SCHD-01 RISK-SUST-04 RISK-CHAR-02 RISK-CHAR-03		
Plausible		RISK-CLNT-03 RISK-PASS-03		RISK-SUST-02	
Likely					
Very Likely					



## Compliance matrix

In order to check whether the design requirements have been met, it is important to generate the so-called compliance matrix, which encompasses all of the requirements, followed by a column which indicates whether each one has been met, has not been met, or is inconclusive at this point without further analysis (denoted by the abbreviation "F/A"). This chapter provides this compliance matrix.

**Table 16.1:** *User requirements as provided by the client*

Requirement	Description	Compliance	Chapter
REQ-USR-PERF-01 	The aircraft shall have a maximum range greater than or equal to 1200 km plus a reserve range of 300 km.	✓	Chapter 4
REQ-USR-PERF-02	The aircraft shall be able to use primary and secondary airfields with hardened runways longer than 1500 m.	✓	Chapter 4
REQ-USR-PERF-03 	The aircraft shall be able to carry a payload greater than or equal to 800 kg.	✓	Chapter 4
REQ-USR-SAFE-01	The design shall comply with EASA CS-23 regulations.	✓	All chapters
REQ-USR-SUST-01 	The aircraft's propulsion system shall be driven by a more sustainable energy source than existing similar aircraft.	✓	Chapter 7
REQ-USR-BDGT-01 	At least 80% of the aircraft's empty weight shall be recyclable or reusable.	✓	Chapter 12
REQ-USR-BDGT-02 	The carbon footprint including indirect emissions per passenger-kilometre of the aircraft shall be no greater than that of an average car with 2 passengers.	✓	Chapter 12
REQ-USR-COST-01	The aircraft shall be priced competitively with respect to other available options in the medium range (500-1200 km) market.	✓	Chapter 13
REQ-USR-COST-02	The aircraft shall be designed for an existing and lasting market demand.	✓	Chapter 13

**Table 16.2:** *Stakeholder requirements*


Requirement	Description	Compliance	Chapter
SH-PAS-REQ-01	The cost per flight-hour shall be no more than 2350 USD.	✓	Chapter 14
SH-PAS-REQ-03	A nominal flight from Amsterdam to Munich shall be completed in under two flight hours.	✓	Chapter 4
SH-PAS-REQ-05	The passengers shall be able to look out of a window.	✓	Chapter 5
SH-PAS-REQ-07	The aircraft shall be equipped with a lavatory.	✓	Chapter 5
SH-PAS-REQ-08	The probability of a fatal accident shall be less than 1 in 16 million per passenger trip. <sup>1</sup>	F/A	-
SH-PDT-REQ-01	The design process shall not take more than 3500 hours of combined labour.	✓	All chapters
SH-OP-REQ-01	The aircraft shall be reliable/operational for 20 years.	✓	Chapter 14
SH-OP-REQ-02	The aircraft shall have a safety factor of 1.5.	✓	Chapter 8
SH-OP-REQ-03a	More than 80% of the aircraft operational empty weight shall have a "second life"/be recyclable.	✓	Chapter 12
SH-OP-REQ-05	The aircraft shall allow for ease of maintenance.	✓	Chapter 14
SH-AfO-REQ-01	The aircraft shall fit within its designated storage place.	✓	Chapter 14
SH-AfO-REQ-02	The aircraft shall fit within the designated gate/ramp area.	✓	Chapter 14
SH-AfO-REQ-03	The aircraft shall be safely refuelled/charged in less than 2 hours time with one pump.	✓	Chapter 14
SH-AfO-REQ-04	The aircraft shall have a refuelling/charging port on the outside, that is accessible from the ground.	✓	Chapter 14

<sup>1</sup><https://www.lesserlawfirm.com/is-flying-safer-than-driving/#:~:text=It%20is%20estimated%20that%20the,several%20things%20must%20be%20considered> [accessed 21-04-2022]



SH-Afo-REQ-06	The noise produced by the aircraft shall not exceed the amount stipulated in Wet geluidhinder <sup>2</sup> .	F/A	-
SH-Afo-REQ-05	The aircraft shall be able to communicate with air traffic control in adherence to the requirements stipulated in CS23.	F/A	-
SH-OM-REQ-02	The entire aircraft shall be manufactured within 40 man hours.	✓	Chapter 11
SH-RC-REQ-02	The recycling of the aircraft components shall be commercially viable.	✓	Chapter 3
SH-RC-REQ-03	The aircraft systems shall be recycled at costs lower than <b>TBD</b> USD/kg.	F/A	-
SH-RC-REQ-05	The aircraft systems shall be recycled using less than <b>TBD</b> energy.	F/A	-
SH-RC-REQ-06	The aircraft systems shall be recycled using less than <b>TBD</b> man hours.	F/A	-
SH-GV-REQ-02	The aircraft shall be designed under the governmental aircraft regulations.	✓	All chapters
SH-GV-REQ-03	The aircraft shall be designed for less than <b>TBD</b> noise pollution factor.	F/A	-
SH-GV-REQ-04	The aircraft shall be operated for a carbon footprint of less than 61.15 g per passenger kilometer during operation.	✓	Chapter 12
SH-GV-REQ-05	The aircraft shall adhere to the regulations stipulated in CS23.	✓	All chapters
SH-PLA-REQ-02	The aircraft shall produce less than 50 dB when outside of the airfield, measured in front of people's homes. <sup>3</sup> .	F/A	-

**Table 16.3:** System requirements from requirement tree

Requirement	Description	Compliance	Chapter
<i>Resources Requirements</i>			
REQ-MC-RSC-01	The project shall be completed with the available resources.	✓	All chapters
REQ-MC-RSC-04	The project shall be completed using the facilities of the TU Delft.	✓	All chapters
REQ-MC-RSC-05	The aircraft shall be operational within 10 years of the development start.	F/A	-
<i>Legal and Safety Requirements</i>			
REQ-MC-LS-01	The aircraft shall abide to legislation stipulated by governmental law.	F/A	-
REQ-MC-LS-02	The noise levels produced by the aircraft shall not exceed the ones stipulated by Wet geluidhinder. <sup>4</sup>	F/A	-
REQ-MC-LS-03	The aircraft shall abide to the rules set by wet luchtvaart. <sup>5</sup>	F/A	All chapters
REQ-MC-LS-04	The aircraft shall comply with EASA CS-23 regulations.	✓	All chapters
REQ-MC-LS-05 	The aircraft shall have a maximum take-off weight of no more than 5670 kg.	✓	Chapter 4
REQ-MC-LS-06	An aircraft of more than 2722 kg shall have a gradient of climb after take-off of at least 4% with: engines at take-off power, landing gear extended, flaps in take-off position and a climb speed of at least 1.1 $V_{MC}$ or 1.2 $V_{S1}$ .	✓	Chapter 4
REQ-MC-LS-08	The aircraft shall have a positive steady gradient of climb at an altitude of 122 m (400 ft) above the take-off surface with: The critical engine in-operative and its propeller in the minimum drag position, the remaining engine at take-off power, the landing gear retracted, the wing flaps in the take-off position(s), a climb speed equal to that achieved at 15 m (50 ft).	F/A	-

<sup>2</sup><https://www.infomil.nl/onderwerpen/geluid/regelgeving/wet-geluidhinder/wet-geluidhinder-'/> [accessed 22-04-2022]

<sup>3</sup><https://bewijsrapportage.nl/waarom/geluidsoverlast/#:~:text=Gebleken%20is%20dat%20continu%20geluid,en%20's%20nachts%2040%20decibel.> [accessed 22-04-2022]

<sup>4</sup><https://www.infomil.nl/onderwerpen/geluid/regelgeving/wet-geluidhinder/wet-geluidhinder-'/> [accessed 22-04-2022]

<sup>5</sup><https://wetten.overheid.nl/BWBR0005555/2021-07-10> [accessed 26-04-2022]













REQ-MC-LS-09	The aircraft shall have a steady gradient of climb of at least 0.75% at an altitude of 457 m (1 500 ft) above the take-off or landing surface with: the critical engine in-operative and its propeller in the minimum drag position, the remaining engine at maximum continuous power, the landing gear and flaps retracted, and a climb speed not less than $1.2 V_{S1}$ .	F/A	-
REQ-MC-LS-10	The approach speed $V_{REF}$ shall be at least equal to or greater than $V_{MC}$ and/or $1.3 V_{S0}$ .	F/A	-
REQ-MC-LS-11	The aircraft shall have a steady approach speed when landing of at least $V_{REF}$ , that must be maintained down to 15 m height at a gradient of descent no greater than 5.2%.	F/A	-
REQ-MC-LS-12	During a balked landing the aircraft shall have a steady climb gradient of at least 2.5% with: not more than the power or thrust that is available 8 seconds after initiation of movement of the power controls from the minimum flight-idle position, the landing gear extended, the wing flaps in the landing position and a climb speed equal to $V_{REF}$ .	F/A	-
REQ-MC-LS-13	The interior of the aircraft shall comply with the emergency regulations in CS23.	F/A	-
REQ-MC-LS-14	The interior of the aircraft shall not be built with flammable materials.	F/A	-
<i>Sustainability Requirements</i>			
REQ-MC-SUS-01	The aircraft shall be more sustainable than other competitive small aircraft.	✓	Chapter 3
REQ-MC-SUS-02 	The aircraft shall be operated for a carbon footprint of less than 61.15 g per passenger kilometer (average car carrying 2 passengers) during operation.	✓	Chapter 12
REQ-MC-SUS-03 	At least 80% of the aircraft's empty weight shall be recyclable or reusable.	✓	Chapter 12
REQ-MC-SUS-06	The aircraft shall not produce harmful emissions in concentrations which are dangerous for human health.	✓	Chapter 3
REQ-MC-SUS-08	The manufacturing process shall have an environmental impact lower than comparable aircraft.	✓	Chapter 3
<i>Market Requirements</i>			
REQ-MC-MKT-02	The aircraft shall have a unit price which is lower or equal to 6.50 million USD.	F/A	-
REQ-MC-MKT-03	The combined business and fuel cost shall be less than 1557 USD per flight hour	✓	Chapter 13
<i>Operations Requirements</i>			
REQ-MC-OPS-02	The aircraft shall be operable in crosswind conditions up to 25 knots.	F/A	-
REQ-MC-OPS-03	The aircraft shall be able to load/load-off passengers without the help of external equipment.	✓	Chapter 5
REQ-MC-OPS-04	The aircraft shall have a refueling point on the outside of the aircraft which is accessible without using a ladder.	✓	Chapter 6
REQ-MC-OPS-05	The aircraft shall be able to carry at least 6 passengers.	✓	Chapter 4
REQ-MC-OPS-09	The aircraft shall be visible in all operable weather conditions.	F/A	-
REQ-MC-OPS-12	The aircraft shall not tip over during taxiing.	✓	Chapter 5
REQ-MC-OPS-13	The aircraft shall be able to loiter for at least 30 minutes.	✓	Chapter 4

Table 16.4: Subsystem Requirements

Requirement	Description	Compliance	Chapter
<i>Structural Requirements</i>			
REQ-TC-STR-01 	The wing shall withstand all load factors during all mission phases. (CS.23.337)	✓	Chapter 8
REQ-TC-STR-02	The wing shall provide 1.4 m clearance when the engine is mounted on the wings.	✓	Chapter 8
REQ-TC-STR-03	Fuselage shall withstand a pressure difference of 21246 Pa at the maximum operational altitude.	✓	Chapter 5
REQ-TC-STR-04	Pressure altitude in fuselage shall not be more than 4572m in cases where pressurisation system malfunctions.	✓	Chapter 5
REQ-TC-STR-05	The Fuselage shall be able to fit the passengers, crew members and other possible payloads.	✓	Chapter 5
REQ-TC-STR-06	The Fuselage shall provide emergency exits as specified in CS23.803, CS23.805 and CS23.807.	✓	Chapter 5
REQ-TC-STR-07 	The structure of the aircraft shall ensure safe operations with an upward acceleration of 3.0g. (CS.23.561)	✓	Chapter 4
REQ-TC-STR-08 	During emergency landings, the structure shall provide escape possibilities with forward accelerations up to 9.0g. (CS.23.561)	F/A	-
<i>Propulsion Requirements</i>			
REQ-TC-PRO-01 	The propulsion system shall provide a minimum thrust of 4097 N.	✓	Chapter 7
REQ-TC-PRO-03	There shall be at least an 18cm (for nose wheel landing gear) or 23 cm (for tailwheel landing gear) between each propeller and the ground in the most critical condition.	✓	Chapter 7
REQ-TC-PRO-04	The propeller shall not hit the ground when with the critical tyre completely deflated and landing gear strut bottomed.	✓	Chapter 7
REQ-TC-PRO-05	There shall be at least 25 mm radial clearance between blade tips and the aircraft structure.	✓	Chapter 7
REQ-TC-PRO-06	There shall be at least 12.7 mm longitudinal clearance between propeller blades and stationary parts of the aircraft.	✓	Chapter 7
REQ-TC-PRO-07	In case of a propeller propulsion system the pilots should not be within +5 degrees of the propeller with respect to the longitudinal axis of the fuselage.	✓	Chapter 7
REQ-TC-PRO-09	During climb a minimum climb rate of 12 m/s shall be possible.	✓	Chapter 4
<i>Aerodynamic Requirements</i>			
REQ-TC-AER-01 	The wing shall have a lift coefficient $C_L$ of 1.5.	✓	Chapter 8
REQ-TC-AER-02	The wing shall provide a $C_L/C_D$ ratio of <b>42.86</b> in cruise.	✓	Chapter 8
REQ-TC-AER-03	The wing shall have high lift devices that provide a $\Delta C_L$ of at least 0.5.	✓	Chapter 8
REQ-TC-AER-05 	The size of the wing should be able to produce the required lift equal to 55152 N for the critical flight condition (MTOW, stall, clean configuration).	✓	Chapter 8
<i>Material Requirements</i>			
REQ-TC-MAT-01 	The materials used for each component shall not fail under any condition in the flight envelope.	F/A	-
REQ-TC-MAT-02 	By mass, at least 80% of the materials used on the aircraft shall recyclable.	✓	Chapter 12
REQ-TC-MAT-03	The materials used during production of the aircraft shall not be hazardous to workers or the environment.	✓	Chapter 3
<i>Control and Stability Requirements</i>			
REQ-TC-CAS-02 	The aircraft shall be statically stable along all axes for any given CG within the range of CG's possible during all phases of the mission	✓	Chapter 4
REQ-TC-CAS-03 	The aircraft shall be controllable for any given CG within the range of the CG's possible during all phases of the mission.	✓	Chapter 4
REQ-TC-CAS-04	The velocity derivative of the stick force shall be positive in each condition.	F/A	-
REQ-TC-CAS-05	The aircraft shall be dynamically stable along all axis.	F/A	-
<i>Landing Gear Requirements</i>			
REQ-TC-GEAR-01	Most aft CG shall be in front of the virtual line, going through the main landing gear and angled forward by the scrape angle.	✓	Chapter 5

<b>REQ-TC-GEAR-02</b>	After take-off it shall be possible to store all gears inside the aircraft.	✓	Chapter 5
<b>REQ-TC-GEAR-03</b>	The landing gear shall withstand the load created during a landing with the following descent speed: $4.4 \frac{W}{S}^{\frac{1}{4}}$ m per second, except that this velocity need not be more than 3.0 m (10 ft) per second and may not be less than 2.1 m (7 ft) per second (CS23.473(d)).	F/A	-
<b>REQ-TC-GEAR-04</b>	During landing the brakes shall not be loaded more than prescribed by the manufacturer of the brakes.	F/A	-
<b>REQ-TC-GEAR-05</b>	Load on nose wheel shall be 0.08% to 0.12% of the weight.	✓	Chapter 5
<b>REQ-TC-GEAR-06</b>	Landing gear shall be able to carry the maximum take-off weight of 5622 kg.	F/A	-
<b>REQ-TC-GEAR-07</b>	The main landing gear shall be positioned such that the scrape back angle is at least 12 degrees.	✓	Chapter 5
<i>Interior Requirements</i>			
<b>REQ-TC-INT-01</b>	During cruise the floor shall be angled compared to the horizon at most 2 degrees.	✓	Chapter 8
<b>REQ-TC-INT-02</b>	The aircraft shall provide seat belts for every person on board while seated.	F/A	-
<b>REQ-TC-INT-03</b>	The seat pitch shall be at least 30 inch.	✓	Chapter 5
<b>REQ-TC-INT-04</b>	The aisle width shall be at least 20 inch.	✓	Chapter 5
<b>REQ-TC-INT-05</b>	All seats shall be equipped with arm rests.	✓	Chapter 5
<b>REQ-TC-INT-06</b>	Each passenger and crew member shall be well ventilated, where the carbon monoxide concentration may not exceed one part in 20 000 parts of air (CS23.831).	F/A	-

As can be seen, the majority of the requirements have been met, but there is still a considerable number of requirements which need a more in-depth analysis and further design. The team concludes that the requirement analysis was a little bit too detailed for the level of development that could be achieved within the available DSE time and resources. Nevertheless, the formulated requirements for which the Sustainable Air Taxi has not been designed yet are still useful for future design steps.

## Conclusions and Recommendations

The contents of this report represent the design of the Sustainable Air Taxi up to the final review stage of the DSE. However, this is not yet a complete design, but a preliminary one, because of the reduced available time. Hence, it could be further developed in the future. This chapter provides the conclusions drawn so far and it discusses the team's recommendations for future work on the design.

### 17.1. Conclusions

This section deals with formulating the conclusions of Group 18 on all relevant aspects, from design considerations to the overall integration of this design in the market.

First of all, the technical performance of the design is discussed in relation with its main goals. The Sustainable Air Taxi's main performance parameters are summarized in Table 17.1. The main objective that was rigorously kept in mind during the design of the aircraft is the high recyclability and a greener alternative to conventional combustion-based propulsion systems, which have a great negative impact on the environment (aviation is responsible for 2-5% of the global  $CO_2$  emissions). A comparison is made between the proposed design and two similar propeller driven conventional aircraft in the same mass range as the Air Taxi, namely the Textron Aviation's King Air 260 and the Piaggio 180 Avanti.

**Table 17.1:** Overview of main performance parameters of the Sustainable Air Taxi

Parameter	Maximum Range	Maximum Payload	Cruise Altitude	Cruise Speed	Maximum Take-off Mass	Number of passengers
Value	1500 km	800 kg	5000 m	475 $\frac{km}{h}$	5622 kg	6

The King Air 260 has a maximum take-off mass of 5670 kg, a maximum payload capacity of 984 kg and maximum cruise altitude and maximum cruise speed of 10668 m and 574  $\frac{km}{h}$ , respectively. It can achieve a maximum range of 3185 km and it carries up to 9 people.<sup>1</sup> On the other side, the Piaggio P180 is rated at a maximum take-off mass of 5488 kg and maximum net payload of 794 kg and it flies at 589  $\frac{km}{h}$  at approximately 12500 m (long range cruise configuration) to achieve a range of around 2800 km (it can fly at over 700  $\frac{km}{h}$  for a shorter range as well) and it can transport up to 8 passengers and 2 crew members.<sup>2</sup> As can be observed, similar conventional aircraft of similar weights are better than the Air Taxi in terms of performance. However, as stated above, this is not an unexpected outcome, because the design process was focused towards having a final product that outmatches the competitors with respect to its environmental impact. The Sustainable Air Taxi can carry 6 passengers, but it is heavier than one would expect for such a capacity and range. This is because of the unconventional propulsion system based on an electric powertrain powered by hydrogen fuel cells, which requires a large storage tank, adding to the overall length and structural weight of the aircraft. In spite of this, all of the major client-imposed requirements referring both to performance and sustainability are met, which are summarized in Table 17.2.

<sup>1</sup><https://beechcraft.txtav.com/king-air-260> [accessed 09-06-2022]

<sup>2</sup><http://www.avantievo.piaggioaerospace.it/> [accessed 09-06-2022]

**Table 17.2:** *Overview of major client requirements*

<b>Performance</b>	
<b>REQ-USR-PERF-01</b>	Aircraft shall achieve a maximum range of at least 1200km + reserves
<b>REQ-USR-PERF-02</b>	Aircraft shall be able to use primary and secondary airfields with hardened runways of at least 1500m
<b>REQ-USR-PERF-03</b>	Aircraft shall carry a payload of at least 800kg
<b>Sustainability</b>	
<b>REQ-USR-SUST-01</b>	Aircraft's propulsion system shall be driven by a more sustainable energy source than existing similar aircraft
<b>Engineering Budgets</b>	
<b>REQ-USR-BDGT-01</b>	At least 80% of the aircraft's empty weight shall be recyclable or reusable

There are certain key design features which enable the Air Taxi to be deemed as a sustainable concept relative to current aircraft. On one side, a lot of attention was paid to the material selection for the aircraft, reason why numerous materials certified for aeronautical applications were investigated. Ironically, the best option in terms of recycling prospects is aluminium, which has been the natural choice for aircraft for decades, before the composites starting winning ground. What is different about the Sustainable Air Taxi, however, is that the internal structure of the wing is entirely designed out of one aluminium alloy (Al7050), rather than employing multiple materials for different components. While the latter method may be more optimized as far as overall performance and mass budget is concerned, the proposed configuration allows for a much greater recycling capability. During the research and meetings the team has made throughout the DSE, it was found that aircraft recycling companies have a tough time with recycling most of the aircraft components specifically because of the multiple alloys used in them. These require very intensive labor and costs associated with material separation, making recycling these parts economically unfeasible. The philosophy behind the Air Taxi was to design the aircraft such that the safety and performance requirements are coordinated with the sustainability ones in relation to the current reality and capabilities of processing aircraft reaching their end of life.

On the other side, the operational emissions of aircraft were another crucial aspect to address. Conventional propulsion systems on aircraft are responsible for very large  $CO_2$ , nitrogen oxides, sulphur oxides,  $CO$  etc. emissions, which have both a global warming and a pollution potential. This is associated with the combustion working principles of typical jet and propeller driven aircraft. This is the reason why the second main point of focus was designing a greener propulsion system. After the necessary trade-offs were performed, a hydrogen based electric powertrain was chosen. The system comprises fuel cells which convert the hydrogen to electricity, which is then directed to two powerful electric motors driving the aluminium propellers. A small battery is also included to perform the functions of the APU and to assist the fuel cells in any emergency, power demanding situation. As the only byproducts of fuel cells are water vapors, the operation of the Sustainable Air Taxi is essentially emission free. Nevertheless, this is not the whole story. In order to account for every possible factor contributing to the environmentally damaging potential, the group also analysed the production and supply chain of hydrogen, considering today's available infrastructure and practices. It was found that hydrogen can also have long term polluting effects if it escapes in the atmosphere in great quantities, such as leading to an increase in the ozone concentration in the upper atmosphere. This is crucial, because hydrogen is the lightest element known to man and it disperses or leaks very quickly in the surrounding air. This is why the fuel cell system features a so called purge valve, which catches the unreacted hydrogen escaping the fuel cells and redirects it back to the cells when the required pressure builds up. Furthermore, the current supply chain of hydrogen, from production to delivery, results in significant emissions of  $CO_2$ ,  $CO$ ,  $CH_4$  and  $H_2$  leaks. Regardless, a thorough analysis showed that, even though a lot of improvement is required in today's hydrogen supply chain in order to make it more environmentally friendly in the long run, hydrogen is still a better option compared to conventional aviation fuels, which damage the surrounding nature at a more elevated level, both during production and during operations. All of the above, combined with the hope that more greener propul-

sion designs will eventually bring the motivation for further developments in the associated required airport infrastructure and production techniques, represent arguments for the feasibility and opportunity that Group 18's design brings for a better aviation future.

## 17.2. Recommendations for the Future

The DSE project represents a proposition towards a new aircraft design that follows clear sustainability requirements towards both recyclability and zero emission flight. The team has come up with a design making use of a hybrid propulsion system based on electric motors and a conventional battery. Powering the electric motors as well as recharging the battery will be done by means of polymer electrolyte membrane fuel cells fuelled with hydrogen that is stored as a liquid at cryogenic temperatures.

As this was an exercise planned for a short duration, the analysis for each system is not fully complete, and only a certain level of detail was achieved in each case. Considering this, the team came up with several recommendations for each system and the steps that may be completed in the future in order to create a design as efficient and as sustainable as possible. The most important systems are represented by the propulsion unit, containing the electric motors and the fuel cell systems, the fuel tank design, the APU battery and the materials used for the structure of the aircraft.

### Propulsion System

The design of the propulsion system entailed gathering the data resulting from the initial sizing of the aircraft, interpreting the data, analysing and selecting the sub-components of the propulsion system accordingly. These components were the electric motors and the propellers, respectively.

As far as the electric motors are concerned, these were chosen according to the obtained driving engine shaft power requirement of 1022 kW - this power requirement corresponds to both the cruise and climb phase, as obtained in Section 4.3. MagniX's magni650 640 kW motors were chosen for this purpose, as they are the only palpable and commercially available option able of meeting this requirement. Because the total shaft power required per engine is actually slightly lower than the nominal power output of 560 kW of the motors, one could argue that the propulsion system is over designed. However, the magni650 were the only tested and available electric motors designed **specifically for aircraft** that could be found on the market with power outputs of over 500 kW.

Another option would be to rely on Wright's new electric motors which are currently under development. According to the company's website<sup>3</sup>, their electric motors will be scalable from 500 kW to 2 MW, according to the needs of the client. Wright Spirit is a modified BAe 146 which should fly using four electric engines powered by the company's new electric motors by 2026, but multiple test flights using one and two electric engines are scheduled in the next two years. If this technology proves airworthy, then it may provide a better alternative for the Air Taxi.

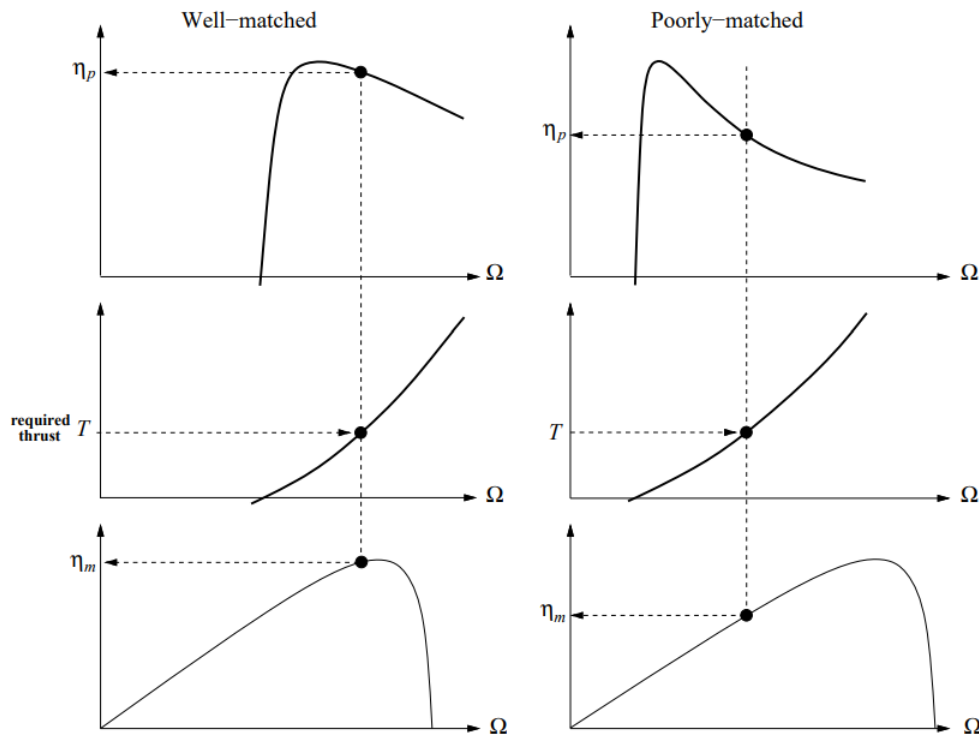
Concerning the propellers, an option from Hartzell Propeller Inc. is chosen, judging by the performance requirements of the Beechcraft King Air 350 and our own requirements. This choice originates from the philosophy of having a propeller which is proven to operate in very similar conditions to the ones expected for the Air Taxi to encounter. The analysis did not cover certain aspects in a quantitative rather than a qualitative way, such as the required blade pitch for every flight phase, altitude and speed. It is known that the propeller is a constant speed propeller and it can be deduced from the King Air 350's specifications what it is optimised for. Furthermore, all the calculations made for the propeller performance assume a propeller efficiency of 85%, efficiency on which the preliminary aircraft sizing is also based. Data for the propeller concerning the variation of its efficiency with parameters such as the advance ratio and the power coefficient are not available, neither

<sup>3</sup><https://www.weflywright.com/technology> [accessed 02-06-2022]



from the manufacturer, nor from other sources, as far as the team could find. Thus, it is left as a future plan to detail this analysis and to verify whether the selected propeller model would encounter any performance damaging conditions during the Air Taxi's mission. This could entail checking its efficiency for the cruise conditions, calculating or finding the exact required pitch values for all conditions.

According to [17], "The equilibrium operating speed  $\omega$  of the motor/propeller combination occurs when the torques are equal". Hence, the torque of the motor and the one of the propeller should ideally be matched. This also means that, in order to maximize the total efficiency of the motor-propeller ensemble, the chosen motor and propeller peak efficiencies have to occur at the operational conditions. Alternatively, instead of a constant speed propeller, a design using a gearbox could be used to find other suitable operational points for the propeller and motor using different RPM and torque such that the equivalent efficiency of the system is maximised [42]. However, in order to find this optimized balance, it is required to know the efficiency ranges for both the propeller and the electric motor, which are currently unavailable. This is thus left as a recommendation for further analysis for the moment. In the end, the required result should resemble as closely as possible the left-hand-side of Figure 17.1, which displays general examples of a well-matched propeller-motor ensemble and a badly matched one, respectively. As can be seen, the efficiency peaks of both the motor and the propeller should lie more or less around the same rotational speed.



**Figure 17.1:** Generic examples of well and poorly matched propeller-electric motor ensembles [17]

### Fuel Cell

The fuel cell system that is implemented in the design of the sustainable air taxi is a polymer electrolyte membrane fuel cell that is the most suitable for mobile applications such as an aircraft. This type of fuel cell is useful because of its high power density and volumetric density, which leads to a vast power produced with relatively low volume and weight.

The main inputs for the PEMFC are hydrogen, oxygen and water. The hydrogen is stored locally in the form of a cryogenically cooled liquid, while the oxygen is fed to the fuel cell from the atmospheric air. As of right now,

the reduction reaction that is happening inside the fuel cell is not fully efficient and it is around 30% lower than the theoretical maximum dictated by thermodynamics.

One of the recommendations for this part is to analyse improvement methods for the efficiency of the fuel cells. One way to do this is to create an electrode membrane that has better conductivity for the electrons, with efficient porosity levels and high catalytic activity. New materials can be developed and tested for this subpart. In addition to this, the use of noble metals such as platinum may be changed if a suitable alternative is found. Of course, when considering new materials, aspects related to sustainability and recyclability should also be taken in account as this is a design that is closely following this ideology.

The efficiency of the PEMFC can also be improved by refining the architecture of the fuel cell, such that the humidity, as well as the temperature control can be better influenced. This can be done in two ways; either by creating systems that can recirculate and recycle the heat, water and unreacted hydrogen, as it was proposed in the Sustainable Air Taxi design, or by changing the internal architecture of the membrane such that the temperature control and the humidity can be done automatically without outside inputs. Another improvement that can be done (and considering literature studies, it has already started) is to create a sustainable supply chain for the hydrogen production, such that the whole process is as close to fully green as possible.

Finally, other types of fuel cells such as solid oxide fuel cells (SOFC), molten carbonate fuel cells (MCFC), alkaline fuel cells (AFC), etc. may be tested for aircraft applications and if their efficiencies are suitable, then they may be improved and fully adapted for integration. New fuel cell designs have to be carefully considered as some of them may use fuels that can do more harm than good.

It is considered that overall, the whole fuel cell system may be well improved in the future, and that in future years, 2030 to 2035, the power and volumetric densities of the fuel cells should be way higher than right now. This will be achieved due to the development towards more sustainable practices in mobile applications. In addition to this, the production of the various materials as well as the hydrogen fuel will be more sustainable in the future, based on the same considerations.

### **Tank Design**

Regarding the tank design future technologies can improve the volume efficiency significantly. MLI foam has very promising thermal conductivity's, but this material is currently still under development. Scientific research about MLI mentions a thermal conductivity for MLI which requires only a foam thickness of several millimeters, resulting in much thinner insulation material compared to the EPS foam from the current airtaxi (11.5 *cm*). Thinner insulation material will result in an bigger shell radius, resulting in more volume such that the tank can be shorter. A shorter tank will directly allow the fuselage to be shorter.

Furthermore, the tank refuelling is highly dependent on the hydrogen infrastructure at airports. A modern hydrogen tank can be the best design possible, but without hydrogen at an airport the Air Taxi can not fly. Because of this, it is necessary to analyse at which airports it will be possible to refuel hydrogen within the near future. Airports without hydrogen infrastructure are not feasible destinations for the Air Taxi, so this might influence the market space.

### **Battery**

Initially, the Sustainable Air Taxi was thought of as a hybrid electric design in which the battery would bring a major contribution to the operation of the aircraft. Nonetheless, during the design process the team arrived at the conclusion that the fuel cells are theoretically capable of delivering the required power during all phases. This is partly due to the soft requirements on the take-off distance (the aircraft was designed for a take-off roll of at least 1500 *m*). As a result, the battery's importance was drastically reduced, to the extent at which it is only

used as an APU and as a redundancy in case of emergency situations, such as an aborted landing.

The group recommends that in the future an analysis is made for the optimization of the aircraft weight, by combining the fuel cells with a bigger battery, such that both are used during the operational phase at full potential. The analysis would work based on iterations using various realistic efficiencies and power densities for both components, until the weight of the aircraft finally converges to the minimum achievable weight. Even so, this does not necessarily guarantee that the design would be better overall, as one must consider the bigger picture. A heavier battery would also mean that the charging times would increase drastically, which would add to the waiting times during refuelling. Thus, the ground operations and logistics of the Air Taxi would have to suffer because of this, so a fine balance between all these aspects needs to be maintained.

### **Fuselage structure and landing gear loads**

The fuselage and landing gear design done in Chapter 5 is still preliminary, and the fuselage structure is not designed in this report. In further design stages, the structural design of the fuselage needs to be addressed, first by determining the load cases that it must handle. Since it was shown in Subsection 5.2.3 that pressurization loads are not of primary concern due to the low cruise altitude, the structure will mostly be designed to bear the aerodynamic loads from the vertical and horizontal tail surfaces, the loads introduced to the fuselage at the location of the wing-fuselage connection, the loads caused in flight by the inertia of the fuselage itself, and the loads introduced by the landing gear when the aircraft is on the ground. These loads will determine the design of the fuselage frames, skin, longerons, etc. In addition, the stress concentrations around large holes and cut-outs such as windows, doors, and access hatches on the airframe must be assessed and reinforced where necessary. Finite element analysis can be done in later stages on the fuselage structure once it is modelled, and from there, design iterations can be done.

### **Control and Stability**

The control and stability analysis in this report is limited to longitudinal static stability and controllability calculations for sizing and positioning the horizontal tail. In later design stages, the dynamic stability of the aircraft must be analysed. This includes the lateral stability and the dynamic eigenmodes of the aircraft. For these analyses, a number of stability and control derivatives are required, which are difficult to obtain and therefore require in-depth simulations. Based on these, the rudder and elevator control surfaces on the tail will also need to be designed to make sure the aircraft complies with all CS23 requirements on dynamic stability and control forces.

# References

- [1] C. Winnefeld, T. Kadyk, B. Bensmann, U. Krewer, and R. Hanke-Rauschenbach, "Modelling and designing cryogenic hydrogen tanks for future aircraft applications," *energies*, 01 2018.
- [2] E. Padgett and G. Kleen, "D.o.e. hydrogen and fuel cells program record." online, aug 2020. <https://www.hydrogen.energy.gov/pdfs/20005-automotive-fuel-cell-targets-status.pdf>.
- [3] Y. Qiu, H. Yang, L. Tong, and L. Wang, "Research progress of cryogenic materials for storage and transportation of liquid hydrogen," *Metals*, 11 2021.
- [4] D. Verstraete, "The potential of liquid hydrogen for long range aircraft propulsion," 4 2009.
- [5] Y. Wang, H. Yuan, A. Martinez, P. Hong, H. Xu, and F. R. Bockmiller, "Polymer electrolyte membrane fuel cell and hydrogen station networks for automobiles: Status, technology, and perspectives," *Advances in Applied Energy*, vol. 2, no. 100011, 2021.
- [6] P. S. rao, K. Sividasan, and P. Balasubramanian, "Structure-property correlation on aa 2219 aluminium alloy weldments," vol. 3, 1996.
- [7] A. Gomeza and H. Smithb, "Liquid hydrogen fuel tanks for commercial aviation: Structural sizing and stress analysis," *Aerospace science and technology*, vol. 95, no. 105438, 2019.
- [8] W. Johnson and J. Fesmire, "Cylindrical cryogenic calorimeter testing of six types of multilayer insulation systems," *Cryogenics*, vol. 89, 2017.
- [9] D. Lee, S. Cha, J. Kim, J. Kim, S. Kim, and J. Lee, "Practical prediction of the boil-off rate of independent-type storage tanks," *Marine Science and Engineering*, vol. 36, 2020.
- [10] M. Hoogeslag, B. Kumbaroğlu, T. Falat, T. Abdelrazek, J. Svensson, M. Krikke, S. Priboi, V. Buzetelu, B. Leeuwen, J. Vermeulen, "Midterm report group 18 - sustainable air taxi," May 2022.
- [11] M. Hoogeslag, B. Kumbaroğlu, T. Falat, T. Abdelrazek, J. Svensson, M. Krikke, S. Priboi, V. Buzetelu, B. Leeuwen, J. Vermeulen, "Baseline report group 18 - sustainable air taxi," 2022.
- [12] toyota, "Outline of the mirai." online, 2014. <https://www.toyota-europe.com/world-of-toyota/feel/environment/better-air/fuel-cell-vehicle>.
- [13] H.-t. Lee, "A technique for matching propeller, motor, and airframe of an electric powered aircraft based on efficiency maps," in *AIAA SCITECH 2022 Forum*, p. 0885, 2022.
- [14] S. Gudmundsson, "Chapter 15 - thrust modeling for propellers," in *General Aviation Aircraft Design (Second Edition)* (S. Gudmundsson, ed.), pp. 597–656, Butterworth-Heinemann, second edition ed., 2022.
- [15] D. Raymer, *Aircraft design: a conceptual approach*. American Institute of Aeronautics and Astronautics, Inc., 2012.
- [16] EASA, *Easy Access Rules for Normal, Utility, Aerobatic and Commuter Category Aeroplanes*. 2018.
- [17] T. Pthrust, "Dc motor/propeller characterization 03 mar 05,"
- [18] ROHACELL® HERO Product Information Thermal Insulator.
- [19] *Certified High-Pressure Gas Product SUS316/SUS316L*.
- [20] "Stability analysis of water-lubricated journal bearings for fuel cell vehicle air compressor," *Tribology International*, vol. 95, pp. 342–348, 2016.
- [21] Y. Zhao, Y. Liu, G. Liu, Q. Yang, L. Li, and Z. Gao, "Air and hydrogen supply systems and equipment for pem fuel cells: a review," *International Journal of Green Energy*, vol. 19, no. 4, pp. 331–348, 2022.
- [22] T. Diepenhorst, R. Lin, A. M. Sedik, T. Song, and J. Sotsky, "Fuel cell air intake system," *Michigan Engineering*, 2009.
- [23] J. Larminie and A. Dicks, *Fuel Cell Systems Explained*. Wiley, second ed., 2003.
- [24] F. Oliviero, *Aircraft aerodynamic analysis: Mobile surfaces of the wing*. TU Delft, 2020.
- [25] A. W. Network, *Business Commercial Aviation Second Quarter 2021*, vol. 117. 2021.
- [26] A. W. Network, *Business Commercial Aviation Second Quarter 2015*. 2015.

- [27] A. W. Network, *Business Commercial Aviation Third Quarter 2019*. 2019.
- [28] A. W. Network, *Business Commercial Aviation Second Quarter 2022*. 2022.
- [29] Y. Chang, Y. Qin, Y. Yin, J. Zhang, and X. Li, "Humidification strategy for polymer electrolyte membrane fuel cells – a review," *Applied Energy*, vol. 230, pp. 643–662, 2018.
- [30] Y. Nonobe, "Development of the fuel cell vehicle mirai," *IEEE Transactions on Electrical and Electronic Engineering*, vol. 12, no. 1, pp. 5–9.
- [31] C. McFarland and R. K. Agarwal, "A simple model of thermal insulation design for cryogenic liquid hydrogen tank," *Mechanical Engineering and Materials Science Independent Study*, vol. 176, no. 1, pp. –,
- [32] G. Vonhoff, *Conceptual Design of Hydrogen Fuel Cell Aircraft*. PhD thesis, Delft University of Technology, Delft, Feb. 2021.
- [33] R. O'Hayre, S.-W. Cha, W. G. Colella, and F. B. Prinz, *Fuel Cell Fundamentals*. Wiley, third ed., 2016.
- [34] J. B. Lu, G. H. Wei, F. J. Zhu, X. H. Yan, and J. L. Zhang, "Pressure effect on the pemfc performance," *Fuel Cells*, vol. 19, no. 3, pp. 211–220, 2019.
- [35] B. Blunier and A. Miraoui, "Air management in pem fuel cells: State-of-the-art and perspectives," in *2007 International Aegean Conference on Electrical Machines and Power Electronics*, pp. 245–254, 2007.
- [36] D. F. Rogers, "Propeller efficiency rule of thumb," *American Bonanza Society*, 2010.
- [37] D. J. Roskam, *Airplane Design: Part IV: Layout of Landing Gear and Systems*, vol. 4. Roskam Aviation and Engineering Corporation, 2000.
- [38] D. J. Roskam, *Airplane Design: Part I*.
- [39] E. Torenbeek, *Synthesis of Subsonic Airplane Design*. Delft University Press, 1982.
- [40] R. Vos, J. A. Melkert, and B. T. C. Zandbergen, "Aerospace design and systems engineering elements i: The design of the fuselage," 2020.
- [41] R. Vos and J. A. Melkert, "Aerospace design and systems engineering elements i: Wing positioning, landing gear and empennage design," 2020.
- [42] L. A. A. (LAA), "Electric propulsion systems," tech. rep., LAA, may 2020.
- [43] H. Li, "Effect of operating backpressure on pem fuel cell performance," *ECS Transactions*, vol. 19, pp. 65–76, 01 2009.
- [44] EASA, "Certification specifications and acceptable means of compliance for normal, utility, aerobatic, and commuter category aeroplanes cs-23." online, jul 2015. <https://www.easa.europa.eu/downloads/18858/en>.
- [45] A. technology Institute, "Fuel cells - roadmap report." online, mar 2022. <https://www.ati.org.uk/wp-content/uploads/2022/03/FZO-PPN-COM-0033-Fuel-Cells-Roadmap-Report.pdf>.
- [46] W. Electric, "Wright spirit white paper." online, apr 2022. accessible at: <https://docsend.com/view/faijijzkvqdcjg>.
- [47] L. Hoogenboom and R. Spaan, "Shear stiffness and maximum shear stress of tubular members," *International offshore and polar engineering conference seoul*, vol. 15, 06 2005.
- [48] J. J. Berton and D. M. Nark, "Low-noise operating mode for propeller-driven electric airplanes," *Journal of Aircraft*, vol. 56, no. 4, pp. 1708–1714, 2019.
- [49] G. D. Brewer, *Hydrogen Aircraft Technology*. CRC press, 1991.
- [50] D. Raymer, *Aircraft Design: A conceptual approach fourth edition*. American Institute of aeronautics and astronautics, 1991.
- [51] H. P. Inc., *MANUAL REVISION TRANSMITTAL Manual 159 Application Guide*. Hartzell Propeller Inc., may 2022.
- [52] M. Miroshnikov, K. Kato, G. Babu, N. K. Thangavel, K. Mahankali, E. Hohenstein, H. Wang, S. Satapathy, K. P. Divya, H. Asare, *et al.*, "Made from henna! a fast-charging, high-capacity, and recyclable tetrakislawsonsone cathode

- material for lithium ion batteries,” *ACS Sustainable Chemistry & Engineering*, vol. 7, no. 16, pp. 13836–13844, 2019.
- [53] L. Gaines, K. Richa, and J. Spangenberg, “Key issues for li-ion battery recycling,” *MRS Energy & Sustainability*, vol. 5, 2018.
- [54] A. Datta, W. Ng, and M. Patil, “Hydrogen fuel cell and battery hybrid architecture for range extension of electric vtol (evtol) aircraft,” *Journal of The American Helicopter Society*, vol. 66, 2021.
- [55] F. Xu, S. Mu, and M. Pan, “Recycling of membrane electrode assembly of pemfc by acid processing,” *International Journal of Hydrogen Energy*, vol. 35, no. 7, pp. 2976–2979, 2010. 2008 International Hydrogen Forum (HyForum2008).
- [56] C. Rans and J. Melkert, *Lecture notes Structural Analysis and Design: Crippling, Johnson-Euler parabola and buckling of a stiffened panel*.
- [57] M. Whiston, I. Azevedo, S. Litster, K. Whitefoot, C. Samaras, and J. Whitacre, “Expert assessments of the cost and expected future performance of proton exchange membrane fuel cells for vehicles,” vol. 116, no. 11, 2019.
- [58] P. Barua, T. Sousa, and D. Scholtz, “Empennage statistics and sizing methods for dorsal fins,” tech. rep., Hamburg University of Applied Sciences, april 2013.
- [59] D. Ciliberti, *An improved preliminary design methodology for aircraft directional stability prediction and vertical tailplane sizing*. PhD thesis, University of Naples Federico II, Mar. 2016.
- [60] U. Breuer, *Flap Design Case Study. In: Commercial Aircraft Composite Technology*. Springer, 2016.
- [61] R. Steven, “Foamcore blow-molded structural components for transportation applications,” vol. -, no. -, 2015.
- [62] A. Johanning and D. Scholz, “A first step towards the integration of life cycle assessment into conceptual aircraft design,” tech. rep., Hamburg University of Applied Sciences, 2013.
- [63] T. Lewis, “A life cycle assessment of the passenger air transport system using three flight scenarios.” -, 2013.
- [64] S. Rondinelli, R. Sabatini, and A. G. M. Gardi, “Challenges and benefits offered by liquid hydrogen fuels in commercial aviation,” tech. rep., RMIT University, 2014.
- [65] T. Gibon, “Norwegian university of science and technology, industrial ecology, tep4223 life cycle assessment, materials: Aluminium,” Nov. 2020.
- [66] T. Gibon, “Norwegian university of science and technology, industrial ecology, tep4223 life cycle assessment, materials: Steel,” Nov. 2020.
- [67] R. Alderliesten, “Aircraft and spacecraft loads: Translating loads to stresses,” 2018.
- [68] J. G. Kaufman, K. Anderson, and J. Weritz, “Fatigue of aluminium alloys,” tech. rep., ASM international, 2019.
- [69] E. National Academies of Sciences, Medicine, et al., *Commercial aircraft propulsion and energy systems research: reducing global carbon emissions*. National Academies Press, 2016.
- [70] E. Cetinkaya, I. Dincer, and G. Naterer, “Life cycle assessment of various hydrogen production methods,” *International Journal of Hydrogen Energy*, vol. 37, 2011.
- [71] *EU Reference Scenario 2016*.
- [72] T. Gibon and A. Arvesen, *Life Cycle Assessment Electricity*.
- [73] *British Petroleum: Statistical Review of World Energy*, 2021.
- [74] C. Sato, R. J. Carbas, E. A. Marques, A. Akhavan-Safar, and L. F. da Silva, *Effect of disassembly on environmental and recycling issues in bonded joints*, ch. 14.
- [75] I. Dincer and C. Zamfirescu, *Sustainable Hydrogen Production*, ch. 3.
- [76] J. Melkert and R. Vos, “A/c preliminary sizing (class 1 weight estimation method).” <https://brightspace.tudelft.nl/d21/le/content/213451/viewContent/1472129/View>, mar 2020. Delft University of Technology, AE1222-II.
- [77] R. Derwent, “Hydrogen for heating: Atmospheric impacts: A literature review,” *UK Department for Business, Energy & Industrial Strategy, BEIS Research Paper*, vol. 2018, p. 21, 2018.

## DSE project logic diagrams

### A.1. DSE diagrams

Regarding the project logic diagrams of the DSE the functional flow diagram and the functional breakdown structure are included in Figure A.1 and Figure A.2 respectively. Both diagrams were also included in the baseline report [11], and after some minor updates they are also attached to this final report.

### A.2. Post DSE diagrams

After 10 weeks of design the airtaxi got a preliminary shape, and after the DSE there are still a lot of opportunities for the design. In this appendix the future plans of the airtaxi will be discussed. It shall be noted that these plans are optional, and it depends on the team members and clients if they want to continue with it.

In Figure A.3 the post DSE Gantt chart can be seen. There is a monthly interval, since it will be a long term project. Each stage of the project can be created more detailed once it is approaching. The blue months are holidays, which means the entire team has 2 months of holiday per year. The detailed design phase and the production phase will take approximately 1.5 years, which means the first Air Taxi can be expected in september 2025.



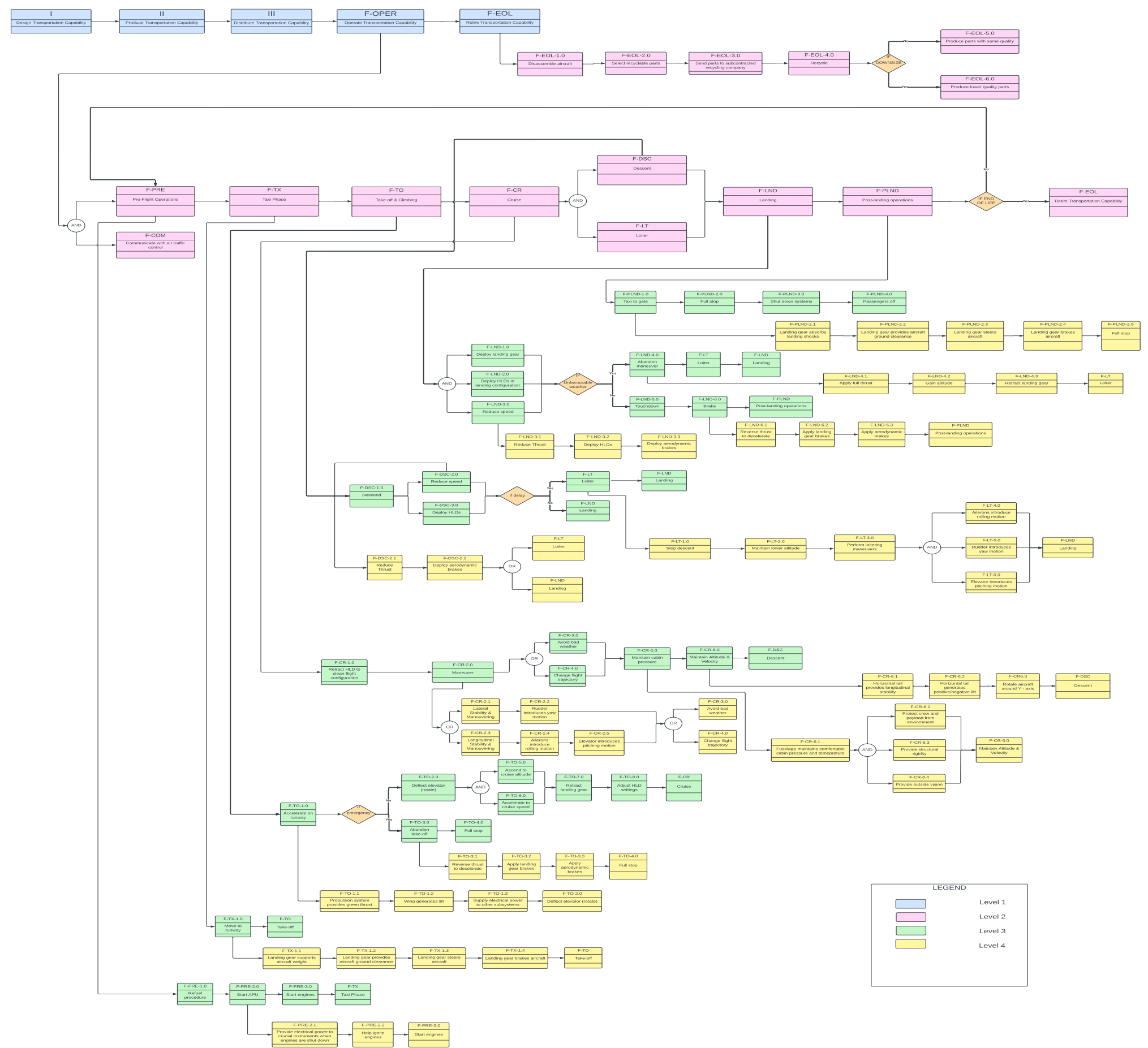


Figure A.1: Functional Flow Diagram v2.0

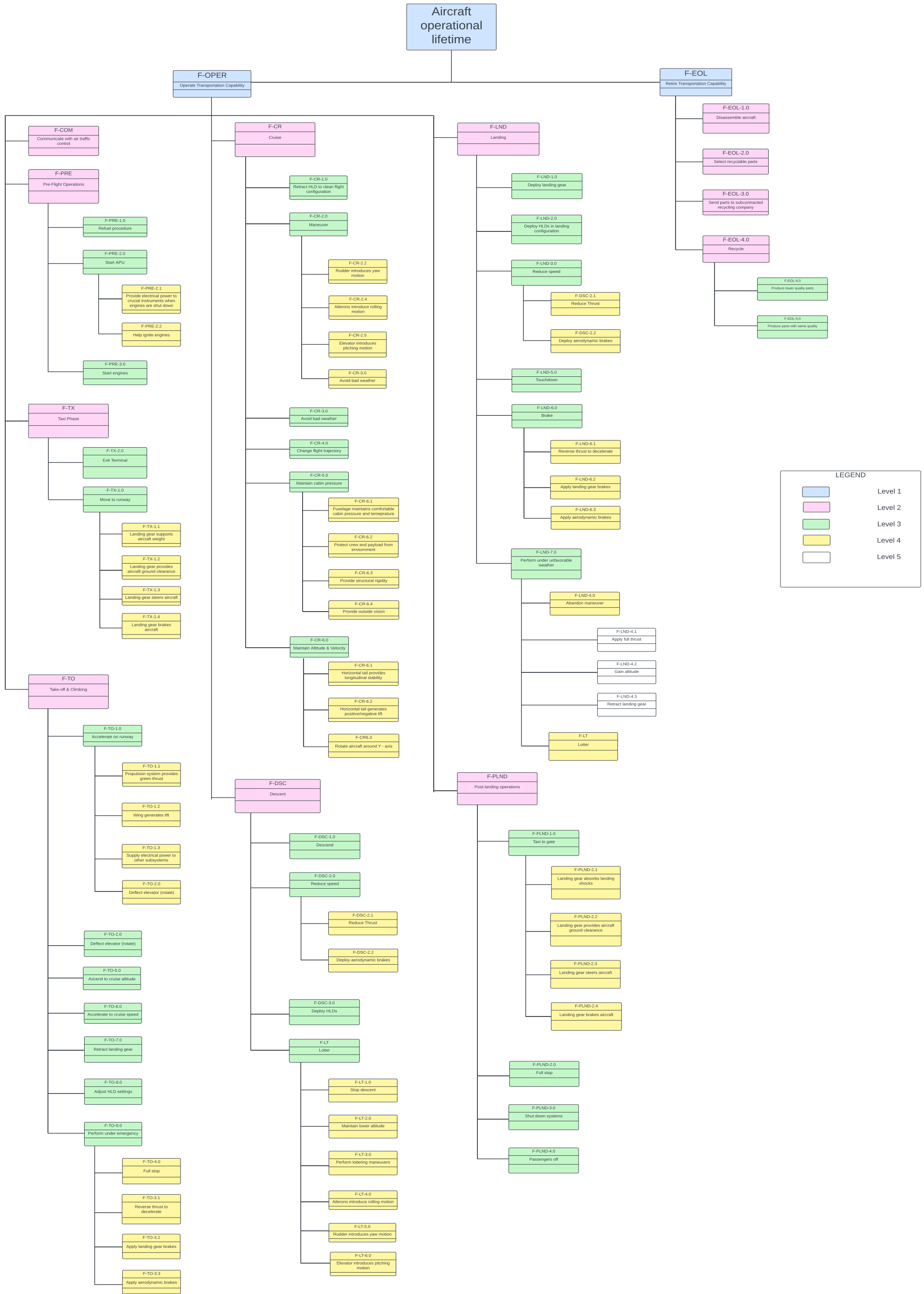


Figure A.2: Functional Break-Down Structure v2.0

## GANTT CHART

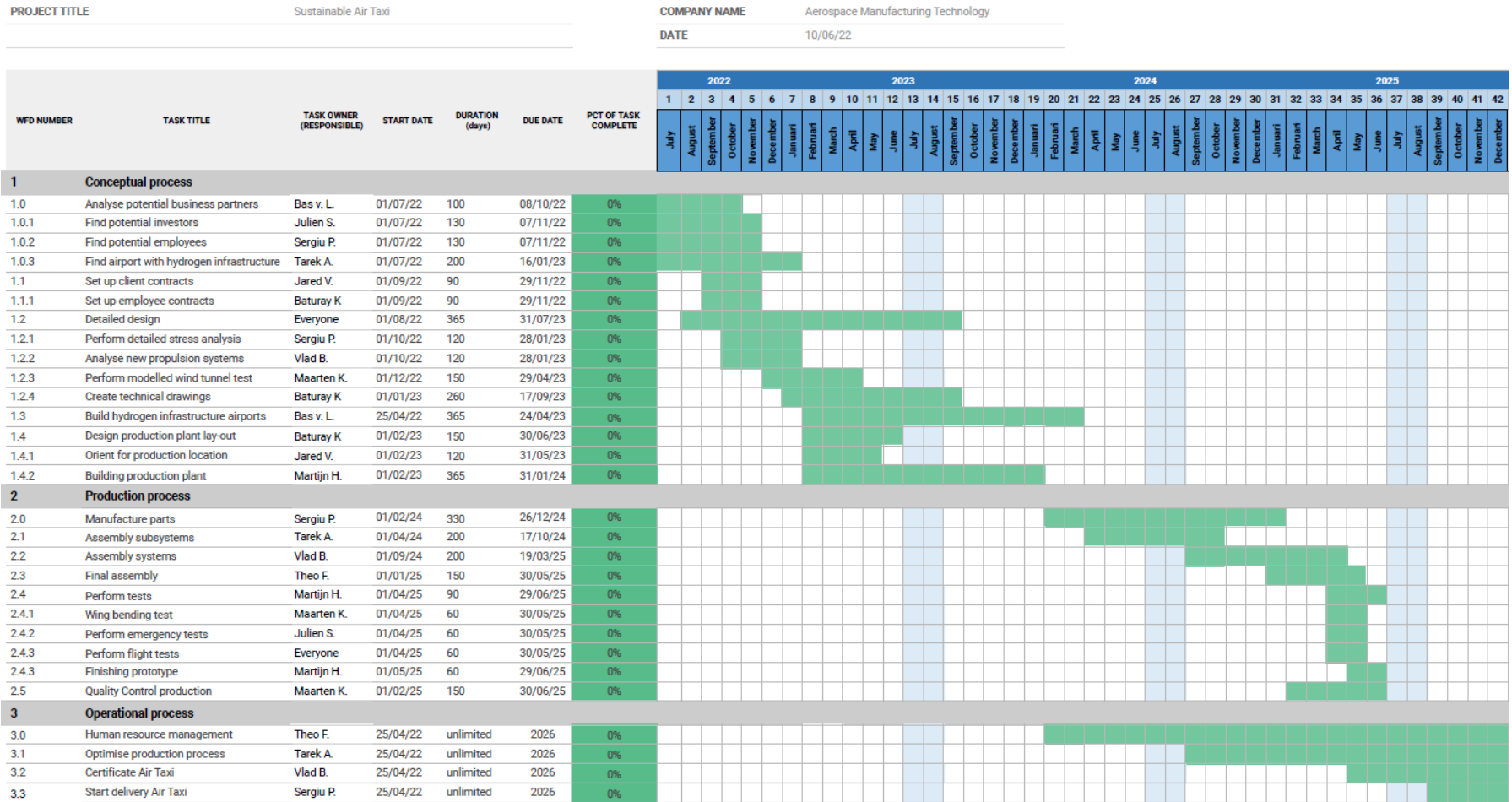


Figure A.3: Post DSE Gantt chart

